新制
工
655
京大附図

APPLICATIONS OF CATASTROPHE THEORY TO STRUCTURAL INSTABILITIES

by

HIDENORI ISAMI

December, 1985

APPLICATIONS OF CATASTROPHE THEORY TO STRUCTURAL INSTABILITIES

by

HIDENORI ISAMI

December, 1985

PREFACE

In natural and social sciences, a sudden and discontinuous change of the state may occur as the external causes vary continuously: buckling and collapse of structures, the flutter of aircrafts, the onset of turbulence in a fast-moving fluid, the phase transition of fluids, the fracture of a crystal lattice, the evolutionary stability of stars and planetary masses, the charged water drops of thunderstorms in an electric field, the heat conduction and fluid flow in thermodynamics and so far. The discontinuous instability phenomena can never be completely interpreted in the classical Newton's mechanics using solutions of unified differential equations.

Thom proposed the philosophical concepts of the **catastrophe** theory in order to clarify the topological aspect of the sudden discontinuities in "Structural Stability and Morphogenesis"(1972). An instability may be determined from a potential function with several internal state variables and some external control parameters. When the control parameters vary continuously, the number of the local minima representing the stable equilibrium states through the potential function may change in a discontinuous way. The Thom's Theorem classifies the structurally stable equilibria of the gradient system, and says that, for the essential state variables ≤ 2 and the control parameters ≤ 4, the canonical form of the potential function is just equivalent to either of the seven elementary catastrophes: fold, cusp, swallowtail, butterfly, hyperbolic umbilic, elliptic umbilic and parabolic umbilic.

The catastrophe theory has been applied to the instability problems of several disciplines of pure mathematics, mechanical engineering, hydrodynamics, thermodynamics, crystallography, cosmology, economics, social sciences and biology.

In civil engineering field, the catastrophe theory provides an effective means for reasonable understanding of static instability or buckling. The internal state variables and the external control parameters in the catastrophe theory correspond to the generalized coordinates and the loading parameters & initial imperfection parameters in the elastic stability theory, respectively. Especially, a question must be answered how imperfections affect the load-carrying capacity of structures; **imperfection sensitivity of structures.** The catastrophe theory significantly contributes to such problems. The load-carrying capacity of structures corresponds to a singular point on the equilibrium surface of structures. Thus, the imperfection sensitivity can be expressed in terms of the bifurcation set in the catastrophe theory.

This dissertation aims to apply the catastrophe theory to evaluation procedures of the ultimate strength of typical civil engineering structures in both the elastic and elasto-plastic ranges. The paper is divided into three parts: the PART I states an introduction to both structural instability theory and the catastrophe theory from two view points of pure mathematics and engineering, the PART II discusses on a proposal of the catastrophe analysis of elastic structures by the use of discretizations and modal transforms, and the PART III formulates a new approach to a unified expression of ultimate strength of compressed slender structural members. The present procedures do not need the so-called nonlinear analysis to evaluate successively the equilibrium states up to the ultimate strength of the structure in elastic and elasto-plastic ranges.

The chapter 1 of the PART I is concerned with an introduction to the interpretation of the concepts such as equilibrium, stability and imperfection sensitivity of conservative structural systems using the general elastic stability theory and the catastrophe theory. In the chapter 2 of the PART I, brief reviews are presented on the catastrophe theory and its applications in engineering sciences from a knowledge of the singularity theory of mappings in pure mathematics. The main mathematical background is provided item by item in the APPENDIX of the PART I.

The chapter 1 of the PART II is concerned with an elastic catastrophe analysis of discrete structural systems with large degrees of freedoms. The present numerical analysis makes use of discretization methods and diffeomorphic modal transformations in the light of the Thom and Thompson's theories. The chapter 2 of the PART II gives a direct computational algorithm to determine the imperfection sensitivity curves or surfaces from the singularity condition in the catastrophe theory. The chapter 3 of the PART II is a comparative study on "inextensible" column models neglecting the axial deformations through the present analysis for continuous and discrete systems. In the chapter 4 of the PART II, the present catastrophe analysis is also applied to axially "extensible" columns, compressed rectangular unstiffened plates and compressed rectangular stiffened plates through the static condensation procedure. A simplified element method adopted herein is briefly described in the APPENDIX A. Also, the standardization of the structural potential function to the Thom's catastrophe unfolding is in the APPENDIX B.

In the chapter 1 of the PART III, a unified new approach is proposed to the prediction of ultimate strength of slender structural members in the elasto-plastic range. The fundamental concepts of the approach is discussed in details. Then, numerical illustrations of the present approach are demonstrated for axially compressed steel columns. In the chapter 2 of the PART III, the present approach is formulated for compressed plates with and without stiffeners. Especially, for stiffened plates, the approach is also applied to independent two modes of the global and local bucklings of the stiffened plate. Furthermore, using the present approach, a Monte Carlo simulation is performed on appropriate statistical distributions of the residual stresses and the initial deflections for compressed plates and stiffened plates. Then, the most frequent combinations of such imperfections can be explicitly determined. The chapter 3 of the PART III formulates the simplified approach for compressed cylindrical shells with considerations of interaction between both asymmetric and axi-symmetric buckling modes. Finally, some experimental data in this PART III were acquired in the CATS, computer aided testing system, at Kyoto University in the APPENDIX.

ACKNOWLEDGMENTS

The author wishes to express appreciation to Professor Yoshiji Niwa of Kyoto University for his general guidance, constant encouragement and support, and valuable criticisms during the course of his studies at the Structural Mechanics Laboratory in Kyoto University since 1977 through 1983. The author wishes to express appreciation to Professor Yoshikazu Yamada and Professor Naruhito Shiraishi of Kyoto University for their encouragement and valuable criticisms during his studies.

The author also wishes to express appreciation to Associate Professor Eiichi Watanabe of Kyoto University for his fundamental and advanced disciplines, constant encouragement and support, helpful suggestions and criticisms throughout the thesis.

The author wishes to extend appreciation to Lecturer Takuo Fukui of Fukui University, Associate Professor Masayasu Ohtsu of Kumamoto University and Lecturer Michihiro Kitahara of Tokai University for their fundamental disciplines and encouragement during his studies. He also wishes to extend appreciation to the following people for his collaboration and assistance: Messrs. K. Iwashimizu, S. Suzuki, Y. Fukumori, T. Asano, T. Yamanouchi, T. Nomura, T. Miyajima, A. Hayashi and A. Fukuda during his school age and his research.

Finally, but not the least, the author wishes to extend appreciation to Principal Hiroyasu Mitani and many staffs of Kohchi National College of Technology for their encouragement and support since 1983.

APPLICATIONS OF CATASTROPHE THEORY TO STRUCTURAL INSTABILITIES

CONTENTS

PART II

CATASTROPHE ANALYSIS OF ELASTIC STRUCTURES

PART III

CATASTROPHE ANALYSIS OF ELASTO-PLASTIC STRUCTURES

PART I

INTRODUCTION TO INSTABILITY AND CATASTROPHE

CHAPTER 1

INSTABILITY AND CATASTROPHE

1.1 General Remarks

Pioneer works on the stability of an equilibrium state of a structure in classical engineering mechanics were initiated by Euler and Lagrange in the eighteenth century. Euler invented his calculus of variations for a bifurcation problem on his "Euler strut". Lagrange introduced the analytical energy approach to mechanics through his fundamental energy theorem using the associated total potential energy.

In the nineteenth century, Poincaré produced a general bifurcation theory in a mathematical sense so as to clarify many qualitative characteristics of solutions for a set of differential equations. He classified them into two typical forms of **limit point** and **bifurcation point.** Hamilton developed the vector fields for a set of first-order differential equations. Also, Liapunov gave the mathematical definitions of stability, and proposed the general energy function with his name. These investigations on nonlinear problems of equilibrium states in pure and applied mathematics will be briefly described in the next chapter 2 of this PART I.

Koiter unified a general bifurcation theory of an elastic continuum under conservative loading in engineering science, and discussed its stability, post-bifurcation and imperfection sensitivity within his energy approach framework[1,2]. He had already proposed an algebraic energy function with the essential instability modes after eliminating the other inessential ones. Furthermore, discussions on the nonlinear branching, postbuckling and imperfection sensitivity of continuous elastic structures were made by Koiter, Budiansky and Hutchinson[3-6]. Especially, Hutchinson extended such a general theory to problems of instabilities in the plastic range[7-10].

Research groups at University College London, associated with Thompson, Hunt, Roorda, Supple, Croll and their colleagues, have provided a great number of significant contributions to study the nonlinear branching of discrete or discretized conservative structural systems using their generalized coordinates[11-24]. Thompson and Hunt summarized their remarkable investigations in the famous monograph, "A General Theory of Elastic Stability"(1973)[25], which played the most important role in engineering applications of Poincaré's dynamics to finite discrete coordinate systems. Also, Huseyin developed his multi-parameter stability theory of elastic structures under combined loading[26-32]. Sewell made a static perturbation procedure to trace equilibrium paths near critical points in structural buckling problems[33-37]. Moreover, Thompson, Hunt, Roorda, Chilver, Supple and Johns have clarified the stability, postbuckling and imperfection sensitivity at the two-fold compound branchings[38-50]. Also, independently, Ho established a reasonable estimation procedure of elastic buckling loads in nonlinear systems[51-53].

Thompson and Hunt have unified the general bifurcation theory of elastic conservative systems[54-64] from a knowledge of the catastrophe theory by Thom and Zeeman[65-68]. The interaction concepts between such two theories of Koiter-Thompson and Thom will be interpreted as follows:

Table 1.1.1 Classification of Static Instabilities of Engineeing Structures.

Classification / Stand-Point	Name of Structures / Type	Columns	Beams	Arches	Plates	Stiffened Plates	Rigid Frames	Trusses	Shells
View Point	Global	✓	✓	✓			✓	✓	✓
	Partial	✓	✓	✓		✓	✓	✓	✓
	Local	✓	✓	✓	✓	✓			
Types of Instability (*CATAS-TROPHE*)	Limit Point, Snap-through (*FOLD*)			✓					✓
	Asymmetric Buckling (*FOLD*)	✓				✓	✓	✓	✓
	Stable Symmetric (*CUSP*)	✓	✓		✓	✓	✓	✓	
	Unstable Symmetric (*DUAL CUSP*)	✓	✓	✓	✓	✓	✓	✓	✓

In civil engineering field, the possibility of various instability phenomena may increase with large degree of freedoms of structures. For typical structures, **Table 1.1.1** shows that the instabilities can be classified into global, partial and local ones from the analytist view point, and that they can be also identified by the canonical forms of catastrophe potential functions. In this table, the types of catastrophes are marked only of so-called distinct critical points, and the possibility of interactive or coincident instabilities, e.g., umbilics, may exist for each type of structures marked in more than two items.

Practical structures have unavoidable imperfections such as initial displacements, residual stresses and load eccentricities in their manufacture and construction. Then, a question must be answered how such imperfections affect the load-carrying capacity of structures. In other words, discussions will concentrate on the well-known **imperfection sensitivity of structures.** The catastrophe theory provides significant reasonable contributions on such problems [62,64,69]. The load-carrying capacity of the structure is assumed to be the maximum value of a single loading parameter among several control ones as mentioned in the next section. The maximum corresponds to a singular point on the equilibrium surface of the structure. Thus, the relation between the load-carrying capacity and several imperfections in the stability theory can be expressed in terms of the catastrophe map in the catastrophe theory[64,69-71].

The catastrophe map means a projection of a set of singular points on the equilibrium surface into the control-parameter space. The projection yields the **bifurcation set** in the control-parameter space, and the set explains the imperfection sensitivity curves, surfaces or spaces. For examples, the so-called "one-half power law" of the asymmetric buckling and the "two-thirds power law" of the unstable symmetric buckling are of the bifurcation sets for distinct critical points, which are clarified by Roorda's experiments[14] and Koiter-Thompson theory[1,25]. At the same time, these sets are interpreted as those of fold and dual cusp catastrophes.

Simultaneous buckling problems are focused on when two distinct instability phenomena take place with coincidence and near-coincidence of the loading parameter. Then, in a mathematical sense, the Hessian matrix of the potential function is degenerate. Thompson, Hunt, Huseyin, Hansen and others have classified such two-fold compound bifurcation points of the "semi-symmetric" potential function into three umbilic subtypes[42,54,72-77].

This chapter presents an introduction to equilibrium, stability and imperfection sensitivity of conservative structural systems within frameworks of the general theory of elastic stability and the catastrophe theory[78,79]. A classification of critical points in both the distinct and the simultaneous cases will be briefly described for ideal perfect systems with no initial imperfections. Then, topological meanings of the use of the catastrophe map will be explained in order to evaluate the load-carrying capacity in engineering practice.

1.2 Elastic Conservative System

A potential function of structural system can be regarded as a function of the internal state variables $\mathbf{x}=(x_1,x_2,\ldots,x_N)$ for prescribed external control parameters $\mathbf{c}=(c_1,c_2,\ldots,c_K)$. The potential function is defined by[62,69,71]

$$V(\mathbf{x}, \mathbf{c}) = V(x_i, c_j) \tag{1.2.1}$$

which may be regarded as a single-valued real function of (N+K) independent variables, **x** and **c**, and is assumed to be infinitely differentiable with respect to them[71,80,81].

The system considered is also assumed to be conservative and to behave elastically in the material sense except for the PART III in this dissertation. Further, the system is assumed to obey the following two Liapunov's axioms[82]:

(1) For a fixed value **c**, the system is in an equilibrium state if and only if its potential function is taken to be stationary at such state with respect to **x**.
(2) For a fixed value **c**, the system is in a stable equilibrium if and only if its potential function has a local minimum value at such state with respect to **x**. The system is governed by the so-called Perfect-Delay convention in a mathematical sense[80,81,83].

Figs. 1.2.1 show the concept of stability of equilibrium state. **Fig. 1.2.1**(a) is "stable" state at which the potential function has a local minimum value, and says that the system keeps the current equilibrium state for an infinitesimal perturbation of potential function near the state. **Fig. 1.2.1**(b) is "unstable" state at which the potential function has a local maximum value, and means that the system transforms an other equilibrium state with lower value of the potential function for a perturbation. Moreover, **Fig. 1.2.1**(c) is "neutral" state at which the potential function has a constant stationary value, and says that the system keeps any equilibrium state without regard to a given perturbation.

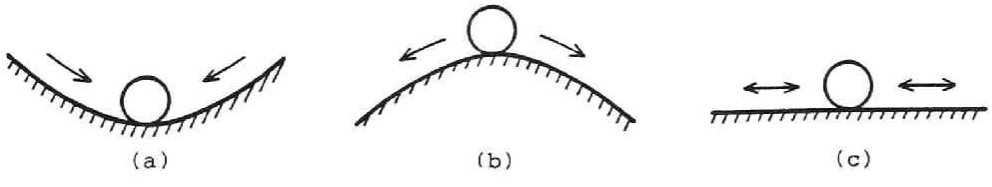

Fig. 1.2.1 Stationary Equilibrium States.
(a) Stable (b) Unstable (c) Neutral

Now, in this dissertation, the change of control parameters may be more slow, but it may be more sensitive to the potential function than that of the state variables. The latter may vary abruptly. That is, the former are assumed to be slow-time scale, while the latter to be fast-time scale[84]. Thus, a perturbation of potential function may be found to be given by that of its control parameters in the case of considering the instability phenomenon through the catastrophe theory.

A great significant problem will arise on the correspondence of the state variables and the control parameters in both the catastrophe theory by Thom and Zeeman and the elastic stability theory of structural mechanics by Koiter and Thompson. The state variables correspond to the generalized coordinates for a discrete system, and are designated as $\mathbf{Q}=(Q_1, Q_2,...,Q_N)$. Whereas the control parameters become both the magnitudes of applied conservative loads and unavoidable initial imperfections such as initial displacements, residual stresses and load eccentricities in manufacture and construction of structural system. The imperfection parameters can be also regarded as some equivalent loading parameters[55,60,61], so that the multi-parameter stability theory has been proposed by Huseyin et al[32,85]. Here, in this dissertation, the control parameters consist of a single loading one and several initial displacement ones.

The following peculiar correspondence between variables and parameters is carried out for the buckling problem of slender structures or models in the dissertation. The control parameters are designated as $\mathbf{\Lambda} = (\Lambda_o, \Lambda_1,..., \Lambda_{K-1})$ such that $\Lambda_o = \Lambda$ is the loading parameter and the remainders Λ_i (i=1,...,K-1) are the initial displacement ones. The "perfect" system means that it has no initial displacements and has only a single loading parameter, that is, $\Lambda_o = \Lambda$, $\Lambda_i = 0$ (i=1,...,K-1). On the other hand, the "imperfect" system possesses a single loading parameter and at least more than one non-zero initial displacement parameters.

1.3 Classification of Instabilities

1.3.1 General remarks

In the elastic conservative system, for fixed control parameters $\mathbf{\Lambda}$, the gradient of its potential function defines a set of equilibrium points. That is, an equilibrium surface is given by a set of solutions of N equilibrium equations

$$\mathbf{grad}\ V = \mathbf{0} \quad \text{or} \quad \frac{\partial V}{\partial Q_i} = 0 \qquad (i=1,...,N) \qquad \text{for prescribed } \mathbf{\Lambda} \qquad (1.3.1)$$

This set yields some equilibrium surfaces in the $(\mathbf{Q}, \mathbf{\Lambda})$ space when $\mathbf{\Lambda}$ varies.

A structural instability which occurs at a singular point on such an equilibrium surface can be classified from a knowledge of its topological aspects [59]. The classification is accomplished by studying on the behavior of "equilibrium paths" on the equilibrium surface when $\Lambda_o = \Lambda$ changes for both the ideal perfect system and the corresponding imperfect system [14,16,18,25, 82,86].

In this section, consider a ideal perfect system; K=1 with only a single loading parameter and no initial displacements. This case has been powerfully studied by Thompson et al. since 1960's[19-25]. Then, for a prescribed value Λ, a single-value solution of Eq. (1.3.1) is expressed by

$$Q_i = Q^F_i(\Lambda) \qquad (i=1,\ldots,N) \qquad (1.3.2)$$

where the superscript "F" refers to the fundamental solution in the equilibrium surface.

Now, consider the stability of structural system using a perturbation of the potential function V due to that of the state variables Q_i from the fundamental equilibrium state, $Q^F_i(\Lambda)$, for a given loading parameter Λ. Thus, an infinitesimal perturbation of the potential function, V, can be expressed by

$$\delta V(q_i, \Lambda) = V(Q^F_i + q_i, \Lambda) - V(Q^F_i, \Lambda) \qquad (1.3.3)$$

when the loading parameter Λ remains fixed. In which, $(q_1,\ldots,q_N)$ are incremental generalized coordinates from the fundamental one Q^F_i.

The perturbation of a potential function defines the stability of the system in the following manner:

(i) if $\delta V > 0$, then the system is in a stable equilibrium state,
(ii) if $\delta V < 0$, then the system is in an unstable equilibrium state, and
(iii) if $\delta V = 0$, then the system may be in a neutral equilibrium state.

Three possible equilibrium states are graphically shown in **Figs. 1.2.1.**

An explicit form of the perturbation δV can be determined in terms of the Taylor expansion of V with respect to the q_i (or Q_i) about the origin (or the fundamental point F). The form follows

$$\delta V(q_i, \Lambda) = \delta V^{(1)} + \delta V^{(2)} + \delta V^{(3)} + \delta V^{(4)} + \ldots \qquad (1.3.4)$$

where

$$\delta V^{(1)} = V_i(\Lambda) q_i \ ,$$

$$\delta V^{(2)} = \frac{1}{2} V_{ij}(\Lambda) q_i q_j \ ,$$

$$\delta V^{(3)} = \frac{1}{6} V_{ijk}(\Lambda) q_i q_j q_k \ ,$$

$$\delta V^{(4)} = \frac{1}{24} V_{ijk\ell}(\Lambda) q_i q_j q_k q_\ell \ ,$$

for a prescribed loading parameter Λ. Also, V_i, V_{ij}, V_{ijk} and $V_{ijk\ell}$ denote the first, second, third and forth partial derivatives with respect to the q_i (or Q_i), respectively. All the derivatives are evaluated at the origin $q_i=0$ (or the fundamental point $Q_i = Q^F_i$. Further, the subscripts, i, j, k,... obey the summation convention form 1 to N. The q_i means an infinitesimal incremental displacement δq_i in a neighborhood of the origin.

When the system stays in an equilibrium state satisfying a set of Eq. (1.3.1), the first term $\delta V^{(1)}$ in the right hand of Eq. (1.3.4) disappeares for any displacement perturbation q_i (i=1,...,N). Thus, in the first approximation, the second

term clarifies the stability of equilibrium states of the system.

(i) if $\delta V^{(2)} > 0$, or if the determinant of the "stability matrix" or the "Hessian matrix"

$$\det[\, V_{ij}(\Lambda)] = \det\left[\frac{\partial^2 V}{\partial q_i \partial q_j}(\Lambda)\right] \qquad (i,j=1,\ldots,N)$$

is positive definite at the origin, then the system is in a stable equilibrium state.

(ii) if $\delta V^{(2)} < 0$, or if the Hessian determinant is negative definite at the origin, then the system is in an unstable equilibrium state.

(iii) if $\delta V^{(2)} = 0$, or if the Hessian determinant vanishes at the origin, then the system is in an uncertain equilibrium state.

$$\det[\, V_{ij}(\Lambda)] = 0 \qquad (i,j=1,\ldots,N) \qquad (1.3.5)$$

The above first two conditions assert that, for a specified Λ, the potential function V can be expressed by a "structurally stable" Morse function in the topological sense at the origin or the fundamental point F. While the third condition can be replaced for

(iii)* An eigenvalue characteristic equation

$$V_{ij}(\Lambda)\, q_j = 0 \qquad (i,j=1,\ldots,N) \qquad (1.3.6)$$

has more than one eigenvalues vanishing at the origin for a peculiar value $\Lambda = \Lambda^C$.

A discontinuous and sudden catastrophe phenomenon may occur at this point $(Q_i, \Lambda) = (Q_i^C, \Lambda^C)$, which is equivalent to an isolated "degenerate" point. Herein, the point F is especially designated as the capital superscript "C", named "critical". Thus, incrementals of state variables and loading parameter from the point (Q_i^C, Λ^C) can be rewritten by

$$Q_i = Q_i^C + q_i \quad (i=1,,,,N) \quad \text{and} \quad \Lambda = \Lambda^C + \lambda \qquad (1.3.7)$$

Then, the critical point (Q_i^C, Λ^C) is transformed into the origin $(q_i, \lambda) = (0,0)$ in the new coordinates.

By the use of these notations, a determination of the sign of the quadratic term $\delta V^{(2)}$ is made through a convenient diagonalization process of its Hessian matrix $V_{ij}(\lambda)$. For this purpose, a linear transformation $\Phi_{ij}(\lambda)$ will be introduced in a neighborhood of the critical origin C $(q_i, \lambda) = (0,0)$, and a new coordinate system u_i can be further defined as follows:

$$q_i = \Phi_{ij}(\lambda)\, u_j \qquad (i=1,\ldots,N;\ j=1,\ldots,n;\ n<<N) \qquad (1.3.8)$$

where the transform $\Phi_{ij}(\lambda)$ is commonly taken as the eigenvector-matrix whose components consist of n eigenvectors corresponding to the n lower eigenvalues of Eq. (1.3.6). That is, herein, it equals to $\Phi_{ij}(0)$ when $\lambda = 0$. The critical point C appears at the origin $(u_i, \lambda) = (0,0)$ in the new coordinate.

Therefore, for a prescribed incremental loading parameter λ near zero, a new potential function is obtained by

$$D(u_i, \lambda) = V(Q_i^c + q_i, \Lambda^c + \lambda) - V(Q_i^c, \Lambda^c + \lambda) \tag{1.3.9}$$

in a neighborhood of the critical origin $(u_i,\lambda)=(0,0)$.

Moreover, the potential function is expressed in the Taylor expansion in a neighborhood of the critical origin $u_i=0$ for prescribed λ near zero

$$D(u_i, \lambda) = D^{(1)} + D^{(2)} + D^{(3)} + D^{(4)} + \cdots$$

$$= D_i(\lambda)u_i + \frac{1}{2} D_{ij}(\lambda)u_iu_j + \frac{1}{6} D_{ijk}(\lambda)u_iu_ju_k + \cdots \tag{1.3.10}$$

where each derivative with respect to the coordinate u_i is evaluated at the origin C $(u_i, \lambda)=(0,0)$. Since the system stays in an equilibrium state, the first linear terms in the right hand side vanish for all i (i=1,...,n). The second quadratic terms may be diagonalized through Eq. (1.3.8).

$$D_{ij}(\lambda) = C_i(\lambda)\,\delta_{ij} \qquad \text{(i,j: not summed)} \tag{1.3.11}$$

where $C_i(\lambda)$ (i=1,...,n) are called "stability coefficients", and δ_{ij} denotes the well-known Kronecker's delta. Then, the quadratic terms are written as the form of

$$\frac{1}{2} C_i(\lambda)u_i^2 \tag{1.3.12}$$

which determine the stability of the system considered.

(i) If $C_i(\lambda) > 0$ for all i, then the system is in a stable equilibrium state,
(ii) if $C_i(\lambda) < 0$ for certain i, then the system is in an unstable equilibrium, and
(iii) if $C_i(\lambda) = 0$ for more than one i, then the system is in a "critical" equilibrium state.

In two cases of (i) and (ii), the potential function D of Eq. (1.3.9) can be expressed in the general quadratic form, i.e., the Morse function of Eq. (1.3.12). On the other hand, the case (iii) says that its critical origin $u_i=0$ is "non-Morse" or "degenerate" point. This paper treats such a singular point. Since $C_i(0)=0$ when $\lambda=0$, the singular point is commonly classified into two types of equilibrium points through the mathematical bifurcation theory by Poincaré[87], Koiter[1] and Thompson[25,54,62] as follows:

(a) Limit Point or Snap Through Point

An equilibrium path near this point has a local minimum value at which the system may lose its stability, and may jump an another stable equilibrium state. This condition can be written by

$$D_i^0 = \frac{\partial^2 D}{\partial u_i \partial \lambda} \neq 0 \qquad (i=1,\ldots,n) \tag{1.3.13}$$

which is evaluated at the point.

(b) Bifurcation Point

More than two independent equilibrium paths intersect at this point, and the system may exchange its stability from a stable equilibrium to an unstable one, or vice versa. This condition can be written by

$$D^{o}_{i} = 0 \qquad (i=1,\ldots,n) \qquad (1.3.14)$$

Similar classification has been also developed by Huseyin in his multi-parameter stability theory of elastic systems[32,85]. He called the type(a) "general", and the type(b) "special".

Now, consider m-fold compound critical points such that

$$D^{c}_{i} = 0, \quad (i=1,\ldots,n) \qquad D^{c}_{ii} = C_{i} = 0 \quad (i=1,\ldots,m) \quad \text{and} \quad D^{c}_{\alpha\alpha} = C_{\alpha} \neq 0 \quad (\alpha = m+1,\ldots,n) \qquad (1.3.15)$$

where the superscript "c" refers to the evaluation of each derivative at the critical origin C, and the subscript "i" and "α" are reordered herein. In other words, this condition equals that the Hessian matrix $D^{c}_{ij}=D_{ij}(0)$ has "rank" (n-m) and "corank" m in a topological manner.

Under this situation, the quadratic form is the Morse function consisting of only the **inessential** state variables, u_{α}(α =m+1, ...,n). More than cubic terms remain in functions of all the state variables u_{i} (i=1,2,...,n). The main objective in this chapter is to describe a brief discussion on an explicit expression of potential function, involving the **essential** stable variables u_{i} (i=1,2,...,m) and the loading parameter λ. For this purpose, effects of the inessential state variables u on the third and higher order terms of the potential function must be investigated using reasonable strategies. Koiter especially developed a powerful procedure selecting some essential eigenmodes of instabilities in kinematically possible displacement field[1,88]*. Also, Thompson and Hunt proposed an alternative method, which can provide a potential function an explicit expression including the **active** state variables and the control parameters through elimination of the **passive** state variables[56, 59,60,62].

Now, (n-m) equilibrium equations for the inessential state variables

$$D_{\alpha} = 0 \qquad (\alpha = m+1,\ldots,n) \qquad (1.3.16)$$

leads to (n-m) real single-value solutions

$$u_{\alpha} = u_{\alpha}(u_{i}, \lambda) \qquad (i=1,\ldots,m; \quad \alpha = m+1,\ldots,n) \qquad (1.3.17)$$

which give functions of the essential variables and the loading parameter. These solutions require great complicated calculations since they are (n-m) nonlinear simultaneous equations with (n-m) unknown variables u_{α}. Such difficulties can be dissolved by expanding algebraically the considered potential function.

Upon substitution of Eq. (1.3.17) into Eq. (1.3.9), a new potential function A is defined by

* In a mathematical sense, this process is called the **Liapunov-Schmidt Reduction**[37, in chapter I-2].

$$A(u_i, \lambda) = D[u_i, u_\alpha(u_j, \lambda), \lambda] \qquad (i,j=1,\ldots,m;\ \alpha=m+1,\ldots,n) \qquad (1.3.18)$$

Then, two potential functions of D and A give the identical important informations about both equilibrium and stability of the system considered. An equivalence between these two potential functions can be discussed fully in the chapter 1 of PART II. The instability phenomena at the critical origin $(u_i,\lambda)=(0,0)$ $(i=1,\ldots,n)$ being m-fold compound critical point of the potential functions of D can be realized as those at the origin $(u_i,\lambda)=(0,0)$ $(i=1,\ldots,m)$ of new potential function A. Thus, each potential derivative of A at any point on the equilibrium states is associated with that of D through formal algebraic computations by Thompson et al. and Niwa et al.[25,54,78,79].

$$A^F_i = D^F_i = 0\ , \qquad A^C_i = D^C_i = 0\ ,$$

$$A^{oF}_i = D^{oF}_i\ , \qquad A^{oC}_i = D^{oC}_i\ ,$$

$$A^F_{ij} = D^F_{ij}\ , \qquad A^C_{ij} = D^C_{ij}\ , \qquad A^C_{ii} = D^C_{ii} = 0\ ,$$

$$A^{oF}_{ij} = D^{oF}_{ij}\ , \qquad A^{oC}_{ij} = D^{oC}_{ij}\ ,$$

$$A^F_{ijk} = D^F_{ijk}\ , \qquad A^C_{ijk} = D^C_{ijk}\ ,$$

$$A^F_{ijk\ell} = D^F_{ijk\ell} - 3\sum_{\alpha=m+1}^{n} \frac{D^F_{\alpha ij} D^F_{\alpha k\ell}}{D^F_{\alpha\alpha}}$$

$$A^C_{ijk\ell} = D^C_{ijk\ell} - 3\sum_{\alpha=m+1}^{n} D^C_{\alpha ij} D^C_{\alpha k\ell} / D^C_{\alpha\alpha} \qquad (1.3.19)$$

where the subscripts refer to the partial derivative with respect to the essential state variables u_i $(i=1,\ldots,m)$ and the superscript "o" refers to the partial derivative with respect to the loading parameter λ. In which, such derivatives of the potential function A are evaluated at any points on the equilibrium states, including the fundamental and the critical points on equilibrium paths.

Using these values, the potential function A can be explicitly expanded in the Taylor form about the critical origin, i.e., m-fold compound critical point. For fixed value of λ near zero, the potential function in a neighborhood of the origin C

$$A(u_i, \lambda) = A^C_i(\lambda)u_i + \frac{1}{2}A^C_{ij}(\lambda)u_iu_j + \frac{1}{6}A^C_{ijk}(\lambda)u_iu_ju_k + \frac{1}{24}A^C_{ijk\ell}(\lambda)u_iu_ju_ku_\ell \qquad (1.3.20)$$

can be obtained as a linear function of λ. Since the system stays in the fundamental equilibrium state, the first terms in the right hand side disappear in order to solve a set of u_i for prescribed λ. These solutions yield both the fundamental and the postbuckling paths in the equilibrium space.

Of course, the m-fold critical point is given by the origin $(u_i, \lambda)=(0,0)$. Furthermore, the second terms vanish at such a point

$$A^c_i(0) = 0 \quad \text{and} \quad A^c_{ij}(0) = 0 \qquad (i,j=1,\ldots,m) \qquad (1.3.21)$$

Therefore, discussions on the stability problems of the system depend on investigating the features of the cubic and higher terms at the point.

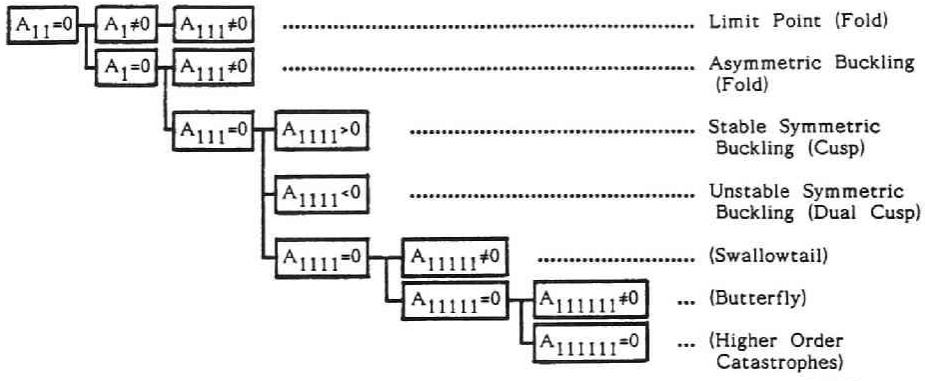

Fig. 1.3.1 Classification of Distinct Critical Points. [25]

1.3.2 Distinct critical point

Thompson and Hunt accomplished a refined classification of a discrete critical point for m=1 by means of a reasonable perturbation procedure in their general theory of elastic stability[19-25], and they associated it with the concepts of the catastrophe theory[54-64]. This classification is shown in **Fig. 1.3.1.** The typical equilibrium paths are drawn in **Figs. 1.4.1, 1.4.2, 1.4.3** and **1.4.4** for limit point, asymmetric point of bifurcation, stable symmetric point of bifurcation and unstable symmetric point of bifurcation, respectively. In these figures, solid lines denote stable equilibrium paths, whereas dashed lines denote unstable ones. Moreover, Q(or q) and ε provide an essential state variable after eliminating the remainder inessential state variables and the corresponding initial imperfection.

A distinct critical point can be generally classified into two types: limit point and bifurcation point as previously denoted, (a)limit point and (b)bifurcation point, and is rewritten in the following.

[L] Limit point or snap through point

The system loses the stability at this point, which is unstable itself. The first approximation in the potential function of the perfect system is expressed in a neighborhood of the critical origin $(u_1, \lambda)=(0,0)$

$$A(u_1,\lambda) = \frac{1}{6} A_{111}u^3_1 + A^o_1 u_1 \lambda \qquad (1.3.22)$$

which can be obtained from representing the linear term of λ in Eq. (1.3.20) by the use of Eq. (1.3.19). Therefore, each coefficient of the above form is not a function of λ, but constant, evaluated at $(u_1,\lambda)=(0,0)$. Then, an equilibrium equation is defined by

$$\frac{\partial A}{\partial u_1} = \frac{1}{2} A_{111} u_1^2 + A_1^o \lambda = 0 \tag{1.3.23}$$

which leads to a parabolic equilibrium path near the origin

$$\lambda = - \frac{A_{111}}{2 A_1^o} u_1^2 \tag{1.3.24}$$

It is shown in **Fig. 1.4.1** at $Q=Q^c+u_1$ and $\Lambda = \Lambda^c + \lambda$. This instability may be realized in structural systems such as a shallow arch loaded laterally and a complete or oblate spherical shell under external pressure. Furthermore, it may be possible to associate this point with the common behavior of imperfect structures at the maximum-load point in elastic and elasto-plastic ranges.

[B] Bifurcation points

The system exchanges the stability at this point, which may be uncertain itself. The stability of the point itself can be determined from only characteristics of the point itself. Moreover, these points are classified into the following three types: asymmetric point of bifurcation, stable symmetric point of bifurcation and unstable symmetric point of bifurcation in terms of each geometrical feature of the point itself.

[A] Asymmetric point of bifurcation

The first approximation in the potential function of the perfect system is expressed near the critical origin $(u_1,\lambda)=(0,0)$

$$A(u_1, \lambda) = \frac{1}{6} A_{111} u_1^3 + \frac{1}{2} A_{11}^o u_1^2 \lambda \tag{1.3.25}$$

where each coefficient is a constant value evaluated at the origin, similarly to the above case. Then, an equilibrium equation is defined by

$$\frac{\partial A}{\partial u_1} = \frac{1}{2} A_{111} u_1^2 + A_{11}^o u_1 \lambda = 0 \tag{1.3.26}$$

It yields two solutions

$$u_1 = 0 \quad \text{or} \quad \lambda = - \frac{A_{111}}{2A_{11}^o} u_1 \tag{1.3.27}$$

which denotes the trivial fundamental equilibrium path or the linear postbuckling one, respectively, as shown in **Fig. 1.4.2** at $q=u_1$ and $\Lambda = \Lambda^c + \lambda$.

This bifurcation may be realized in buckling problems of structural systems such as a rigid frame, a spherical shell under external pressure and eccentrically stiffened plates in global modes under in-plane compression.

[S] Stable symmetric point of bifurcation

[U] Unstable symmetric point of bifurcation

The first approximation in the potential function of the perfect system is expressed near the origin $(u_1, \lambda)=(0,0)$

$$A(u_1, \lambda) = \frac{1}{24} A_{1111} u_1^4 + \frac{1}{2} A^o_{11} u_1^2 \lambda \qquad (1.3.28)$$

where each coefficient is constant. Then, an equilibrium equation is

$$\frac{\partial A}{\partial u_1} = \frac{1}{6} A_{1111} u_1^3 + A^o_{11} u_1 \lambda = 0 \qquad (1.3.29)$$

It leads to two solutions

$$u_1 = 0 \quad \text{or} \quad \lambda = -\frac{A_{1111}}{6A^o_{11}} u_1^2 \qquad (1.3.30)$$

which denotes the fundamental equilibrium path or the parabolic postbuckling one, respectively. Since commonly $A^o_{11}<0$, **Figs. 1.4.3** and **1.4.4** draw such equilibrium paths for [S] when $A_{1111}>0$ and for [U] when $A_{1111}<0$ at $q=u_1$ and $\Lambda = \Lambda^c + \lambda$.

These bifurcations may be realized in buckling problems of structural systems such as the well-known Euler column, compressed unstiffened plates and compressed symmetrically stiffened plates in global modes for the former bifurcation. The latter bifurcation point may appear in structural systems such as a laterally loaded shallow or deep arch, a column on elastic foundations, a rigid frame, a cylindrical or elliptic shell under pressure and/or axial load.

Thompson and Hunt gave fine relationships between the structural potential function with either of these four distinct critical points and the catastrophe unfolding for four cuspoids. Both the first[L] and the second [A] correspond to the **fold** catastrophes. The third[S] and the fourth[U] correspond to the **cusp** and the **dual cusp** catastrophes, respectively [54-64]. The remainder cuspoids of **swallowtail** and **butterfly**, involving the higher order terms of the essential state variables in the catastrophe theory, have been studied by Hui and Hansen in terms of Koiter's theory[89].

1.3.3 Two-fold compound critical points

When m=2, it is well known that the two-fold compound instabilities appear at their simultaneous critical points. Supple investigated the coupled branchings for two-degree-of-freedom structural systems, and clarified the interactive buckling phenomena within a framework of tracking the postbuckling equilibrium paths[16,46,47]. Also, Johns and Chilver presented the stability and the imperfection sensitivity of structures at coincident and/or near-coincident critical

points[48-50]. They investigated on the simultaneous buckling problems in terms of the elastic stability theory. On the other hand, using both the concepts of the general elastic stability theory and the catastrophe theory, Thompson, Hunt, Roorda and their colleagues have clarified the two-fold compound bifurcations of the "semi-symmetric" potential function, which is symmetric with respect to certain one state mode and unsymmetric with respect to another mode[38-45,54,72-77,90-93,99,100]. Recently, Gaspar proposed the concept of a "critical imperfection territory" instead of the imperfection sensitivity surface[94-96,101]. Huseyin and Mandadi made an independent investigation on similar classifications of the same form of potential functions through the catastrophe theory and their multi-parameter stability theory[32,75-77]. Also, Hansen and Hui have applied the catastrophe theory to the single- and two-mode buckling problems in the Koiter's elastic stability theory[72-74,89].

From many researchers' attempts, the two-fold compound bifurcations have some umbilic characteristics of the semi-symmetric potential functions. The first approximation in the potential function of the perfect system is expressed in a neighborhood of the critical compound origin $(u_1,u_2, \lambda)=(0,0,0)$

$$A(u_1,u_2, \lambda) = \frac{1}{6} A_{111}u_1^3 + \frac{1}{2} A_{122}u_1u_2^2 + \frac{1}{2} (A^o_{11}u_1^2 + A^o_{22}u_2^2) \lambda \tag{1.3.31}$$

where each coefficient is also constant. Then, simultaneous equilibrium equations are

$$\frac{\partial A}{\partial u_1} = \frac{1}{2} A_{111}u_1^2 + \frac{1}{2} A_{122}u_2^2 + A^o_{11}u_1 \lambda = 0 \tag{1.3.32a}$$

$$\frac{\partial A}{\partial u_2} = A_{122}u_1u_2 + A^o_{22}u_2 \lambda = 0 \tag{1.3.32b}$$

The second equation yields

$$u_2 = 0 \quad \text{or} \quad A_{122}u_1 + A^o_{22} \lambda = 0 \tag{1.3.33}$$

If $u_2 = 0$, the first equation leads to

$$u_1 = 0 \quad \text{or} \quad \frac{1}{2}A_{111} u_1 + A^o_{11} \lambda = 0 \tag{1.3.34}$$

Eliminating λ from Eq. (1.3.32a) and the second equation of Eq. (1.3.33), projected solutions into the (u_1,u_2) plane are determined as:

$$u_2^2 = a\, u_1^2 \tag{1.3.35}$$

where

$$a = \frac{2A^o_{11}}{A^o_{22}} - \frac{A_{111}}{A_{122}}$$

Therefore, the following three types of equilibrium paths can be obtained, and they are

(i) trivial fundamental equilibrium path

$$u_1 = u_2 = 0 \qquad \text{for all } \lambda \tag{1.3.36}$$

(ii) uncoupled postbuckling equilibrium path

$$u_2 = 0 \quad \text{and} \quad \frac{1}{2} A_{111} u_1 + A^{o}_{11} \lambda = 0 \tag{1.3.37}$$

(iii) coupled postbuckling equilibrium paths

$$A_{122} u_1 + A^{o}_{22} \lambda = 0 \quad \text{and} \quad u_2^2 = a\, u_1^2 \tag{1.3.38}$$

if a<0, then the third coupled paths never exist. Thus, the canonical aspects of the equilibrium paths are shown in **Figs. 1.4.5, 1.4.6** and **1.4.7** at $\Lambda = \Lambda^c + \lambda$.

[M] Monoclinal point of bifurcation

As shown in **Fig. 1.4.5,** there exist two paths of (i) and (ii) in a neighborhood of the critical point when a<0. This may be realized in structural systems such as a column on elastic foundations and compressed stiffened plates with coincidence of local and global modes. If a>0, then the signs of A_{111} and A_{122} estimate the possibility of the following two bifurcation points.

[H] Homeoclinal point of bifurcation

If $A_{111} \cdot A_{122} > 0$, then there exist three paths of (i), (ii) and (iii) in **Fig. 1.4.6.** The uncoupled path and the projection of the coupled paths onto the (u_1, λ)-plane have equal sign of slopes on the (u_1, λ)-plane. This may be realized in simultaneous buckling problems such as infinitely wide stiffened plates under compression and complete spherical shells under external pressure.

[An] Anticlinal point of bifurcation

If $A_{111} \cdot A_{122} < 0$, then there exist also three paths of (i), (ii) and (iii) in **Fig. 1.4.7.** However, the uncoupled path and the projection of the coupled paths onto the (u_1, λ)-plane have opposite sign of slopes (u_1, λ)-plane. This may be realized in the similar simultaneous bifurcation problems.

Both the former [M] and [H] correspond to the **hyperbolic umbilic** catastrophe, while, in the latter case [An], the **elliptic umbilic** catastrophe appears.*

Such a sub-classification of umbilics was proposed by Thompson et al. using several partial derivatives of the Taylor expansion of potential function considered. Huseyin et al. led to the similar results using nonlinear perturbation process. The subclassification is listed in **Table 1.3.1**[42,43,54,72-77].

Table 1.3.1 Sub-classification of Semi-Symmetric Bifurcation Points. [42,54]

	A_{111} & A_{122}	
	same sign	opposite sign
a < 0	monoclinal	void
a > 0	homeoclinal	anticlinal

* If a>0, $A_{111}=0$ and $A_{122}\neq 0$, then there exist three paths of (i), (ii) $u_2=0$, $\Lambda = \Lambda^c$, and (iii) with the paraclinal point of bifurcation for the **parabolic umbilic** catastrophe neglecting its fourth-order term.

1.4 Imperfection Sensitivity

Consider a system with only a single loading parameter and several initial displacement ones, regarded as control parameters. Such an "imperfect" system is associated with the corresponding "perfect" system with only loading parameter and no other initial displacements. The control parameters are designated as a vector $(\Lambda_0, \Lambda_1, \ldots, \Lambda_{K-1})$, whose component $\Lambda_0 = \Lambda$ denotes the loading parameter and the remainders Λ_i (i=1,...,K-1) denote the initial displacement ones as mentioned above.

In this dissertation, an imperfect system will be considered to be a perturbation of the corresponding perfect system. For this purpose, incremental control parameters can be defined by

$$\Lambda_i = \Lambda_i^c + \lambda_i \qquad (i=0,1,\ldots,K-1) \qquad (1.4.1)$$

where

$$\Lambda_0^c = \Lambda^c, \qquad \Lambda_i^c = 0 \qquad (i=1,\ldots,K-1)$$

when λ_i denote initial displacements, and $\lambda_0 = \lambda$ indicates an incremental loading parameter from the critical value Λ^c.

The imperfect system is defined such that it leads to the perfect system when there exist no initial displacements. Therefore, upon the procedures similar to Eq. (1.3.9) for the perfect system and from Eqs. (1.2.1), (1.3.2), (1.3.3), (1.3.7) and (1.4.1), the reduced potential function of the imperfect system is assumed to take the following form

$$D(u_i, \lambda_j) = V(Q_i^c + q_i, \Lambda_j^c + \lambda_j) - V(Q_i^c, \Lambda_j^c + \lambda_j) \qquad (1.4.2)$$

in a neighborhood of the critical origin $(u_i, \lambda_j)=(0,0)$. In which,

$$q_i = \Phi_{ij}(\lambda_0)\, u_j \qquad (i=1,\ldots,N;\ j=1,\ldots,n;\ n<<N) \qquad (1.4.3)$$

for the imperfect system. In this paper, u_j are assumed to be determined from the eigenvector matrix $\Phi_{ij}(\lambda_0)$ independently of initial displacement parameters λ_j (j=1,...K-1) except for the loading parameter λ_0. This is the reason why discussions on the instability behavior is completed if imperfect systems are taken into account for only the essential eigenmodes of the corresponding perfect systems. It is obviously found that a perfect system is regarded as one when all the control parameters λ_j equal to be zero from Eqs. (1.3.9) and (1.4.2).

Moreover, another linear transform similar to Eq. (1.4.3) is adopted for initial displacement parameters λ_i (i=1,...,K-1), that is,

$$\lambda_i = \Psi_{ij}(\lambda_0)\, \varepsilon_j \qquad (i=1,\ldots K-1;\ j=1,\ldots,k-1;\ k<<K) \qquad (1.4.4)$$

where the transformation matrix $\Psi_{ij}(\lambda_0)$ is chosen so that the partial derivatives evaluated at the critical origin $(u_i, \lambda_0, \lambda_j)=(0,0,0)$

$$D_i^j = \frac{\partial^2 D}{\partial u_i \partial \varepsilon_j} \qquad (i=1,\ldots,n;\ j=1,\ldots,k-1) \qquad (1.4.5)$$

constructs a diagonalized matrix after reordering. If the form of initial displacements is the same as that of the relevant buckling modes, then $\Psi_{ij}(\lambda_o)$ in Eq. (1.4.4) can be taken to be $\Phi_{ij}(\lambda_o)$ in Eq. (1.4.3). Detail descriptions on this will be provided in the chapter I of PART II.

Under Eqs. (1.3.15), (1.3.16) and (1.3.17), the previous procedure for elimination of the inessential state variables can be expanded in the case of imperfect systems,

$$D^c_i = 0, \quad (i=1,\ldots,n) \qquad D^c_{ii} = 0 \quad (i=1,\ldots,m) \quad \text{and} \qquad D^c_{\alpha\alpha} \neq 0 \quad (\alpha = m+1,\ldots,n) \tag{1.4.6}$$

where the superscript "c" refers to the evaluation of each partial derivative at the critical origin $(u_i,\lambda_o,\varepsilon_j)=(0,0,0)$. Then, (n-m) real single-value solutions are assumed to be

$$u_\alpha = u_\alpha(u_i, \lambda_o, \varepsilon_j) \quad (i=1,\ldots,m;\ \alpha=m+1,\ldots,n;\ j=1,\ldots,k-1) \tag{1.4.7}$$

which yield a resultant potential function

$$A(u_i, \lambda_o, \varepsilon_j) = D[u_j, u_\alpha(u_j, \lambda_o, \varepsilon_k), \lambda_o, \varepsilon_\ell\ ] \tag{1.4.8}$$

It is apparently shown that this potential function must be defined so that Eq. (1.4.8) when $\lambda_o=\lambda$, $\varepsilon_j=0$ is equivalent to Eq. (1.3.18) in a neighborhood of the critical origin $(u_i, \lambda_o, \varepsilon_j)=(0,0,0)$. An explicit form of the potential function of the imperfect system can be determined from evaluation of its Taylor expansion near the critical origin $(u_i, \lambda_o, \varepsilon_j)=(0,0,0)$. That is, for prescribed control parameters $(\lambda_o, \varepsilon_j)$ near (0,0), the Taylor expansion of the imperfect system can be estimated similarly to Eq. (1.3.20) for the perfect system. Also, the form and the number k of the essential control parameters can be topologically proved from the concepts of the **universal unfolding** in the singularity theory of mappings [62,69,81,83].

Using such an explicit expression of the potential function $A(u_i, \lambda_o, \varepsilon_j)$ in Eq. (1.4.8), a projection of a set of singular points on equilibrium surface into the control-parameter space leads to the "bifurcation sets", i.e., the imperfection sensitivity curves or surfaces in the stability problems of structural mechanics.

The imperfection sensitivity curves or surfaces mean that universal explicit expression of relation between the essential initial displacement parameters ε_j (j=1,...,k-1) and the loading parameter λ provides the load-carrying capacity of the system. For examples, the "one-half power law" for asymmetric buckling and the "two-thirds power law" for unstable symmetric buckling are those of the well-known imperfection sensitivity of structures, which have been already investigated theoretically and experimentally [1,3,4,11,13, 18,25,32,97].

Figs. 1.4.1, **1.4.2**, **1.4.3** and **1.4.4** show the imperfection sensitivity curves for the typical four distinct instabilities when m=1 and k=1. **Figs. 1.4.5**, **1.4.6** and **1.4.7** show the imperfection sensitivity surfaces for two-fold compound instabilities when m=2 and k=2. The correlation between Thom's and Thompson' theories is summarized in **Table 1.3.2**[54,55](Also, see **Table 2.5.1** in this PART).

The significant relationships and meanings between the bifurcation set in the catastrophe theory and the imperfection sensitivity surface in the structural in-

Table 1.3.2 Relationships between Catastrophes and Instabilities. [54,55]

CATASTROPHES (THOM)		INSTABILITIES (THOMPSON & HUNT)	
fold	$V=x^3+ux$	$\frac{1}{6}D_{111}u_1^3 + D_1^o\lambda u_1$	limit point
cusp	$V=\pm x^4+ux^2+vx$	$\frac{1}{24}A_{1111}u_1^4 + \frac{1}{2}A_{11}^o\lambda u_1^2 + A_1^1\epsilon_1 u_1$	stable sym. bifurcation unstable sym. bifurcation
swallow tail	$V=x^5+ux^3+vx^2+wx$	m = 1, k = 3	rare
butterfly	$V=\pm x^6+ux^4+vx^3+wx^2+tx$	m = 1, k = 4	rare
hyperbolic umbilic	$V=x^3+y^3+wxy-ux-vy$	$\frac{1}{6}A_{111}u_1^3 + \frac{1}{2}A_{122}u_1u_2^2$ $+\frac{1}{2}\lambda(A_{11}^o u_1^2 + A_{22}^o u_2^2)$ $+ A_1^1\epsilon_1 u_1 + A_2^2\epsilon_2 u_2$	moniclinal bifurcation homeoclinal bifurcation
elliptic umbilic	$V=x^3-3xy^2+w(x^2+y^2)-ux-vy$		anticlinal bifurcation
parabolic umbilic	$V=x^2y\pm y^4+wx^2+ty^2-ux-vy$	m = 2, k = 4	rare

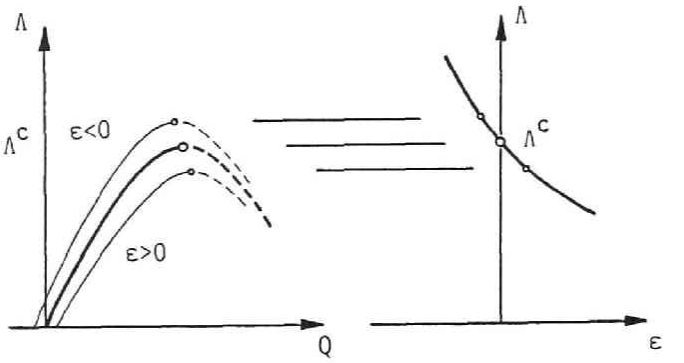

Fig. 1.4.1 **Limit Point Instability with Fold Catastrophe.** [25, 64]
(a) Equilibrium Paths (b) Imperfection Sensitivity Curve

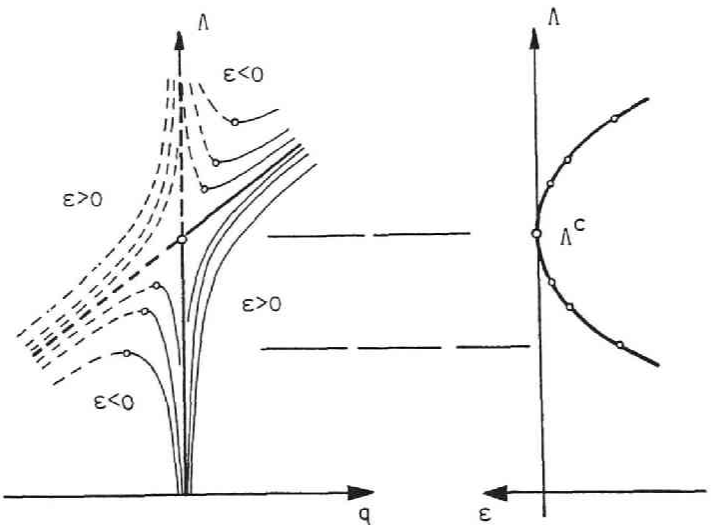

Fig. 1.4.2 **Asymmetric Point of Bifurcation with Fold Catastrophe.** [25, 64]
(a) Equilibrium Paths (b) Imperfection Sensitivity Curve

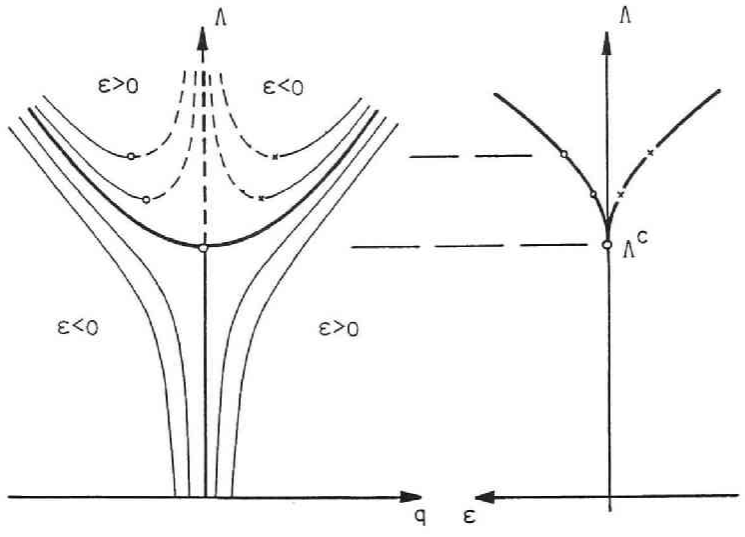

Fig. 1.4.3 **Stable Symmetric Point of Bifurcation with Cusp Catastrophe.** [25,64]
(a) Equilibrium Paths (b) Imperfection Sensitivity Curve

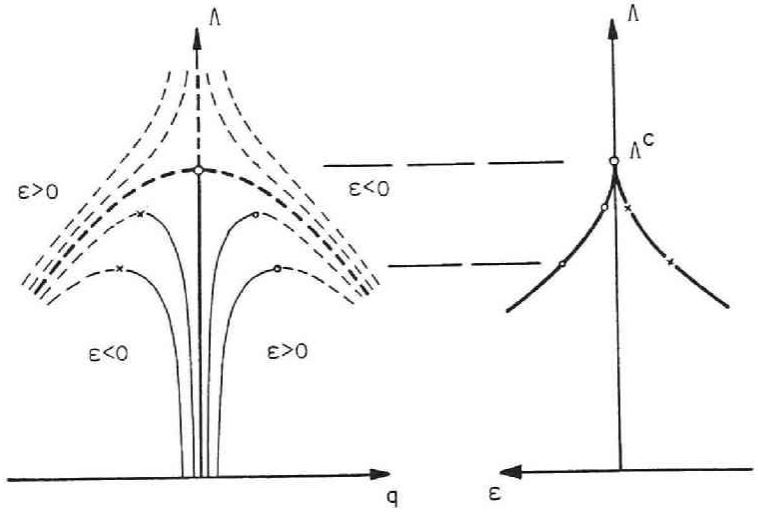

Fig. 1.4.4 **Unstable Symmetric Point of Bifurcation with Dual Cusp Catastrophe.**
(a) Equilibrium Paths (b) Imperfection Sensitivity Curve [25,64]

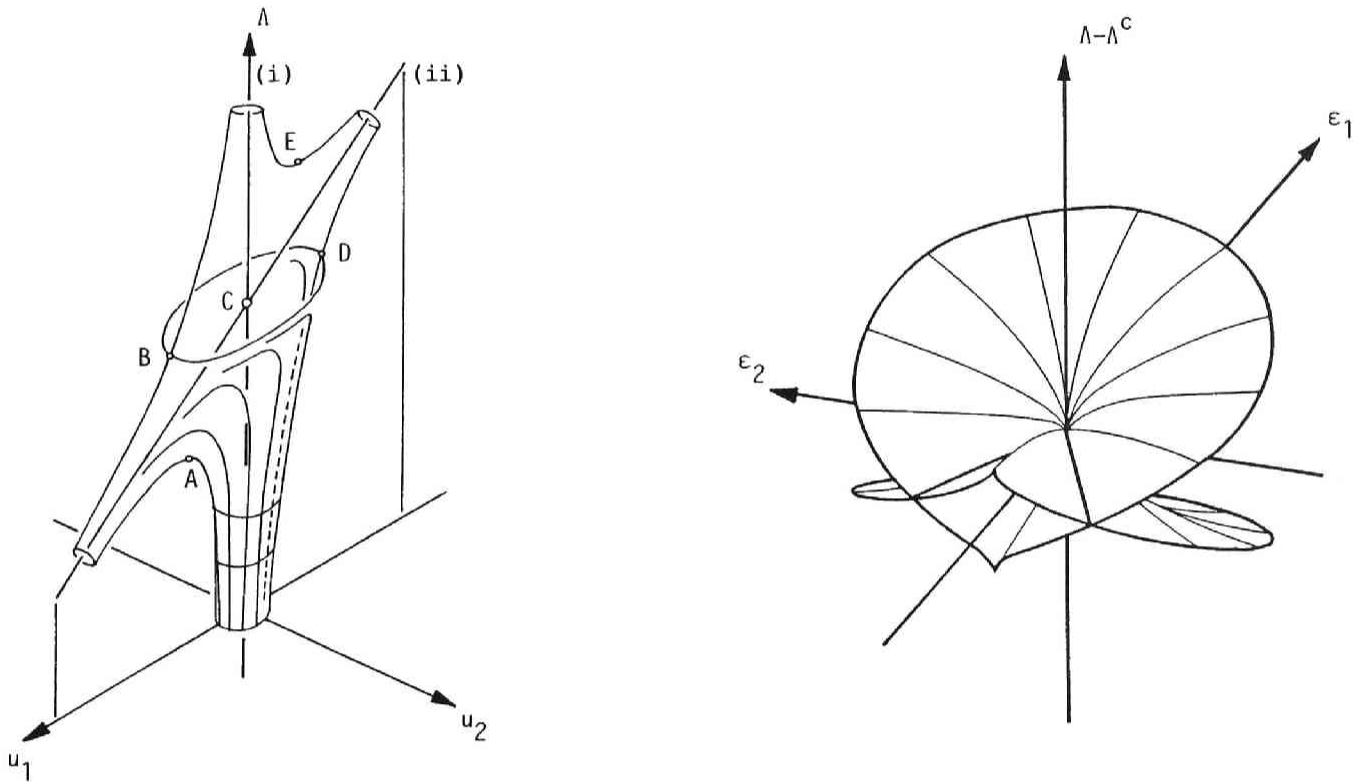

Fig. 1.4.5 Monoclinal Point of Bifurcation with Hyperbolic Umbilic Catastrophe. [25,64]
(a) Equilibrium Paths (b) Imperfection Sensitivity Surfaces

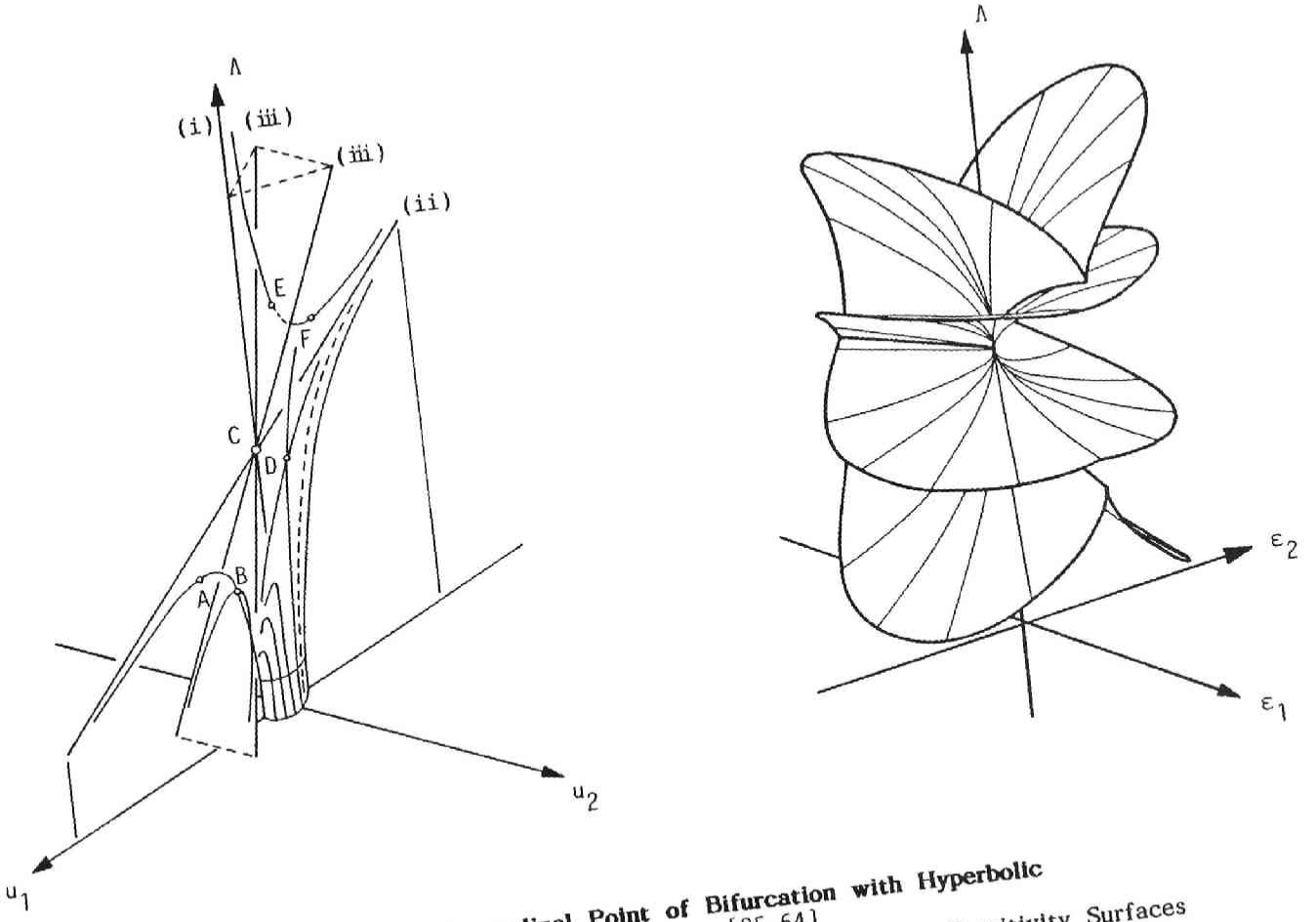

Fig. 1.4.6 **Homeoclinal Point of Bifurcation with Hyperbolic Umbilic Catastrophe.** [25,64]
(a) Equilibrium Paths (b) Imperfection Sensitivity Surfaces

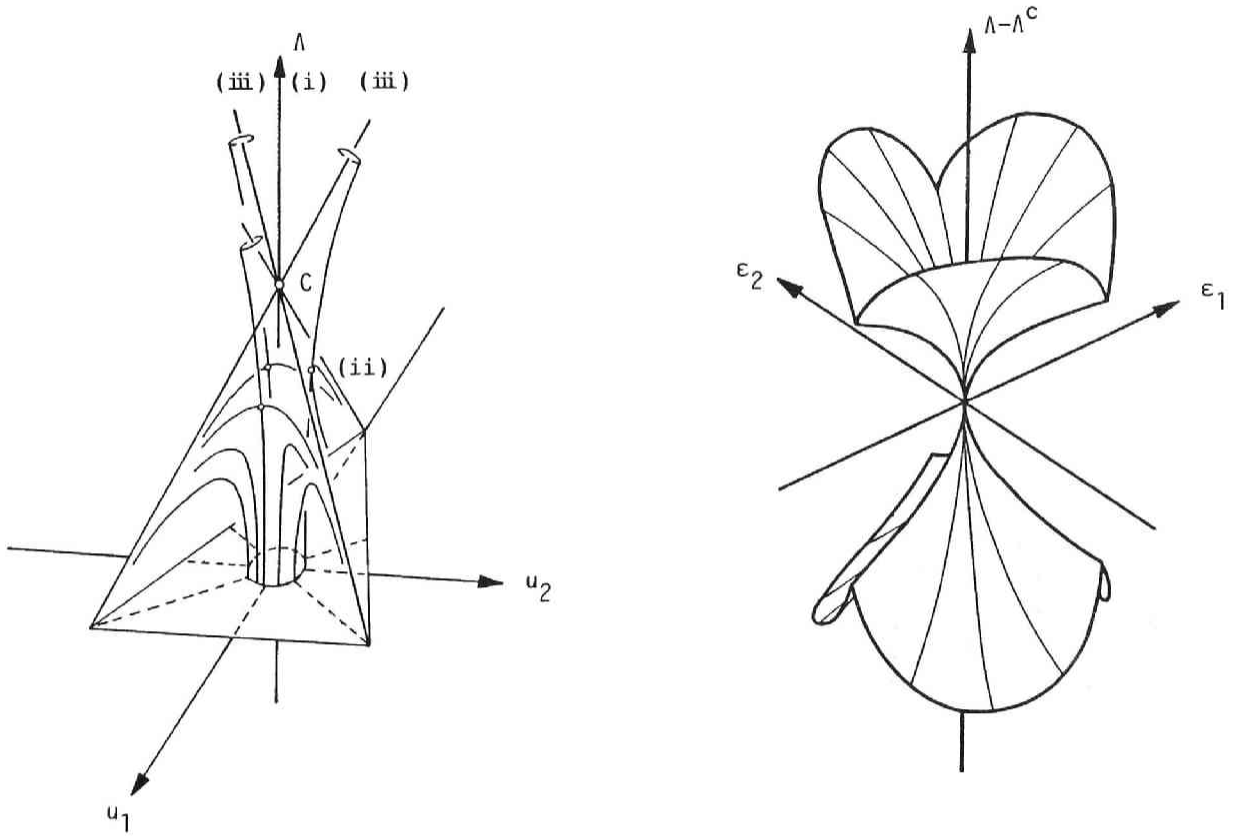

Fig. 1.4.7 Anticlinal Point of Bifurcation with Elliptic Umbilic Catastrophe. [25, 64]
(a) Equilibrium Paths (b) Imperfection Sensitivity Surfaces

stability problems will be mentioned in the chapter 1 of PART II. Furthermore, the canonical procedure to evaluate it qualitatively and quantitatively is proposed in the chapter 2 of the PART II using the singularity theory.

1.5 Conclusions

This chapter reviews on the general theory of elastic stability in a topological sense using the catastrophe theory, and classifies the static instability phenomena on the basis of the canonical form of the potential function in order to predict the imperfection sensitivity of structures. The main conclusions are:

(1) A potential function of structural system can be defined by a function of the generalized internal state variables and several external control parameters.

(2) The generalized state variables correspond to the active and essential instability modes, while the control parameters correspond to a single loading parameter and the associated initial modes.

(3) An explicit form of the potential function of the imperfect system can be evaluated by only significant informations on partial derivatives at the critical point of the potential function of the associated perfect systems.

(4) An effect of the initial displacements on the load-carrying capacity of the system is obtained from the bifurcation set in the catastrophe theory, and its evaluation procedure will be explained in the chapter 2 of the next PART.

Bibliographies of Chapter 1 in PART I

1) Koiter,W.T., Over de Stabiliteit van het Elastische Evenwicht. Thesis, Delft, 1945 (English translations: On the Stability of Elastic Equilibrium. NASA Technical Transactions, F10, 833, National Aeronautics and Space Administration, 1967 and Technical Report AFFDL-TR-70-25, Air Force Flight Dynamics Laboratory, 1970).
2) Koiter,W.T., Elastic stability and post-buckling behavior. Nonlinear Problems (ed. R.H. Langer), Publication No. 8 of the Mathematical Research Center, United States Army, University of Wisconsin Press, pp. 257-275, 1963.
3) Hutchinson,J.W. and W.T.Koiter, Post-buckling theory. Applied Mechanics Reviews, Vol. 23, pp. 1353-1366, 1970.
4) Budiansky,B., Theory of buckling and post-buckling behavior of elastic structures. Advances in Applied Mechanics (ed. C.-S.Yih), Vol. 14, Academic Press, pp. 1-65, 1974.
5) Koiter,W.T., Current trends in the theory of buckling. Buckling of Structures (ed. B.Budiansky), IUTAM, International Union of Theoretical and Applied Mechanics, Springer-Verlag, pp. 1-16, 1976.
6) Koiter,W.T., Elastic stability, buckling and post-buckling behaviour. Proceedings of the IUTAM Symposium on Finite Elasticity (eds. D.E.Carlson and R.T.Shield), Martinus Nijhoff Publishers, pp. 13-24, 1981.
7) Hutchinson,J.W., On the postbuckling behavior of imperfection-sensitive structures in the plastic range. Journal of Applied Mechanics, Transactions of American Society of Mechanical Engineers, Vol. 39, pp. 155-162, 1972.

8) Hutchinson,J.W., Post-bifurcation behavior in the plastic range. Journal of the Mechanics and Physics of Solids, Vol. 21, pp. 163-190, 1973.
9) Hutchinson,J.W., Imperfection-sensitivity in the plastic range. Journal of the Mechanics and Physics of Solids, Vol. 21, pp. 191-204, 1973.
10) Hutchinson,J.W., Plastic buckling. Advances in Applied Mechanics (ed. C.-S.Yih), Vol. 14, Academic Press, pp. 67-144, 1974.
11) Roorda,J., Stability of structures with small imperfections. Journal of the Engineering Mechanics Division, Proc. ASCE, Vol. 91, No. EM4, pp. 87-106, 1965.
12) Roorda,J., The buckling behaviour of imperfect structural systems. Journal of the Mechanics and Physics of Solids, Vol. 13, pp. 267-280, 1965.
13) Roorda,J., On the buckling of symmetric structural systems with first and second order imperfections. International Journal of Solids and Structures, Vol. 4, pp. 1137-1148, 1968.
14) Roorda,J., Buckling of Elastic Structures. Special Publications Series, Solid Mechanics Division, University of Waterloo Press, 1980.
15) Supple,W.J., On the change in buckling pattern in elastic structures. International Journal of Mechanical Sciences, Vol. 10, pp. 737-745, 1968.
16) Supple,W.J., Structural Instability. IPC Science and Technology Press, 1973.
17) Croll,J.G.A., Continuum perturbation method in the buckling analysis of conservative systems. International Journal of Mechanical Sciences, Vol. 13, pp. 605-613, 1971.
18) Croll,J.G.A. and A.C.Walker, Elements of Structural Stability. Macmillian Press, 1972.
19) Thompson,J.M.T., Discrete branching points in the general theory of elastic stability. Journal of the Mechanics and Physics of Solids, Vol. 13, pp. 295-310, 1965.
20) Thompson,J.M.T., A general theory for the equilibrium and stability of discrete conservative systems. Journal of Applied Mathematics and Physics (Zeitschrift für Angewandte Mathematik und Physik), Vol. 20, pp. 797-846, 1969.
21) Thompson,J.M.T. and A.C.Walker, A general theory for the branching analysis of discrete structural systems. International Journal of Solids and Structures, Vol. 5, pp. 281-288, 1969.
22) Thompson,J.M.T., The branching analysis of perfect and imperfect discrete structural systems. Journal of the Mechanics and Physics of Solids, Vol. 17, pp. 1-10, 1969.
23) Thompson,J.M.T., A new approach to elastic branching analysis. Journal of the Mechanics and Physics of Solids, Vol. 18, pp. 29-42, 1970.
24) Thompson,J.M.T., Basic theorems of elastic stability. International Journal Engineering Sciences, Vol. 8, pp. 307-313, 1970.
25) Thompson,J.M.T. and G.W. Hunt, A General Theory of Elastic Stability. John Wiley & Sons, 1973.
26) Huseyin,K., The convexity of the stability boundary of symmetric structural systems. Acta Meccanica, Vol. 8, pp. 205-211, 1969.
27) Huseyin,K., The stability boundary of systems with one degree of freedoms (Part I and II). Meccanica, Vol. 5, pp. 306-311 and 312-316, 1970.
28) Huseyin,K., Fundamental principles in the buckling of structures under combined loading. International Journal of Solids and Structures, Vol. 6, pp. 479-487, 1970.
29) Huseyin,K., The elastic stability of structural systems with independent loading parameters. International Journal of Solids and Structures, Vol. 6, pp. 677-691, 1970.
30) Huseyin,K., Singular critical points in the general theory of elastic stability. Meccanica, Vol. 7, pp. 58-68, 1972.

31) Huseyin,K., On the estimation of the stability boundary of symmetric structural systems. International Journal of Non-Linear Mechanics, Vol. 7, pp. 31-50, 1972.
32) Huseyin,K., Non-Linear Theory of Elastic Stability. Noordhoff, 1974.
33) Sewell,M.J., The static perturbation technique in buckling problems. Journal of the Mechanics and Physics of Solids, Vol. 13, pp. 247-265, 1965.
34) Sewell,M.J., A general theory of equilibrium paths through critical points I and II. Proceedings of the Royal Society of London, Series A, Vol. 306, pp. 201-223 and 225-238, 1968.
35) Sewell,M.J., On the connection between stability and the shape of the equilibrium surface. Journal of the Mechanics and Physics of Solids, Vol. 14, pp. 203-230, 1969.
36) Sewell,M.J., A method of post-buckling analysis. Journal of the Mechanics and Physics of Solids, Vol. 17, pp. 219-233, 1969.
37) Sewell,M.J., On the branching of equilibrium paths. Proceedings of the Royal Society of London, Series A, Vol. 315, pp. 499-518, 1970.
38) Thompson,J.M.T. and G.W.Hunt, A theory for the numerical analysis of compound branching. Journal of Applied Mathematics and Physics (Zeitschrift für Mathematik und Physik), Vol. 22, pp. 1001-1015, 1971.
39) Thompson,J.M.T. and W.J.Supple, Erosion of optimum design by compound branching phenomena. Journal of the Mechanics and Physics of Solids, Vol. 21, pp. 135-144, 1973.
40) Thompson,J.M.T., Optimization as a generator of structural instability. Letter to editor, International Journal of Mechanical Sciences, Vol. 14, pp. 627-629, 1972.
41) Hunt,G.W., Imperfection-sensitivity of semi-symmetric branching. Proceedings of the Royal Society of London, Series A, Vol. 357, pp. 193-211, 1977.
42) Hunt,G.W., Imperfection and near-coincidence for semisymmetric bifurcations. Bifurcation Theory and Applications in Scientific Disciplines, Annals of the New York Academy of Science, Vol. 316, pp. 572-589, 1979.
43) Hunt,G.W., An algorithm for the nonlinear analysis of compound bifurcation. Philosophical Transactions of the Royal Society of London, Series A, Vol. 300, pp. 443-471, 1981.
44) Roorda,J. and A.J.Reis, Nonlinear interactive buckling: sensitivity and optimality. Journal of Structural Mechanics, Vol. 5, pp. 207-232, 1977.
45) Reis,A.J. and J.Roorda, Post-buckling behaviour under mode interaction. Journal of the Engineering Mechanics Division, Proc. ASCE, Vol. 105, No. EM5, pp. 609, 621, 1979.
46) Supple,W.J., Coupled branching configurations in the elastic buckling of symmetric structural systems. International Journal of Mechanical Sciences, Vol. 9, pp.97-112, 1967.
47) Supple,W.J., Initial post-buckling behaviour of a class of elastic structural systems. International Journal of Non-Linear Mechanics, Vol. 4, pp. 23-36, 1969.
48) Johns,K.C. and A.H.Chilver, Multiple path generation at coincident branching points. International Journal of Mechanical Sciences, Vol. 13, pp. 899-910, 1971.
49) Johns,K.C., Simultaneous buckling in symmetric structural systems. Journal of the Engineering Mechanics Division, Proc. ASCE, Vol. 98, No. EM4, pp. 835-848, 1972.
50) Johns,K.C., Imperfection sensitivity of coincident buckling systems. International Journal of Non-Linear Mechanics, Vol. 9, pp. 1-21, 1974.
51) Ho,D., Higher order approximations in the calculation of elastic buckling loads of imperfect systems. International Journal of Non-Linear Mechanics, Vol. 6, pp. 649-661, 1971.

52) Ho,D., The influence of imperfections on systems with coincident buckling loads. International Journal of Non-Linear Mechanics, Vol. 7, pp. 311-321, 1972.
53) Ho,D., Buckling load of non-linear systems with multiple eigenvalue. International Journal of Solids and Structures, Vol. 10, pp. 1315-1330, 1974.
54) Thompson,J.M.T. and G.W.Hunt, Towards a unified bifurcation theory. Journal of Applied Mathematics and Physics (Zeitschrift für Angewandte Mathematik und Physik), Vol. 26, pp. 581-603, 1975.
55) Thompson.J.M.T., Designing against catastrophe. Modern Trends in Cybernetics and Systems, Proceedings of the 3rd International Congress of Cybernetics and Systems, Vol. 2, Section 2 (Systems and Models), Bucharest, Romania, August 25-29, Springer-Verlag, pp. 445-454, 1975.
56) Thompson,J.M.T. and G.W.Hunt, A bifurcation theory for the instabilities of optimization and design. Synthese, Vol. 26, pp. 315-351, 1977.
57) Thompson,J.M.T., Instabilities, bifurcations and catastrophes. Physics Letters, Vol. 51A, pp. 201-203, 1975.
58) Thompson,J.M.T. and G.W.Hunt, The instability of evolving systems. Interdisciplinary Science Reviews, Vol. 2, pp. 240-262, 1977.
59) Thompson,J.M.T., J.K.Y.Tan and K.C.Lim, On the topological classification of postbuckling phenomena. Journal of Structural Mechanics, Vol. 6, pp. 383-414, 1978.
60) Thompson,J.M.T., Bifurcational aspects of catastrophe theory. Bifurcation Theory and Applications in Scientific Disciplines, Annals of the New York Academy of Sciences, Vol. 316, pp. 553-571, 1979.
61) Thompson,J.M.T., Catastrophe theory and its rule in applied mechanics. Theoretical and Applied Mechanics (ed. W.T.Koiter), North-Holland, pp. 451-458, 1980.
62) Thompson,J.M.T., Instability and Catastrophes in Sciences and Engineering. John Wiley & Sons, 1982.
63) Thompson,J.M.T. and G.W.Hunt(eds.), Collapse: The Buckling of Structures in Theory and Practice. Proceedings of the IUTAM Symposium, International Union of Theoretical and Applied Mechanics, Cambridge University Press, 1983.
64) Thompson,J.M.T. and G.W.Hunt, Elastic Instability Phenomena. John Wiley & Sons, 1984.
65) Thom,R., Structural Stability and Morphogenesis (translated from the French by D.H. Fawler), Benjamin, 1975.
66) Thom,R., Structural stability, catastrophe theory, and applied mathematics. SIAM Reviews, Society for Industrial and Applied Mathematics, Vol. 19, pp. 189-201, 1976.
67) Zeeman,E.C., Catastrophe theory. Scientific American, Vol. 234, pp. 65-83, 1976.
68) Zeeman,E.C., Catastrophe Theory: Selected Paper 1972-1977. Addison-Wesley, 1977.
69) Gilmore,R., Catastrophe Theory for Scientists and Engineers. John Wiley & Sons, 1981.
70) Poston,T. and I.Stewart, Taylor Expansions and Catastrophes. Research Notes in Mathematics, No. 7, Pitman, 1976.
71) Poston,T. and I.Stewart, Catastrophe Theory and Its Applications. Pitman, 1978.
72) Hansen,J.S., Some two-mode buckling problems and their relation to catastrophe theory. AIAA J., Vol. 15, pp. 1638-1644, 1977.

73) Hui,D. and J.S.Hansen, Two-mode buckling of an elastically supported plate and its relation to catastrophe theory. Journal of Applied Mechanics, Transactions of American Society of Mechanical Engineers, Vol. 47, pp. 607-612, 1980.
74) Hui,D.and J.S.Hansen, The parabolic umbilic catastrophe and its application in the theory of elastic stability. Quarterly of Applied Mathematics, Vol. 39, pp. 210-220, 1981.
75) Huseyin,K. and V.Mandadi, On the imperfection sensitivity of compound branching. Ingenieur-Archiv, Vol. 46, pp. 213-222, 1977.
76) Huseyin,K. and V.Mandadi, Classification of critical conditions in the general theory of stability. Mechanical Research Communications, Vol. 4, pp. 11-15, 1977.
77) Mandadi,V. and K.Heseyin, The effects of symmetry on the imperfection-sensitivity of coincident critical points. Ingenieur-Archiv, Vol. 47, pp. 35-45, 1978.
78) Isami,H., Applications of Catastrophe Theory to Static Instability Phenomena by Discretization and Modal Transforms. Thesis submitted to the Faculty of Engineering of Kyoto University in partial fulfillment of the requirements for the degree of Master of Engineering, 1980 (in Japanese).
79) Niwa,Y., E.Watanabe and H.Isami, Catastrophe analysis of structures by discretization and modal transforms. Memoirs of the Faculty of Engineering, Kyoto University, Vol. 43, pp. 67-87, 1981.
80) Lu,Y.-C., Singularity Theory and an Introduction to Catastrophe Theory, 2nd corrected printing. Springer-Verlag, 1976.
81) Lander,L., Differential Germs and Catastrophes. London Mathematical Society Lecture Notes, No. 17, Cambridge University Press, 1975.
82) Leipholz,H., Stability of Elastic Systems. Sijthoff and Noordhoff, 1980.
83) Noguchi,H., Catastrophes. Mathematics in Engineering Sciences, No. 13, Science Library, Saiensu-Sha, 1977 (in Japanese).
84) Sewell,M.J., Elementary catastrophe. Problem Analysis in Science and Engineering (eds. F.H. Branin,Jr. and K.Huseyin), Academic Press, pp. 391-426, 1977.
85) Huseyin,K., The multi-parameter stability theory and its relation to catastrophe theory. Problem Analysis in Science and Engineering (eds. F.H. Branin,Jr. and K.Huseyin), Academic Press, pp. 229-255, 1977.
86) Britvec,S.J., The Stability of Elastic Systems. Pergamon Press, 1973.
87) Gurel,O., Poincare's bifurcation analysis. Bifurcation Theory and Applications in Scientific Disciplines, Annals of the New York Academy of Sciences, Vol. 316, pp. 5-26, 1979.
88) Haftka,R.T., R.H.Mallet and W.Nachbar, A Koiter-Type Method for Finite Element Analysis of Nonlinear Structural Behavior. Vol. 1: The Modified Structural Method. Technical Report AFFDL-TR-70-130, Air Force Flight Dynamics Laboratory, 1970.
89) Hui,D. and J.S.Hansen, The swallowtail and butterfly cuspoids and their application in the initial post-buckling of single-mode structural systems. Quarterly of Applied Mathematics, Vol. 38, pp. 17-36, 1980.
90) Thompson,J.M.T. and Z.Gaspar, A buckling model for the set of umbilic catastrophes. Mathematical Proceedings of Cambridge Philosophical Society, Vol. 82, pp. 497-507, 1977.
91) Gaspar,Z., Buckling models for higher catastrophes. Journal of Structural Mechanics, Vol. 5, pp. 357-368, 1977.
92) Hunt,G.W., N.A.Reay and T.Yoshimura, Local diffeormorphisms in the bifurcational manifestations of the umbilic catastrophes. Proceedings of the Royal Society of London, Series A, Vol. 369, pp. 47-65, 1979.

93) Hunt,G.W., Symmetries of elastic buckling. Engineering Structures, Vol. 4, pp. 21-28, 1982.
94) Gaspar,Z., Critical imperfection territory. Journal of Structural Mechanics, Vol. 11, pp. 297-325, 1983.
95) Gaspar,Z., Imperfection sensitivity and catastrophe theory. Collapse: The Buckling of Structures in Theory and Practice (eds. J.M.T.Thompson and G.W.Hunt), Proc. IUTAM Symposium, International Union of Theoretical and Applied Mechanics, Cambridge University Press, pp. 175-181, 1983.
96) Gaspar,Z., Computation of imperfection-sensitivity at two-fold branching points. Zeitschrift fur Angewandte Mathematik und Mechanik, Vol. 63, pp. 359-370, 1983.
97) Chajes,A., Post-buckling behavior. Journal of Structural Engineering, Proc. ASCE, Vol. 109, pp. 2450-2462, 1983.
98) Isami,H., A topological aspect of imperfection sensitivity of structures. Bulletin of Kohchi Technical College, No. 20, pp. 85-94, 1984.
99) Hunt,G.W. and K.A.J.Williams, Closed-form and asymmetric solution for an interactive buckling model. Journal of the Mechanics and Physics of Solids, Vol. 32, pp. 101-118, 1984.
100) Hunt,G.W. and K.A.J.Williams, On truncation of the structural potential function. Mathematical Proceedings of Cambridge Philosophical Society, Vol. 95, pp. 495-510, 1984.
101) Gasper,Z., Imperfection sensitivity at near-coincidence of two critical points. Journal of Structural Mechanics, Vol. 13, pp. 43-65, 1985.

CHAPTER 2

SINGULARITY THEORY AND CATASTROPHE THEORY

2.1 General Remarks

Many phenomena in natural process may take place suddenly and discontinuously as the relevant external control parameters change continuously: buckling and collapse of slender structures, the flutter of aircrafts, the onset of turbulence in a fast-moving fluid, the phase transition of fluids, the fracture of a crystal lattice, the evolutionary stability of stars and planetary masses, the charged water drops of thunderstorms in an electric field, the heat conduction and fluid flow in thermodynamics, and so on. Such discontinuous phenomena can not be systematically interpreted by the classical Newton's mechanics in which any continuous phenomena can be specified as solutions of unified differential equations with any smooth changes of control parameters.

Thom introduced the concept of the structural stability to understand some topological aspect of the sudden discontinuity in natural process. He also applied the concept of the transversality to a canonical form of mappings. Furthermore, he proposed such mathematical ideas of the catastrophe theory as fundamentals in biology, and published the well-known powerful paper, "Stabilite Structurelle et Morphogeneses"(1972), which was translated into English, "Structural Stability and Morphogenesis"(1975) by Fowler[1].

It may be very difficult for our engineers to understand completely the topological concepts of the catastrophe theory since the concepts are rigorously derived from the singularity theory of mappings in pure mathematics. Each instability phenomenon may be regarded as one governed by a potential function of the system considered. The equilibrium states of the system may be those for which the corresponding potential function is locally minimized. Then, they can construct an equilibrium space, i.e., a set of critical points named in pure mathematics. The potential function has almost multiple local minima, then there may exist more than one stable equilibria of the system. When the external control parameters vary continuously, the number of the local minima will change in a discontinuous way. As a result, the allowable stable state will be exchanged suddenly into other unknown states. Such discontinuous phenomena may occur at a singular point in the equilibrium space. One of several topological forms of the potential function in a neighborhood of the point locally determines the structurally stable characteristics.

The Thom's Theorem allows one to classify the structurally stable equilibria of the "gradient system" under a small number of control parameters and to describe how these equilibria change as the parameters vary. The theorem asserts that, for the number of state variables < 2 and the number of control parameters < 4, the typical form of potential function is just equivalent to either of the well-known seven elementary catastrophes: **fold**, **cusp**, **swallowtail**, **butterfly**, **hyperbolic umbilic**, **elliptic umbilic** and **parabolic umbilic**.

The useful applications of the catastrophe theory have been accomplished in the problems of several disciplines of mechanical engineering, hydrodynamics, thermodynamics, crystallography, cosmology, meteorology, economics, social sciences and biology as well as pure mathematics.

In this chapter, a historical review on the study of the catastrophe theory within a frame of the singularity theory will be briefly discussed. Furthermore, the chapter presents a simple interpretation of the Thom's Theorem in a topological manner accessible to our engineers. The local forms both of potential functions and of families of potential functions will be considered herein through the concepts of the Implicit Function Theorem, the Morse Lemma, the Splitting Lemma and the Thom's Theorem. The main mathematical background is provided on brief items in APPENDIX of PART I.

2.2 Historical Reviews

The study on the qualitative properties of nonlinear ordinary differential equations in dynamical systems was firstly by Poincaré just last century. He formulated the fundamental ideas of structural stability, dynamic stability and critical set, which form the current necessarities of mathematical bifurcation theory. For examples, his achievements were surveyed by Gurel in concise expressions[2]. Liapunov provided the mathematical definitions of stability using the generalized energy functions with his name at the end of last century[3]. Then, the precise concept of structural stability was introduced by mathematicians Andronov and Pontryagin in 1930's. Smale translated the qualitative dynamics motivated by Poincaré into the modern mathematical terminologies of the differential topology by Andronov et al., and systemized the topological theory in dynamical systems. Within a frame work of singularity of mappings, Morse developed the structures of some canonical forms of functions in a neighborhood of isolated critical point. Mather also made important contributions for the singularity of C^{∞} -mappings. Furthermore, Whitney discussed on the typical forms of mappings of singularities.

Thus, as mentioned at the previous section in this chapter, at the beginning of 1970's, Thom introduced the concept of transversality in order to explain the structural stability, and applied the transversality to the canonical expressions of singularities, i.e., catastrophes, for families of potential functions[1]. He also associated the catastrophe theory with applied mathematics in terms of structural stability[4].

The rapid growths of the catastrophe theory to applied mathematics, engineerings, economics, biology and social sciences have recently been accomplished. Many introduction papers of the catastrophe theory to those who not pure mathematicians appeared in the middle of 1970's, e.g., by Zeeman[5], Sussmann[6], Chillingworth[8], Stewart[8], Sewell[9] and Golubitsky[10].

Zeeman made the most significant contributions to the development of the catastrophe theory in pure and applied mathematics. He proposed a mechanical model to illustrate visually the catastrophes, then the model has been called the Zeeman's catastrophe machine[11,12,13]. Also, he classified some elementary catastrophes of small codimension in view of topology[14], and graphically described a higher-order catastrophe of the double cusp[15]. Moreover, he reviewed on researches of the catastrophe theory in applied mathematics and sciences[16]. No one exists who applied the catastrophe theory to the buckling problem of Euler strut[17].

While, in the middle of 1970's, the remarkable advances of the catastrophe theory were made within a topology of singularity theory by Lu[18], Lander[19], and et al. Particularly, Poston and Stewart clarified the relationships between catastrophes and the Taylor expansions being unfolding germs in terms of brief

and rigorous mathematical representations[20]. They surveyed on applied catastrophe theory[21]. Recently, Stewart discussed on its applications to physics, chemistry and fluid mechanics[22]. Hilton edited the well-known Lecture Note series on the structural stability in the catastrophe theory[23]. Also, Gurel et al. published the proceedings of the mathematical bifurcation theory and the catastrophe theory in mathematics and sciences[24].

Independently of these investigations, useful researches on mathematical bifurcations through the singularity theory have been made by Golubitsky and Schaeffer [25,26,27,49].

In Japan, the journal of Mathematical Sciences made up special editions on the catastrophe theory just after Thom's book[28,29,30]. Noguchi has rigorously investigated the applied catastrophe theory through Japanese translations of Zeeman et al.[31,32,33]. Fujii and Yamaguchi examined the numerical realization of the structure of singularities by means of their group theory[34-38].

Several applications of the catastrophe theory to the buckling of structures in mechanical engineering have been carried out since Zeeman's pioneer works of Euler column. Thompson and Hunt unified a bifurcation theory between catastrophe theory and elastic stability theory in order to evaluate the imperfection sensitivity of structures[39]. They explained the static instabilities in structural mechanics using the unified theory, and wrote many important introduction papers [40-46]. Using such theory, the imperfection sensitivity, i.e., the load-carrying capacity of structures can be expressed in the form of an explicit function of unavoidable imperfections. Recently, they summarized the applications of the catastrophe theory to engineering sciences in [47,48].

A great number of researches on such structural instabilities in the light of the catastrophe theory has been reported by Thompson, Hunt and colleagues. Further, Hansen and Hui, Huseyin and Mandadi, Sewell, Niwa, Watanabe and Isami have been discussed on the imperfection sensitivity of structures. Also, Niwa et al. have attempted to expand the catastrophe theory in order to predict the strength of steel structures in the elasto-plastic range. These contributions will be explained in the following PART III.

2.3 Family of Potential Functions

Now, consider the mathematical system governed by a potential function

$$U_{\mathbf{c}} : \mathbf{R}^N \rightarrow \mathbf{R} \quad \text{or} \quad U_{\mathbf{c}} = U_{\mathbf{c}}(\mathbf{x}),\ \mathbf{x} \in \mathbf{R}^N \tag{2.3.1}$$

when the external control parameters $\mathbf{c} \in \mathbf{R}^K$ remain fixed. In which, $\mathbf{R}^N$ represents the internal state space, described by the state variables $\mathbf{x}$. These terminologies were firstly introduced by Thom, and also Zeeman called $\mathbf{R}^N$ and $\mathbf{R}^K$ the state (or behavior) space and the control (or parameter) space, respectively. Particularly, it is reasonably natural to name $\mathbf{R}^K$ as the unfolding space in view of the topological meanings. Furthermore, $\mathbf{R}^N$ and $\mathbf{R}^K$ refer to an N- and a K-dimensional Euclidian space, respectively. In structural mechanics, the former correspond to the so-called generalized coordinates, while the latter does the control parameters such as loads and unavoidable imperfections.

As the control parameters $\mathbf{c} \in \mathbf{R}^K$ vary continuously, a change in the potential function, $U_{\mathbf{c}}$, leads to each state of the system itself. Then, for each point $\mathbf{c}$, there exists a smooth map, i.e., continuous and differential map

$$U : \mathbf{R}^N \times \mathbf{R}^K \rightarrow \mathbf{R} \quad \text{or} \quad U = U(\mathbf{x},\mathbf{c}) \tag{2.3.2}$$

The map constructs a family of potential functions on $\mathbf{R}^N$ characterized by $\mathbf{R}^K$, and it is called an **unfolding** of $U_{\mathbf{c}}$. Then, U may be regarded as a set of perturbations of $U_{\mathbf{c}}$.

$$U = \{ U_{\mathbf{c}} \mid \mathbf{c} \in \mathbf{R}^K \} \quad \text{or} \quad U(\mathbf{x},\mathbf{c}) = U_{\mathbf{c}}(\mathbf{x}), \quad \mathbf{c} \in \mathbf{R}^K \tag{2.3.3}$$

Therefore, both a potential function $U_{\mathbf{c}}(\mathbf{x})$ for fixed $\mathbf{c}$ and a family of potential functions $U(\mathbf{x},\mathbf{c})$ parameterized by $\mathbf{c}$ can be defined above. In other words, a family of potential functions, $U(\mathbf{x},\mathbf{c})$, may correspond to an unfolding of potential function $U_{\mathbf{c}}$ as mentioned below.

The system will possess more than one minimum or maximum of the potential function $U_{\mathbf{c}}$ for specified control parameters $\mathbf{c}$. Several minima will be accessible to the stable states of the system. Therefore, a question arises: which one minimum of all should be chosen according to a prescribed certain rule ? The question can be answered under either of the following two conventions.

[i] Maxwell's convention This convention specifies the state of the system to be one where the potential function $U_{\mathbf{c}}$ reaches its absolute minimum for given parameters $\mathbf{c}$.

[ii] Perfect-delay convention This convention insists that the state of the system is one determining the local minimum of the potential function $U_{\mathbf{c}}$. The chosen state follows a continuous family of minima until these minima disappear or translate to other different minima as the control parameters $\mathbf{c}$ changes continuously.

The so-called **catastrophe** takes place at the point $\mathbf{c}=\mathbf{c}_0$ where the number of minima will alter. The catastrophe means that the stable state of the system may vary suddenly and discontinuously with the continuous change of the control parameters.

2.4 Thom's Theorem

If, for prescribed $\mathbf{c} \in \mathbf{R}^K$, the gradient of a potential function, $\mathbf{grad}U_{\mathbf{c}}$, is non-zero at a point $\mathbf{x} \in \mathbf{R}^N$, then a new coordinate system near the point can be chosen so that the gradient has only one vanishing direction, denoted as the "1". The Implicit Function Theorem asserts that there exists a smooth change of coordinates such that

$$U_{\mathbf{c}} \cong y_1 \tag{2.4.1}$$

for a new coordinate $\mathbf{y}=(y_1,\ldots,y_N) \in \mathbf{R}^N$.

The stable or unstable equilibrium state of the system considered can be regarded as the one of the minimum or maximum of the potential function $U_{\mathbf{c}}(\mathbf{x})$, respectively, for fixed control parameters $\mathbf{c}$. When the Perfect-delay convention is adopted herein, the stable state corresponds to the local minimum of

$U_c(\mathbf{x})$. Then, $\mathbf{grad}U_c=\mathbf{0}$ at a particular point $\mathbf{x}$ for prescribed $\mathbf{c}$. This defines a set of equilibrium point, surface or space

$$M_U = \{ (\mathbf{x},\mathbf{c}) \in R^N \times R^K \mid \mathbf{grad}U_c=\mathbf{0} \} \subset R^N \times R^K \qquad (2.4.2)$$

which the zero-gradient $\mathbf{grad}U_c=\mathbf{0}$ means the equations of equilibrium

$$\frac{\partial U_c}{\partial x_i}(x) = 0 \qquad (i=1,\ldots,N) \qquad (2.4.3)$$

Now, the equilibrium point is non-degenerate if the Hessian matrix of the potential function with each component

$$U_{ij} = \frac{\partial^2 U_c}{\partial x_i \partial x_j}(x) \qquad (i,j=1,\ldots,N) \qquad (2.4.4)$$

is non-singular at a point $\mathbf{x}$, that is,

$$\det[\, U_{ij} \,]_x \neq 0 \qquad (2.4.5)$$

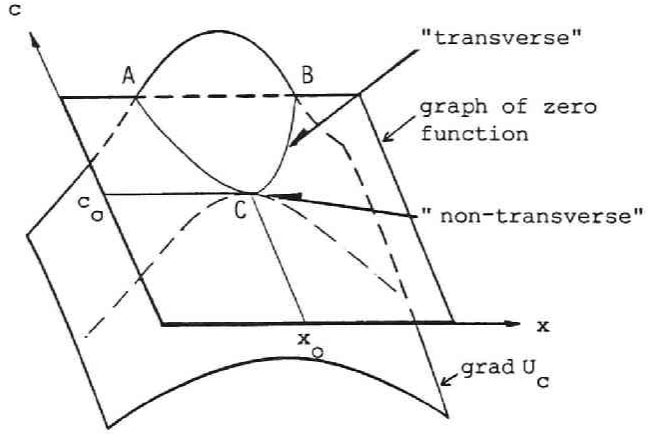

Fig. 2.4.1 Graphs of Zero Function and grad U_c. [21]

This condition means that the graph of $\mathbf{grad}U_c$ meets that of the zero function **transversely**(See, **Fig. 2.4.1**; curves AC and BC, not including the point C). Then, the function U_c is non-degenerate at the point $\mathbf{x}$. Therefore, through the Morse Lemma, there exists a smooth local change of coordinates such that the non-degenerate function becomes a quadratic form in a neighborhood of the origin $\mathbf{0} \in R^N$:

$$U_c \cong - y_1^2 - \ldots - y_s^2 + y_{s+1}^2 + \ldots + y_N^2 \qquad (2.4.6)$$

for a new coordinate $\mathbf{y} \in \mathbf{R}^N$. In which, "s" denotes the index* being the number of the negative eigenvalues of the Hessian matrix U_{ij} at the point $\mathbf{x}$. The non-degenerate equilibrium point is also called an isolated or Morse point. Conversely, if the Hessian

$$\det[\ U_{ij}]_{\mathbf{x}} = 0 \tag{2.4.7}$$

then the equilibrium point is called a degenerate, non-isolated or non-Morse point.

As the control parameters $\mathbf{c}$ vary, a family of potential functions, U, may have such a degenerate equilibrium point $\mathbf{x}$. In other words, since the eigenvalues of the Hessian matrix depends on the control parameters $\mathbf{c}$, more than one eigenvalues may vanish at a point $\mathbf{x}$. The number of non-zero eigenvalues refers to as the **rank** of the Hessian matrix, while, that is not the case, is called its **corank**. Topologically speaking, at the point, the graph of $\mathbf{grad}U_{\mathbf{c}}$ meets that of the zero function **non-transversally**"(See, **Fig. 2.4.1**; the point C). Also, the number and the location of the minima of the potential function $U_{\mathbf{c}}$ changes discontinuously at this point. The one of main objectives of the catastrophe theory is to determine a canonical expression of a potential function at this point.

If M eigenvalues of the Hessian matrix U_{ij} vanish simultaneously at $\mathbf{x}=\mathbf{x}_0 \in \mathbf{R}^N$ when $\mathbf{c}=\mathbf{c}_0 \in \mathbf{R}^K$, then a family of potential functions, $U(\mathbf{x},\mathbf{c})$, can be split into a degenerate part f and a Morse part, using the Splitting Lemma, for a new coordinate $\mathbf{y} \in \mathbf{R}^N$.

$$U(\mathbf{x},\mathbf{c}) \cong f(y_1,\ldots,y_M,\mathbf{c}) \pm y^2_{M+1} \pm \cdots \pm y^2_N \tag{2.4.8}$$

in a neighborhood of the corresponding degenerate point, transformed into the origin $\mathbf{0} \in \mathbf{R}^N$ by an appropriate change of coordinates. In which, $y_1,\ldots,y_M$ associated with the corank M of the Hessian matrix are smooth functions of both the N state variables $x_1,\ldots,x_N$ and the k control parameters $c_1,\ldots,c_k$. The number k is still unknown, but it may be determined from the concepts of the **unfolding**. Of course, k << K. These coordinates $y_1,\ldots,y_M$ are called the **essential** variables. Whereas the remainders $y_{M+1},\ldots,y_N$ are smooth functions of only the $x_1,\ldots,x_N$. They also are called the **inessential** variables, neglected in a catastrophe investigation.

The Splitting Lemma provides no informations about the form of the degenerate function f, but the function f has more that third order terms of the y_i in the Taylor expansions at the origin $\mathbf{0} \in \mathbf{R}^M$ corresponding to the original point $\mathbf{x}=\mathbf{x}_0$ when $\mathbf{c}=\mathbf{c}_0$. The resultant form is accessible in the neighborhood of $(\mathbf{x}_0, \mathbf{c}_0) \in \mathbf{R}^N \times \mathbf{R}^k$.

Since the catastrophe is assumed to take place at the degenerate point $(\mathbf{x}_0, \mathbf{c}_0)$, the Hessian matrix U_{ij} vanishes at the point. That is, the Hessian matrix U_{ij} (i,j=1,2,...,M) is singular at the point. While the remainder (N-M)x(N-M) matrix is non-singular, or Morse. Thom insists that there exists a smooth change of coordinates so that the potential function $U_{\mathbf{c}}$ at the fixed value $\mathbf{c}=\mathbf{c}_0 \in \mathbf{R}^k$ can be expressed in the neighborhood of the transformed origin $\mathbf{0} \in \mathbf{R}^N$ in the canonical form

$$U_{\mathbf{c}}(\mathbf{x}) \cong g(y_1,\ldots,y_M) \pm y^2_{M+1} \pm \cdots \pm y^2_N \tag{2.4.9}$$

where

---

* The index can be determined from the **Sylvester's Law of Inertia.** The quadratic form in Eq. (2.4.6) is called the **Morse s-saddle**(See, APPENDIX in this PART).

$$g : \mathbf{R}^M \rightarrow \mathbf{R}$$

The y_i are new coordinates after such a smooth **differomorphism**, and g refers to the **catastrophe germ.** This form is available in the neighborhood of $\mathbf{x}=\mathbf{x}_0 \in \mathbf{R}^N$ at fixed $\mathbf{c}=\mathbf{c}_0 \in \mathbf{R}^k$. Therefore, the result of Eq. (2.4.9) provides only specific form of f when $\mathbf{c}=\mathbf{c}_0$ in Eq. (2.4.8).

Thus, Thom introduced the concept of the **universal unfolding.** He resolved such insufficiencies of f and g, thinking that $U(\mathbf{x},\mathbf{c})$ may be regarded as a perturbation of $U_{\mathbf{c}}(\mathbf{x})$ in the neighborhood of $(\mathbf{x}_0,\mathbf{c}_0)$. A k-unfolding of g is equivalent to the form near the origin $\mathbf{0} \in \mathbf{R}^N$

$$V(\mathbf{y},\mathbf{c}) = g(\mathbf{y}) + h(\mathbf{y},\mathbf{c}) \tag{2.4.10}$$

where

$$V(\mathbf{y},\mathbf{c}_0) = g(\mathbf{y}) \quad \text{when} \quad \mathbf{c}=\mathbf{c}_0$$

and $\mathbf{y}=(y_1,\ldots,y_M)$, $\mathbf{c}=(c_1,\ldots,c_k)$ and $h(\mathbf{y},\mathbf{c})$ may be associated with some mathematical concepts such as the **truncated Taylor expansion**, the **jet**, the **determinancy**, the **transversality** and the **codimension.** Furthermore, the unknown number k can be evaluated from the versality and universality of the unfolding, that is, V is universe if k is the smallest dimension for which a versal k-unfolding of g exists.

Hence, the original potential function $U(\mathbf{x},\mathbf{c})$ with the degenerate equilibrium point $\mathbf{x}=\mathbf{x}_0 \in \mathbf{R}^N$ when $\mathbf{c}=\mathbf{c}_0 \in \mathbf{R}^k$ can be transformed in the neighborhood of $\mathbf{0} \in \mathbf{R}^N \times \mathbf{R}^k$ into the following canonical form

$$\begin{aligned} U(\mathbf{x},\mathbf{c}) &= V(\mathbf{y},\mathbf{c}) \pm y_{M+1}^2 \pm \cdots \pm y_N^2 \\ &= g(\mathbf{y}) + h(\mathbf{y},\mathbf{c}) \pm y_{M+1}^2 \pm \cdots \pm y_N^2 \end{aligned} \tag{2.4.11}$$

where

$$U_{\mathbf{c}_0}(\mathbf{x}) = U(\mathbf{x},\mathbf{c}_0) = g(\mathbf{y}) \pm y_{M+1}^2 \pm \cdots \pm y_N^2 \quad \text{when} \quad \mathbf{c}=\mathbf{c}_0 \in \mathbf{R}^k$$

Therefore, the catastrophe at the degenerate equilibrium point $(\mathbf{x}_0,\mathbf{c}_0)$ is equivalent to the one at the origin

$$\mathbf{0} = (\mathbf{0},\mathbf{0}) = (\mathbf{y}_0,\mathbf{c}_0) \in \mathbf{R}^M \times \mathbf{R}^k = \mathbf{R}^N \Big|_{y_{M+1}=\cdots=y_N=0} \times \mathbf{R}^k \tag{2.4.12}$$

Of course, a smooth change of parameters from the original $\mathbf{c} \in \mathbf{R}^k$ to the corresponding $\mathbf{c} \in \mathbf{R}^k$ near the origin $\mathbf{0} \in \mathbf{R}^k$ may be necessary to realize such an equivalence, but herein both are designated as the same small letter **c.**

Now, as mentioned above, the compound, but exactly concise procedures to determine the form of $h(\mathbf{y},\mathbf{c})$ have been developed by Mather, Siersma et al. [21,54]. Their details on proof and derivation in pure mathematics are beyond this dissertation. The resultant form of $h(\mathbf{y},\mathbf{c})$ follows a linear combination of parameters **c**

$$h(\mathbf{y},\mathbf{c}) = c_1 b_1(\mathbf{y}) + \ldots + c_k b_k(\mathbf{y}) \tag{2.4.13}$$

where $b_i(\mathbf{y})$ are called the cobases, and can be obtained associating with the jet space using the germ g. Further, their order is one less than that of g.

2.5 Thom's Elementary Catastrophes

All the typical forms of germs $g(\mathbf{y})$ and unfoldings $V(\mathbf{y},\mathbf{c})$ for $k \leq 4$, M=1 or 2 are listed out in **Table 2.5.1**(Also, see **Table I-1.3.2**). The concept of both the catastrophe map and the bifurcation set are also under the Thom's Theorem. Now, as the control parameters $\mathbf{c}$ vary in a neighborhood of the point $\mathbf{c}_0$, then consider a set of degenerate equilibrium points near the point $(\mathbf{x}_0,\mathbf{c}_0)$

$$S_U = \left\{ (\mathbf{x},\mathbf{c}) \in \mathbf{R}^N \times \mathbf{R}^K \;\middle|\; \mathbf{grad} U_{\mathbf{c}} = \mathbf{0} \text{ and } \det[V_{ij}]_{\mathbf{x}} = 0 \right\} \subset M_U \tag{2.5.1}$$

Further, consider a projection

$$\chi : \mathbf{R}^N \times \mathbf{R}^K \longrightarrow \mathbf{R}^K \tag{2.5.2}$$

onto the parameter space, then the restriction of χ on M_U can be written as

$$\chi_U : M_U \longrightarrow \mathbf{R}^K \tag{2.5.3}$$

This projection is called the **catastrophe map.** Particularly, a set of points on $\mathbf{R}^K$ projected by this of S_U on M_U is also called the **bifurcation set**, designated as B_U.

$$B_U = \chi_U(S_U) \tag{2.5.4}$$

The set can be defined for $(\mathbf{x},\mathbf{c})$ in the neighborhood of the point $(\mathbf{x}_0,\mathbf{c}_0)$, and forms a significant point, surface or space in the parameter space. In structural mechanics, the set B_U specifies the well-known imperfection sensitivity curve(s) or surface(s) as stated in the chapter II-2(See, **Fig. II-2.2.1**).

Finally, for the canonical potential form, $V(\mathbf{y},\mathbf{c})$, the catastrophe map and the bifurcation set will be analogously treated from the Thom's Theorem. Hence, the Thom's Theorem says that a family of potential functions

$$U(\mathbf{x},\mathbf{c}) : \mathbf{R}^N \times \mathbf{R}^K \longrightarrow \mathbf{R} \tag{2.5.5}$$

with the degenerate equilibrium point $(\mathbf{x}_0,\mathbf{c}_0)$ is equivalent to either of seven elementary catastrophes

$$V(\mathbf{y},\mathbf{c}) : \mathbf{R}^M \times \mathbf{R}^k \longrightarrow \mathbf{R} \tag{2.5.6}$$

with the degenerate point being the origin $\mathbf{0} \in \mathbf{R}^M x \mathbf{R}^k$.

2.6 Conclusions

This chapter presents an introduction to the catastrophe theory in the light of the singularity theory of mappings in pure mathematics. Then, broad, but

Table 2.5.1 Thom's Elementary Catastrophes

Name	Germ $g(\mathbf{y})$	$h(\mathbf{y},\mathbf{c})$	M	k
fold	x^3	c_1x	M = 1 x = y_1	1
cusp	$\pm x^4$	$c_1x^2+c_2x$		2
swallow tail	x^5	$c_1x^3+c_2x^2+c_3x$		3
butterfly	$\pm x^6$	$c_1x^4+c_2x^3+c_3x^2+c_4x$		4
hyperbolic umbilic	x^3+y^3	$c_1xy+c_2x+c_3y$	M = 2 x = y_1 y = y_2	3
elliptic umbilic	x^3-3xy^2	$c_1(x^2+y^2)+c_2x+c_3y$		
parabolic umbilic	$x^2y\pm y^4$	$c_1x^2+c_2y^2+c_3x+c_4y$		4

$V(\mathbf{y},\mathbf{c})=g(\mathbf{y})+h(\mathbf{y},\mathbf{c})$ is equivalent to the Thom's unfolding(See, **Table I-1.3.2**), where $\mathbf{y}=(y_1,y_2,\ldots,y_M)$ and $\mathbf{c}=(c_1,c_2,\ldots,c_k)$.

concise, historical reviews on the catastrophe theory and its applications in engineering sciences are provided. The main conclusions are:

(1) The system is governed by a potential function, which is a function of internal state variables for fixed value of external control parameters.

(2) There exists a family of potential functions characterized by the control parameters as they vary smoothly.

(3) The stable state of the system corresponds to the one for which the potential function has its local minimum for prescribed control parameters under the Perfect-delay convention.

(4) The catastrophe may take place at a peculiar point where the number of such minima changes suddenly.

(5) The Thom's Theorem asserts that a family of potential functions can be described locally in either typical form of the seven elementary catastrophes or universal unfoldings when the state variables $\leq$ 2 and the control parameters $\leq$ 4.

(6) The bifurcation set in the control-parameter space through the catastrophe map of elementary catastrophe unfolding plays a significant role in order to evaluate the imperfection sensitivity in structural mechanics.

Bibliographies of Chapter 2 in PART I

1) Thom,R., Structural Stability and Morphogenesis (translated form the French by D.H.Fowler). Benjamin, 1975.
2) Gurel,O, Poincare bifurcation analysis. Bifurcation Theory and Applications in Scientific Disciplines, Annals of the New York Academy of Sciences, Vol. 316, pp. 5-26, 1979.
3) Leipholz,H., Stability of Elastic Systems. Sijthoff and Noordhoff, 1980.
4) Thom,R., Structural stability, catastrophe theory, and applied mathematics. SIAM Review, Society for Industrial and Applied Mathematics, Vol. 19, No. 2, pp. 189-201, 1976.
5) Zeeman,E.C., Catastrophe theory. Scientific American, Vol. 234, pp. 65- 83, 1976.
6) Sussmann,H.J., Catastrophe theory. Synthese, Vol. 31, pp. 229-270, 1975.
7) Chillingworth,D., Elementary catastrophe theory. Bulletin of the Institute of Mathematics and Its Applications, Vol. 11, pp. 155-159, 1975.
8) Stewart,I., Catastrophe theory. Mathematical Chronicle, Vol. 5, pp. 140-165, 1977.
9) Sewell,M.J., Elementary catastrophe theory. Problem Analysis in Science and Engineering (eds. F.H.Branin,Jr. and K.Huseyin), Academic Press, pp. 391-426, 1977.
10) Golubitsky,M., An introduction to catastrophe theory and its applications. SIAM Review, Society for Industrial and Applied Mathematics, Vol. 20, No. 2, pp. 352-387, 1978.
11) Zeeman,E.C., A catastrophe machine. Towards a Theoretical Biology, Vol. 4, pp. 276-282, 1972.
12) Poston,T. and A.E.R.Woodcock, Zeeman's catastrophe machine. Mathematical Proceedings of Cambridge Philosophical Society, Vol. 74, pp. 217-226, 1973.

13) Poston,T., Various Catastrophe machines. Structural Stability, the Theory of Catastrophes, and Applications in the Sciences (ed. P.J.Hilton), Lecture Notes in Mathematics, Vol. 525, Springer-Verlag, pp. 111-126, 1976.
14) Zeeman,E.C., The classification of elementary catastrophes of codimension $\leq$ 5. Structural Stability, the Theory of Catastrophes, and Applications in the Sciences (ed. P.J.Hilton), Lecture Notes in Mathematics, Vol. 525, Springer-Verlag, pp. 263-327, 1976.
15) Zeeman,E.C., The umbilic bracelet and the double-cusp catastrophe. Structural Stability, the Theory of Catastrophes, and Applications in the Sciences (ed. P.J.Hilton), Lecture Notes in Mathematics, Vol. 525, Springer-Verlag, pp. 328-366, 1976.
16) Zeeman,E.C., Catastrophe Theory: Selected Papers 1972-1977. Addison-Wesley, 1977.
17) Zeeman,E.C., Euler buckling. Structural Stability, the Theory of Catastrophes, and Applications in the Sciences (ed. P.J.Hilton), Lecture Notes in Mathematics, Vol. 525, Springer-Verlag, pp. 372-395, 1976.
18) Lu.,Y.-C., Singularity Theory and an Introduction to Catastrophe Theory. Springer-Verlag, 1976.
19) Lander,L., Differential Germs and Catastrophes. London Mathematical Society Lecture Notes, No. 17, Cambridge University Press, 1975.
20) Poston,T. and I.Stewart, Taylor Expansions and Catastrophes. Research Notes in Mathematics, No. 7, Pitman, 1976.
21) Poston,T. and I.Stewart, Catastrophe Theory and Its Applications. Pitman, 1978.
22) Stewart,I., Applications of catastrophe theory to the physical sciences. Physica, Vol. 2D, pp. 245-305, 1981.
23) Hilton,P.(ed.), Structural Stability, the Theory of Catastrophes, and Applications in the Sciences. Lecture Notes in Mathematics, Vol. 525, Springer-Verlag, 1976.
24) Gurel,O and O.E.Rossler(eds.), Bifurcation Theory and Applications in Scientific Disciplines. Annals of the New York Academy of Sciences, 1979.
25) Golubitsky,M. and D.Schaeffer, A theory for imperfect bifurcation via singularity theory. Communications on Pure and Applied Mathematics, Vol. 32, pp. 21-98, 1979.
26) Golubitsky,M. and D.Schaeffer, Imperfect bifurcation in the presence of symmetry. Communications in Mathematical Physics, Vol. 67, pp. 205-232, 1979.
27) Golubitsky,M. and D.Schaeffer, An analysis of imperfect bifurcation. Bifurcation Theory and Applications in Scientific Disciplines (eds. O.Gurel and O.E.Rossler), Annals of the New York Academy of Sciences, pp. 127-133, 1979.
28) Dynamical Systems and Catastrophes, Special Edition. Mathematical Sciences, No. 138, Saiensu-Sha, 1974 (in Japanese).
29) Catastrophes, Special Edition. Mathematical Sciences, No. 147, Saiensu-Sha, 1975 (in Japanese).
30) Applied Catastrophes, Special Edition. Mathematical Sciences, No. 196, Saiensu-Sha, 1979 (in Japanese).
31) Zeeman,E.C. and H.Noguchi, Applied Catastrophe Theory: Social Sciences + Collapse Theory. Blue Backs, No. B-244, Kohdansha, 1974 (in Japanese).
32) Noguchi,H., Catastrophes. Science Library, Mathematics in Scientific Engineering, No. 13, Saiensu-Sha, 1977 (in Japanese).
33) Noguchi,H., Topology : Foundation and Procedures. Nihonhyohron-Sha, 1979 (in Japanese).

34) Fujii,H. and M.Yamaguti, Simple buckling - a group theoretical introduction. Theory of Stability, Bifurcation and Buckling in Nonlinear Elasticity and Its Numerical Analysis, Research Report No. 343, Mathematical Institute of Numerical Analysis, Kyoto University, pp. 1-28, 1979.
35) Fujii,H. and M.Yamaguti, Structure of singularities and its numerical realization in nonlinear elasticity. Journal of Mathematics of Kyoto University, Vol. 20, No.3, pp. 489-590.
36) Fujii,H., Group bifurcation theory and finite element method. Mathematics, Vol. 33, No.3, pp. 227-247, 1981 (in Japanese).
37) Yamaguchi,M.(ed.), Nonlinear Phenomena and Their Analyses. An Introduction to Modern Mathematics, Mathematical Seminar Extra Edition, Nihonhyouron-Sha, 1979 (in Japanese).
38) Yamaguchi,M.(ed.), Numerical Analysis and Nonlinear Phenomena. An Introduction to Modern Mathematics, No. 2, Mathematical Seminar Extra Edition, Nihonhyohron-Sha, 1981 (in Japanese).
39) Thompson,J.M.T. and G.W.Hunt, Towards a unified bifurcation theory. Journal of Applied Mathematics and Physics (Zeitschrift für Angewandte Mathematik und Physik), Vol. 26, pp. 581-603, 1975.
40) Thompson,J.M.T., Experiments in catastrophe. Nature, Vol. 254, pp. 392-395, 1975.
41) Thompson,J.M.T., Designing against catastrophe. Modern Trends in Cybernetics and Systems, Proceeding of the 3rd International Congress of Cybernetics and Systems, Vol. 2, Section 2 (Systems and Models), Bucharest, Rumania, Springer-Verlag, pp. 445-454, Aug. 25-29, 1975.
42) Thompson,J.M.T., Instabilities, bifurcations and catastrophes. Physics Letters, Vol. 51A, No. 4, pp. 201-203, 1975.
43) Thompson,J.M.T. and G.W.Hunt, A bifurcation theory for the instabilities of optimization and design. Synthese, Vol. 26, pp. 315-351, 1977.
44) Thompson,J.M.T. and G.W.Hunt, The instability of evolving systems. Interdisciplinary Science Reviews, Vol. 2, No. 3, pp. 240-262, 1977.
45) Thompson,J.M.T., Bifurcational aspects of catastrophe theory. Bifurcation Theory and Applications in Scientific Disciplines (eds. O.Gurel and O.E. Rossler), Annals of the New York Academy of Sciences, Vol. 316, pp. 553-571, 1979.
46) Thompson,J.M.T., Catastrophe theory and its rule in applied mechanics. Theoretical and Applied Mechanics (ed. W.T.Koiter), North-Holland Publishing Company, pp. 451-458, 1980.
47) Thompson,J.M.T., Instability and Catastrophe in Science and Engineering. John Wiley & Sons, 1982.
48) Thompson,J.M.T. and G.W. Hunt, Elastic Instability Phenomena. John Wiley & Sons, 1984.
49) Golubitsky,M. and D.G.Schaeffer, Singularities and Groups in Bifurcation Theory, Vol. 1. Applied Mathematical Sciences, No. 51, Springer-Verlag, 1985.

APPENDIX for PART I

MATHEMATICAL BACKGROUND TO SINGULARITY THEORY

The fundamental mathematical concepts to understand the topology of the singularity theory of mappings will be outlined with only short comments and notes, and their precise proof are referred to mathematical papers[1-10].

A.1 Differential Calculus

The first step follows some basic principles of differential calculus of several variables:

Derivative

A function $f: \mathbf{R}^n \to \mathbf{R}^m$ is **differentiable** at $x \in \mathbf{R}^n$ if there exists a linear map $\lambda : \mathbf{R}^n \to \mathbf{R}^m$ such that

$$\lim_{h \to 0} \frac{|| f(x+h) - f(x) - \lambda(h) ||}{|| h ||} = 0 \qquad \text{(A.1)}$$

where the symbol $|| \ ||$ designates the so-called **norm.** The linear map λ is uniquely determined, and is called the **derivative** of f at x. It can be described as

$$\lambda = D f \Big|_x \qquad \text{(A.2)}$$

Partial Derivative

For $f: \mathbf{R}^n \to \mathbf{R}$ and $x \in \mathbf{R}^n$, if the limit

$$\lim_{h \to 0} \frac{f(x_1, \ldots, x_i + h, \ldots, x_n) - f(x_1, \ldots, x_n)}{h} \qquad \text{(A.3)}$$

exists, then it is called the **i-th partial derivative** of f at x.

$$D_i f \Big|_x \quad \text{or} \quad \frac{\partial f}{\partial x_i}\Big|_x \qquad \text{(A.4)}$$

Thus, if $f: \mathbf{R}^n \to \mathbf{R}^m$ is differentiable at $x \in \mathbf{R}^n$, then $D_i f_j \Big|_x$ exists for all i, j, and $Df\Big|_x$ has the matrix

$$\left[D_i f_j \Big|_x \right] \quad \text{or} \quad \left[\frac{\partial f_j}{\partial x_i} \right]_x \qquad \text{(A.5)}$$

Using this derivative, the Jacobian determinant of f at x is defined by $Jf\Big|_x = \det(Df\Big|_x)$.

Note: $Df\Big|_x$ is non-singular if and only if the Jacobian determinant $Jf\Big|_x = 0$.

Note: f is **continuously differentiable** such that $Df|_x$ exists if all $D_i f_j|_x$ exist and are continuous.

Class ∞

If partial derivatives of a function f up to **order** r exist and are continuous, f is **r-fold differentiable** or **of class r.** A **smooth** function is of class C^∞ ($k=\infty$).

Taylor Series

For any smooth function f: $\mathbf{R} \to \mathbf{R}$, its Taylor series at the origin is defined to be the **formal** power series

$$\sum_{r=0}^{\infty} \frac{1}{r!} D^r f|_0 \, x^r \qquad (A.6)$$

k-jet

The k-jet of smooth function f: $\mathbf{R} \to \mathbf{R}$ is defined by truncating its Taylor series up to **degree** k at the origin

$$j^k f(x) = \sum_{r=0}^{k} \frac{1}{r!} D^r f|_0 \, x^r \qquad (A.7)$$

Note: A function f: $\mathbf{R} \to \mathbf{R}$ has **order** k at the origin if

$$f(0) = D\,f|_0 = \ldots = D^{k-1} f|_0 = 0 \qquad (A.8)$$

Note: Apparently, its Taylor series and its k-jet can be also generalized for smooth functions f: $\mathbf{R}^n \to \mathbf{R}^m$.

A.2 Diffeomorphism

In the second step, the type of change of coordinates is restricted herein in order to hold some important informations of topology.

Diffeomorphism

A change of coordinates is **diffeomorphism** if and only if it must be smooth - differentiable and continuous - and reversible.

Inverse Function Theorem

Let f: $U \to \mathbf{R}^m$ (U is an open set in $\mathbf{R}^n$) be smooth, and let $x \in U$. If the linear map $Df|_x$ is non-singular, then f is a local diffeomorphism at x.

Implicit Function Theorem

If $f: \mathbf{R}^m \times \mathbf{R}^n \to \mathbf{R}^n$ is smooth and $f(x_o,y_o) = c$ at $(x_o,y_o) \in \mathbf{R}^m \times \mathbf{R}^n$, and if a set of solutions at (x,y)

$$\{ (x,y) \mid D f \Big|_{(x_o,y_o)} (x,y) = 0 \} \tag{A.9}$$

is the graph of a function y=y(x) from $\mathbf{R}^m$ to $\mathbf{R}^n$, then a set of solutions

$$\{ (x,y) \mid f(x,y) = c \} \tag{A.10}$$

is also the graph of a smooth function locally near (x_o,y_o).

Equivalence of Functions

Two smooth functions $f, g : \mathbf{R}^n \to \mathbf{R}$ are called to be **equivalent** around $0 \in \mathbf{R}^n$ if there exists a local diffeomorphism $y: \mathbf{R}^n \to \mathbf{R}^n$ around $0 \in \mathbf{R}^n$ and a constant γ such that

$$g(x) = f(y(x)) + \gamma \tag{A.11}$$

around $0 \in \mathbf{R}^n$ (See, **Fig. A.2.1**).

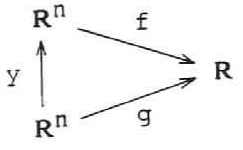

Fig. A.2.1 Equivalence of Functions.

Note: This concept can be also expanded in the case of a family of functions $F: \mathbf{R}^n \times \mathbf{R}^r \to \mathbf{R}$(See, **Fig. A.4.4**).

A.3 Morse Lemma and Splitting Lemma

The third step follows that the main objective of the catastrophe theory is the classification of types of critical points at which the derivative of a smooth real-valued function vanishes.

Critical Point

A point $x \in \mathbf{R}^n$ is a critical point of $f: \mathbf{R}^n \to \mathbf{R}$ if

$$D f\Big|_x = 0 \quad \text{or} \quad \frac{\partial f}{\partial x_1}\Big|_x = \cdots = \frac{\partial f}{\partial x_n}\Big|_x = 0 \tag{A.12}$$

The value f(x) at a critical point is called the **critical value** of f.

Non-degenerate Critical Point

$f: \mathbf{R}^n \to \mathbf{R}$ has a **non-degenerate** critical point at x if $Df\Big|_x = 0$ and if $D^2 f\Big|_x$ is a non-degenerate quadratic form, that is, its rank is equal to the number of variables n. In other words, the **Hessian matrix**

$$H\,f\,|_x = \left[\frac{\partial^2 f}{\partial x_i \partial x_j}\right]_x \tag{A.13}$$

is non-singular, so the **Hessian determinant.**

$$\det\,[\,H\,f\,|_x\,] \neq 0 \tag{A.14}$$

Note: The number of the negative eigenvalues, including their duplications, of the Hessian matrix of f at x is called the **index** of f at x (See, Eq. (A.18)).

Note: Let f: $\mathbf{R}^n \to \mathbf{R}$ be a smooth function, and let the origin $0 \in \mathbf{R}^n$ be a critical point, such that

$$f(0) = D\,f\,|_0 = \ldots = D^{k-1}\,f\,|_0 = 0 \tag{A.15}$$

but

$$D^k\,f\,|_0 \neq 0 \tag{A.16}$$

Then there exists a smooth local change of coordinates under which f takes the form

$$x^k \quad (\,k : \text{odd}\,), \qquad \pm x^k \quad (\,k : \text{even}\,) \tag{A.17}$$

and in the latter case the sign is that of $D^k f|_0$.

Morse Lemma

Let x be a non-degenerate critical point of a smooth function f: $\mathbf{R}^n \to \mathbf{R}$ with the index ℓ. Then, there exists a local coordinate system $(y_1,\ldots,y_N)$ in a neighborhood U of u with $y_i(x)=0$ for all i such that

$$f = f(x) - y_1^2 - \ldots - y_\ell^2 + y_{\ell+1}^2 + \ldots + y_n^2 \tag{A.18}$$

for all $u \in U \subset \mathbf{R}^n$. In which, the quadratic form of the right hand is called the Morse ℓ-saddle.

Note: The Hessian is degenerate at a non-Morse critical point.
Note: If f is a quadratic form itself, the number ℓ can be obtained by the Sylvester's Law of Inertia independently of the coordinate system **y.**

Splitting Lemma

Let f: $\mathbf{R}^n \to \mathbf{R}$ be a smooth function, whose Hessian at $0 \in \mathbf{R}^n$ has **rank** m, i.e., **corank** (n-m). Then f is **equivalent** around $0 \in \mathbf{R}^n$ to a function of the form

$$\pm x_1^2 \pm \quad \ldots \quad \pm x_m^2 + \tilde{f}(x_{m+1},\ldots,x_n) \tag{A.19}$$

where

$$\tilde{f} : \mathbf{R}^{n-m} \to \mathbf{R}$$

is smooth.

Note: This lemma asserts that a smooth function at a degenerate critical point is split into the Morse part on one set of variables and a degenerate part on the remainder set. Thus, from the Morse part being non-degenerate, the behavior of the original function f near the degenerate critical point can be realized as that of the remainder function $\tilde{f}$ with the number of variables equal to the **corank** of the Hessian at such a point.

Note: The corank of the Hessian is also the corank of the function at the critical point.

Note: The concepts of the Morse and Splitting Lemma can be also expanded in the case of a family of functions F: $\mathbf{R}^n \times \mathbf{R}^r \to \mathbf{R}$(See, Section **A.5**).

A.4 Structural Stability and Transversality

Structural Stability

A smooth function f: $\mathbf{R}^n \to \mathbf{R}$ is **structurally stable** if f and f+p are "equivalent" after a suitable translation of origin for all sufficiently small function p (See, for examples, **Figs. A.4.1**).

Note: Any function near the Morse critical point is structurally stable.

Note: A critical point is structurally stable if and only if it is non-degenerate; every degenerate critical point is structurally unstable.

Transversality

Two spaces U, V of $\mathbf{R}^n$ are **transverse** if they meet in a subspace whose dimension is as small as possible. If dim U = s and dim V= t, then this minimal dimension is

$$\max(0, s + t - n) \qquad \text{(A.20)}$$

Note: The transversality is generalized for **affine** subspaces. Then, let X and Y be affine subspaces of $\mathbf{R}^n$ of dimensions s and t, respectively. They meet **transversely** if either

(a) their intersection $X \cap Y$ is empty, or

(b) $s + t \geq n$ and dim $X \cap Y = s + t - n$.

Note: The condition that the Hessian of a smooth function f: $\mathbf{R}^n \to \mathbf{R}$ is non-singular leads to the condition that the Jacobian of the mapping

$$D f = \left(\frac{\partial f}{\partial x_1}, \ldots, \frac{\partial f}{\partial x_n} \right) : \mathbf{R}^n \to \mathbf{R}^m \qquad \text{(A.21)}$$

is non-singular. In other words, the condition is equivalent to the condition that

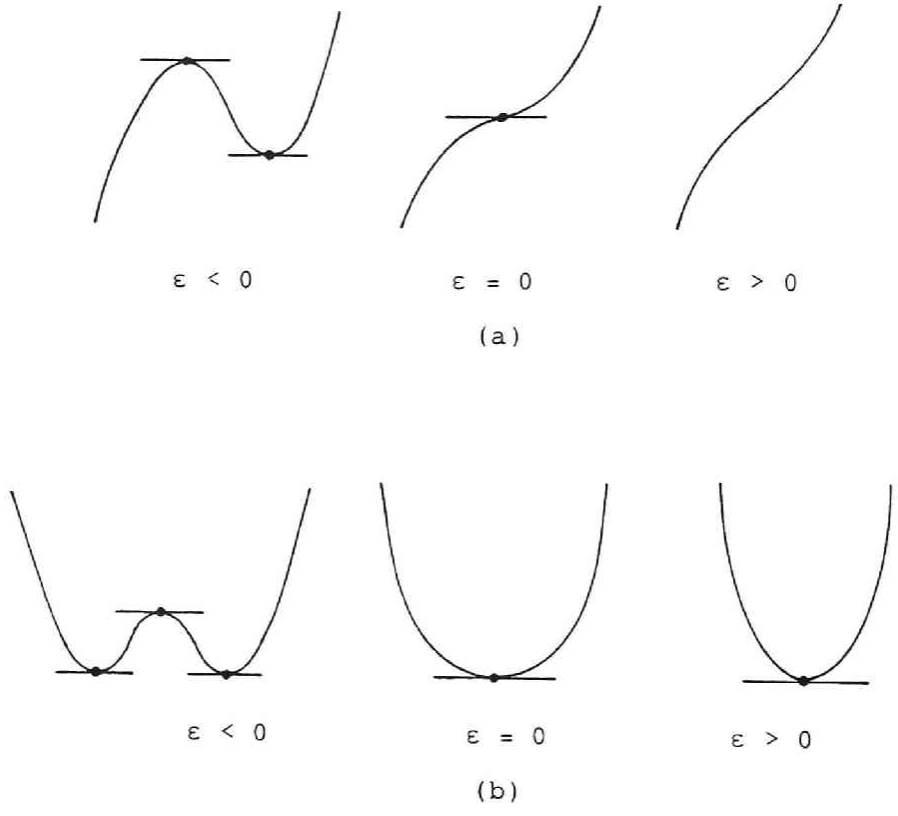

Fig. A.4.1 Structural Stability. [7]
(a) $x^3 + \varepsilon x$ (b) $x^4 + \varepsilon x^2$

the graph of Df meet that of the zero function **transversely**(See, **Fig. A.4.2**; curves AC and BC, not including the point C).

Note: The derivative of the non-Morse function not being structurally stable has a graph which is typical in meeting the zero line **non-transversely**(See, **Fig. A.4.2**; the point C).

Note: Several examples for the transversality are typically shown in **Figs. A.4.3** in the case of two manifolds X and Y.

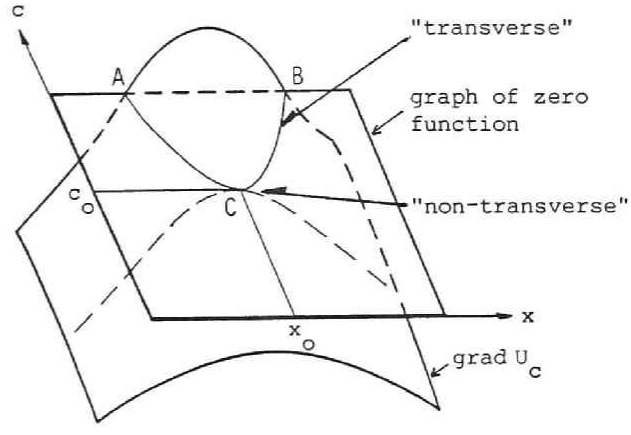

Fig. A.4.2 Transversality [7]

A.5 Family of Functions

In the fifth step, the structural stability of families of functions is briefly described, and the Splitting Lemma for families can be expanded herein.

Equivalence of Families

Two families of functions f, g : R^n x $R^r \to R$ are **equivalent** if there exist e, y, γ defined in a neighborhood of $0 \in R^n$ such that

$$g(x,s) = f(y_s(x),e(s)) + \gamma(s) \qquad (A.22)$$

for all $(x,s) \in R^n$ x R^r in that neighborhood(See, **Fig. A.4.4**). In which, e, y, andγ follows

(a) a diffeomorphism

$$e : R^r \to R^r \qquad (A.23.a)$$

(b) a smooth map

$$y : R^n \text{ x } R^r \to R^r \qquad (A.23.b)$$

such that for each $s \in R^r$ the map

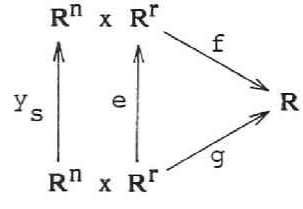

Fig. A.4.4 Equivalence of Families of Functions.

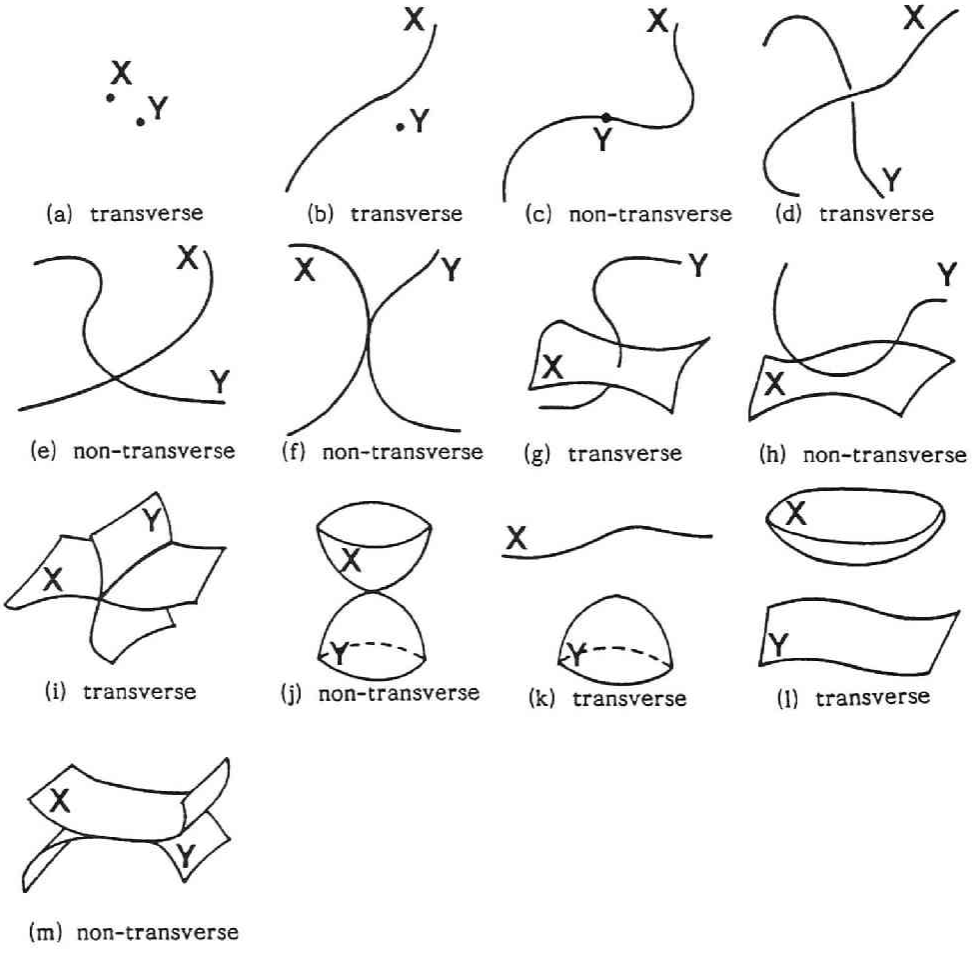

Fig. A.4.3 Some Examples for Transversality. [7]

PART II

CATASTROPHE ANALYSIS OF ELASTIC STRUCTURES

$$y_s : \mathbf{R}^n \to \mathbf{R}^n \text{ or } y_s(x) = y(x,s) \qquad \text{(A.23.c)}$$

is a diffeomorphism.

(c) a smooth map

$$\gamma : \mathbf{R}^n \to \mathbf{R} \qquad \text{(A.23.d)}$$

Structural Stability of Families

A family f: $\mathbf{R}^n$ x $\mathbf{R}^r \to \mathbf{R}$ is **structurally stable** if f is equivalent to any family f+p, where p is a sufficiently small family $\mathbf{R}^n$ x $\mathbf{R}^r \to \mathbf{R}$.

Morse Lemma for Families

Let F: $\mathbf{R}^n$ x $\mathbf{R}^r \to \mathbf{R}$ be smooth. Suppose that the Hessian

$$\left[\frac{\partial^2 F}{\partial x_i \partial x_j} \right] \qquad (i,j=1,\ldots,n) \qquad \text{(A.24)}$$

is non-degenerate at $(x,c)=0 \in \mathbf{R}^n$ x $\mathbf{R}^r$. Then, F is equivalent to a family of the form

$$\pm y_1^2 \pm \ \ldots \ \pm y_n^2 \qquad \text{(A.25)}$$

Splitting Lemma for Families

Let F: $\mathbf{R}^n$ x $\mathbf{R}^r \to \mathbf{R}$ be smooth. Suppose that the Hessian

$$HF_c = \left[\frac{\partial^2 F_c}{\partial x_i \partial x_j} \right]_x \qquad (i,j=1,\ldots,n) \qquad \text{(A.26)}$$

has **corank** m at $(\mathbf{x},\mathbf{c})=(x_1,\ldots,x_n,c_1,\ldots,c_r) \in \mathbf{R}^n$ x $\mathbf{R}^r$. Then F is equivalent to a family of the form

$$\tilde{F}(y_1(x,c),\ldots,y_m(x,c),c) \pm y_{m+1}^2 \pm \ \ldots \ \pm y_n^2 \qquad \text{(A.27)}$$

where

$$\tilde{F} : \mathbf{R}^m \text{ x } \mathbf{R}^r \to \mathbf{R}$$

In the form, $y_1,\ldots,y_m$ are called the **essential** variables, whereas the remainders $y_{m+1},\ldots,y_n$ the **inessential** variables negligible on the study of topology of catastrophes.

A.6 Determinancy and Unfolding

In the sixth step, the significant problem is outlined what beginnings of Taylor series will be typically necessary to realize the essential features of catastrophes of functions considered. From finite Taylor expansions, it can be ex-

actly determined whether the relevant function is typical or not.

k-Determinancy

If, for a smooth function f: $\mathbf{R}^n \to \mathbf{R}$ and any g of order k+1, any function f+g is locally equivalent by a smooth change of coordinates to the k-jet of the function f, $j^k f$ at $0 \in \mathbf{R}^n$, then, f is called **k-determinate** at $0 \in \mathbf{R}^n$.

r-Unfolding

An r-unfolding of a function f: $\mathbf{R}^r \to \mathbf{R}$ is a function

$$F : \mathbf{R}^{n+r} \to \mathbf{R} \tag{A.28}$$

such that

$$F(x_1,\ldots,x_n,0,\ldots,0) = f(x_1,\ldots,x_n) \tag{A.29}$$

Note: Denote

$$F(x_1,\ldots,x_n,c_1,\ldots,c_r) = F_{(c_1,\ldots,c_r)}(x_1,\ldots,x_n) \tag{A.30}$$

the r-unfolding F is regarded as a family of functions $\mathbf{R}^n \to \mathbf{R}$ parameterized by $(c_1,\ldots,c_r)$.

Note: The internal variables, the unfolding variables, the unfolding dimension and the unfolding space are named as x, c, r and $\mathbf{R}^r$.

Note: An r-unfolding of f is **versal** if all other unfoldings of f can be "induced" form it, that is, they are equivalent to it. Moreover, it is **universal** if r is the smallest dimension for which a versal r-unfolding of f exists.

Bibliographies of APPENDIX in PART I

1) Thom,R., Structural Stability and Morphogenesis (translated from the French by D.H.Fowler). Benjamin, 1975.
2) Lander,L., Differential Germs and Catastrophes. London Mathematical Society Lecture Notes, No. 17, Cambridge University Press, 1975.
3) Lu,Y.-C., Singularity Theory and an Introduction to Catastrophe Theory. Springer-Verlag,1976.
4) Poston,T. and I.Stewart, Taylor Expansions and Catastrophes. Research Notes in Mathematics, No. 7, Pitman, 1976.
5) Noguchi,H. and T.Fukuda, Elementary Catastrophes. Kyohritsu Zensho, No. 208, 1976 (in Japanese).
6) Noguchi,H., Catastrophes. Science Library Mathematics in Scientific Engineering, No. 13, Saiensu-Sha, 1977 (in Japanese).
7) Poston.T. and I.Stewart, Catastrophe Theory and Its Applications, Pitman, 1978.
8) Gilmore,G., Catastrophe Theory for Scientists and Engineers. John Wiley & Sons, 1981.
9) Thompson,J.M.T., Instability and Catastrophe in Science and Engineering. John Wiley & Sons, 1982.
10) Golubitsky,M. and D.G.Schaeffer, Singularities and Groups in Bifurcation Theory, Volume 1. Applied Mathematical Sciences, Vol. 51, Springer-Verlag, 1985.

CHAPTER 1

CATASTROPHE ANALYSIS OF STRUCTURES BY DISCRETIZATION AND MODAL TRANSFORMS

1.1 General Remarks

As the degree-of-freedom of structures increases, the possibility of various instability phenomena increases. From the analysists' view point, the instability can be classified into global, partial and local ones, as shown in **Table 1.1.1** of the previous PART I[1]. At the same time, engineering structures may be classified in terms of the types of catastrophe or instability[2,3,4]. The purpose in this chapter is to show whether or not these marked items in the table are correct, and to find the most influential parameter in each of the items. In order for the structures to be accounted for by means of discretization methods, a question must be answered regarding whether or not the structure of singularities can be realized numerically. To answer this question, either a mathematical argument or an engineering computation will be necessary.

In the mathematical field, Poincaré made significant contributions on such problems in view of qualitative interpretations of differential equations. These researches performed by many investigators were briefly surveyed in the previous PART I[5,6]. Among them, recently, Fujii and Yamaguchi tried to answer the question through a nonlinear operator equation in the topological group theory, by use of the shallow arch and shell theory of von Kármán, Donnell and Marguerre [7,8]. Then, a numerical approximation of the problem was performed in a class of finite element schemes with the approximate Hilbert space. As a concluding remark, it was made clear that the numerical realization of the cusp bifurcation in the Hilbert space reveals the imperfections resulting from the use of numerical schemes which are very non-degeneric, and thus can be avoided.

In the engineering field, however, this equation may be equally answered by a comparison of the results such as eigenvalue, eigenmode and load-deflection curves from the discretization methods with those from the closed-form solutions, or with those from the experiments concerned. A great number of the theoretical and numerical analyses of static instability problems using the classical stability theory mainly initiated by Koiter have been developed by many researchers as well as by such experimental investigations[9,10]. Furthermore, Thompson et al. have proposed a unified bifurcation theory between the classical stability theory and the catastrophe theory introduced by Thom and Zeeman[4,11,12]. These were also discussed in the previous PART I with short comments. Thus, in this chapter, further introductions to the objectives of the associated problems will not be provided.

This chapter is also concerned with a catastrophe analysis of static instability problems of multi-degree-of-freedom structural system in the light of the Thom and Koiter-Thompson's theories. The proposed procedure makes use of discretization methods, such as a finite element method and a simplified element method [13,14] through the Lagrangian formulation, and some diffeomorphic modal transformations[15,16] upon the **static condensation** procedure. Also, this method formulates a numerical evaluation of catastrophe characteristics near the critical point. Furthermore, the applicability and the validity of the present analysis of numerical formulations will be discussed within the framework of the topological meanings. Several results as calculated in the subsequent chapters in this PART

II for the normal and unstable behavior of the engineering structures show that, in general, legitimate use of the finite element method and the simplified element method will be surely realize the singularities and instabilities of the canonical prototypes of catastrophe instabilities[15-19].

1.2 Formulation by Discretization

A method of approach to a catastrophe analysis of structures by discretization and modal transforms will be summarized in the flow chart of **Fig. 1.2.1** [14]. Brief descriptions on this procedure are performed in the previous chapter I-1. Herein, the applicability and validity of this method is examined in a topological sense.

1.2.1 Potential function V

Consider a potential function of a discrete structural system with M+N degrees of freedoms[4,13,14,18]

$$U : \mathbf{R}^M \times \mathbf{R}^N \times \mathbf{R}^K \to \mathbf{R} \quad \text{or} \quad U = U(u_i, w_j, \Lambda_k) \tag{1.2.1}$$

under K external control parameters. In which, $\mathbf{R}^M \times \mathbf{R}^N$ refers to an Euclidian behavior space of dimension M+N, representing a set of two types of generalized coordinates, $u_i(i=1,2,...M)$ and $w_j(j=1,2,...,N)$, respectively; $\mathbf{R}^K$ refers to a K-dimensional Euclidian space, representing conveniently a single loading parameter and several imperfection parameters, $\Lambda_k(k=0,1,...,K-1)$(Λ_0 is a single loading parameter). In the catastrophe theory, the former denotes the internal state variables; while the latter the external control parameters. The potential function can be defined by a perturbation one from the fundamental equilibrium state as mentioned in the chapter I-1. Furthermore, as stated in the chapter I-2, this potential can be also regarded as a family of potential functions in a mathematical sense if it is referred to as a set of potential functions when the control parameters Λ_k change continuously. The concept will be applied in evaluation of the form of the universal unfolding[20,21,22].

The equilibrium surface M_U of this system is given by:

$$M_U = \{ (u_i, w_j, \Lambda_k) \mid \frac{\partial U}{\partial u_i} = 0 \ (i=1,...,M), \ \frac{\partial U}{\partial w_j} = 0 \ (j=1,...,N) \} \tag{1.2.2}$$

Now, consider a static instability phenomenon of slender structures such as columns, beams and plates, that is, mainly a bifurcation problem with respect to the generalized coordinates, $w_j(j=1,2,...,N)$. Then, this surface is assumed to have the trivial solution $(u_i, w_j, \Lambda_k)=(u_i, 0, \Lambda_0, 0)$ for the structure with no imperfections. Hence, w_j designates essential variables from this solution, and inessential variables u_i must be eliminated from the original potential function U in Eq. (1.2.1). This is called the **static condensation** procedure.

In general, the variables u_i can be determined from the first M equations in parentheses of Eq. (1.2.2) in the following from:

$$u_i = u_i(w_j, \Lambda_k) \qquad \text{for} \quad \frac{\partial U}{\partial u_i} = 0 \ (i=1,...,M) \tag{1.2.3}$$

Under this condition, the original potential function U and its equilibrium surface M_U can be rewritten as

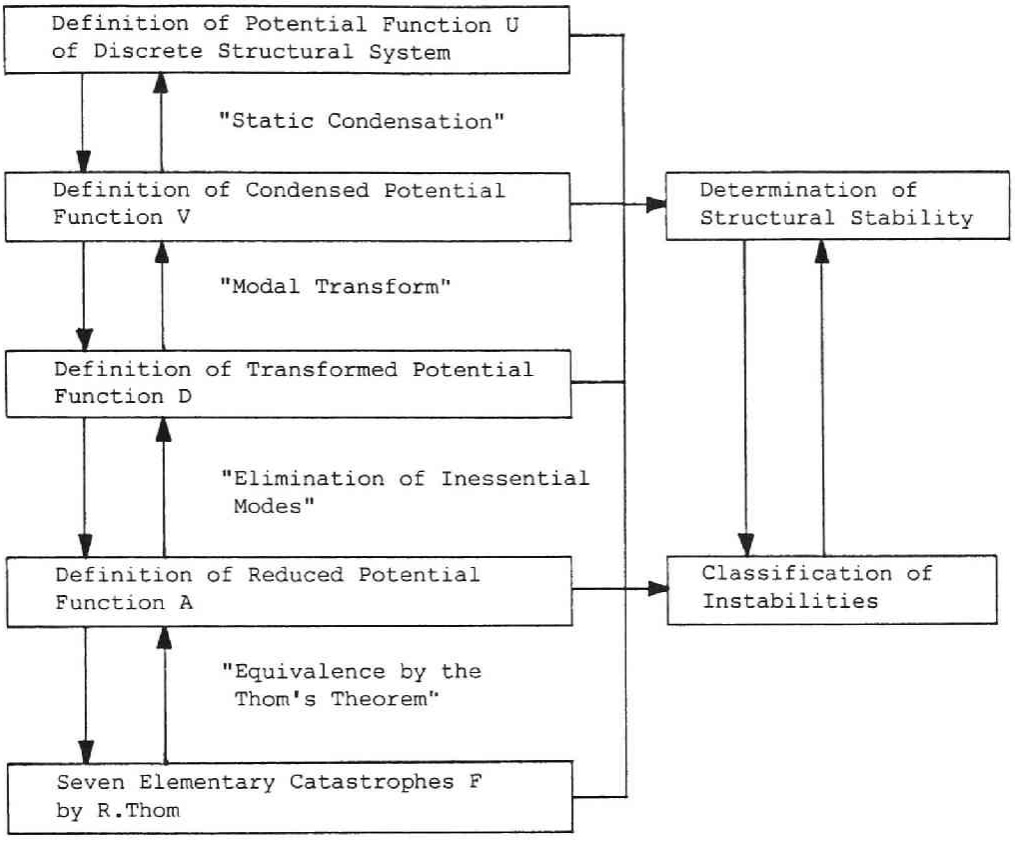

Fig. 1.2.1 Flow Chart of the Proposed Catastrophe Analysis.

$$V : R^N \times R^K \rightarrow R \quad \text{or} \quad V = V(w_i, \Lambda_j) \tag{1.2.4}$$

such that

$$M_V = \{ (w_i, \Lambda_j) \mid \frac{\partial V}{\partial w_i} = 0 \ (i=1,...,N) \} \subset R^N \times R^K$$

$$\text{for} \quad \frac{\partial U}{\partial u_i} = 0 \ (i=1.,,,,M) \tag{1.2.5}$$

This potential function V is defined as a function whose associated original potential function U identically satisfies equations of equilibrium for u_i (i=1,2,...,M). Discussions on the instability of the system will be made hereafter. It indicates the so-called fundamental equilibrium path, w_i=0 for the "perfect" system with only the loading parameter $\Lambda_o = \Lambda$. In other words, the path composes of a part of the section of equilibrium surface, cut by the plane Λ_j=0 (j=1,2,...,K-1). The section also involves the initial postbuckling path under the similar condition.

The catastrophe on this surface M_V can be represented by the bifurcation set Bif χ_V from the catastrophe map χ_V:

$$\chi_V : M_V \rightarrow R^K \tag{1.2.6}$$

Now, an instability phenomenon may occur at a peculiar point S. Then, at the point, the Hessian matrix of the potential function vanishes, that is,

$$\det[V_{ij}(\Lambda_k)]_S = \det[\frac{\partial^2 V}{\partial w_i \partial w_j} (\Lambda_k)]_S = 0 \tag{1.2.7}$$

It is apparently found that, for the **perfect** system, $\Lambda_o = \Lambda$, Λ_j=0 (j=1,2,..,K-1), the condition of Eq. (1.2.7) provides a critical point or a singular point $(w_i, \Lambda, \Lambda_j)=(0, \Lambda^C, 0)$ corresponding to some bifurcations as stated in the chapter I-1. Whereas, as a result, Eq. (1.2.7) under Eq. (1.2.5) commonly determines the well-known load-carrying capacity corresponding to the maximum value of loading parameter Λ for prescribed Λ_j(j=1,...,K-1) of the **imperfect** system.

1.2.2 Potential function D

Discussions on the catastrophe characteristics using potential function V are not realistic since a large degree of freedoms is generally involved. Thus, an eigen equation satisfying Eq. (1.2.7) is given by

$$V_{ij} w_j = 0 \qquad (i,j=1,...,n) \tag{1.2.8}$$

for given control parameters Λ_j near zero. This equation provides the eigenvector matrix whose components consist of n eigenvectors corresponding to n lower essential eigenvalues. The matrix is used for an Affine transformation h_1:

$$h_1 : R^n \rightarrow R^N$$
$$\mathbf{v}=(v_1,...,v_n) \rightarrow \mathbf{w}=(w_1,...,w_N) \qquad (n<<N) \tag{1.2.9}$$

With respect to the control parameters, another transformation similar to h_1 can be used for the imperfection parameters except for the loading one $\lambda_o = \lambda$, and a translation from the critical point to the origin may be used for the loading parameter:

$$h_2 : \mathbf{R}^k \rightarrow \mathbf{R}^K$$

$$\lambda = (\lambda_o, \varepsilon_1, \ldots, \varepsilon_{k-1}) \rightarrow \Lambda = (\Lambda_o, \Lambda_1, \ldots, \Lambda_{K-1}) \quad (k<<K) \tag{1.2.10}$$

Thus, a potential function D can be defined such that

$$D : \mathbf{R}^n \times \mathbf{R}^k \rightarrow \mathbf{R} \quad \text{or} \quad D = D(v_i, \lambda, \varepsilon_j) \tag{1.2.11}$$

where the quadratic terms

$$D_{ij} = \frac{\partial^2 D}{\partial v_i \partial v_j}, \qquad D_i^j = \frac{\partial^2 D}{\partial v_i \partial \varepsilon_j}$$

are diagonalized at the point $(v_i, \lambda, \varepsilon_j)=(0,0,0)$. In which, the imperfection parameters ε_j will be rewritten as λ_j in the next section of this chapter.

Let the equilibrium surface be designated by M_D. Then, the catastrophe map χ_D can be taken so that

$$\chi_D : M_D \rightarrow \mathbf{R}^k \tag{1.2.12}$$

If two transformations h_1 and h_2 are both **diffeomorphism** (See, APPENDIX in PART I), then the potential function V is equivalent to D in a mathematical sense. The equivalence can be proved using their explicit expression of transformations in the next section.

1.2.3 Potential function A

Now, consider the buckling problems treated as structural instabilities. Then, they lead to an evaluation of m instability modes with respect to the essential lowest buckling load $\Lambda_o = \Lambda$, i.e., $\lambda_o = \lambda = 0$. In other words, it means that the Hessian matrix of the potential function D has m zero-eigenvalues at the critical point $(v_i, \lambda, \varepsilon_j)=(0,0,0)$.

Suppose that the corank of the Hessian matrix at the point is

$$\text{corank}[\, D_{ij} \,] = \text{corank}\left[\, \frac{\partial^2 D}{\partial v_i \partial v_j} \,\right] = m \tag{1.2.13}$$

Under this situation, m-fold compound instability phenomena will be taken into account herein[23,24].

Since D_{ij} is diagonal, it can be shown after reordering,

$$\begin{aligned} &D_{ii} = 0 && (i=1,\ldots,m) && (i: \text{ not summed}) \\ &D_{\alpha\alpha} \neq 0 && (\alpha=m+1,\ldots,n) && (\alpha: \text{ not summed}) \end{aligned} \tag{1.2.14}$$

On the equilibrium surface M_D, (n-m) equations of equilibrium, $D_\alpha = 0$, will yield the following diffeomorphisms through the theorem of the Implicit Function Theorem:

$$v_\alpha = g_\alpha(v_i, \lambda, \varepsilon_j) \quad (\alpha = m+1,\ldots,n;\ i=1,\ldots,m;\ j=1,\ldots,k-1) \tag{1.2.15}$$

for prescribed control parameters (λ, ε_j) near zero (0,0).

Furthermore, consider a map ψ such that

$$\psi : \mathbf{v}=(v_1,\ldots,v_n) \rightarrow \mathbf{x}=(v_1,\ldots,v_m, v_{m+1}-g_{m+1},\ldots,v_n-g_n) \tag{1.2.16}$$

in a neighborhood of the critical origin $(v_i, \lambda, \varepsilon_j)=(0,0,0)$. Then, it can be easily shown that the potential function can be written as[15,20,21,25]:

$$D(v_i, \lambda, \varepsilon_j) \quad (D \circ \psi^{-1})(x_i, \lambda, \varepsilon_j) = A(x_1,\ldots,x_m) + \frac{1}{2} \sum_{\alpha=m+1}^{n} D_{\alpha\alpha} x_\alpha^2 \tag{1.2.17}$$

for prescribed (λ, ε_j). This relationship is known as the Splitting Lemma for a family of functions in Eq. (I-2.4.9). A potential function A can be interpreted as:

$$A : \mathbf{R}^m \times \mathbf{R}^k \rightarrow \mathbf{R} \quad \text{or} \quad A = A(x_i, \lambda, \varepsilon_j) \tag{1.2.18}$$

and $A(x_1,\ldots,x_m, \lambda, \varepsilon_j)$ includes terms higher than the third order. Variables $x_i=v_i$ $(i=1,2,\ldots,m)$ are called the **essential state variables**, and variables v_α $(\alpha=m+1,\ldots,n)$ are called the **inessential state variables**, and Thompson et al. called the former **active** and the latter **passive.**

An equivalence between two potential functions D and A can be proved from an existence of the diffeomorphic map ψ, i.e., from the Implicit Function Theorem and the Splitting Lemma. Also, the number of the **essential** control parameters among all k can be determined from the concept of unfoldings in the singularity theory of mappings as mentioned in the chapter I-2. The number is designated as ℓ. This may be strengthened by diagonalization of the terms $A_i^j (j \neq 0)$ similarly to Eq. (1.2.11). Therefore, a potential function can be rewritten by

$$A : \mathbf{R}^m \times \mathbf{R}^\ell \rightarrow \mathbf{R} \tag{1.2.19}$$

Let the equilibrium space be designated as M_A. Then, the catastrophe map may be given by χ_A:

$$\chi_A : M_A \rightarrow \mathbf{R}^\ell \tag{1.2.20}$$

1.2.4 Thom's unfoldings

When $1 \leq m \leq 2$, $1 \leq \ell \leq 4$, the diffeomorphisms g_1 and g_2:

$$g_1 : \mathbf{R}^m \rightarrow \mathbf{R}^m \quad \text{and} \quad g_2 : \mathbf{R}^\ell \rightarrow \mathbf{R}^\ell \tag{1.2.21}$$

will lead to either of the well-known seven elementary catastrophes by Thom[2, 12](See, APPENDIX B in this PART).

The discussions may be graphically summarized in **Fig. 1.2.2.**

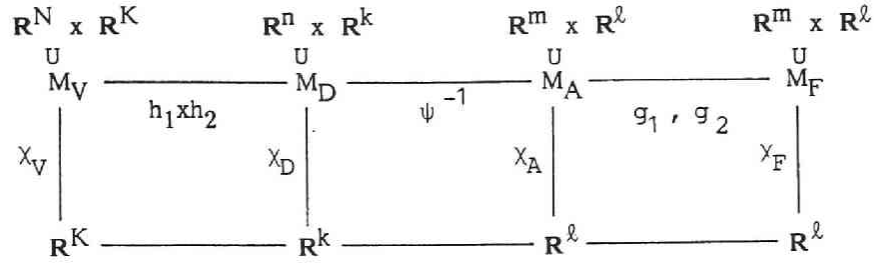

Fig. 1.2.2 Relationship among Four Potential Functions.

1.3 Numerical Formulation

1.3.1 General remarks

In the system, the generalized coordinates describing the state variables will correspond to nodal displacements, and the external control parameters to a loading parameter and nodal initial displacements. That is,

$$\Lambda_o = \Lambda \ , \quad \Lambda_j = \bar{w}_{j+1} \ (j=1,\ldots,K-1) \qquad (N=K+1) \qquad (1.3.1)$$

Let u_i, w_j, $P^u_i(\Lambda)$ and $P^w_j(\Lambda)$ denote the nodal in-plane and out-of-plane displacements, and the equivalent nodal in-plane and out-of-plane forces, respectively. The latter two forces are assumed to be known as linear functions of a single loading parameter $\Lambda_o = \Lambda$ in the fundamental case of instability problems in civil engineering. An explicit form of the potential function including implicit function of the loading parameter can be written as[14]

$$\begin{aligned} U &= U(u_i, w_j, \Lambda, \bar{w}_k) \\ &= \tfrac{1}{2} K^P_{ij} u_i u_j + \tfrac{1}{2} K^B_{ij} w_i w_j + K^S_{ij} u_i w_j + K^{PB}_{kij} u_k w_i \bar{w}_j + \tfrac{1}{2} K^{PB}_{kij} u_k w_i w_j \\ &+ K^{SS}_{ijk} \bar{w}_i w_j w_k + \tfrac{1}{2} K^{SS}_{ijk} w_i w_j w_k + \tfrac{1}{2} K^{BB}_{ijk\ell} \bar{w}_i \bar{w}_j w_k w_\ell \\ &+ \tfrac{1}{2} K^{BB}_{ijk\ell} \bar{w}_i w_j w_k w_\ell + \tfrac{1}{8} K^{BB}_{ijk\ell} w_i w_j w_k w_\ell - P^u_i(\Lambda) u_i - P^w_i(\Lambda) w_i \end{aligned} \qquad (1.3.2)$$

Here, K^P_{ij}, K^B_{ij}, K^S_{ij}, K^{SS}_{ijk}, K^{PB}_{kij} and $K^{BB}_{ijk\ell}$ are constants determined in terms of the geometry of the structure and the mechanical properties. Their superscripts "P" and "B" refer to the in-plane and out-of-plane stiffnesses, respectively. Moreover, the superscript "S" refers to the asymmetric stiffnesses of eccentric stiffeners. The symmetric stiffnesses of the stiffeners are included in these stiffnesses with the superscripts P and B.

Using the principle of virtual work on Eq. (1.3.2), a set of basic equations of equilibrium can be derived considering the potential, U, in a form similar to the nonlinear equations:

$$\begin{Bmatrix} \frac{\partial U}{\partial u_i} \\ \\ \frac{\partial U}{\partial w_j} \end{Bmatrix} = \left[\begin{array}{c|c} K^{uu}_{im} & K^{uw}_{in} \\ \hline K^{wu}_{jm} & K^{ww}_{jn} \end{array}\right] \begin{Bmatrix} u_m \\ \\ w_n \end{Bmatrix} + \frac{1}{2} \begin{Bmatrix} Q^u_i \\ \\ Q^w_j \end{Bmatrix} + \frac{1}{6} \begin{Bmatrix} 0 \\ \\ C^w_j \end{Bmatrix} - \begin{Bmatrix} P^u_i(\Lambda) \\ \\ P^w_j(\Lambda) \end{Bmatrix} = \begin{Bmatrix} 0 \\ \\ 0 \end{Bmatrix} \tag{1.3.3}$$

where

$$K^{uu}_{im} = K^{P}_{im} \ , \qquad K^{uw}_{in} = K^{wu}_{ni} = K^{PB}_{inr}\bar{w}_r + K^{S}_{in} \ ,$$

$$K^{ww}_{jn} = K^{B}_{jn} + K^{BB}_{jnqs}\bar{w}_q\bar{w}_s + K^{SS}_{jnk}\bar{w}_k + K^{SS}_{njk}\bar{w}_k$$

and

$$Q^u_i = K^{PB}_{inr}w_n w_r \ , \qquad Q^w_j = Q^{wu}_j + Q^{ww}_j \ ,$$

$$Q^{wu}_j = 2\, K^{PB}_{mj\ell}u_m w_\ell \ ,$$

$$Q^{ww}_j = 3\, K^{BB}_{jnqs}\bar{w}_n w_q w_s + (K^{SS}_{jnk} + 2\, K^{SS}_{njk})w_k w_n \ ,$$

$$C^w_j = 3\, K^{BB}_{jnqs}w_n w_q w_s \ .$$

Moreover, let Q^u_i, Q^w_j and C^w_j refer to the quadratic pseudo forces in the in-plane and out-of-plane directions, and the cubic pseudo-force in the out-of-plane direction, respectively.

Whether or not the discretization method is legitimate will depend on how and to what extent the singularities can be realized numerically. Then, the critical loads, the buckling modes and the load-displacement relationships will serve as good measures in this respect. Fujii and Yamaguchi have discussed mathematically the numerical realization of the nonlinear behaviors in a Hilbert space[7,8]. Also, for square plates in in-plane compression with and without initial deflections, the load-deflection curves provide good numerical realizations of the nonlinear buckling behaviors by Tateishi, Kageyama, Yamaki and Nomura[26-31].

1.3.2 Potential function V

Here, in this dissertation, consider buckling problems of slender structures with respect to the out-of-plane nodal displacements under in-plane compressive loading controlled by only a single loading parameter $\Lambda_o = \Lambda$. Then, through the **static condensation** procedure as stated in the previous section, in other words, eliminating the in-plane displacements, u_i.

For this purpose, firstly, the in-plane equilibrium equations in Eq. (1.3.3) lead to the in-plane displacement solutions expressed in terms of the out-of-plane displacements and the loading parameter

$$u_j = F_{jm}P^u_m(\Lambda) - F_{jm}K^S_{mk}w_k - F_{jm}K^P_{m\,k\ell}\overline{w}_k w_\ell - \frac{1}{2}F_{jm}K^P_{m\,k\ell}w_k w_\ell \qquad (1.3.4)$$

where

$$F_{jm} = (K^P_{mj})^{-1}$$

that is, F_{jm} refers to the inverse matrix of the in-plane linear stiffness matrix K^P_{mj}.

Now, two types of in-plane controls are taken into account in the post-bifurcation range: (A) load-control and (B) displacement-control. For example, in case of buckling problem of axially compressed rectangular plate structures, the former control means that the resultant axial in-plane displacement components are linearly distributed in the axial direction; whereas the latter means that the axial in-plane displacement components on the loaded edges remain straightly with their prescribed amplitudes.

Then, the two control types are assigned by difference of evaluation of the in-plane nodal forces: The load-control is

$$\text{(A)}\quad P^u_m(\Lambda) = \Lambda P^u_{om} \qquad (m=1,\ldots,M) \qquad (1.3.5a)$$

where P^u_{om} refers to the mode of the in-plane nodal forces prescribed. While, the displacement-control is

$$\text{(B)}\quad P^u_m(\Lambda) = \Lambda P^u_{om} + \rho_m \qquad (m=1,\ldots,M) \qquad (1.3.5b)$$

where ρ_m denotes the magnitude of the nodal forces due to the constrained in-plane displacements whose number is designated as M_c, and

$$\rho_m \neq 0 \qquad (m=\alpha=1,\ldots,M_c)\,, \qquad \rho_m = 0 \qquad \text{(others)} \qquad (1.3.5c)$$

Furthermore, Λ refers to the single loading parameter as stated above, and however each has significantly physical difference under condition of (A) or (B). In the case of the load-control type (A), the parameter Λ indicates the magnitude of uniform applied load itself. Whereas, under the displacement-control (B), the parameter Λ represents the magnitude of a part of uniform load in the response of constrained in-plane displacements. Also, in which, the equivalent out-of-plane nodal force is assumed to be written as

$$P^w_m(\Lambda) = \Lambda P^w_{om} \qquad (m=1,\ldots,N) \qquad (1.3.6)$$

for both control types of (A) and (B).

Apparently, it is found that the type (B) may involve the type (A) when M_c=0. Hence, hereafter, this numerical formulation will be accomplished for only the type (B).

Let the assigned condition of M_c constrained in-plane displacements be given

by

$$u_\alpha = f_{\alpha m} u_m \qquad (\alpha = 1,\ldots,M_c;\ \alpha \neq m;\ m = 1,\ldots,M_b) \tag{1.3.7}$$

where M_b refers to the number of nodes with known equivalent in-plane forces.

Upon substitution of Eqs. (1.3.4) and (1.3.5b) into Eq. (1.3.7), the constrained nodal forces ρ_α are obtained as

$$\rho_\alpha = G_{\alpha k} K^S_{k\ell} w_\ell + \tfrac{1}{2} G_{\alpha k} K^{PB}_{k\ell m} w_\ell w_m + G_{\alpha k} K^{PB}_{k\ell m} \bar{w}_\ell w_m - \Lambda G_{\alpha k} P^u_{ok} \qquad (\alpha = 1,\ldots,M_c) \tag{1.3.8}$$

where

$$G_{\alpha k} = H^*_{\alpha\beta} H_{\beta k} \qquad (\alpha, \beta = 1,\ldots,M_c;\ k = 1,\ldots,M)$$

$$H^*_{\alpha\beta} = (H_{\beta\alpha})^{-1} \qquad (\alpha, \beta = 1,\ldots,M_c)$$

$$H_{\alpha m} = F_{\alpha m} - f_{\alpha p} F_{pm} \qquad (\alpha = 1,\ldots,M_c;\ m = 1,\ldots,M;\ \alpha \neq p;\ p = 1,\ldots,M_b)$$

Using Eqs. (1.3.8) and (1.3.5b), Eq. (1.3.4) can be rewritten as

$$u_j = \Lambda F^*_{jm} P^u_{om} - F^*_{jm} K^S_{mk} w_k - F^*_{jm} K^{PB}_{mk\ell} \bar{w}_k w_\ell - \tfrac{1}{2} F^*_{jm} K^{PB}_{mk\ell} w_k w_\ell \qquad (j = 1,\ldots,M) \tag{1.3.9}$$

where

$$F^*_{jm} = F_{jm} - F_{j\alpha} G_{\alpha m} \qquad (j,m = 1,\ldots,M;\ \alpha = 1,\ldots,M_c)$$

It is apparently shown that the difference between the conditions of (A) and (B) results in that between the forms of F_{jm} in Eq. (1.3.4) and F^*_{jm} in Eq. (1.3.9). Therefore, Eq. (1.3.9) includes Eq. (1.3.4) under the condition (A); $\rho_m = 0$ $(m = 1,\ldots,M)$ and $M_c = 0$. The difference of the control types of (A) and (B) leads to that of the explicit expression of the potential function. This will be discussed in the subsequent chapter 4 of this PART II in details.

Upon substitution of Eq. (1.3.9) into the out-of-plane equilibrium equations of Eq. (1.3.3), the **static condensation** procedure is completely accomplished. Then, a set of equations of equilibrium with only the out-of-plane nodal displacements, w_i, the loading parameter Λ and the initial out-of-plane nodal displacements, $\bar{w}_i$ can be determined. Thus, the condensed potential function $V(w_i, \Lambda, \bar{w}_i)$ can be defined as a function of solely the out-of-plane displacements, w_i, for prescribed Λ and $\bar{w}_j$ such that its equilibrium equations are given by

$$V_i = \frac{\partial V}{\partial w_i} = -\Lambda K^G_{ij} \bar{w}_j + (K^B_{ij} - K^{SP}_{ij} - \Lambda K^G_{ij}) w_j$$

$$+ \left(K^{SS}_{jik} + K^{SS}_{kij} - K^{SPB}_{jik} - K^{SPB}_{kij} \right) \bar{w}_j w_k$$

$$+ \frac{1}{2} \left(K^{SS}_{ijk} + 2\, K^{SS}_{kij} - K^{SPB}_{ijk} - 2\, K^{SPB}_{kij} \right) w_j w_k$$

$$+ K^{BB}_{ijk\ell} \left(\bar{w}_j \bar{w}_k w_\ell + \frac{3}{2} \bar{w}_j w_k w_\ell + \frac{1}{2} w_j w_k w_\ell \right)$$

$$- K^{BPB}_{ijk\ell} \left(\bar{w}_j \bar{w}_k w_\ell + \frac{1}{2} \bar{w}_j w_k w_\ell + w_j \bar{w}_k w_\ell + \frac{1}{2} w_j w_k w_\ell \right) = 0$$

$$(i=1,\ldots,N) \qquad (1.3.10)$$

where

$$K^{G}_{ij} = - K^{PB}_{mij} F^{*}_{mn} P^{u}_{on} , \qquad K^{SP}_{ij} = K^{S}_{mi} F^{*}_{mn} K^{S}_{nj} ,$$

$$K^{SPB}_{ijk} = K^{S}_{mi} F^{*}_{mn} K^{PB}_{njk} , \qquad K^{BPB}_{ijk\ell} = K^{PB}_{mij} F^{*}_{mn} K^{PB}_{nk\ell} ,$$

and herein, the following condition is postulated:

$$R_i - P^{w}_{oi} = 0 \qquad (i=1,\ldots,N)$$

where

$$R_i = K^{S}_{mi} F^{*}_{mn} P^{u}_{on}$$

For a symmetric structural system with respect to the essential out-of-plane displacements, this assumption may be clearly identified since $K^{S}_{ij}=0$ and $K^{SS}_{ijk}=0$. While, for an asymmetric system, the condition may play an important role, In other words, the latter case says that the associated instability may occur on the trivial equilibrium path $(w_i, \Lambda, \bar{w}_i)=(0, \Lambda, 0)$ for any Λ, and furthermore, that the potential function V, whose derivative with respect to w_i can be evaluated from Eq. (1.3.10), may be equivalent to a perturbation of V of Eq. (I-1.3.4). Also, it is clearly found that the equilibrium surface M_V as defined by Eq. (1.2.5) can be explicitly given by Eq. (1.3.10).

1.3.3 Potential function D

Now, consider linear terms of Eq. (1.3.10)

$$\left(K^{B}_{ij} - K^{SP}_{ij} - \Lambda K^{G}_{ij} \right) w_j = 0 \qquad (i,j=1,\ldots,N) \qquad (1.3.11)$$

which present an eigenvalue problem on the lowest value Λ^c of the loading parameter Λ and the associated eigenvector being the lowest instability mode of the out-of-plane displacements. Let Φ_{ij} take the eigenvector matrix, composed of n eigenvectors corresponding to n lower essential eigenvalues[29]. Then, a linear transformation is defined as

$$w_i = \Phi_{ij} v_j \qquad (i=1,...,N;\ j=1,...,n;\ n<<N) \qquad (1.3.12)$$

This is an explicit expression of the Affine transformation h_1 in Eq. (1.2.9). The transformation is **diffeomorphic**, topologically derived from the mapping theory[15,32]. Then, the mapping h_1 is shown to be one-to-one correspondent. Moreover, for the control parameters, another transformation h_2 in Eq. (1.2.10) is taken into account similarly to h_1 in Eqs. (1.2.9) and (1.3.12).

Let λ_j designate the generalized initial displacement transformed through Eq. (1.3.12) from $\bar{w}_i$. Each λ_j corresponds to v_j, and was designated as ε_j in the previous section 1.4 in the PART I. Then, the following transformation can be made with respect to the control parameters:

$$h_2 : \lambda = (\lambda_0, \lambda_1, ..., \lambda_{k-1}) \rightarrow \Lambda = (\Lambda_0, \Lambda_1, ..., \Lambda_{K-1}) \qquad (1.3.13)$$

where

$$\Lambda_o = \Lambda_o^c + \lambda, \qquad \Lambda_i = \bar{w}_{i+1} \qquad (i=1,...,K-1;\ K=N+1)$$

$$\Lambda_o^c = \Lambda^c, \qquad \lambda_o = \lambda \quad ,$$

$$\bar{w}_i = \Phi_{ij} \lambda_j \qquad (i=1,...,N;\ j=1,...,k-1;\ K=N+1;\ k=n+1)$$

Now, let us define a new potential D so that

$$D(v_i, \lambda_j) \cong V(w_i, \Lambda_j) \qquad (1.3.14)$$

Through Eq. (1.3.12), the first partial differentiation of D with respect to yields:

$$D_i = \frac{\partial D}{\partial v_i} = V_j \Phi_{ji} = 0 \qquad (i=1,...,n) \qquad (1.3.15)$$

The explicit form of D_i is given by the product of the right hand side of Eq. (1.3.10) and Φ_{ji}, where w_i has been expressed in terms of v_j by Eq. (1.3.12). That is, equations of equilibrium of the potential function D are written in the form similar to Eq. (1.3.10):

$$D_i = \frac{\partial D}{\partial v_i} = -(\Lambda^c + \lambda)\tilde{K}^G_{ij}\lambda_j + [\tilde{K}^B_{ij} - \tilde{K}^{SP}_{ij} - (\Lambda^c + \lambda)\tilde{K}^G_{ij}]v_j$$

$$+ [\tilde{K}^{SS}_{ijk} + \tilde{K}^{SS}_{kij} - \tilde{K}^{SPB}_{ijk} - \tilde{K}^{SPB}_{kij}]\lambda_j v_k$$

$$+ \frac{1}{2}[\tilde{K}^{SS}_{ijk} + 2\tilde{K}^{SS}_{kij} - \tilde{K}^{SPB}_{ijk} - 2\tilde{K}^{SPB}_{kij}]v_j v_k$$

$$+ \tilde{K}^{BB}_{ijk\ell}[\lambda_j\lambda_k v_\ell + \frac{3}{2}\lambda_j v_k v_\ell + \frac{1}{2} v_j v_k v_\ell]$$

$$- \hat{K}^{BPB}_{ijk\ell} [\ \lambda_j\lambda_k v_\ell + \frac{1}{2}\lambda_j v_k v_\ell + v_j\lambda_k v_\ell + \frac{1}{2} v_j v_k v_\ell\ ]$$

(i=1,...,n) (1.3.16)

where

$$\hat{K}^{G}_{ij} = K^{G}_{mn}\Phi_{mi}\Phi_{nj}\ ,\qquad \hat{K}^{B}_{ij} = K^{B}_{mn}\Phi_{mi}\Phi_{nj}\ ,$$

$$\hat{K}^{SP}_{ij} = K^{SP}_{mn}\Phi_{mi}\Phi_{nj}\ ,\qquad \hat{K}^{SS}_{ijk} = K^{SS}_{mnp}\Phi_{mi}\Phi_{nj}\Phi_{pk}\ ,$$

$$\hat{K}^{SPB}_{ijk} = K^{SPB}_{mnp}\Phi_{mi}\Phi_{nj}\Phi_{pk}\ ,$$

$$\hat{K}^{BB}_{ijk\ell} = K^{BB}_{mnpq}\Phi_{mi}\Phi_{nj}\Phi_{pk}\Phi_{q\ell}\ ,$$

$$\hat{K}^{BPB}_{ijk\ell} = K^{BPB}_{mnpq}\Phi_{mi}\Phi_{nj}\Phi_{pk}\Phi_{q\ell}\ .$$

Furthermore, more than the second order derivatives are feasibly obtained by evaluating them at the critical point as follows:

The quadratic terms are

$$D_{ij} = \frac{\partial^2 D}{\partial v_i \partial v_j} = \hat{K}^{B}_{ij} - \hat{K}^{SP}_{ij} - (\Lambda^c + \lambda)\hat{K}^{G}_{ij}$$

$$+ [\ \hat{K}^{SS}_{ijk} + \hat{K}^{SS}_{jik} - \hat{K}^{SPB}_{ijk} - \hat{K}^{SPB}_{jik}\ ]\lambda_k$$

$$+ [\ \hat{K}^{SS}_{ijk} + \hat{K}^{SS}_{kij} + \hat{K}^{SS}_{jik} - \hat{K}^{SPB}_{ijk} - \hat{K}^{SPB}_{kij} - \hat{K}^{SPB}_{jik}\ ] v_k$$

$$+ \hat{K}^{BB}_{ijk\ell}[\ \lambda_k\lambda_\ell + 3\lambda_k v_\ell + \frac{3}{2} v_k v_\ell\ ]$$

$$- \hat{K}^{BPB}_{ikj\ell}\lambda_k\lambda_\ell - \frac{1}{2}[\ 2\hat{K}^{BPB}_{ijk\ell} + 3\hat{K}^{BPB}_{i\ell kj} + \hat{K}^{BPB}_{ikj\ell}\ ]\lambda_k v_\ell$$

(i,j=1,...,n) (1.3.17a)

The cubic terms are

$$D_{ijk} = \frac{\partial^3 D}{\partial v_i \partial v_j \partial v_k} = \hat{K}^{SS}_{ijk} + \hat{K}^{SS}_{kij} + \hat{K}^{SS}_{jik}$$

$$- \hat{K}^{SPB}_{ijk} - \hat{K}^{SPB}_{kij} - \hat{K}^{SPB}_{jik} + 3\hat{K}^{BB}_{ijk\ell}\lambda_\ell + 3\hat{K}^{BB}_{ijk\ell} v_\ell$$

$$- \frac{1}{2}[\ 2\hat{K}^{BPB}_{ijk\ell} + 3\hat{K}^{BPB}_{ikj\ell} + \hat{K}^{BPB}_{i\ell jk}\ ]\lambda_\ell$$

$$- [\ \tilde{K}^{BPB}_{ijk\ell} + \tilde{K}^{BPB}_{ikj\ell} + \tilde{K}^{BPB}_{i\ell jk}\ ]v_\ell$$

$$(i,j,k=1,...n) \qquad (1.3.17b)$$

The quartic terms are

$$D_{ijk\ell} = \frac{\partial^4 D}{\partial v_i \partial v_j \partial v_k \partial v_\ell} = 3\ \tilde{K}^{BB}_{ijk\ell} - [\ \tilde{K}^{BPB}_{ijk\ell} + \tilde{K}^{BPB}_{ikj\ell} + \tilde{K}^{BPB}_{i\ell jk}\ ]$$

$$(i,j,k,\ell=1,...,n) \qquad (1.3.17c)$$

1.3.4 Potential function A

Let the corank of the Hessian matrix D_{ij} be m. In other words, let us assume an m-fold coincident buckling. Then, from Eq. (1.2.13) and the Implicit Function Theorem, it has been shown that the inessential modes, v_α (α =m+1,...,n), can be expressed in terms of the control parameters and the essential modes, v_i(i=1,...,m), after some reordering in the form of Eq. (1.2.14).

Upon substitution of these expressions into Eq. (1.3.15) or (1.3.16), a new potential A can be defined through the Implicit Function Theorem by the following equation.

$$A(v_i,\ \lambda_j) = D[v_i, v_\alpha(v_j,\ \lambda_k),\ \lambda_\ell\ ] \qquad (1.3.18)$$

where the Roman and Greek subscripts on v refer to the essential and inessential modes, respectively.

The substitution of v_α (α=m+1,...,n) into the equilibrium equations D_α=0 will yield the identities:

$$D_\alpha\ [v_i, v_\alpha(v_j,\ \lambda_k),\ \lambda_\ell\ ] = 0 \qquad (\alpha=m+1,...,n) \qquad (1.3.19)$$

The left-hand side now represents a function of totally (m+k) independent variables. Thus, the relationships between two potential functions of D and A can be easily obtained in Eqs. (I-1.3.19) of the PART I.

As mentioned in the chapter 1 of the PART I, an explicit expression of the potential function A can be determined by the Taylor expansion about the critical point $(v_i,\ \lambda\ ,\ \lambda_j)$=(0,0,0) For any small perturbations of control parameters (λ, λ_j) in a neighborhood of the zero (0,0), the Taylor expansion of the potential function $A(v_i,\ \lambda\ ,\ \lambda_j)$ can be explicitly determined similarly to Eqs. (I-1.3.20), using the relationships between D and A as follows:

$$A(v_i,\ \lambda\ ,\ \lambda_j) = A_i(\ \lambda\ ,\ \lambda_j)v_i + \frac{1}{2}\ A_{ij}(\ \lambda\ ,\ \lambda_k)v_iv_j$$

$$+ \frac{1}{6}\ A_{ijk}(\ \lambda\ ,\ \lambda_\ell\ )v_iv_jv_k + \frac{1}{24}\ A_{ijk\ell}(\ \lambda,\ \lambda_m)v_iv_jv_kv_\ell \qquad (1.3.20)$$

where each coefficient is evaluated at the origin $v_i=0$ in the following form:

$$A_i(\lambda, \lambda_j) = \frac{\partial A}{\partial v_i}\Big|_{v_i=0} = -(\Lambda^c + \lambda)\hat{K}^G_{ij}\lambda_j = A_i^{jc}\lambda_j \quad (j\neq 0) \qquad (i=1,\ldots,m)$$

$$A_i^{jc} = \frac{\partial^2 A}{\partial v_i \partial \lambda_j}\Big|_{(v_i,\lambda,\lambda_j)=(0,0,0)} = -\Lambda^c \hat{K}^G_{ij} \quad (j\neq 0) \qquad (i,j=1,\ldots,m)$$

$$\begin{aligned} A_{ij}(\lambda, \lambda_j) &= \frac{\partial^2 A}{\partial v_i \partial v_j}\Big|_{v_i=0} = \hat{K}^G_{ij} - \hat{K}^{SP}_{ij} - (\Lambda^c + \lambda)\hat{K}^G_{ij} \\ &\quad + [\hat{K}^{SS}_{ijk} + \hat{K}^{SS}_{jik} - \hat{K}^{SPB}_{ijk} - \hat{K}^{SPB}_{jik}]\lambda_k \\ &\quad + [\hat{K}^{BB}_{ijk\ell} - \hat{K}^{BPB}_{ijk\ell}]\lambda_k\lambda_\ell \\ &= A^c_{ij} + A^{oc}_{ij}\lambda + A^{kc}_{ij}\lambda_k \quad (k\neq 0) \end{aligned} \qquad (i,j=1,\ldots,m)$$

$$A^c_{ij} = \hat{K}^B_{ij} - \hat{K}^{SP}_{ij} - \Lambda^c \hat{K}^G_{ij}, \qquad (i,j=1,\ldots,m)$$

$$A^{oc}_{ij} = \frac{\partial^3 A}{\partial v_i \partial v_j \partial \lambda}\Big|_{(v_i,\lambda,\lambda_j)=(0,0,0)} = -\hat{K}^G_{ij}, \qquad (i,j=1,\ldots,m)$$

$$\begin{aligned} A_{ijk}(\lambda, \lambda_\ell) &= \frac{\partial^3 A}{\partial v_i \partial v_j \partial v_k}\Big|_{v_i=0} = \hat{K}^{SS}_{ijk} + \hat{K}^{SS}_{kij} + \hat{K}^{SS}_{jik} \\ &\quad - \hat{K}^{SPB}_{ijk} - \hat{K}^{SPB}_{kij} - \hat{K}^{SPB}_{jik} \\ &\quad + (3\hat{K}^{BB}_{ijk\ell} - \hat{K}^{BPB}_{ijk\ell} - \hat{K}^{BPB}_{ikj\ell} - \hat{K}^{BPB}_{i\ell jk}] \\ &= A^c_{ijk} + A^{\ell c}_{ijk}\lambda_\ell \quad (\ell\neq 0) \end{aligned} \qquad (i,j,k=1,\ldots,m)$$

$$\begin{aligned} A^c_{ijk} &= \frac{\partial^3 A}{\partial v_i \partial v_j \partial v_k}\Big|_{(v_i,\lambda,\lambda_j)=(0,0,0)} = \hat{K}^{SS}_{ijk} + \hat{K}^{SS}_{kij} + \hat{K}^{SS}_{jik} \\ &\quad - \hat{K}^{SPB}_{ijk} - \hat{K}^{SPB}_{kij} - \hat{K}^{SPB}_{jik} \end{aligned} \qquad (i,j,k=1,\ldots,m)$$

$$A^{\ell c}_{ijk} = \frac{\partial^4 A}{\partial v_i \partial v_j \partial v_k \partial \lambda_\ell}\Big|_{(v_i,\lambda,\lambda_j)=(0,0,0)} = 3\hat{K}^{BB}_{ijk\ell} - [\hat{K}^{BPB}_{ijk\ell} + \frac{3}{2}\hat{K}^{BPB}_{ikj\ell} + \frac{1}{2}\hat{K}^{BPB}_{i\ell jk}]$$

$$(i,j,k,\ell=1,\ldots,m)$$

$$A_{ijk\ell}(\lambda, \lambda_j) = \frac{\partial^4 A}{\partial v_i \partial v_j \partial v_k \partial v_\ell}\Big|_{v_i=0}$$

$$= 3\,\overset{\gamma BB}{K}_{ijk\ell} - [\,\overset{\gamma BPB}{K}_{ijk\ell} + \overset{\gamma BPB}{K}_{ikj\ell} + \overset{\gamma BPB}{K}_{i\ell jk}]$$

$$= A^c_{ijk\ell} = \frac{\partial^4 A}{\partial v_i \partial v_j \partial v_k \partial v_\ell}\Big|_{(v_i,\lambda,\lambda_j)=(0,0,0)} \qquad (i,j,k,\ell=1,\ldots,m)$$

in which the superscript "C" denotes the critical point $(v_i, \lambda, \lambda_j)=(0,0,0)$.

This potential function forms a family of potential functions by perturbing λ and λ_j near the zero (0,0), and itself means an universal unfolding of the associated one when $(\lambda, \lambda_j)=(0,0)$ as briefly mentioned in the chapter I-2. Then, neglect more than the second order terms of control parameters of λ and λ_j, and for their fixed value near the origin (0, 0), a canonical form of a family of potential functions can be obtained as

$$A(v_i, \lambda, \lambda_j) = \frac{1}{24}A^c_{ijk\ell}v_iv_jv_kv_\ell + \frac{1}{6}A^{\ell c}_{ijk}\,v_iv_jv_k\lambda_\ell$$

$$+ \frac{1}{6}A^c_{ijk}v_iv_jv_k + \frac{1}{2}A^c_{ij}v_iv_j + \frac{1}{2}A^{oc}_{ij}\lambda v_iv_j$$

$$+ \frac{1}{2}A^{kc}_{ij}v_iv_j\lambda_k + A^{jc}_{i}v_i\lambda_j \qquad (1.3.21)$$

where the terms $\lambda v_i \lambda_j$ and $v_iv_jv_k\lambda_\ell$ disappear since they may be higher order than the remainder terms in Eq. (1.3.21), in other words, more than the second order terms of control parameters (λ, λ_j) are neglected herein. From the quadratic terms $A^c_{ij}(\lambda, \lambda_j)$ in Eq. (1.3.20) and A^{oc}_{ij} in Eq. (1.3.21), the following significant eigenvalue problem can be defined at the critical point $(v_i, \lambda, \lambda_j)=(0,0,0)$:

$$\det\,[\,\overset{\gamma B}{K}_{ij} - \overset{\gamma SP}{K}_{ij} - \Lambda^c\overset{\gamma G}{K}_{ij}\,] = 0 \qquad (1.3.22)$$

which presents peculiar eigenvalues Λ^c corresponding to the m-fold primary modes of bifurcation buckling. The lowest eigenvalue among them is called the primary buckling load of the structure considered, and it is rewritten as Λ^c hereafter.

Also, this typical form* of the potential function A can be derived from the **universal unfolding** of the singularity theory of mappings in the PART I-2[20,21,25]. These concepts are briefly interpreted in the previous PART I. Some numerical illustrations using the numerical formulation of catastrophe analysis by discretization and modal transforms will be demonstrated in the subsequent chapters.

---

* See, APPENDIX B in this PART II. APPENDIX B summerizes the relationships between the structural potential function and the Thom's unfolding using some diffeomrohisms.

1.4 Conclusions

This chapter presents a numerical formulation of catastrophe analysis in order to evaluate static instabilities of multi-degree-of-freedom structural systems in civil engineering field. The main conclusions are:

(1) The present procedure makes use of discretization methods such as a finite element method and a simplified element method, and also of several modal transformations.

(2) The method finally leads to the determination of the canonical form of potential function by means of evaluating the Taylor coefficients at the critical point of the associated instability in the light of the Thom and Thompson's theories.

(3) The instability phenomena for the original potential function with the multiple state variables can be numerically realized as those for either of the Thom's seven elementary catastrophes with one or two state variables through some diffeomorphisms.

(4) The proposed procedure can be mainly applied to bifurcation problems having no prebuckling equilibrium solutions. Then, several features of bifurcation, postbuckling and imperfection sensitivity will be predicted herein.

(5) It is clearly found that this method will be also applicable to the common instability problems with linear or nonlinear prebuckling equilibrium solution, since the solution can be regarded as the fundamental one, that is, its potential function can be defined as a perturbation from the fundamental state.

(6) Some numerical demonstrations will be performed in the subsequent chapters in this PART II on the typical civil engineering structures or structural elements such as columns, plates and stiffened plates.

Bibliographies of Chapter 1 in PART II

1) Konishi,I. (ed.), Steel Bridges, Volume I. Maruzen, 1977 (in Japanese).
2) Thom,R., Structural Stability and Morphogenesis (translated from the French by D.H. Fowler). Benjamin, 1975.
3) Thompson,J.M.T. and G.W.Hunt, A General Theory of Elastic Stability. John Wiley & Sons, 1973.
4) Thompson,J.M.T., Instabilities and Catastrophes in Science and Engineering. John Wiley & Sons, 1982.
5) Hilton,P.(ed.), Structural Stability, the Theory of Catastrophes, and Applications in the Sciences. Lecture Notes in Mathematics, No. 525, Springer-Verlag, 1976.
6) Lu,Y.-C., Singularity Theory and an Introduction to Catastrophe Theory, 2nd Correcting Printing. Springer-Verlag, 1976.
7) Fujii,H. and M.Yamaguchi, Simple buckling - a group theoretical introduction -. Report of Study on the Theory and Numerical Analysis of Stability, Bifurcation and Buckling in Non-Linear Theory of Elasticity, Research Institute for Mathematical Sciences, Kyoto University, pp. 1-28, 1979.

8) Fujii,H. and M.Yamaguchi, Structure of singularities and its numerical realization in nonlinear elasticity. Journal of Mathematics of Kyoto University., Vol. 20, pp. 489-590, 1980.
9) Hutchinson,J.W. and W.T.Koiter, Post-buckling theory. Applied Mechanics Reviews, Vol. 23, pp. 1353-1366, 1970.
10) Koiter,W.T., Over de Stabiliteit van het Elastische Evenwicht. Thesis, Delft, 1945 (English translations: On the Stability of Elastic Equilibrium. NASA Technical Transactions, F10, 833, National Aeronautics and Space Administration, 1967 and Technical Report AFFDL-TR-70-25, Air Force Flight Laboratory, 1970).
11) Thompson,J.M.T. and G.W.Hunt, Elastic Instability Phenomena. John Wiley & Sons, 1984.
12) Zeeman,E.C., Catastrophe Theory: Selected Papers 1972-1977. Addison-Wesley, 1977.
13) Watanabe,E. and Y.Yamada, On the behavior and ultimate strength of longitudinally stiffened flanges of steel box girders. Proceedings of the Japan Society of Civil Engineers, No. 252, pp. 127-142, 1976.
14) Watanabe,E. and Y.Yamada, Compressive strength of plates with close-sectional ribs. Proceedings of the Japan Society of Civil Engineers, No. 278, pp. 133-147, 1978.
15) Niwa,Y., E.Watanabe and H.Isami, Catastrophe analysis of structures by discretization and modal transforms. Memoirs of the Faculty Engineering, Kyoto University, Vol. 43, pp. 67-87, 1981.
16) Isami,H., Applications of Catastrophe Theory to Static Instabilities of Structures by Discretization and Modal Transforms. Thesis presented to the Faculty of Engineering of Kyoto University in partial fulfillment of the requirements for Master of Engineering, 1980 (in Japanese).
17) Niwa,Y., E.Watanabe and H.Isami, Catastrophes of elastic column structures. Memoirs of the Faculty of Engineering, Kyoto University, Vol. 45, pp. 71-97, 1983.
18) Isami,H., A topological aspect of imperfection sensitivity of structures. Bulletin of Kohchi Technical College, No. 20, pp. 85-94, 1984.
19) Niwa,Y., E.Watanabe and H.Isami, On prediction of large deflection of compressed rectangular plates by catastrophe theory. Proceedings of Structural Mechanics, Vol. 31A, pp. 25-35, 1985 (in Japanese).
20) Gilmore,R., Catastrophe Theory for Scientists and Engineers. John Wiley & Sons, 1981.
21) Poston,T. and I.Stewart, Catastrophe Theory and Its Applications. Pitman, 1978.
22) Lander,L., Differential Germs and Catastrophes. London Math. Soci. Lecture Notes, No. 17, Cambridge University Press, 1975.
23) Thompson,J.M.T. and G.W.Hunt, Towards a unified bifurcation theory. Journal of Applied Mathematics and Physics (Zeitschrift für Angewandte Mathematik und Physik), Vol. 26, pp. 581-603, 1975.
24) Hunt,G.W., Imperfection-sensitivity of semi-symmetric branching. Proceedings of the Royal Society of London, Series A, Vol. 357, pp. 193-211, 1977.
25) Noguchi,H. and T.Fukuda, Elementary Catastrophes. Kyoritsu-Zensho, No. 208, 1976 (in Japanese).
26) Tateishi,A., A study on the Utilization of Static Instability Analysis by a Discretization Method. Thesis presented to the Faculty of Engineering of Kyoto University in partial fulfillment of the requirements for Master of Engineering, 1980 (in Japanese).

27) Kageyama,M., A Study on the Utilization of Geometrical and Material Nonlinear Analysis. Thesis presented to the Faculty of Engineering of Kyoto University in partial fulfillment of the requirements for Master of Engineering, 1980 (in Japanese).
28) Yamaki,N., Postbuckling behaviour of rectangular plates with small initial curvature loaded in edge compression. Journal of Applied Mechanics, Transactions of American Society of Mechanical Engineers, Vol. 26, pp. 407-414, 1959.
29) Bathe,K.J., Numerical Methods in Finite Element Analysis. Prentice-Hall, 1976.
30) Hirao,T., Fundamental Study on the Utilization of Elasto-Plastic Large-Deflection Nonlinear Analysis. Thesis presented to the Faculty of Engineering of Kyoto University in partial fulfillment of the requirements for the degree of Bachelor of Engineering, 1981 (in Japanese).
31) Nomura,T., A Study on the Utilization of Elasto-plastic Large-Deflection Analysis of Plate Structures. Thesis presented to the Faculty of Engineering of Kyoto University in partial fulfillment of the requirements for the degree of Master of Engineering, 1985 (in Japanese).
32) Watanabe,E., A Study on the Catastrophe and Static Load-Carrying Capacity of Structures. Thesis presented to the Graduate Faculty of Kyoto University in partial fulfillment of the requirements for the degree of Doctor of Engineering, 1986.

CHAPTER 2

EVALUATION ALGORITHM OF IMPERFECTION SENSITIVITY

2.1 General Remarks

Several comprehensive studies on the relationship between the general elastic bifurcation theory and the catastrophe theory have been developed by Thompson and Hunt. They revealed that an elastic structural instability under conservative loading can be classified in the form of either of Thom's seven elementary catastrophes[1-6].

According to the Thom's theorem, an instability near the prescribed critical point in the relevant space can be realized as that near the origin in the space after certain consistent transform. The consequent potential energy A near the critical origin can written by[7-12]

$$A : \mathbf{R}^m \times \mathbf{R}^k \rightarrow \mathbf{R} \quad \text{or} \quad A = A(v_i, \lambda, \varepsilon_j)$$

where v_i refers to the essential i-th instability mode, and $(v_1,...,v_m)$ spans the state space $\mathbf{R}^m$ in the catastrophe theory. Also, ε_j refers to the imperfection mode corresponding to v_j; λ designates an assigned conservative loading parameter. Then, the control space is spanned by (λ, ε_j) so that k=m+1. An explicit form of the potential energy can be defined by the Taylor's expansion near the critical origin[7,8,13].

Thompson and Hunt investigated the imperfection sensitivity surfaces of structures using a perturbation procedure with the discrete generalized coordinates[3,6,14,15]. Hunt proposed a perturbation algorithm for the compound instabilities with the parabolic, hyperbolic and elliptic umbilic catastrophes[16-21]. Such umbilics were also illustrated by Gasper for simple strut models[22,23,24]. Moreover, the swallowtail and the butterfly catastrophes as well as the umbilics were examined by Hui and Hansen through Koiter's general stability theory for beam, plate and shell models[25-28].

This chapter discusses on a direct computational algorithm to evaluate the effect of imperfections on the elastic load-carrying capacity of structures through the singularity condition in the catastrophe theory without using a perturbation process. The bifurcation set representing such imperfection sensitivity is explained briefly with topological meanings. For some simple typical examples in structural engineering, the bifurcation sets will be spatially drawn in three-dimensional load-imperfections space by the use of the proposed formulation.

2.2 Imperfection Sensitivity

Let a potential energy of an elastic conservative structure be mathematically rewritten as:

$$\begin{aligned} A : \mathbf{R}^m \times \mathbf{R}^k &\rightarrow \mathbf{R} \\ (v_i, \lambda, \varepsilon_j) &\rightarrow A = A(v_i, \lambda, \varepsilon_j) \end{aligned} \qquad (2.2.1)$$

Under the principle of the stationary potential energy, the necessary and sufficient condition for equilibrium states of the structures can be described by

$$M_A = \{(v_i, \lambda, \varepsilon_j) \mid \frac{\partial A}{\partial v_i} = 0 \ (i=1,2,\ldots,n)\} \subset \mathbf{R}^m \times \mathbf{R}^k \tag{2.2.2}$$

which constitutes the equilibrium surface in an (m+k)-dimensional Euclidian space $\mathbf{R}^m \times \mathbf{R}^k$.

Then, on the surface M_A, a set of singular points S_A is obtained by means of the condition of the zero-determinant of the Hessian matrix of the potential energy:

$$S_A = \{(v_i, \lambda, \varepsilon_j) \mid \frac{\partial A}{\partial v_i} = 0 \text{ and } \det[\frac{\partial^2 A}{\partial v_i \partial v_j}] = 0\} \subset M_A \quad (i,j=1,\ldots,m) \tag{2.2.3}$$

These (m+1) equations may be resolved in terms of k=m+1 control variables being one loading parameter λ and n imperfection parameters $\varepsilon_j (j=1,\ldots,m)$ for given state variables $v_j (j=1,\ldots,m)$.

On the other hand, in the singularity theory of mappings, the catastrophe map χ_A is referred to as a projection of M_A to the control space $(\lambda, \varepsilon_j) \in \mathbf{R}^k$, that is,

$$\begin{aligned} \chi_A : M_A &\to \mathbf{R}^k \\ (v_i, \lambda, \varepsilon_j) &\to (\lambda, \varepsilon_j) \end{aligned} \tag{2.2.4}$$

Then, the bifurcation set $B_A \subset \mathbf{R}^k$ is obtained as

$$B_A = \chi_A(S_A) \tag{2.2.5}$$

As the map is not **one-to-one correspondent**, assume a projection ϕ to exist in the following form:

$$\begin{aligned} \phi : \mathbf{R}^{m+1} &\to M_A \\ (v_i, \lambda) &\to (v_i, \lambda, \varepsilon_j) \end{aligned} \tag{2.2.6}$$

such that the projection is one-to-one correspondent. It means that each imperfection ε_j can be solved for any prescribed values of v_i and λ. Thus, a chained map is determined by

$$\begin{aligned} \chi_A \phi : \mathbf{R}^{m+1} &\to \mathbf{R}^k \\ (v_i, \lambda) &\to (\lambda, \varepsilon_j) \end{aligned} \tag{2.2.7}$$

where $k=m+1$. The map becomes singular if and only if the Jacobian of $\chi_A \phi$ is equal to be zero:

$$J(\chi_A \phi) = \det \left[\begin{array}{ccc|c} \frac{\partial \lambda}{\partial v_1} & \frac{\partial \lambda}{\partial v_2} & \cdots \frac{\partial \lambda}{\partial v_m} & \frac{\partial \lambda}{\partial \lambda} \\ \hline \frac{\partial \varepsilon_1}{\partial v_1} & \frac{\partial \varepsilon_1}{\partial v_2} & \cdots \frac{\partial \varepsilon_1}{\partial v_m} & \frac{\partial \varepsilon_1}{\partial \lambda} \\ \vdots & \vdots & \vdots & \vdots \\ \frac{\partial \varepsilon_m}{\partial v_1} & \frac{\partial \varepsilon_m}{\partial v_2} & \cdots \frac{\partial \varepsilon_m}{\partial v_m} & \frac{\partial \varepsilon_m}{\partial \lambda} \end{array}\right] = 0 \tag{2.2.8}$$

This relationship determines a set of singular points at which the one-to-one correspondence of $\chi_A\phi$ vanishes(See, **Fig. 2.2.1**). Therefore, the bifurcation set B_A can be appreciated to be the set of singular points on M_A as follows:

$$B_A = \{(\lambda,\varepsilon_j) \mid \frac{\partial A}{\partial v_i} = 0 \text{ and } J(\chi_A\phi) = 0 \text{ for a given } (v_1,v_2,\ldots,v_m)\} \subset R^k \qquad (2.2.9)$$

Meanings of two sets of S_A and B_A in Eqs. (2.2.3) and (2.2.9) are entirely identified, and indicate the imperfection sensitivity surfaces in the control space R^k.

2.3 Distinct Instabilities

2.3.1 Fold catastrophe

The first illustration is a typical **fold** catastrophe, which may be realized in a structural models such as a rigid frame and complete or oblate spherical shell under external pressure [3,11,15,29]. The mathematical form of the potential energy can be expressed for m=1 and k=2 from Eq. (2.2.1):

$$A : R^1 \times R^2 \to R \qquad (v_1, \lambda, \varepsilon_1) \to A = A(v_1, \lambda, \varepsilon_1) \qquad (2.3.1a)$$

or in the Taylor's expansion

$$A(v_1,\lambda,\varepsilon_1) = \frac{1}{6} A_{111} v_1^3 + \frac{\lambda}{2} A_{11}^{o} v_1^2 + A_1^1 v_1 \varepsilon_1 \qquad (2.3.1b)$$

whose coefficients are evaluated at the critical origin. The subscript "1" denotes the differentiation with respect to the instability mode v_1; whereas the superscript "o" and "1" refers to the differentiation with respect to the loading parameter λ and the imperfection parameter ε_1 corresponding to v_1, respectively. That is,

$$A_{111} = \frac{\partial^3 A}{\partial v_1^3} \quad , \quad A_{11}^{o} = \frac{\partial^3 A}{\partial v_1^2 \partial \lambda} \quad , \quad A_1^1 = \frac{\partial^2 A}{\partial v_1 \partial \varepsilon_1}$$

These notations will be adopted hereafter in this chapter.

Then, the equilibrium surface M_A in Eq. (2.2.2) is given by

$$M_A = \{(v_1,\lambda,\varepsilon_1) \mid A_1 = \frac{\partial A}{\partial v_1} = \frac{1}{2} A_{111} v_1^2 + \lambda A_{11}^{o} v_1 + A_1^1 \varepsilon_1 = 0\} \subset R^1 \times R^2 \qquad (2.3.2)$$

Moreover, the set of singular points on M_A is obtained from Eq. (2.2.3), and is written by

$$S_A = \{(v_1,\lambda,\varepsilon_1) \mid A_1 = 0 \text{ and } A_{11} = \frac{\partial^2 A}{\partial v_1^2} = A_{111} v_1 + \lambda A_{11}^{o} = 0\} \subset M_A \qquad (2.3.3)$$

Now, let a projection ϕ in Eq. (2.2.6) defined explicitly as:

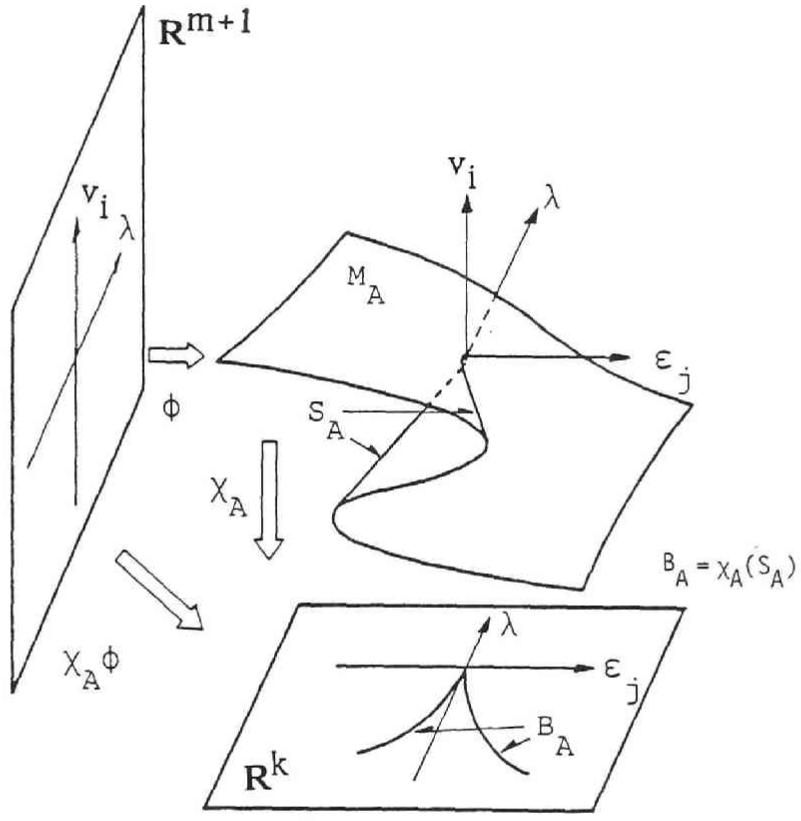

Fig. 2.2.1 Catastrophe Map and Bifurcation Set. [10]

$$\phi : (v_1, \lambda) \rightarrow (v_1, \lambda, -\frac{A_{111}}{2A_1^1} v_1^2 - \frac{A_{11}^0}{A_1^1} \lambda v_1) \tag{2.3.4}$$

Hence, the zero-determinant condition of the Jacobian of $\chi_A \phi$ in Eq. (2.2.7) is given by

$$\det \begin{bmatrix} \frac{\partial \lambda}{\partial v_1} & \frac{\partial \lambda}{\partial \lambda} \\ \frac{\partial \varepsilon_1}{\partial v_1} & \frac{\partial \varepsilon_1}{\partial \lambda} \end{bmatrix} = \det \begin{bmatrix} 0 & 1 \\ -\frac{A_{111}}{A_1^1} v_1 - \frac{A_{11}^0}{A_1^1} \lambda & -\frac{A_{11}^0}{A_1^1} v_1 \end{bmatrix} = 0 \tag{2.3.5}$$

Therefore, it is clear that the bifurcation set in Eq. (2.2.9) through Eqs. (2.3.2) and (2.3.5) is completely identified with the set S_A in Eq. (2.3.3). An explicit form of the bifurcation set can be determined by

$$\lambda_f = \pm \frac{(2A_{111} A_1^1 \varepsilon_1)^{\frac{1}{2}}}{A_{11}^0} \tag{2.3.6}$$

which means that the imperfection sensitivity obeys the **one-half power law.**

The bifurcation set is drawn in two-dimensional control space (λ, ε_1). However, it can be drawn spatially in three-dimensional space $(\lambda, \varepsilon_1, \varepsilon_2)$ adding another void parameter ε_2 as shown in **Fig. 2.3.1**[29]. The parameter ε_2 may be arbitrary, but must correspond to another mode v_2 independently of the mode v_1.

2.3.2 Dual cusp catastrophe

The second example includes a typical **dual cusp** catastrophe, which may be realized in the models such as a laterally loaded arch, a column on an elastic foundation, a pony truss and a cylindrical or elliptic shell under external pressure and axial load [3,11,15,29]. Then, the potential energy in Eq. (2.2.1) for m=1 and k=2 leads to

$$\begin{aligned} A : \mathbf{R}^1 \times \mathbf{R}^2 &\rightarrow \mathbf{R} \\ (v_1, \lambda, \varepsilon_1) &\rightarrow A = A(v_1, \lambda, \varepsilon_1) \end{aligned} \tag{2.3.7a}$$

or

$$A(v_1, \lambda, \varepsilon_1) = \frac{1}{24} A_{1111} v_1^4 + \frac{\lambda}{2} A_{11}^0 v_1^2 + A_1^1 v_1 \varepsilon_1 \tag{2.3.7b}$$

which characterizes a **cusp** or **dual cusp** catastrophe whether A_{1111} is positive or negative.

In this case, the equilibrium surface M_A yields

$$M_A = \{ (v_1, \lambda, \varepsilon_1) \mid A_1 \equiv \frac{\partial A}{\partial v_1} = \frac{1}{6} A_{1111} v_1^3 + \lambda A_{11}^0 v_1 + A_1^1 \varepsilon_1 = 0 \} \subset \mathbf{R}^1 \times \mathbf{R}^2 \tag{2.3.8}$$

and the set of singular points on M_A is

$$S_A=\{(v_1,\lambda,\varepsilon_1)\,|\,A_1=0 \text{ and } A_{11}\equiv\frac{\partial^2 A}{\partial v_1^2}=\frac{1}{2}A_{1111}v_1^2+\lambda A_{11}^{\circ}=0\}\subset M_A \tag{2.3.9}$$

Similarly to the case of the previous **fold** catastrophe, a projection ϕ is defined as follows:

$$\phi:(v_1,\lambda)\rightarrow(v_1,\lambda,-\frac{A_{1111}}{6A_1^1}v_1^3-\frac{A_{11}^{\circ}}{A_1^1}\lambda v_1) \tag{2.3.10}$$

Therefore, from the zero-determinant condition in Eq. (2.2.8), the bifurcation set B_A in Eq. (2.2.9) being equivalent to the set S_A can be revealed apparently.

Thus, the imperfection sensitivity surface is expressed by the **two-thirds power law:**

$$\lambda_d=\pm\frac{(A_{1111})^{\frac{1}{3}}(3A_1^1\varepsilon_1)^{\frac{2}{3}}}{2A_{11}^{\circ}} \tag{2.3.11}$$

Assuming the null parameter ε_2 similar to the **fold** catastrophe, the bifurcation set is visually drawn in **Fig. 2.3.2**[29].

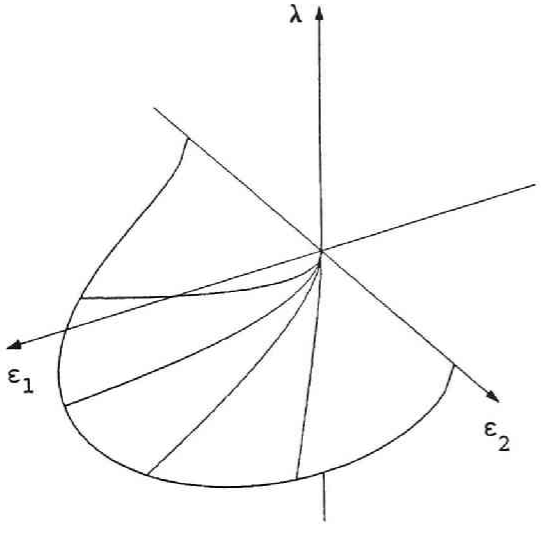

Fig. 2.3.1 Bifurcation Set for Fold Catastrophe.

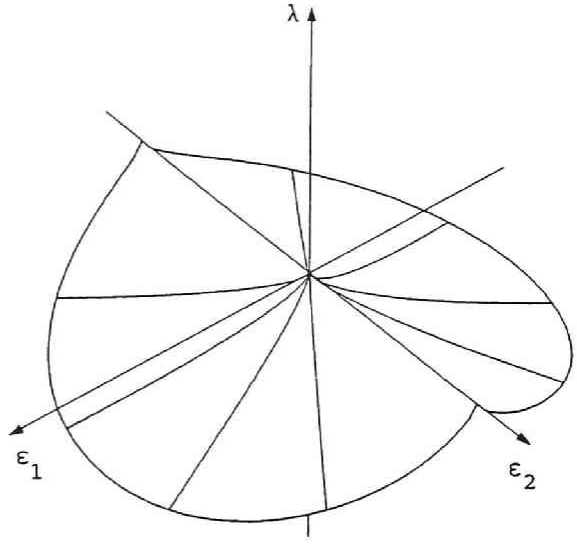

Fig. 2.3.2 Bifurcation Set for Dual Cusp Catastrophe.

2.4 Compound Instabilities

The third illustrations have some **umbilic** characteristics, which may be realized in the compound instabilities such as struts on an elastic foundation and stiffened plates subjected to in-plane loading. The typical form of the potential

energy is assumed to be given for m=2 and k=3:

$$A : R^2 \times R^3 \rightarrow R$$
$$(v_1, v_2, \lambda, \varepsilon_1, \varepsilon_2) \rightarrow A = A(v_1, v_2, \lambda, \varepsilon_1, \varepsilon_2) \tag{2.4.1a}$$

or

$$A(v_1,v_2,\lambda,\varepsilon_1,\varepsilon_2) = \frac{1}{6} A_{111} v_1^3 + \frac{1}{2} A_{122} v_1 v_2^2 + \frac{\lambda}{2} (A^{\circ}_{11} v_1^2 + A^{\circ}_{22} v_2^2) + A^1_1 v_1 \varepsilon_1 + A^2_2 v_2 \varepsilon_2 \tag{2.4.1b}$$

Then, the equilibrium surface M_A is obtained by

$$M_A = \left\{ (v_1,v_2,\lambda,\varepsilon_1,\varepsilon_2) \;\middle|\; \begin{array}{l} A_1 = \frac{\partial A}{\partial v_1} = \frac{1}{2} A_{111} v_1^2 + \frac{1}{2} A_{122} v_2^2 + \lambda A^{\circ}_{11} v_1 + A^1_1 \varepsilon_1 = 0 \\ A_2 = \frac{\partial A}{\partial v_2} = A_{122} v_1 v_2 + \lambda A^{\circ}_{22} v_2 + A^2_2 \varepsilon_2 = 0 \end{array} \right\} \tag{2.4.2}$$

The set of singular points can be defined from the zero-determinant condition of the Hessian matrix of Eq. (2.4.2) in the following form:

$$\det\left[\frac{\partial^2 A}{\partial v_i \partial v_j} \right] = A_{11} \cdot A_{22} - (A_{12})^2 = (A_{111} v_1 + \lambda A^{\circ}_{11})(A_{122} v_1 + \lambda A^{\circ}_{22}) - (A_{122} v_2)^2 = 0 \tag{2.4.3}$$

Eqs. (2.4.2) and (2.4.3) provide the set of singular points S_A in Eq. (2.2.3).

In the mapping theory, a projection ϕ is obtained by

$$\phi : (v_1,v_2,\lambda) \rightarrow (v_1, v_2, \lambda, -\frac{A_{111}}{2A^1_1} v_1^2 - \frac{A_{122}}{2A^1_1} v_2^2 \quad \frac{A^{\circ}_{11}}{A^1_1} \lambda v_1 , \; - \frac{A_{122}}{A^2_2} v_1 v_2 - \frac{A^{\circ}_{22}}{A^2_2} \lambda v_2) \tag{2.4.4}$$

The bifurcation set B_A in Eq. (2.2.9) can be represented as the set S_A substituting Eqs. (2.4.2) and (2.4.3) into Eq. (2.2.3):

$$S_A = \{ (\lambda,\varepsilon_1,\varepsilon_2) \mid A_1 = A_2 = 0 \text{ and } (A_{111} v_1 + \lambda A^{\circ}_{11})(A_{122} v_1 + \lambda A^{\circ}_{22}) - (A_{122} v_2)^2 = 0 \} \tag{2.4.5}$$

Now, the form of bifurcation sets for the **fold** and **dual cusp** catastrophes was shown to be definitely described by Eq. (2.3.6) and (2.3.11), respectively.

However, it is very difficult to make an explicit expression of bifurcation set for the **umbilics.** Therefore, Thompson and Hunt clarified the umbilic characteristics using a manipulative perturbation algorithm[1,4]. In this chapter, a non-perturbing direct procedure will be presented in the following manner:

Firstly, some equilibrium paths on M_A in Eq. (2.4.2) for perfect structures $\varepsilon_1 = \varepsilon_2 = 0$ are obtained as follows:

$$v_1 = v_2 = 0 \qquad \text{for all } \lambda \tag{2.4.6a}$$

$$v_2 = 0, \quad \frac{1}{2} A_{111} v_1 + \lambda A^{o}_{11} = 0 \tag{2.4.6b}$$

and

$$A_{122} v_1 + \lambda A^{o}_{22} = 0, \quad v_2 = \pm \left(\frac{2A^{o}_{11}}{A^{o}_{22}} - \frac{A_{111}}{A_{122}} \right)^{\frac{1}{2}} v_1 \tag{2.4.6c}$$

if and only if $2A^{o}_{11}/A^{o}_{22} > A_{111}/A_{122}$. Eq. (2.4.6a) provides a trivial fundamental path imbeded on the λ-axis. Eq. (2.4.6b) shows an uncoupled secondary line on the plane representing the asymmetric postbuckling path with respect to only v_1. Moreover, Eq. (2.4.6c) indicates two coupled secondary lines spread spatially in (v_1, v_2, λ) space. This case is previously discussed in details in the chapter 1 of PART I.

Secondly, consider imperfection sensitivity for imperfect structure $\varepsilon_1 \neq 0$, $\varepsilon_2 = 0$. Then, from Eq. (2.4.2), $v_2 = 0$ is reasonably satisfied. The following two imperfection sensitivity surfaces can be easily calculated.

$$\lambda = \lambda_{\ell} \equiv \pm \frac{(2A_{111} A^{1}_{1} \varepsilon_1)^{\frac{1}{2}}}{A^{o}_{11}} \tag{2.4.7a}$$

and

$$\lambda = \lambda_{b} \equiv \pm \frac{(2A_{122} A^{1}_{1} \varepsilon_1)^{\frac{1}{2}}}{A^{o}_{22} \left(\frac{2A^{o}_{11}}{A^{o}_{22}} - \frac{A_{111}}{A_{122}} \right)^{\frac{1}{2}}} \tag{2.4.7b}$$

It is found that Eq. (2.4.7a) is identically equal to the imperfection sensitivity of the **fold** catastrophe with respect to only v_1 or ε_1 referring to Eq. (2.3.6). Subscript " ℓ " refers to the set of **limit points** with the asymmetric bifurcation point. Also, Eq. (2.4.7b) gives the imperfection sensitivity for the **secondary bifurcation points** with respect to v_1 only, being designated by the subscript "b" if $2A^{o}_{11}/A^{o}_{22} > A_{111}/A_{122}$.

Finally, for computation of general imperfection sensitivity of imperfect structures, ε_1: any, $\varepsilon_2 \neq 0$, three equations in Eq. (2.4.5) will be solved simultaneously and directly. The consequent imperfection sensitivity surface can be obtained by

$$\lambda = \lambda_u \equiv \pm \frac{(A_{122})^3 x^4 - A_{111}(A_2^2)^2\varepsilon_2^2}{A_2^2(A_{111}A_{22}^o - A_{122}A_{11}^o)\, x\, \varepsilon_2} \quad \text{when} \quad \frac{A_{11}^o}{A_{22}^o} \neq \frac{A_{111}}{A_{122}} \tag{2.4.8}$$

where x designates an available real root of the following eighth order equation:

$$A_{22}^o(A_{122})^4(A_{111}A_{22}^o - 2A_{122}A_{11}^o)\, x^8$$
$$+ A_{122}(A_2^2)^2[\,3(A_{122})^2(A_{11}^o)^2 - 2A_{111}A_{122}A_{11}^oA_{22}^o + (A_{111})^2(A_{11}^o)^2]\varepsilon_1^2\, x^4$$
$$+ 2(A_2^2)^2A_1^1(A_{111}A_{22}^o - A_{122}A_{11}^o)^2\varepsilon_1\varepsilon_2^2\, x^2 \quad A_{111}(A_{11}^o)^2(A_2^2)^4\varepsilon_2^4 = 0 \tag{2.4.9}$$

If $A_{11}^o/A_{22}^o = A_{111}/A_{122}$, that is, in the case of the spherical shell conditions named by Thompson and Hunt[15], then an alternative implicit expression for Eq. (2.4.8) leads to

$$[\,\tfrac{1}{2}(A_{22}^o)^2A_{111}\lambda_s^2 \quad (A_{122})^2A_1^1\varepsilon_1\,]^2 = (A_{122})^3A_{111}(A_2^2)^2\varepsilon_2^2$$
$$\text{for} \quad \lambda_s^2 > \frac{2(A_{122})^2A_2^2}{(A_{22}^o)^2A_{111}}\,\varepsilon_1 \tag{2.4.10}$$

Hence, the **umbilic** imperfection sensitivity surfaces can be defined from Eqs. (2.4.7) and (2.4.8), or Eqs. (2.4.7) and (2.4.10). These results confirm the closed-form solutions obtained by Thompson et al[15]. For evaluation without complicated calculations, a polar coordinate (ε,θ) for the Cartesian $(\varepsilon_1,\varepsilon_2)$ is adopted:

$$\varepsilon_1 = \varepsilon\cos\theta \quad , \quad \varepsilon_2 = \varepsilon\sin\theta \qquad \text{for} \quad 0 \leq \theta < 2\pi \tag{2.4.11}$$

Then, Eqs. (2.4.7), (2.4.8) and (2.4.10) can be rewritten explicitly for a given ε on the line of θ =constant:

$$\lambda_\ell \equiv \pm \frac{(2A_{111}\dot{A}_1\varepsilon)^{\frac{1}{2}}}{A_{11}^o} \qquad \text{for} \quad \theta = 0 \text{ or } \pi \tag{2.4.12}$$

$$\lambda_b \equiv \pm \frac{(2A_{122}\dot{A}_1\varepsilon)^{\frac{1}{2}}}{A_{22}^o\left(\frac{2A_{11}^o}{A_{22}^o} - \frac{A_{111}}{A_{122}}\right)^{\frac{1}{2}}} \qquad \text{for} \quad \theta = 0 \text{ or } \pi \tag{2.4.13}$$

$$\lambda_u \equiv \pm \frac{(A_{122})^3x^4 - A_{111}(\dot{A}_2)^2\varepsilon^2}{\dot{A}_2(A_{111}A_{22}^o - A_{122}A_{11}^o)\, x\, \varepsilon} \quad \text{when} \quad \frac{A_{11}^o}{A_{22}^o} \neq \frac{A_{111}}{A_{122}}$$
$$\text{for } 0 < \theta < 2\pi,\ \theta \neq \pi \tag{2.4.14}$$

where x is a proper real root of the following equation from Eq. (2.4.9):

$$A_{22}^{o}(A_{122})^{4}(A_{111}A_{22}^{o} - 2A_{122}A_{11}^{o})x^{8}$$

$$+ A_{122}(\dot{A}_2)^{2}[3(A_{122})^{2}(A_{11}^{o})^{2} - 2A_{111}A_{122}A_{11}^{o}A_{22}^{o} + (A_{111})^{2}(A_{22}^{o})^{2}]\varepsilon^{2}x^{4}$$

$$+ 2A_{1}(\dot{A}_2)^{2}(A_{111}A_{22}^{o} - A_{122}A_{11}^{o})\varepsilon^{3}x^{2} - A_{111}(A_{11}^{o})^{2}(\dot{A}_2)^{4}\varepsilon^{4} = 0 \qquad (2.4.15)$$

and furthermore,

$$\lambda_s = \pm \left[\frac{2(A_{122})^{2}\dot{A}_1 - (A_{122})^{3}A_{111}(\dot{A}_2)^{2}}{\frac{1}{2}A_{111}(A_{22}^{o})^{2}}^{\frac{1}{2}} \varepsilon \right]^{\frac{1}{2}}$$

$$\text{for } 0 < \theta < 2\pi,\ \theta \neq \pi \qquad (2.4.16)$$

in these equations

$$\dot{A}_1 = A_1^1 \cos\theta \quad \text{and} \quad \dot{A}_2 = A_2^2 \sin\theta \quad \text{for } 0 \leq \theta < 2\pi \qquad (2.4.17)$$

Also, the superscript " $\cdot$ " designates the differentiation with respect to the radius imperfection parameter ε on each θ ray.

Some illustrated drawings of the bifurcation sets for the **hyperbolic umbilics** are performed in such manner. The first example as shown in **Figs. 2.4.1** corresponds to the imperfection sensitivity with the **monoclinal point of bifurcation**[11]. The instability has two equilibrium paths in Eqs. (2.4.6a) and (2.4.6b) for the perfect structure, and the bifurcation sets can be expressed in terms of λ_ℓ, λ_b and λ_u.

The second illustration represents the imperfection sensitivity with the **homeoclinal point of bifurcation**, including three equilibrium paths in Eqs. (2.4.6) for the perfect structure. The bifurcation sets are drawn in **Figs. 2.4.2** for λ_ℓ, λ_b, and λ_u[11].

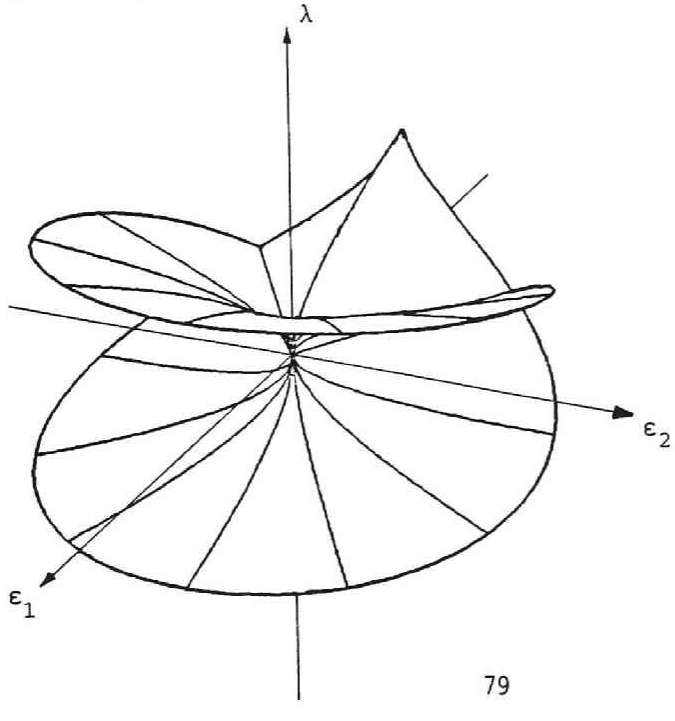

Fig. 2.4.1 Bifurcation Set for Hyperbolic Umbilic Catastrophe with Monoclinal Bifurcation.

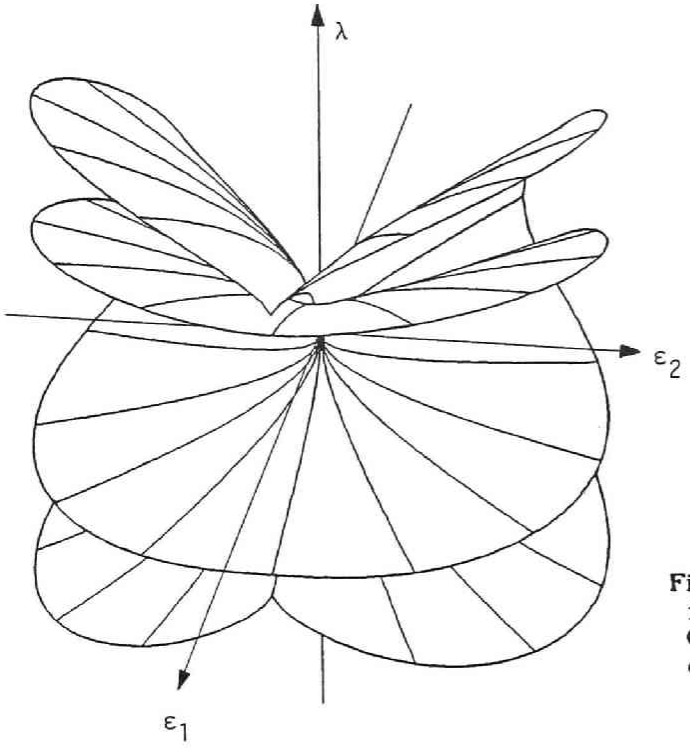

Fig. 2.4.2 Bifurcation Set for Hyperbolic Umbilic Catastrophe with Homeoclinal Bifurcation.

2.5 Conclusions

A direct computational approach for evaluating the imperfection sensitivity of structures was presented in terms of the bifurcation set through the catastrophe theory. The main conclusions are:

(1) The singularity condition on the equilibrium surface is definitely consistent with the zero-determinant condition of the associated map. $\chi_A \Phi$.

(2) The bifurcation set for a typical **fold** catastrophe can be explicitly realized by the 1/2-power rule λ_f.

(3) The bifurcation set for a typical **dual cusp** catastrophe can be realized by the 2/3-power rule λ_d.

(4) The bifurcation sets for typical **hyperbolic umbilic** catastrophes can be consequently composed of λ_ℓ, λ_b, λ_u (or λ_s) and their combinations.

(5) Each bifurcation set may be visually drawn in the three-dimensional load-imperfections space, and may confirm Thompson's results.

Bibliographies of Chapter 2 in PART II

1) Thom,R., Structural Stability and Morphogenesis(translated from the French by D.H.Fowler). Benjamin, 1975.
2) Zeeman,E.C., Catastrophe Theory: Selected Paper 1972-1977. Addison Wesley, 1977.
3) Thompson,J.M.T. and G.W.Hunt, Towards a unified bifurcation theory. Journal of Applied Mathematics and Physics (Zeitchrift für Angewandte Mathematik und Physik), Vol. 26, pp. 581-603, 1975.
4) Thompson,J.M.T. and G.W.Hunt, The instability of evolving systems. Interdisciplinary Science Reviews, Vol. 2, pp. 240-262, 1977.
5) Thompson,J.M.T., Instabilities and Catastrophes in Science and Engineering. John Wiley & Sons, 1982.
6) Thompson,J.M.T. and G.W.Hunt, Elastic Instability Phenomena. John Wiley & Sons, 1984.
7) Poston,T. and I.Stewart, Catastrophe Theory and Its Applications. Pitman, 1978.
8) Gilmore,R., Catastrophe Theory for Scientists and Engineers. John Wiley & Sons, 1981.
9) Thompson,J.M.T., Bifurcational aspects of catastrophe theory. Bifurcation Theory and Applications in Scientific Disciplines, Annals of the New York Academy of Sciences, Vol. 316, pp. 553-571, 1979.
10) Noguchi,H. and T.Fukuda, Elementary Catastrophes. Kyoritsu-Zensho, No. 208, 1976 (in Japanese).
11) Niwa,Y., E.Watanabe and H.Isami, Catastrophe analysis of structures by discretization and modal transforms. Memoirs of the Faculty of Engineering, Kyoto University, Vol. 43, pp. 67-87, 1981.
12) Isami,H., A topological aspect of imperfection sensitivity of structures. Bulletin of Kohchi Technical College, No. 20, pp. 85-94, 1984.
13) Poston,T. and I.Stewart, Taylor Expansions and Catastrophes. Research Notes in Mathematics, No. 7, Pitman, 1976.
14) Thompson,J.M.T. and G.W.Hunt, A General Theory of Elastic Stability. John Wiley & Sons, 1973.
15) Thompson,J.M.T., J.K.Y.Tan and K.C.Lim, On the topological classification of postbuckling phenomena. Journal of Structural Mechanics, Vol. 6, pp. 383-414, 1978.
16) Hunt,G.W., Imperfection-sensitivity of semi-symmetric branching. Proceedings of the Royal Society of London, Series A, Vol. 357, pp. 193-211, 1977.
17) Hunt,G.W., N.A.Reay and T.Yoshimura, Local diffeomorphisms in the bifurcational manifestations of the umbilic catastrophes. Proceedings of the Royal Society of London, Series A, Vol. 369, pp. 47-65, 1979.
18) Hunt,G.W., Imperfections and near-coincidence for semisymmetric bifurcations. Bifurcation Theory and Applications in Scientific Disciplines, Annals of the New York Academy of Sciences, Vol. 316, pp. 572-589, 1979.
19) Hunt,G.W., An algorithm for the nonlinear analysis of compound bifurcation. Philosophical Transactions of the Royal Society of London, Series A, Vol. 300, pp. 443-471, 1981.
20) Hunt,G.W., Symmetries of elastic buckling. Engineering Structures, Vol. 4, pp. 21-28, 1982.
21) Hunt,G.W., Elastic stability: in structural mechanics and applied mathematics. Journal of Structural Mechanics, Vol. 11, pp. 123-147, 1983.
22) Gaspar,Z., Buckling models for higher catastrophes. Journal of Structural Mechanics, Vol. 5, pp. 357-368, 1977.
23) Thompson,J.M.T. and Z. Gaspar, A buckling model for the set of umbilic catastrophes. Mathematical Proceedings of Cambridge Philosophical Society,

Vol. 82, pp. 497-507, 1977.
24) Gaspar,Z., Computation of imperfection-sensitivity at two-fold branching points. Zeitschrift für Mathematik und Mechanik, Vol. 63, pp. 359-370, 1983.
25) Hansen,J.S., Some two-mode buckling problems and their relation to catastrophe theory. AIAA J., Vol. 5, pp. 1638-1644, 1977.
26) Hui,D. and J.S.Hansen, Two-mode buckling of an elastically supported plate and its application to catastrophe theory. Journal of Applied Mechanics, Trans. American Society of Mechanical Engineering, Vol. 47, pp. 607-612, 1980.
27) Hui,D. and J.S.Hansen, The swallowtail and butterfly cuspoids and their application in the initial post-buckling of single-mode structural systems. Quarterly of Applied Mathematics, Vol. 38, pp. 17-36, 1980.
28) Hui,D. and J.S.Hansen, The parabolic umbilic catastrophe and its application in the theory of elastic stability. Quarterly of Applied Mathematics, Vol. 39, pp. 201-220, 1981.
29) Niwa,Y., E.Watanabe and H.Isami, Catastrophes of elastic column structures. Memoirs of the Faculty of Engineering, Kyoto University, Vol. 45, pp. 71-97, 1983.

CHAPTER 3

APPLICATIONS TO ELASTIC COLUMN STRUCTURES

3.1 General Remarks

The load-carrying capacity of structures is generally adversely affected by imperfections such as initial deformations, eccentricities and residual stresses. This is what is called the **imperfection sensitivity of structures.**

It is general practice to solve the elasto-plastic and geometrically nonlinear equilibrium equations for evaluating the load-carrying capacity. For this purpose, such numerical procedures as Newton-Raphson's, perturbation, incremental and homotopy continuation methods are commonly used. Consequently, the load-carrying capacity of structures can be plotted against the initial imperfections. However, these results can only be obtained in a discrete numerical form and are generally time-consuming.

In this respect, an application of the catastrophe theory to the strength prediction of structures may be found to be useful as stated in the previous PART I. The load-carrying capacity of structures can be evaluated explicitly by means of the bifurcation set of the catastrophe map. The catastrophe map, herein, is defined to be a map of singular points of equilibrium surface on the control space, spanned by a loading parameter and several imperfection parameters. The mapped surface is called the **bifurcation set**, designating the adverse effects of the initial imperfections. It can be evaluated without resorting to the solution process of the nonlinear simultaneous equations.

This chapter provides a comparative study on the continuous analyses and discrete analyses for column models in relation to the models by Thompson et al. and Niwa et al[1-5]. The first symmetric buckling model corresponds to an Elastica model, normal simple struts and rings, struts on an elastic foundation and normal thin plates subjected to in-plane loading. The stability of such models has been analyzed by Thompson in terms of the differential equation, continuous method and finite element method[6]. The second unstable symmetric buckling model corresponds to a laterally loaded shallow arch, a column on an elastic foundation, pony truss and a cylindrical or elliptic shell subjected to an external pressure and the axial load. Furthermore, the third asymmetric buckling model corresponds to a rigid frame in the well-known Roorda's experiments[7,8], and in Britvec's analysis[9], to a complete spherical or oblate spheroidal shell under external pressure.

All proposed models are assumed to be elastic conservative systems. Therefore, the necessary and sufficient condition of the equilibrium of the systems is the total potential energy being stationary, whereas the condition of the stability of the equilibrium systems is the second variation of the total potential energy being positive definite[10]. Furthermore, these column models are assumed to be **inextensible** along their neutral axis. The load is assumed to act conservatively in the axial direction, being controlled by a single loading parameter. Thus, the total potential energy of a column structure can be expressed in terms of a single loading parameter, the lateral deflections and prescribed initial deflections. The initial deflections are assumed in the same modes as the considered buckling ones. The other imperfection parameters such as load eccentricities and residual stresses are not considered herein.

Thus, several interesting comparisons can be among those three catastrophe analyses: the two-degree-of-freedom analysis, the continuous analysis and the discrete analysis. The applicability and the feasibility of the proposed method are discussed in the later section.

3.2 Continuous Analysis

3.2.1 General remarks

A continuous analysis on stable symmetric, unstable symmetric and asymmetric buckling models will be presented. The discussions will be made as brief as possible here, and detailed descriptions may be provided in references by Niwa, Watanabe and Isami[3,4,5].

Let W(X) and $W_0(X)$ designate the lateral additional and initial deflection of column structures, respectively, where X refers to the coordinate taken along the deformed neutral axis of the column. **Fig. 3.2.1** illustrates a simply supported column, referred to as the stable symmetric buckling model[1,6].

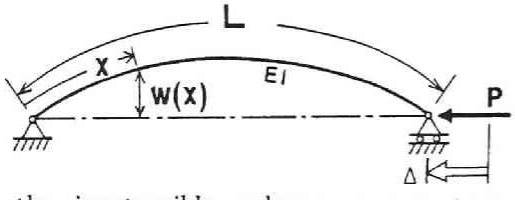

Fig. 3.2.1 Simply Supported Column Model.

In the inextensible column, a curvature κ_x at the coordinate X can be designated as:

$$\left.\begin{aligned}\kappa_x &= W_{,xx}\,[1-(W_{,x}+W_{0,x})^2]^{-1/2} \\ &\cong W_{,xx}+\frac{1}{2}W_{,xx}W_{,x}^2\end{aligned}\right\} \qquad (3.2.1)$$

where $W_{,x}=dW/dX$ and $W_{,xx}=d^2W/dX^2$.

Also, a shortening Δ at the right end as shown in **Fig. 3.2.1** can be shown as:

$$\begin{aligned}\Delta &= \int_0^L [1-\{1-(W_{,x}+W_{0,x})^2\}^{1/2}]\,dx \\ &\cong \int_0^L \left(\frac{1}{2}W_{,x}^2+W_{,x}W_{0,x}+\frac{1}{8}W_{,x}^4\right)dx\end{aligned} \qquad (3.2.2)$$

where L is the constant total length of the column structure. In Eqs. (3.2.1) and (3.2.2), the terms of $(W_{0,x})^2$ and the higher order terms of $W_{,x}$ are assumed to be negligible.

Let us introduce the following non-dimensionalized parameters:

$$x=\frac{X}{L}, \qquad w=\frac{W}{L}, \qquad w_0=\frac{W_0}{L}, \qquad \lambda=\frac{PL^2}{EI} \qquad (3.2.3)$$

where EI refers to the constant flexural rigidity of the column structure, and P refers to the axial load applying at the right end.

Table 3.2.1 Various Approximations of Flexural Curvatures and Edge Shortening.

Approximation	Curvature κ_x	Shortening Δ	Remarks
1	$W_{,xx}$	$\int_0^L\left(\frac{1}{2}W_{,x}^2+W_{,x}W_{0,x}\right)dx$	Linear Eigen-Value Problem
2	$W_{,xx}+\frac{1}{2}W_{,xx}W_{,x}^2$	$\int_0^L\left(\frac{1}{2}W_{,x}^2+W_{,x}W_{0,x}\right)dx$	
3	$W_{,xx}$	$\int_0^L\left(\frac{1}{2}W_{,x}^2+W_{,x}W_{0,x}+\frac{1}{8}W_{,x}^4\right)dx$	
4	$W_{,xx}+\frac{1}{2}W_{,xx}W_{,x}^2$	$\int_0^L\left(\frac{1}{2}W_{,x}^2+W_{,x}W_{0,x}+\frac{1}{8}W_{,x}^4\right)dx$	Present Analysis, Eqs. (3.2.1) & (3.2.2)

Then, the non-dimensionalized total potential energy V can be obtained by the sum of the flexural strain energy and the external work under the axial load:

$$\left.\begin{aligned} V(w,\lambda,w_0)=&\frac{1}{2}\int_0^1(w_{,xx}^2+w_{,x}^2w_{,x}^2)\,dx\\ &-\lambda\int_0^1\left(\frac{1}{2}w_{,x}^2+w_{,x}w_{0,x}+\frac{1}{8}w_{,x}^4\right)dx\end{aligned}\right\} \qquad (3.2.4)$$

where $w_{,x}=dw/dx$, $w_{0,x}=dw_0/dx$, and $w_{,xx}=d^2w/dx^2$.

Usually, however, both the second term of κ_x in Eq. (3.2.1) and the third term of Δ in Eq. (3.2.2) are not taken into account for linear bifurcation problems. **Table 3.2.1** shows several possible combinations of approximations of curvature and edge shortening. It can be shown, firstly, that the potential energy based on **Approximation 1** leads only to a linear eigenvalue problem. Secondly, the potential energy based on **Approximation 2** or **3** can be shown to fail in evaluating rigorously either the flexural strain or the external work. Finally, the potential energy on **Approximation 4** in the last row is considered to be sufficiently rigorous, and is adopted herein in order to approximate the geometrical nonlinearity.

3.2.2 Stable symmetric buckling model

Fig. 3.2.1 illustrates an arbitrary deformed state of the model. The non-dimensionalized total potential energy is given by Eq. (3.2.4). This equation may be interpreted as the map with a lateral deflection w as the state variable, and the load λ and the lateral initial deflection w_0 being the control parameters.

The perfect column model without any initial imperfections has, in general, distinct bifurcation buckling points. The primary buckling mode is of a half sine wave. Therefore, the modal transforms h_1 x h_2 given by

$$h_1:\ w(x)=v_1\sin\pi x, \qquad \text{and } h_2:\ w_0(x)=\varepsilon_1\sin\pi x \qquad (3.2.5)$$

can be adopted to transform directly the total potential energy V into a new potential A. In Eq. (3.2.5), v_1 and ε_1 refer to the parameters indicating the magnitude of the buckling mode and that of the initial deflection of the same mode, respectively.

Upon transformation through Eq. (3.2.5), the Taylor expansion of the imperfect total potential energy A around the critical point $(v_1, \lambda, \varepsilon_1)=(0, \pi^2, 0)$ of the perfect system, leads to[11,12,13]

$$A(v_1, \lambda, \varepsilon_1)=\frac{1}{24} A^c_{1111} v_1^4+\frac{1}{2} A^{oc}_{11}(\lambda-\lambda_c) v_1^2+A^{1c}_1 v_1 \varepsilon_1 \tag{3.2.6}$$

where

$$\left.\begin{aligned} A^c_{1111}&=\frac{3}{8}\pi^6, & A^{oc}_{11}&=-\frac{\pi^2}{2}, \\ A^{1c}_1&=-\frac{\pi^4}{2}, & \lambda_c&=\pi^2. \end{aligned}\right\}$$

Then, an equilibrium equation is

$$\frac{\partial A}{\partial v_1} = \frac{1}{6} A^c_{1111} v_1^3 + A^{oc}_{11} \lambda v_1 + A^{1c}_1 \varepsilon_1 = 0 \tag{3.2.7}$$

This provides the fundamental solution $v_1=0$ for $\varepsilon_1=0$ and the typical nonlinear equilibrium path

$$\frac{\Lambda}{\Lambda^c} = 1 + C_4 v_1^2 + C_\varepsilon \frac{\varepsilon_1}{v_1} \tag{3.2.8}$$

where

$$C_4 = \frac{-A^c_{1111}}{6 A^{oc}_{11} \Lambda^c} \qquad C_\varepsilon = \frac{-A^{1c}_1}{A^{oc}_{11} \Lambda^c}$$

Since $A^c_{1111} > 0$, Eq. (3.2.6) indicates the stable symmetric bifurcation buckling corresponding to Thom's typical **cusp** catastrophe[14,15]. It is well-known, however, that the bifurcation set of the cusp catastrophe does not provide any realistic meaning on the stability problems in structural mechanics. In such case, the load-carrying capacity of the model should be evaluated using a certain yield criterion of the material in the elasto-plastic range. However, such elasto-plastic characteristics are beyond the scope of this chapter, and will be investigated in the subsequent PART III of this dissertation.

3.2.3 Unstable symmetric buckling model

Let us consider a column similar to the stable symmetric model, but with an elastic foundation at the right end as shown in **Fig. 3.2.2.** Then, the non-dimensionalized total potential energy of the model is given by

$$V(w, \lambda, w_0)=\frac{1}{2}\int_0^1 (w_{,xx}^2+w_{,xx}^2 w_{,x}^2)\, dx$$
$$-\lambda\int_0^1\left(\frac{1}{2}w_{,x}^2+w_{,x} w_{0,x}+\frac{1}{8}w_{,x}^4\right) dx+\frac{k}{2}w_L^2 \tag{3.2.9}$$

where $w_L=W_L/L$, $k=KL^3/EI$ and K refers to the spring constant of the elastic foundation.

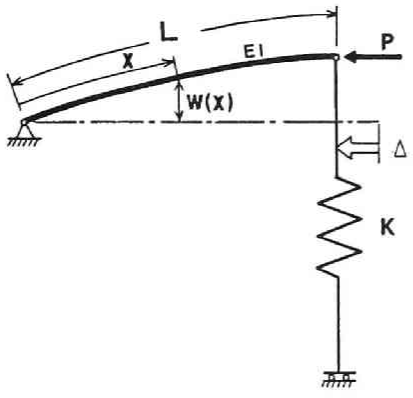

Fig. 3.2.2 Unstable Symmetric Buckling Model.

Then, the following three typical instability phenomena can be shown to take place depending upon the magnitude of the non-dimensionalized spring rigidity k of the elastic foundation.

(i) when $k>\pi^2$

A distinct bifurcation with the mode 2:

$$w(x)=v_2 \sin \pi x$$

may occur at the critical point $(v_2, \lambda, \varepsilon_2)=(0, \pi^2, 0)$. The mode corresponds to a half sine waveform for the column buckling configuration.

Then, the non-dimensionalized total potential energy of the imperfect model near the critical point can be expanded to the following form:

$$A(v_2, \lambda, \varepsilon_2)=\frac{1}{24}A^{c}_{2222}v_2^4+\frac{1}{2}A^{uc}_{22}(\lambda-\lambda_c)v_2^2+A^{2r}_{2}v_2\varepsilon_2, \qquad (3.2.10)$$

where

$$\left.\begin{aligned} A^{c}_{2222}&=\frac{3}{8}\pi^6, & A^{uc}_{22}&=-\frac{\pi^2}{2} \\ A^{2r}_{2}&=-\frac{\pi^4}{2}, & \lambda_c&=\pi^2. \end{aligned}\right\}$$

Eq. (3.2.10) predicts the stable symmetric bifurcation buckling corresponding to Thom's **cusp** catastrophe. This model can behave similarly to the simply supported column without any significant effect due to the elastic foundation. Also, the nonlinear equilibrium solution is expressed in the form similar to Eq. (3.2.8) by replacing the subscript "1" for the "2".

(ii) when $k<\pi^2$

A distinct bifurcation with the mode 1:

$$w(x)=v_1 x$$

may occur at the critical point $(v_1, \lambda, \varepsilon_1)=(0, k, 0)$. The mode corresponds to a rigid-body straight line configuration for the elastic foundation.

The non-dimensionalized total potential energy of the imperfect model near the critical point can be expanded to the following form:

$$A(v_1, \lambda, \varepsilon_1)=\frac{1}{24}A^c_{1111}v_1^4+\frac{1}{2}A^{oc}_{11}(\lambda-\lambda_c)v_1^2+A^{1c}_1 v_1\varepsilon_1, \tag{3.2.11}$$

where

$$\left.\begin{aligned} &A^c_{1111}=-3k, && A^{oc}_{11}=-1,\\ &A^{1c}_1=-k, && \lambda_c=k. \end{aligned}\right\}$$

Since $A^c_{1111} < 0$, Eq. (3.2.11) predicts the unstable symmetric bifurcation buckling corresponding to Thom's typical **dual cusp** catastrophe. Then, the nonlinear equilibrium solution completely equals to Eq. (3.2.8). The sign of A^c_{1111} plays an important role to predict the strength of the model. The load-carrying capacity λ_m of the model can be identified as the bifurcation set corresponding to the imperfection sensitivity surface. The surface can be expressed by the following non-dimensionalized form[16](See, Eq. (II-2.3.1))

$$\bar{\lambda}_m=\frac{\lambda_m}{\lambda_c}=1\pm\frac{1}{2A^{oc}_{11}\lambda_c}(A^c_{1111})^{1/3}(3A^{1c}_1\varepsilon_1)^{2/3} \tag{3.2.12}$$

near the critical point $(v_1, \lambda, \varepsilon_1)=(0, k, 0)$. This sensitivity is usually referred to the **two-thirds power law.**

(iii) when $k=\pi^2$

The bifurcations of (i) and (ii) may occur simultaneously. Near the two-fold critical point $(v_1, v_2, \lambda, \varepsilon_1, \varepsilon_2)=(0, 0, k, 0, 0)$, the non-dimensionalized total potential energy of the model can be expanded to the following form:

$$\begin{aligned} A(v_1, v_2, \lambda, \varepsilon_1, \varepsilon_2)=&\frac{1}{24}A^c_{1111}v_1^4+\frac{1}{24}A^c_{2222}v_2^4\\ &+\frac{1}{2}(A^{oc}_{11}v_1^2+A^{oc}_{22}v_2^2)(\lambda-\lambda_c)\\ &+A^{1c}_1 v_1\varepsilon_1+A^{2c}_2 v_2\varepsilon_2, \end{aligned} \tag{3.2.13}$$

where

$$\left.\begin{aligned} &A^c_{1111}=-3\pi^2, && A^c_{2222}=\frac{3}{8}\pi^8, && A^c_{1122}=0,\\ &A^{oc}_{11}=-1, && A^{oc}_{22}=-\frac{1}{2}\pi^2, && A^{1c}_1=-\pi^2,\\ &A^{2c}_2=-\frac{1}{2}\pi^4, && \lambda_c=\pi^2. \end{aligned}\right\}$$

Eq. (3.2.11) predicts the compound bifurcation buckling of the stable symmetric and the unstable symmetric buckling corresponding to the **double cusp** catastrophe, not indicated in Thom's seven elementary catastrophes. Then, the nonlinear equilibrium solution is clearly obtained by two independent equations of equilibrium, whose forms are both similar to Eq. (3.2.8). This catastrophe will not be discussed any further in this dissertation[17].

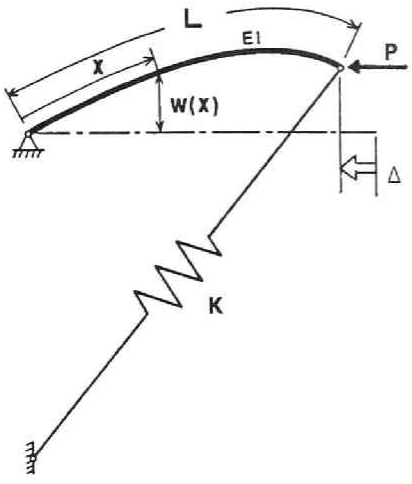

Fig. 3.2.3 Asymmeric Buckling Model.

3.2.4 Asymmetric buckling model

The third model is a column similar to the unstable symmetric buckling model, but having an asymmetric elastic foundation at the right end as shown in **Fig. 3.2.3.** Then, the non-dimensionalized total potential energy of the model can be obtained as

$$\left.\begin{aligned} V(w,\lambda,w_0)&=\frac{1}{2}\int_0^1 (w,_{xx}^{2}+w,_{xx}^{2}w,_{x}^{2})\,dx \\ &-\lambda\int_0^1\left(\frac{1}{2}w,_{x}^{2}+w,_{x}w_{0},_{x}+\frac{1}{8}w,_{x}^{4}\right)dx \\ &+\frac{k}{4}w_L^2+\frac{k}{8}w_L^3-\frac{k}{64}w_L^4+\frac{k}{4}\delta^2-\frac{k}{2}w_L\delta+\frac{k}{8}w_L^2\delta, \end{aligned}\right\} \quad (3.2.14)$$

where

$$\delta\equiv\int_0^1\left(\frac{1}{2}w,_{x}^{2}+w,_{x}w_{0},_{x}+\frac{1}{8}w,_{x}^{4}\right)dx.$$

Let us consider the modal transform h_1 x h_2:

$$h_1:\ w(x)=v_1x+v_2\sin\pi x \qquad h_2:\ w_0(x)=\varepsilon_1x+\varepsilon_2\sin\pi x. \quad (3.2.15)$$

Upon substitution of Eq. (3.2.15) into Eq. (3.2.14), the potential energy V can be rewritten as D:

$$D(v_1, v_2, \lambda, \varepsilon_1, \varepsilon_2)=\frac{1}{8}\left(\frac{3}{8}k-\lambda\right)v_1^4+\frac{\pi^2}{4}\left(\pi^2-\lambda+\frac{3}{8}k\right)v_1^2v_2^2$$
$$+\frac{\pi^4}{16}\left(\pi^2-\frac{3}{4}\lambda+\frac{k}{4}\right)v_2^4-\frac{k}{8}v_1^3-\frac{\pi^2}{8}kv_1v_2^2\Bigg\}$$
$$+\frac{\pi^2}{4}(\pi^2-\lambda)v_2^2-\lambda v_1\varepsilon_1-\frac{\pi^2}{2}\lambda v_2\varepsilon_2. \tag{3.2.16}$$

The following three typical instability phenomena can be shown to take place depending upon the magnitude of the spring constant k:

(i) when $k>2\pi^2$

A distinct bifurcation with the mode 2:

$$w(x)=v_2\sin\pi x$$

may occur at the critical point $(v_2, \lambda, \varepsilon_2)=(0, \pi^2, 0)$. Taking into account the interaction term $v_1 v_2^2$, the non-dimensionalized total potential energy of the imperfect model near the critical point can be expanded to the form

$$A(v_2, \lambda, \varepsilon_2)=\frac{1}{24}A^c_{2222}v_2^4$$
$$+\frac{1}{2}A^{oc}_{22}(\lambda-\lambda_c)v_2+A^{2c}_2v_2\varepsilon_2, \tag{3.2.17}$$

where

$$A^c_{2222}=D^c_{2222}-3(D^c_{122})^2/D^c_{11}=\frac{-3\pi^4(2\pi^4+\pi^2k)}{16\left(\frac{k}{2}-\pi^2\right)}<0,$$
$$A^{oc}_{22}=D^{oc}_{22}=-\frac{\pi^2}{2},\ A^{2c}_2=D^{2c}_2=-\frac{\pi^4}{2},\ \lambda_c=\pi^2.$$

Since $A^c_{2222} < 0$, Eq. (3.2.17) predicts the unstable symmetric bifurcation buckling corresponding to Thom's **dual cusp catastrophe**, similar to Eq. (3.2.11). Then, the bifurcation set near the critical point is in the form similar to Eq. (3.2.12), and is given by

$$\tilde{\lambda}_m=\frac{\lambda_m}{\lambda_c}=1\pm\frac{1}{2A^{oc}_{22}\lambda_c}(A^c_{2222})^{1/3}(3A^{2c}_2\varepsilon_2)^{2/3} \tag{3.2.18}$$

(ii) when $k<2\pi^2$

A distinct bifurcation with the mode 1:

$$w(x)=v_1x$$

may occur at the critical point $(v_1, \lambda, \varepsilon_1)=(0, k/2, 0)$. The non-dimensionalized total potential energy of the imperfect model near the critical point can be expanded to the form

$$A(v_1, \lambda, \varepsilon_1)=\frac{1}{6}A^c_{111}v_1^3$$
$$+\frac{1}{2}A^{oc}_{11}(\lambda-\lambda_c)v_1^2+A^{1c}_1v_1\varepsilon_1, \tag{3.2.19}$$

where

$$A^c_{111}=D^c_{111}=-\frac{3}{4}k,\quad A^{oc}_{11}=-1,\quad A^{1c}_{1}=-\frac{k}{2},\quad \lambda_c=\frac{k}{2}.$$

Since $A^c_{111} \neq 0$, Eq. (3.2.19) predicts the symmetric bifurcation buckling corresponding to Thom's typical **fold catastrophe.** Then, an equilibrium equation is

$$\frac{\partial A}{\partial v_1} = \frac{1}{2}A^c_{111}v_1^2 + A^{oc}_{11}\lambda v_1 + A^{1c}_{1}\varepsilon_1 = 0 \qquad (3.2.20)$$

This yields the fundamental solution $v_1 = 0$ for $\varepsilon_1 = 0$ and the typical nonlinear equilibrium path

$$\frac{\Lambda}{\Lambda^c} = 1 + C_3 v_1 + C_\varepsilon \frac{\varepsilon_1}{v_1} \qquad (3.2.21)$$

where

$$C_3 = \frac{-A^c_{111}}{2A^{oc}_{11}\Lambda^c} \qquad C_\varepsilon = \frac{-A^{1c}_{1}}{A^{oc}_{11}\Lambda^c}$$

includes the primary postbuckling straight line when $\varepsilon_1 = 0$. The bifurcation set is referred to as the **one-half power law**(See, Eq. (II-2.3.6))

$$\tilde{\lambda}_m=\frac{\lambda_m}{\lambda_c}=1\pm\frac{1}{A^{oc}_{11}\lambda_c}(2A^c_{111}A^{1c}_{1}\varepsilon_1)^{1/2}. \qquad (3.2.22)$$

where, since $A^{oc}_{11} < 0$ and $A^{1c}_{1} < 0$ in general, Eq. (3.2.22) is valid only if $\varepsilon_1<0$ for $A^c_{111} < 0$.

(iii) when $k=2\pi^2$

The bifurcations of (i) and (ii) may occur simultaneously. Near this critical point $(v_1, v_2, \lambda, \varepsilon_1, \varepsilon_2)=(0, 0, k/2, 0, 0)$, the total potential energy of the imperfect model can be expanded to the form of

$$\begin{aligned}A(v_1, v_2, \lambda, \varepsilon_1, \varepsilon_2)=&\frac{1}{6}A^c_{111}v_1^3+\frac{1}{2}A^c_{122}v_1v_2^2\\&+\frac{1}{2}(A^{oc}_{11}v_1^2+A^{oc}_{22}v_2^2)(\lambda-\lambda_c)\\&+A^{1c}_{1}v_1\varepsilon_1+A^{2c}_{2}v_2\varepsilon_2\end{aligned} \qquad (3.2.23)$$

where

$$\left.\begin{aligned}&A^c_{111}=D^c_{111}=-\frac{3}{2}\pi^2,\quad A^c_{122}=D^c_{122}=-\frac{\pi^4}{2},\\&A^{oc}_{11}=D^{oc}_{11}=-1,\quad A^{oc}_{22}=D^{oc}_{22}=-\frac{\pi^2}{2},\quad A^{1c}_{1}=D^{1c}_{1}=-\pi^2,\\&A^{2c}_{2}=D^{2c}_{2}=-\frac{\pi^4}{2},\qquad \lambda_c=\pi^2.\end{aligned}\right\}$$

Since

$$A^c_{111}\cdot A^c_{122}=\frac{3}{4}\pi^6>0, \qquad 2\frac{A^{oc}_{11}}{A^{oc}_{22}}-\frac{A^c_{111}}{A^c_{122}}=\frac{1}{\pi^2}>0,$$

Eq. (3.2.23) predicts the semi-symmetric bifurcation buckling, that is, the Thompson's **homeoclinal bifurcation buckling,** corresponding to Thom's **hyperbolic umbilic catastrophe**[18]. Then, equations of equilibrium are

$$\frac{\partial A}{\partial v_1}=\frac{1}{2}A^c_{111}v_1^3+\frac{1}{2}A^c_{122}v_2^2+A^{oc}_{11}\lambda v_1+A^{1c}_{1}\varepsilon_1=0$$

$$\frac{\partial A}{\partial v_2}=A^c_{122}v_1v_2+A^{oc}_{22}\lambda v_2+A^{2c}_{2}\varepsilon_2=0 \qquad (3.2.24)$$

The fundamental path when $\varepsilon_1=\varepsilon_2=0$ is solved in the chapter I-1.3 in details. Moreover, the typical nonlinear equilibrium solutions are obtained from the above simultaneous nonlinear equations using a particular nonlinear procedure. However, this dissertation aims to estimate the strength of slender structures without solving such nonlinear equations, so that this purpose follows the catastrophe theory in the form of the bifurcation set(See, Section **2.4** in this PART). Detailed discussions on the bifurcation sets for each model just mentioned will be described in the section 4 of this chapter.

3.3 Discrete Analysis

3.3.1 General remarks

A catastrophe analysis by discretization methods will be presented herein. The discretizations adopted herein are both the finite element method (abbreviated as FEM) using the ACM cubic shape function and the simplified element method (SEM), idealizing the column to consist of chains of rigid bars and a flexural spring using the linear shape function, first introduced by Watanabe et al[19]. These discrete numerical analyses are compared with the continuous analyses. All of the assumptions made for the continuous analysis are also adopted herein. Moreover, the D.O.F. at each nodal point is two for FEM and one for SEM, respectively. The total D.O.F. in the SEM is much less than that in the FEM.

The discrete total potential energy corresponding to Eq. (3.2.4) can be expressed

$$V(w_i,\lambda,w_{0j})=\frac{1}{2}K^{B1}_{ij}w_iw_j+\frac{1}{2}K^{B2}_{ijkl}w_iw_jw_kw_l$$
$$-\frac{\lambda}{2}K^{G1}_{ij}w_iw_j-\frac{\lambda}{8}K^{G2}_{ijkl}w_iw_jw_kw_l$$
$$-\lambda K^{G1}_{ij}w_iw_{0j} \qquad (3.3.1)$$

where K^{B1}_{ij} and K^{B2}_{ijkl} refer to the linear and nonlinear flexural stiffness matrices, respectively, whereas, K^{G1}_{ij} and K^{G2}_{ijkl} refer to the linear and nonlinear geometrical matrices, respectively. Each subscript i, j, k, *l* obeys the summation convention upto the total D.O.F.= N.

3.3.2 Stable symmetric buckling model

For the perfect model $w_{oj}=0$ (j=1,...,N), the characteristic equation at the critical point:

$$\det\,(K^{B1}_{ij}-\lambda K^{G1}_{ij})=0 \qquad (i,j=1,...,N) \qquad (3.3.2)$$

provides n eigenvector matrices, ϕ_{ij} (i=1,...N; j=1,...n) where n eigenvectors are chosen corresponding to their smaller n eigenvalues.

Then, the following modal transform is adopted:

$$w_i=\phi_{ij}v_j \qquad (i=1,...,N;\ j=1,...,n;\ 1\leq n<<N) \qquad (3.3.3)$$

This transform diagonalizes the Hessian matrix of the total potential energy in Eq. (3.3.1) at the critical point. Upon substitution of Eq. (3.3.3) into Eq. (3.3.1), the diagonalized potential energy D can be defined as:

$$\begin{aligned} D(v_i,\lambda,\varepsilon_j)=&\frac{1}{2}\tilde{K}^{B1}_{ij}v_iv_j+\frac{1}{2}\tilde{K}^{B2}_{ijkl}v_iv_jv_kv_l\\ &-\frac{\lambda}{2}\tilde{K}^{G1}_{ij}v_iv_j-\frac{\lambda}{8}\tilde{K}^{G2}_{ijkl}v_iv_jv_kv_l\\ &-\lambda\tilde{K}^{G1}_{ij}v_i\varepsilon_j \end{aligned} \qquad (3.3.4)$$

Furthermore, herein, the transform similar to Eq. (3.3.3) is adopted for the initial deflection w_{oi} (i=1,...,N), that is,

$$w_{0i}=\phi_{ij}\varepsilon_j \qquad (i=1,...,N;\ j=1,...,n;\ 1\leq n<<N) \qquad (3.3.5)$$

where ε_j corresponds to v_j (j=1,...,n) and

$$\begin{aligned} \tilde{K}^{B1}_{ij}&=K^{B1}_{mn}\phi_{mi}\phi_{nj},\\ \tilde{K}^{G1}_{ij}&=K^{G1}_{mn}\phi_{mi}\phi_{nj},\\ \tilde{K}^{B2}_{ijkl}&=K^{B2}_{mnpq}\phi_{mi}\phi_{nj}\phi_{pk}\phi_{ql},\\ \tilde{K}^{G2}_{ijkl}&=K^{G2}_{mnpq}\phi_{mi}\phi_{nj}\phi_{pk}\phi_{ql}. \end{aligned} \qquad (3.3.6)$$

Table 3.3.1 shows the numerical results by the discrete analyses of the model, with those through the continuous analysis and one degree-of-freedom analysis. The convergence of the buckling load λ_c and the 4th derivatives A^C_{1111} with respect to the number of discrete elements is illustrated in **Fig. 3.3.1.** It may be seen that the discretization method can surely realize the instability phenomena of the continuous model.

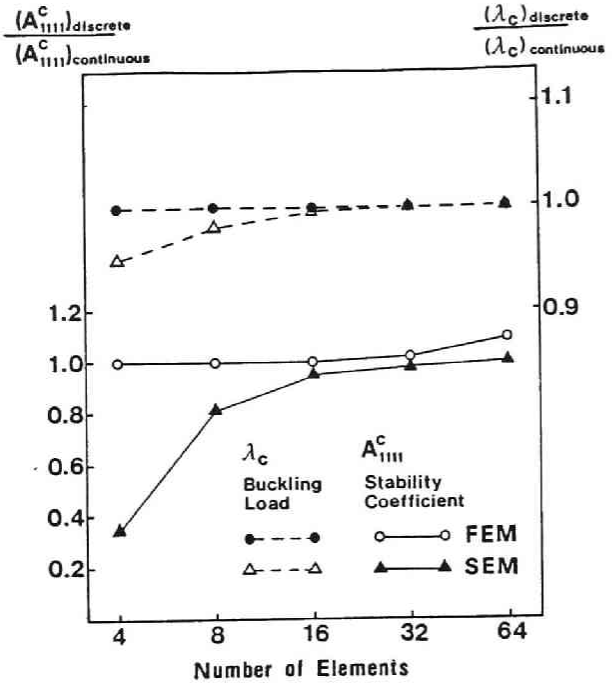

Fig. 3.3.1 Convergence of Buckling Strengths and Stability Curvatures.

3.3.3 Unstable symmetric buckling model

The discrete total potential energy corresponding to Eq. (3.2.9) is given by

$$V(w_i, \lambda, w_{0j})=\frac{1}{2}(K^{B1}_{ij}+K^{S}_{ij})w_iw_j+\frac{1}{2}K^{B2}_{ijkl}w_iw_jw_kw_l$$
$$-\frac{\lambda}{2}K^{G1}_{ij}w_iw_j-\frac{\lambda}{8}K^{G2}_{ijkl}w_iw_jw_kw_l$$
$$-\lambda K^{G1}_{ij}w_iw_{0j} \qquad (3.3.7)$$

where $K^S_{ji}=k\delta_{is}\delta_{js}$, superscript "S" refers to the spring stiffness, whereas subscript "s" refers to the nodal point on the elastic foundation, and δ_{ij} designates Kronecker's delta.

For simplicity, a new stiffness parameter κ will be introduced:

$$\kappa\equiv\frac{\pi^2EI}{KL^3}=\frac{\pi^2}{k}, \qquad k=\frac{KL^3}{EI} \qquad (3.3.8)$$

instead of the non-dimensionalized spring stiffness k.

Similarly to the continuous analysis, the following typical three instability phenomena may be found to occur, depending on the magnitude of κ :

$0<\kappa<1$: stable symmetric bifurcation (cusp catastrophe)

$\kappa=1$: double cusp catastrophe

$\kappa>1$: unstable symmetric bifurcation (dual cusp catastrophe)

Tables 3.3.2(a), (b) and (c) show the numerical results with those of the two-degree-of-freedom analysis and the continuous analysis. As an example, the bifurcation set for $\kappa=1.5$ in the continuous analysis is illustrated in **Fig. 3.3.2.**

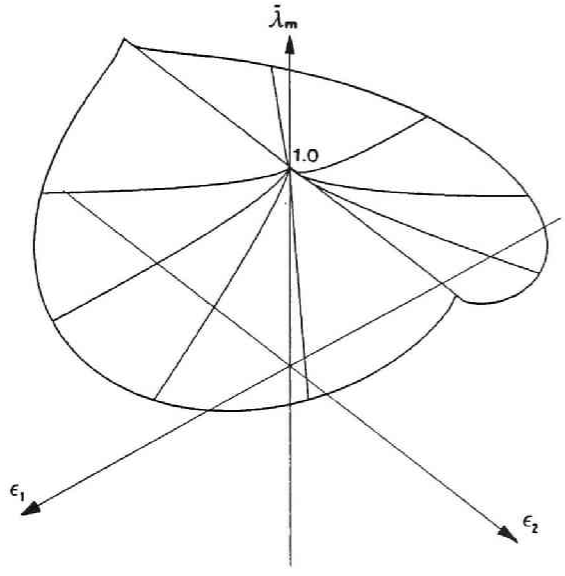

Fig. 3.3.2 Imperfection Sensitivity for Dual Cusp Catastrophe of Unstable Symmetric Model. $\kappa = 1.5$

3.3.4 Asymmetric buckling model

The discrete total potential energy corresponding to Eq. (3.2.14) is given by

$$V(w_i, \lambda, w_{0j})=\frac{1}{2}(K_{ij}^{B1}+K_{ij}^{S4})w_iw_j-\frac{\lambda}{2}K_{ij}^{G1}w_iw_j-\lambda K_{ij}^{G1}w_iw_{0j}$$
$$+\frac{1}{2}(K_{ijk}^{S2}+K_{ijk}^{S5})w_iw_jw_k-\frac{\lambda}{8}K_{ijkl}^{G2}w_iw_jw_kw_l$$
$$+\frac{1}{2}(K_{ijkl}^{B2}+K_{ijkl}^{S1}+K_{ijkl}^{S3}+K_{ijkl}^{S6})w_iw_jw_kw_l \qquad (3.3.9)$$

where

$$K_{ijkl}^{S1}=\frac{1}{8}kK_{ij}^{G1}K_{kl}^{G1}, \qquad K_{ijk}^{S2}=-\frac{1}{2}k\delta_{is}K_{jk}^{G1},$$
$$K_{ijkl}^{S3}=\frac{1}{8}k\delta_{is}\delta_{js}K_{kl}^{G1}, \qquad K_{ij}^{S4}=\frac{1}{2}k\delta_{is}\delta_{js}$$
$$K_{ijk}^{S5}=\frac{1}{4}k\delta_{is}\delta_{js}\delta_{ks}, \qquad K_{ijkl}^{S6}=-\frac{1}{32}k\delta_{is}\delta_{js}\delta_{ks}\delta_{ls},$$

and subscript "s" corresponds to the nodal point on the elastic foundation.

Then, the following typical three instability phenomena may be found to occur depending on the magnitude of κ introduced in Eq. (3.3.8):

Table 3.3.1 Stable Symmetric Buckling. - Cusp Catastrophe -

	CONTINUOUS METHOD	DISCRETIZATION METHODS										
		1-D.O.F.	Finite Element Method					Simplified Element Method				
Elements		2	4	8	16	32	64	4	8	16	32	64
D.O.F.		1	8 (3,5)	16 (7,9)	32 (15,17)	64 (31,32)	128 (63,65)	3	7	15	31	63
λ_c	9.870	8.000	9.875	9.870	9.870	9.870	9.870	9.373	9.743	9.838	9.862	9.868
A_1^{1c}	-48.705	-32.000	-48.684	-48.699	-48.708	-48.708	-48.708	-43.922	-47.468	-48.393	-48.630	-48.689
A_{11}^{oc}	-4.935	-4.000	-4.930	-4.934	-4.935	-4.935	-4.935	-4.686	-4.872	-4.919	-4.931	-4.934
A_{1111}^{c}	360.521 (1.000)	128.000 (0.355)	360.118 (0.999)	360.986 (1.001)	362.534 (1.006)	368.596 (1.022)	392.834 (1.090)	127.889 (0.355)	294.062 (0.816)	343.340 (0.952)	356.190 (0.988)	359.436 (0.997)

Table 3.3.2(a) Unstable Symmetric Buckling. - Cusp Catastrophe -

$$\kappa \equiv \pi^2 EI/(KL^3) = 0.5$$

	CONTINUOUS METHOD	DISCRETIZATION METHODS										
		2-D.O.F.	Finite Element Method					Simplified Element Method				
Elements		2	4	8	16	32	64	4	8	16	32	64
D.O.F.		2	9 (4,5)	17 (8,9)	33 (16,17)	65 (32,33)	129 (64,65)	4	8	16	32	64
λ_c	9.870	8.000	9.870	9.870	9.870	9.870	9.870	9.373	9.743	9.838	9.862	9.868
Mode	2	2	2	2	2	2	2	2	2	2	2	2
A_2^{2c}	-48.705	-32.000	-48.684	-48.699	-48.708	-48.708	-48.708	-43.922	-47.468	-48.393	-48.630	-48.689
A_{22}^{oc}	-4.935	-4.000	-4.930	-4.934	-4.935	-4.935	-4.935	-4.686	-4.872	-4.919	-4.931	-4.934
A_{2222}^{c}	360.521 (1.000)	128.000 (0.355)	360.118 (0.999)	360.987 (1.001)	362.534 (1.006)	368.596 (1.022)	392.834 (1.090)	127.889 (0.355)	294.062 (0.816)	343.340 (0.952)	356.190 (0.988)	359.436 (0.997)

Table 3.3.2(b) Unstable Symmetric Buckling. - Double Cusp Catastrophe -

$\kappa \equiv \pi^2 EI/(kL^3) = 1.0$

	CONTINUOUS METHOD	DISCRETIZATION METHODS										
		2-D.O.F.	Finite Element Method					Simplified Element Method				
Elements		2	4	8	16	32	64	4	8	16	32	64
D.O.F.		2	9 (4,5)	17 (8,9)	33 (16,17)	65 (32,33)	129 (64,65)	4	8	16	32	64
λ_{c1}	9.870	8.000	9.870	9.870	9.870	9.870	9.870	9.870	9.870	9.870	9.870	9.870
λ_{c2}	9.870	8.000	9.875	9.870	9.870	9.870	9.870	9.373	9.743	9.838	9.862	9.868
Mode	1 , 2	1 , 2	1 , 2	1 , 2	1 , 2	1 , 2	1 , 2	1 , 2	1 , 2	1 , 2	1 , 2	1 , 2
A_1^{1c}	-9.870	-8.000	-9.870	-9.870	-9.870	-9.870	-9.870	-9.870	-9.870	-9.870	-9.870	-9.870
A_2^{2c}	-48.705	-32.000	-48.684	-48.699	-48.708	-48.708	-48.708	-43.922	-47.468	-48.393	-48.630	-48.689
A_{11}^{oc}	-1.000	-1.000	-1.000	-1.000	-1.000	-1.000	-1.000	-1.000	-1.000	-1.000	-1.000	-1.000
A_{22}^{oc}	-4.935	-4.000	-4.930	-4.934	-4.935	-4.935	-4.935	-4.686	-4.872	-4.919	-4.931	-4.934
A_{1111}^{c}	-29.609 (1.000)	-29.610 (1.000)	-29.605 (1.000)	-29.595 (1.000)	-29.553 (0.999)	-29.388 (0.993)	-28.724 (0.970)	-28.118 (0.950)	-29.230 (0.987)	-29.514 (0.997)	-29.585 (0.999)	-29.603 (1.000)
A_{2222}^{c}	360.521 (1.000)	128.000 (0.355)	360.671 (1.000)	361.022 (1.001)	362.535 (1.006)	368.596 (1.022)	392.784 (1.090)	127.889 (0.355)	294.062 (0.816)	343.340 (0.952)	356.190 (0.988)	359.437 (0.997)

Table 3.3.2(c) Unstable Symmetric Buckling. - Dual Cusp Catastrophe -

$\kappa \equiv \pi^2 EI/(KL^3) = 1.5$

	CONTINUOUS METHOD	DISCRETIZATION METHODS										
		2-D.O.F.	Finite Element Method					Simplified Element Method				
Elements		2	4	8	16	32	64	4	8	16	32	64
D.O.F.		2	9 (4,5)	17 (8,9)	33 (16,17)	65 (32,33)	129 (64,65)	4	8	16	32	64
λ_c	6.580	6.580	6.580	6.580	6.580	6.580	6.580	6.580	6.580	6.580	6.580	6.580
Mode	1	1	1	1	1	1	1	1	1	1	1	1
A_1^{1c}	-6.580	-6.580	-6.580	-6.580	-6.580	-6.580	-6.580	-6.580	-6.580	-6.580	-6.580	-6.580
A_{11}^{oc}	-1.000	-1.000	-1.000	-1.000	-1.000	-1.000	-1.000	-1.000	-1.000	-1.000	-1.000	-1.000
A_{1111}^{c}	-19.739 (1.000)	-19.740 (1.000)	-19.736 (1.000)	-19.725 (0.999)	-19.684 (0.997)	-19.518 (0.989)	-18.854 (0.955)	-19.739 (1.000)	-19.739 (1.000)	-19.739 (1.000)	-19.739 (1.000)	-19.739 (1.000)

$0 < \kappa < 0.5$: unstable symmetric bifurcation (dual cusp catastrophe)

$\kappa = 0.5$: homeoclinal bifurcation (hyperbolic umbilic catastrophe)

$\kappa > 0.5$: asymmetric bifurcation (fold catastrophe)

Tables 3.3.3(a), (b) and (c) show the numerical results with those of the two-degree-of-freedom analysis and the continuous analysis. The bifurcation sets in the continuous analysis are illustrated in **Figs. 3.3.3, 3.3.4** and **3.3.5** for κ =0.25, 0.5 and 0.75, respectively[5,20,21].

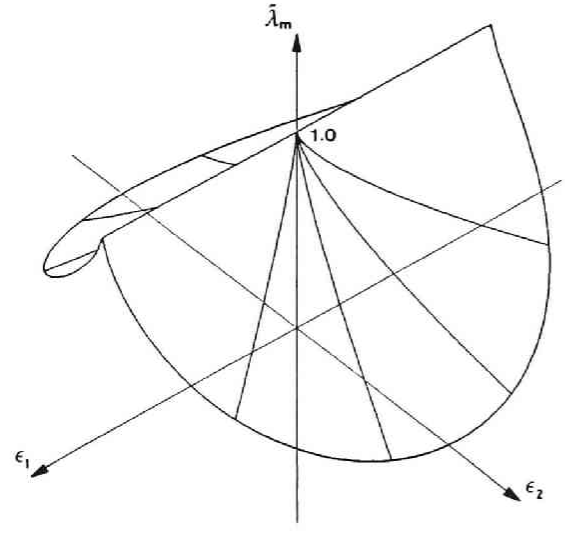

Fig. 3.3.3 Imperfection Sensitivity for Dual Cusp Catastrophe of Asymmetric Model. κ = 0.25

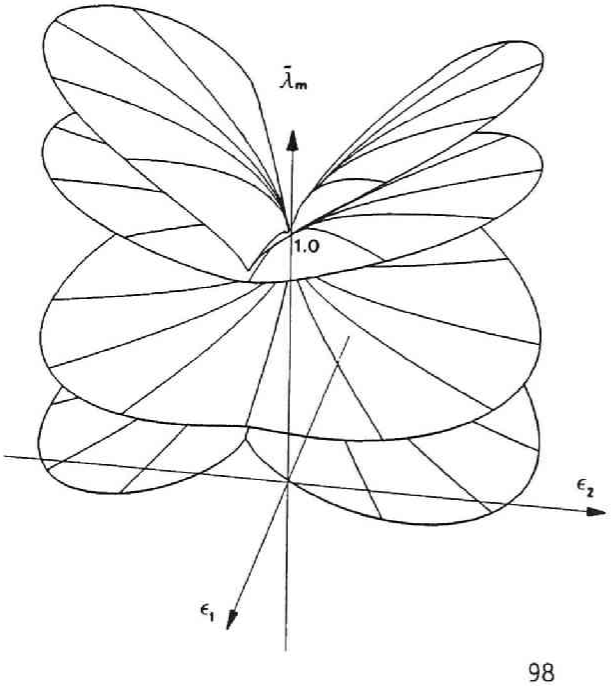

Fig. 3.3.4(a) Imperfection Sensitivity for Hyperbolic Umbilic Catastrophe of Asymmetric Model.
- All Sheets - κ = 0.5

Table 3.3.3(a) Asymmetric Buckling. - Dual Cusp Catastrophe -

$\kappa \equiv \pi^2 EI/(KL^3) = 0.25$

	CONTINUOUS METHOD	DISCRETIZATION METHODS									
		2-D.O.F.	Finite Element Method					Simplified Element Method			
Elements		2	4	8	16	32	64	4	8	16	32	64
D.O.F.		2	9 (4,5)	17 (8,9)	33 (16,17)	65 (32,33)	129 (64,65)	4	8	16	32	64
λ_c	9.870	8.000	9.875	9.870	9.870	9.870	9.870	9.373	9.743	9.838	9.862	9.868
Mode	2	2	2	2	2	2	2	2	2	2	2	2
A_2^{2c}	-48.705	-32.000	-48.684	-48.699	-48.708	-48.708	-48.708	-43.922	-47.468	-48.393	-48.630	-48.689
A_{22}^{0c}	-4.935	-4.000	-4.930	-4.934	-4.935	-4.935	-4.935	-4.686	-4.872	-4.919	-4.931	-4.934
D_{11}^{c}	9.870	11.739	9.865	9.870	9.870	9.870	9.870	10.367	9.996	9.901	9.878	9.872
D_{122}^{c}	-97.409	-78.957	-97.307	-97.403	-97.409	-97.409	-97.409	-92.504	-96.164	-97.096	-97.331	-97.390
D_{2222}^{c}	1802.605	1075.480	1799.186	1802.880	1804.604	1810.678	1834.916	1428.387	1699.504	1776.166	1795.938	1800.941
A_{2222}^{c}	-1081.563 (1.000)	-517.724 (0.479)	-1080.282 (0.999)	-1080.811 (0.999)	-1079.442 (0.998)	-1073.442 (0.992)	-1049.131 (0.970)	-1047.833 (0.969)	-1075.861 (0.994)	-1080.404 (0.999)	-1081.160 (1.000)	-1081.397 (1.000)

Table 3.3.3(b) Asymmetric Buckling. - Hyperbolic Umbilic Catastrophe -

$\kappa \equiv \pi^2 EI/(KL^3) = 0.5$

	CONTINUOUS METHOD	DISCRETIZATION METHODS									
		2-D.O.F.	Finite Element Method					Simplified Element Method			
Elements		2	4	8	16	32	64	4	8	16	32	64
D.O.F.		2	9 (4.5)	17 (8,9)	33 (16,17)	65 (32,33)	129 (64,65)	4	8	16	32	64
λ_{c1}	9.870	8.000	9.870	9.870	9.870	9.870	9.870	9.870	9.870	9.870	9.870	9.870
λ_{c2}	9.870	8.000	9.875	9.870	9.870	9.870	9.870	9.373	9.743	9.838	9.862	9.868
Mode	1 , 2	1 , 2	1 , 2	1 , 2	1 , 2	1 , 2	1 , 2	1 , 2	1 , 2	1 , 2	1 , 2	1 , 2
A_1^{1c}	-9.870	-8.000	-9.870	-9.870	-9.870	-9.870	-9.870	-9.870	-9.870	-9.870	-9.870	-9.870
A_2^{2c}	-48.705	-32.000	-48.684	-48.699	-48.708	-48.708	-48.708	-43.922	-47.468	-48.393	-48.630	-48.689
A_{11}^{0c}	-1.000	-1.000	-1.000	-1.000	-1.000	-1.000	-1.000	-1.000	-1.000	-1.000	-1.000	-1.000
A_{22}^{0c}	-4.935	-4.000	-4.930	-4.934	-4.935	-4.935	-4.935	-4.686	-4.872	-4.919	-4.931	-4.934
A_{111}^{c}	-14.804 (1.000)	-12.000 (0.811)	-14.804 (1.000)	-14.804 (1.000)	-14.804 (1.000)	-14.804 (1.000)	-14.804 (1.000)	-14.804 (1.000)	-14.804 (1.000)	-14.804 (1.000)	-14.804 (1.000)	-14.804 (1.000)
A_{122}^{c}	-48.705 (1.000)	-32.000 (0.657)	-48.654 (0.999)	-48.701 (1.000)	-48.704 (1.000)	-48.705 (1.000)	-48.713 (1.000)	-46.252 (0.950)	-48.082 (0.987)	-48.584 (0.997)	-48.665 (0.999)	-48.695 (1.000)

Table 3.3.3(c) Asymmetric Buckling. - Fold Catastrophe -

$\kappa \equiv \pi^2 EI/(KL^3) = 0.75$

	CONTINUOUS METHOD	DISCRETIZATION METHODS										
		2-D.O.F.	Finite Element Method					Simplified Element Method				
Elements		2	4	8	16	32	64	4	8	16	32	64
D.O.F.		2	9 (4,5)	17 (8,9)	33 (16,17)	65 (32,33)	129 (64,65)	4	8	16	32	64
λ_c	6.580	6.580	6.580	6.580	6.580	6.580	6.580	6.580	6.580	6.580	6.580	6.58(
Mode	1	1	1	1	1	1	1	1	1	1	1	1
A_1^{1c}	-6.580	-6.580	-6.580	-6.580	-6.580	-6.580	-6.580	-6.580	-6.580	-6.580	-6.580	-6.58(
A_{11}^{oc}	-1.000	-1.000	-1.000	-1.000	-1.000	-1.000	-1.000	-1.000	-1.000	-1.000	-1.000	-1.00(
A_{111}^{c}	-9.870 (1.000)	-9.870 (1.000)	-9.870 (1.000)	-9.870 (1.000)	-9.870 (1.000)	-9.870 (1.000)	-9.870 (1.000)	-9.870 (1.000)	-9.870 (1.000)	-9.870 (1.000)	-9.870 (1.000)	-9.87((1.00(

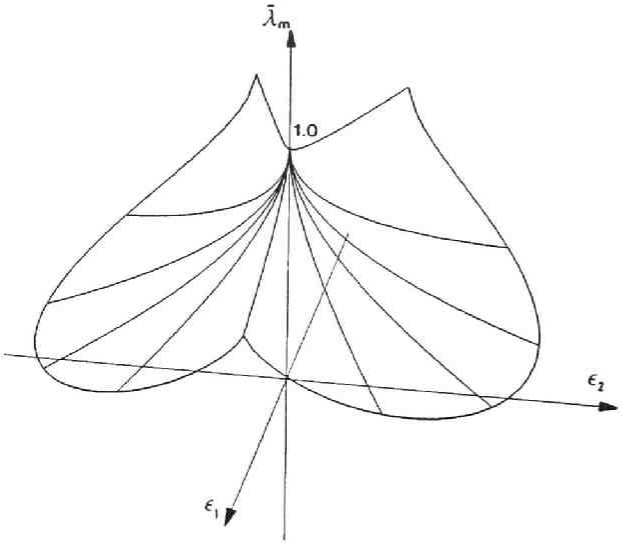

Fig. 3.3.4(b) Imperfection Sensitivity for Hyperbolic Umbilic Catastrophe of Asymmetric Model. κ = 0.5 - Only the Lowest Sheet -

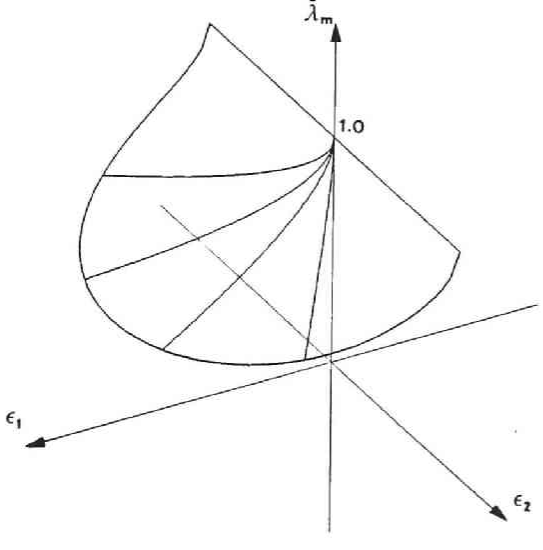

Fig. 3.3.5 Imperfection Sensitivity for Fold Catastrophe with Asymmetric Model. κ = 0.75

3.4 Discussions

Detailed discussions will be presented herein based on **Tables 3.2.1, 3.3.1, 3.3.2** and **3.3.3**, and **Figs. 3.3.1, 3.3.2, 3.3.3, 3.3.4** and **3.3.5**, comparing the numerical results of both the continuous and discrete analyses.

Table 3.2.1 shows how the degree of the order of the approximation for either a curvature κ_x or a shortening Δ may affect the form of the total potential energy. The first order approximations in the first row give a linear eigenvalue problem, from which only the critical bifurcation buckling load and its buckling mode can be evaluated. The fourth order approximations in the last row are found to describe the geometrical nonlinearity with sufficient accuracy. The second and third rows in the table indicate that the potential energies fail to evaluate rigorously either the flexural strain energy or the external work.

Three tables in the previous section 3 provide a complete comparison among the numerical results of stability coefficients as A^c_{111} , A^c_{1111} for the one-degree-of-freedom, two-degree-of-freedom, continuous and discrete analyses. Furthermore, in these tables, the two figures in parentheses in the second row, pertaining to the FEM, refer to the D.O.F. of the lateral deflection and that of the rotation, respectively. The value in parentheses in the rows of stability coefficients such as A^c_{111} , A^c_{1111} indicate the ratio of the value of each coefficient through discrete analyses to the value of the corresponding coefficient through the continuous analyses.

Table 3.3.1 shows the numerical results for the stable symmetric buckling model. **Fig. 3.3.1** illustrates the convergence of the buckling loads and the 4th order stability coefficients A^c_{1111} with respect to the number of finite elements. Obviously, the discrete analyses can be shown to realize the instability phenomena, predicted by the continuous analysis. The FEM used herein, however, may seem to tend to estimate the values of A^c_{1111} slightly larger than the SEM, with an increase of the number of elements.

The numerical results are shown in **Table 3.3.2** for the unstable symmetric buckling model. In this case, the discrete analysis can be also shown to realize the continuous model. Similarly, the FEM will tend to overestimate slightly the values of A^c_{1111}, , A^c_{2222} etc., in comparison with the SEM.

Fig. 3.3.2 illustrates a bifurcation set for $\kappa=1.5$ in the continuous analysis. The surface of the bifurcation set represents the **dual cusp** catastrophe with respect to the buckling model 1, **i.e.**, the mode for the buckling of the column structure. It is symmetric with respect to the plane of $\varepsilon_1=0$. Furthermore, it has no dependence on the value of ε_2 , which is called the two-thirds power law. For example, if ε_1 = 1/1000, ε_2 = 0, then $\bar{\lambda}_m$ = 0.985. The load-carrying capacity will thus be reduced by 1.5 %, compared to the buckling load.

Table 3.3.3 shows the numerical results for the asymmetric buckling model. The bifurcation sets in the continuous analysis are illustrated in **Figs. 3.3.3, 3.3.4** and **3.3.5** for κ =0.25, 0.5 and 0.75, respectively.

The bifurcation set for κ =0.25 is shown in **Fig. 3.3.3.** The surface of the bifurcation set corresponds to the dual cusp catastrophe with respect to the buckling mode 2, **i.e.**, the straight line rigid-body mode. It is symmetric with respect to the plane $\varepsilon_2=0$ independent of ε_1 . For example, if $\varepsilon_1=0$, ε_2 = 1/1000. then $\bar{\lambda}_m$ = 0.971, so that the load-carrying capacity will be reduced by

2.9 % compared to the buckling load.

Fig. 3.3.4 illustrates the bifurcation sets of a typical hyperbolic umbilic catastrophe for κ =0.5. The bifurcation point has been called the homeoclinal bifurcation point of the semi-symmetric buckling by Thompson. For example, if ε_1 = 0, ε_2 = 1/1000, then $\bar{\lambda}_m$ = 0.851, and if ε_1 = 1/1000, ε_2 = 0, then $\bar{\lambda}_m$ = 0.937. Thus, the load-carrying capacity will be reduced by 14.9 % and 6.4 %, respectively, from the buckling load.

Fig. 3.3.5 illustrates the bifurcation set of a fold catastrophe with respect to the buckling mode 1 for κ =0.75. It will exist only if $\varepsilon_1 > 0$ independently on ε_2 . For example, if ε_1 = 1/1000, ε_2 = 0, then $\bar{\lambda}_m$ = 0.923, whereby the load-carrying capacity will be reduced by 7.7 % from the buckling load.

From three numerical results, the effects of the initial imperfections on the load-carrying capacity may be found to be significantly sensitive for the asymmetric buckling model. The imperfection sensitivity to the mode 2, ε_2 of the compound buckling for κ =0.5, may seem to be much greater than that of a distinct buckling of the mode 2 for κ =0.25.

Next, several discussions on the error and convergence of each stability coefficient may be made. The values of the stability coefficients calculated by a discrete analysis may converge to those in a continuous analysis, as the number of discretized elements increases. Especially, the stability coefficients through the SEM may converge rapidly to the value through the continuous analysis. The value by the FEM, on the other hand, may have a tendency to overestimate slightly, as the number of elements becomes larger as mentioned previously. The FEM provides a very accurate value of the buckling loads regardless of any kinds of models and any buckling modes.

The values of the stability coefficients for the rigid buckling mode 1 of the elastic foundation can be evaluated precisely for any modes, and in any analyses. Those for the mode 2 of the column structures, however, may contain slight errors depending on the degree of approximation of the mode shape.

3.5 Conclusions

For several simple elastic conservative column structures, both continuous and discrete analyses were performed. The numerical results were compared with the two-degree-of-freedom analyses. The main conclusions are:

(1) The discrete analysis can be shown to realize the instability phenomena, predicted by the continuous analysis. The results of the discrete analysis are shown to converge to those of the continuous analysis generally, as the number of discrete finite elements increases.

(2) The imperfection sensitivity of structures can be evaluated qualitatively and quantitatively by means of the bifurcation set in the control space through the catastrophe theory.

(3) For a legitimate evaluation of the **cusp** and **dual cusp** catastrophe, the 4th order terms of the buckling mode in the total potential energy must be considered rigorously in expressions for both the strain energy and the external work.

(4) The stable symmetric buckling model is shown to indicate the typical **cusp** catastrophe.

(5) The unstable symmetric buckling model can be shown to indicate the typical **dual cusp** catastrophe for a relatively small stiffness of the elastic foundation, the **cusp** catastrophe for a relatively large stiffness, and the compound **double cusp** catastrophe at a certain critical stiffness value.

(6) The asymmetric buckling model can be shown to indicate the typical **fold** catastrophe for a relatively small stiffness of the inclined elastic foundation, the **dual cusp** catastrophe for a relatively large stiffness, and the compound **hyperbolic umbilic** catastrophe at a certain critical stiffness value.

(7) The value of each stability coefficient calculated by discretization methods may generally converge to that by the continuous analyses.

(8) The value of each stability coefficient calculated by the FEM may tend to overestimate slightly in comparison with the SEM, as the number of discrete finite elements increases.

(9) The true load-carrying capacity of the column structures should be investigated, taking into account such things as the extensibility, the elasto-plasticity of the material and the residual stresses of the cross section.

Bibliographies of Chapter 2 in PART II

1) Thompson,J.M.T. and G.W.Hunt, A General Theory of Elastic Stability. John Wiley & Sons, 1973.
2) Niwa,Y., E.Watanabe and N.Nakagawa, Catastrophe and imperfection sensitivity of two-degree-of-freedom systems. Proceedings of the Japan Society of Civil Engineers, No. 307, pp. 99-111, 1981.
3) Niwa,Y., E.Watanabe and H.Isami, Catastrophe analysis of structures by discretization and modal transforms. Memoirs of the Faculty of Engineering, Kyoto University, Vol. 43, pp. 67-87, 1981.
4) Niwa,Y., E.Watanabe and H.Isami, Catastrophes of elastic column structures. Memoirs of the Faculty of Engineering, Kyoto University, Vol. 45, pp. 71-97, 1983.
5) Isami,H., A topological aspect of imperfection sensitivity of structures. Bulletin of Kohchi Technical College, No. 20, pp. 85-94, 1984.
6) Thompson,J.M.T. and G.W.Hunt, Comparative perturbation studies of the Elastica. International Journal of Mechanical Sciences, Vol. 11, pp. 999-1014, 1969.
7) Roorda,J., Stability of structures with small imperfections. Journal of the Engineering Mechanics Division, Proc. ASCE, Vol. 91, No. EM1, pp. 87-106, 1965.
8) Roorda,J., Buckling of Elastic Structures. Special Publications Series, Solid Mechanics Division, University of Waterloo Press, 1980.
9) Britvec,S.J., The Stability of Elastic Systems. Pergamon Press, 1973.
10) Huseyin,K., Vibrations and Stability of Multiple Parameter Systems. Mechanics of Elastic Stability, Sijthoff & Noordoff, 1978.
11) Poston,T. and I.Stewart, Catastrophe Theory and Its Applications. Pitman, 1978.

12) Poston,T. and I.Stewart, Taylor Expansions and Catastrophes. Research Notes in Mathematics, No. 7, Pitman, 1976.
13) Gilmore,R., Catastrophe Theory for Scientists and Engineers. John Wiley & Sons, 1981.
14) Zeeman,E.C., Euler buckling. Structural Stability, the Theory of Catastrophes, and Applications in the Sciences, Lecture Notes in Mathematics, Vol. 525, Springer-Verlag, pp. 373-395, 1976.
15) Thom,R., Structural Stability and Morphogenesis (translated from the French by D.H.Fowler). Benjamin, 1975.
16) Thompson,J.M.T. and G.W.Hunt, Towards a unified bifurcation theory. Journal of Applied Mathematics and Physics (Zeitschrift für Angewandte Mathematik und Physik), Vol. 26, pp. 581-603, 1975.
17) Zeeman,E.C., The umbilic bracelet and the double-cusp catastrophe. Structural Stability, the Theory of Catastrophes, and Applications in the Sciences, Lecture Notes in Mathematics, Vol. 525, Springer-Verlag, pp. 328-366, 1976.
18) Thompson,J.M.T., J.K.T.Tan and K.C.Lim, On the topological classification of post-buckling phenomena. Journal of Structural Mechanics, Vol. 6, pp. 384-414, 1978.
19) Yamada,Y., E.Watanabe and R.Ito, Compressive strength of plates with close-sectional ribs. Proceedings of the Japan Society of Civil Engineers, No. 278, pp. 133-147, 1978.
20) Hunt,G.W., An algorithm of the nonlinear analysis of compound bifurcation. Philosophical Transactions of the Royal Society of London, Series A, Vol. 300, pp. 443-471, 1981.
21) Huseyin,K. and V.Mandadi, On the imperfection-sensitivity of compound branching. Ingenieur-Archiv, Vol. 46, pp. 213-222, 1977.

CHAPTER 4

APPLICATIONS TO ELASTIC COLUMN AND PLATE STRUCTURES THROUGH STATIC CONDENSATION PROCEDURE

4.1 General Remarks

This chapter is concerned with applications of the catastrophe analysis proposed in the previous chapter II-1 to evaluating elastic initial postbuckling characteristics of several structural models such as columns, unstiffened plates and stiffened plates. The numerical formulation is made through discretization and modal transforms[1,2]. Then, it includes the static condensation procedure and the load- and displacement-control types as previously stated in the chapter II-1 if these strategies are necessary.

Firstly, the three prototypes of structural buckling models in the chapter II-3 are also adopted herein[3-7]. However, each model in this chapter differs from the original one with an **inextensible** column, that is, it consists of an **extensible** column and an elastic spring representing an elastic foundation. Such an extensibility of column is commonly neglected to estimate its Euler buckling load [8,9]. Based on both the theoretical and numerical results, an effect of extensibility of column on its stability characteristics at the critical point will be investigated briefly. Furthermore, the imperfection sensitivity surfaces of the model are drawn spatially in terms of the bifurcation sets[4,10-12].

Secondly, the primary buckling of compressed rectangular plates will be studied using the proposed catastrophe analysis under the two control types of load and displacement[1,2]. Especially, the obtained initial postbuckling and the typical nonlinear equilibrium solutions are compared with those by Timoshenko, Coan, Yamaki, Williams and Rhodes for compressed square plates under various supporting conditions[8,13-18] and control types as mentioned in the chapter II-1. Then, a validity and an applicability will be made clear of the present catastrophe analysis.

Finally, such applications of the present catastrophe analysis lead to compound bifurcation problems when compressed stiffened plate buckles simultaneously in both modes of an Euler-type column for a stiffener and of an isolated local plate between stiffeners[1,19-24]. Moreover, the imperfection sensitivity surfaces of the stiffened plate for the simultaneous bifurcations as well as a distinct asymmetric bifurcation one with only the primary global mode are shown spatially in the form of three-dimensional surfaces[10,12,19,25].

4.2 Elastic Extensible Columns

The three typical buckling models of compressed columns in the chapter II-3 are also considered herein. In the previous chapter, it is assumed that the column is **inextensible** on the neutral axis, neglecting the axial deformations. Then, the prototypes of catastrophes such as cusp, fold and umbilics are investigated in order to evaluate their imperfection sensitivity surfaces[3,4,5]. However, the column models considered in this chapter is assumed to be **extensible** in the neutral-axis direction. Therefore, an effect of the extensibility of column on its stability will be briefly studied in view of the analytical and numerical interpretations.

Figs. 4.2.1, 4.2.2 and **4.2.3** show the stable symmetric, the unstable symmetric and the asymmetric buckling models corresponding to **Figs. 3.2.1, 3.2.2** and **3.2.3** in the chapter II-3, respectively. Also, **Tables 4.2.1, 4.2.2** and **4.2.3** list the numerical results by the present analyses of the three extensible column models. In which, the two computations of a finite element method (abbreviated as FEM) and a simplified element method (SEM) in APPENDIX[26-29] are compared each other. They are performed for column models having the number of discrete elements of 32 with the maximum number of out-of-plane deflections of 65 and 32 by the FEM and the SEM, respectively. Note that all the proposed results are obtained with respect to the buckling deflection modes whose amplitudes are non-dimensionalized by the undeformed column-span length L.

From these calculations, it is found that, for the asymmetric buckling (fold) and the semi-symmetric compound buckling (umbilic) associated with the cubic terms of the potential function, some instabilities of the extensible column models can be similarly realized into those in the case of the inextensible models in the chapter II-3. Then, all the numerical results are identical, regardless of the procedures of the FEM and the SEM with increase of the number of discrete elements. The asymmetric and the semi-symmetric bucklings are both related to evaluations of the cubic terms of the potential function at the critical point[30,31]. The cubic terms are defined by directly deriving from the changes of large geometrical configurations of the model, and they never depend on whether the column is extensible or not.

However, it is shown that, for the extensible columns, the symmetric bifurcations obtained from the quartic terms of the potential function can not be completely realized similarly to those of the inextensible models in the chapter II-3. Then, the numerical computations by the SEM provide no postbuckling strength of column models with respect to the symmetric buckling except in the case of the unstable symmetric bifurcation of the asymmetric models in **Fig. 4.2.3.** Also, all FEM's results give the stable symmetric buckling characteristics. In order to clarify the reason of such inconsistencies, an analytical discussion will be carried out as follows:

Let U(X) and W(X) denote the in-plane axial displacement and the out-of-plane lateral deflection at the axial point X, where X refers to the axial coordinate of the original perfect column model, differently from the inextensible neutral axis X in the previous chapter II-3. Then, an axial strain ε_x at the point X is given by

$$\left.\begin{aligned} &\varepsilon_x = \varepsilon_{ox} - Z\,\kappa_x \\ &\text{where} \\ &\varepsilon_{ox} = U_{,x} + \frac{1}{2} W^2_{,x}\,, \qquad \kappa_x = W_{,xx} \\ &\text{and} \\ &U_{,x} = \frac{dU}{dX}\,, \quad W_{,x} = \frac{dW}{dX}\,, \quad W_{,xx} = \frac{d^2W}{dX^2} \end{aligned}\right\} \qquad (4.2.1)$$

In which, ε_{ox} and κ_x represent the well-known Green's strain tensor of column and the first approximation of its curvature in **Table II-3.2.1**, respectively. Also, the coordinate perpendicular to the axis X is designated as Z, whose direction coincides with that of the deflection W. An accurate expression of the curvature

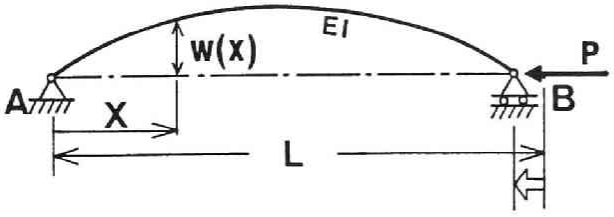

Fig. 4.2.1 Stable Symmetric Buckling Model.

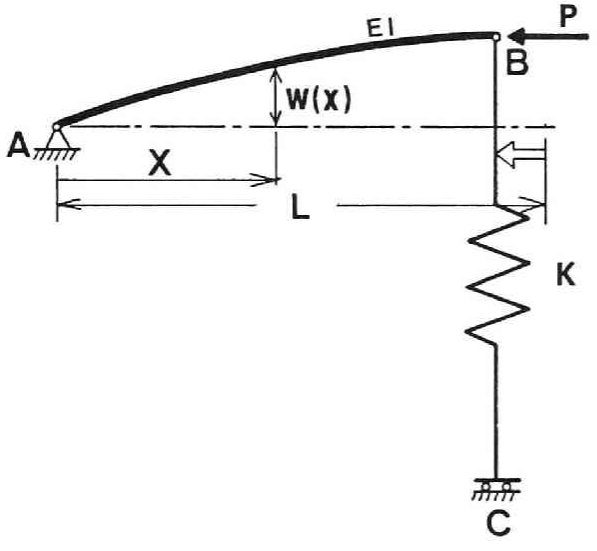

Fig. 4.2.2 Unstable Symmetric Buckling Model.

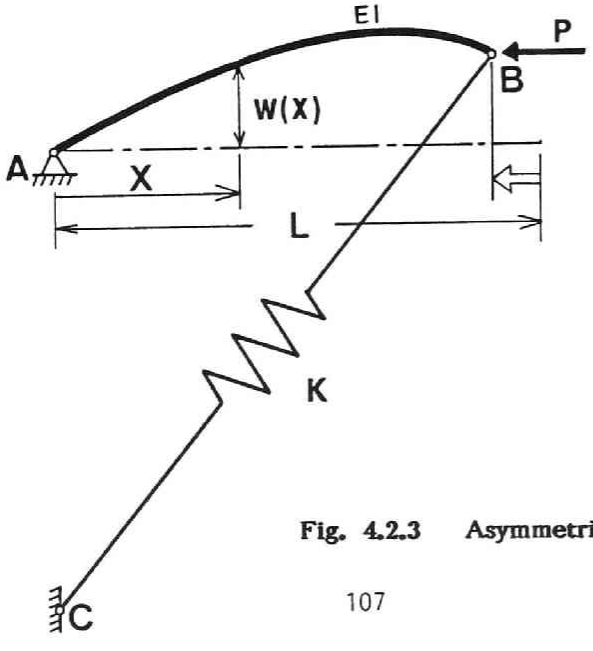

Fig. 4.2.3 Asymmetric Buckling Model.

Table 4.2.1 Stable Symmetric Buckling Model.

	Continuous Method*	Discretization Methods							
		Finite Element Method				Simplified Element Method			
Elements		4	8	16	32	4	8	16	32
D.O.F.		12 (4,8)	24 (8,16)	48 (16,32)	96 (32,64)	7 (4,3)	15 (8,7)	31 (16,15)	63 (32,31)
Mode	1	1	1	1	1	1	1	1	1
Λ^c	9.870	9.870	9.870	9.870	9.870	9.372	9.743	9.838	9.870
A_1^{1c}	-48.705	-48.699	-48.699	-48.699	-48.699	-43.927	-47.458	-48.393	-48.551
A_{11}^{oc}	-4.935	-4.934	-4.934	-4.934	-4.934	-4.687	-4.871	-4.919	-4.919
A_{1111}^c	360.521	130329.36	35669.76	11109.12	10884.48	order (10^{-14} - 10^{-12})			
C**	1.234	445.733	122.077	38.020	37.251	order (10^{-14} - 10^{-12})			

* Results for "inextensible" columns.

** Stability curvature $C = -A^c_{1111}/(6A^{oc}_{11}\Lambda^c)$

Table 4.2.2(a) Unstable Symmetric Buckling Model.

$K = \pi^2 EI/kL^3 = 0.75$

	Continuous Method *	Discretization Methods							
		Finite Element Method				Simplified Element Method			
Elements		4	8	16	32	4	8	16	32
D.O.F.		13 (4,9)	25 (8,17)	49 (16,33)	97 (32,65)	8 (4,4)	16 (8,8)	32 (16,16)	64 (32,32)
Mode	2	2	2	2	2	2	2	2	2
Λ^c	9.870	9.870	9.870	9.870	9.870	9.372	9.743	9.838	9.870
A_2^{2c}	-48.705	-48.699	-48.699	-48.699	-48.699	-43.927	-47.458	-48.393	-48.551
A_{22}^{oc}	-4.935	-4.934	-4.934	-4.934	-4.934	-4.687	-4.871	-4.919	-4.919
A_{2222}^c	360.521	130329.36	35669.76	11109.12	10884.48	order (10^{-14} - 10^{-12})			
C **	1.234	445.733	122.077	38.020	37.251	order (10^{-14} - 10^{-12})			

* Results for "inextensible" columns.

** Stability curvature $C = -A^c_{2222}/(6A^{oc}_{22}\Lambda^c)$

Table 4.2.2(b) Unstable Symmetric Buckling Model.

$K = \pi^2 EI/kL^3 = 1.0$

	Continuous Method*	Discretization Methods							
		Finite Element Method				Simplified Element Method			
Elements		4	8	16	32	4	8	16	32
D.O.F.		13 (4,9)	25 (8,17)	49 (16,33)	97 (32,65)	8 (4,4)	16 (8,8)	32 (16,16)	64 (32,32)
Mode	1,2	1,2	1,2	1,2	1,2	1,2	1,2	1,2	1,2
Λ_1^c	9.870	9.874	9.870	9.870	9.870	9.870	9.870	9.870	9.870
Λ_2^c	9.870	9.870	9.870	9.870	9.870	9.372	9.743	9.838	9.870
A_1^{1c}	-9.870	-9.864	-9.860	-9.860	-9.860	-9.860	-9.860	-9.860	-9.860
A_2^{2c}	-48.705	-48.699	-48.699	-48.699	-48.699	-43.927	-47.458	-48.393	-48.551
A_{11}^{oc}	-1.000	-0.999	-0.999	-0.999	-0.999	-0.999	-0.999	-0.999	-0.999
A_{22}^{oc}	-4.935	-4.934	-4.934	-4.934	-4.934	-4.687	-4.871	-4.919	-4.919
A_{1111}^c	-29.609	49.267	319.104	2227.20	16475.52	order ($10^{-13} - 10^{-12}$)			
A_{2222}^c	360.521	130239.36	35667.84	11111.04	1089.408	order ($10^{-13} - 10^{-12}$)			
C_1**	-0.500	0.832	5.394	37.647	278.487	order ($10^{-13} - 10^{-12}$)			
C_2	1.234	445.733	122.077	38.020	37.251	order ($10^{-13} - 10^{-12}$)			

* Results for "inextensible" columns.

** Stability curvatures $C_1 = -A_{1111}^c/(6A_{11}^{oc}\Lambda_1^c)$, $C_2 = -A_{2222}^c/(6A_{22}^{oc}\Lambda_2^c)$

Table 4.2.2(c) Unstable Symmetric Buckling Model.

$K = \pi^2 EI/kL^3 = 1.25$

	Continuous Method*	Discretization Methods							
		Finite Element Method				Simplified Element Method			
Elements		4	8	16	32	4	8	16	32
D.O.F.		13 (4,9)	25 (8,17)	49 (16,33)	97 (32,65)	8 (4,4)	16 (8,8)	32 (16,16)	64 (32,32)
Mode	1	1	1	1	1	1	1	1	1
Λ^c	7.896	7.896	7.896	7.896	7.896	7.896	7.896	7.896	7.896
A_1^{1c}	-7.896	-7.896	-7.896	-7.896	-7.896	-7.896	-7.896	-7.896	-7.896
A_{11}^{oc}	-1.000	-0.999	-0.999	-0.999	-0.999	-0.999	-0.999	-0.999	-0.999
A_{1111}^c	-23.687	49.267	319.296	2227.20	16477.44	order ($10^{-13} - 10^{-12}$)			
C**	-0.500	0.832	5.394	37.647	278.487	order ($10^{-13} - 10^{-12}$)			

* Results for "inextensible" columns.

** Stability curvature $C = -A_{1111}^c/(6A_{11}^{oc}\Lambda^c)$

Table 4.2.3(a) Asymmetric Buckling Model.

$\kappa = \pi^2 EI/kL^3 = 0.25$ - Dual Cusp Catastrophe -

	Continuous Method*	Discretization Methods							
		Finite Element Method				Simplified Element Method			
Elements		4	8	16	32	4	8	16	32
D.O.F.		13 (4,9)	25 (8,17)	49 (16,33)	97 (32,65)	8 (4,4)	16 (8,8)	32 (16,16)	64 (32,32)
Mode	2	2	2	2	2	2	2	2	2
Λ^c	9.870	9.884	9.880	9.880	9.880	9.382	9.753	9.848	9.872
A_1^{1c}	-48.705	-48.679	-48.703	-48.704	-48.704	-43.923	-47.469	-48.392	-48.626
A_{11}^{oc}	-4.935	-4.924	-4.929	-4.930	-4.930	-4.681	-4.867	-4.914	-4.926
D_{11}^c	9.870	9.849	9.854	9.853	9.830	10.351	9.980	9.887	9.815
D_{122}^c	-97.409	-97.208	-97.302	-97.308	-97.309	-92.409	-96.065	-96.996	-97.231
D_{2222}^c	1802.605	131679.09	37108.90	12550.97	12324.62	1301.081	1402.942	1433.487	1438.508
A_{2222}^c	-1081.563	128800.81	34226.52	9667.93	9434.78	-1173.875	-1371.151	-1421.239	-1451.110
C **	-3.701	—	—	—	—	-4.454	-4.814	-4.894	-4.974

* Results for "inextensible" columns.

** Stability curvature $C = -A_{2222}^c/(6A_{22}^{oc}\Lambda_2^c)$

Table 4.2.3(b) Asymmetric Buckling Model.

$\kappa = \pi^2 EI/kL^3 = 0.5$

- Hyperbolic Umbilic Catastrophe -

	Continuous Method *	Discretization Methods							
		Finite Element Method				Simplified Element Method			
Elements		4	8	16	32	4	8	16	32
D.O.F.		13 (4,9)	25 (8,17)	49 (16,33)	97 (32,65)	8 (4,4)	16 (8,8)	32 (16,16)	64 (32,32)
Mode	1,2	1,2	1,2	1,2	1,2	1,2	1,2	1,2	1,2
Λ_1^c	9.870	9.872	9.872	9.872	9.872	9.872	9.872	9.872	9.872
Λ_2^c	9.870	9.880	9.875	9.875	9.877	9.377	9.748	9.843	9.867
A_1^{1c}	-9.870	-9.864	-9.864	-9.864	-9.864	-9.864	-9.864	-9.864	-9.864
A_2^{2c}	-48.705	-48.690	-48.578	-48.704	-48.704	-43.922	-47.467	-48.392	-48.626
A_{11}^{oc}	-1.000	-0.999	-0.999	-0.999	-0.999	-0.999	-0.999	-0.999	-0.999
A_{22}^{oc}	-4.935	-4.927	-4.932	-4.932	-4.932	-4.684	-4.869	-4.916	-4.928
A_{111}^c	-14.804 (1.000)	-14.778 (0.998)	-14.778 (0.998)	-14.778 (0.998)	-14.778 (0.998)	-14.778 (0.998)	-14.778 (0.998)	-14.778 (0.998)	-14.778 (0.998)
A_{122}^c	-48.705 (1.000)	-48.629 (0.998)	-48.676 (0.999)	-48.679 (0.999)	-48.679 (0.999)	-45.364 (0.931)	-48.057 (0.987)	-48.523 (0.996)	-48.640 (0.999)

* Results for "inextensible" columns.

Table 4.2.3(c) Asymmetric Buckling Model.

$\kappa = \pi^2 EI/kL^3 = 0.75$ - Fold Catastrophe -

	Continuous Method *	Discretization Methods							
		Finite Element Method				Simplified Element Method			
Elements		4	8	16	32	4	8	16	32
D.O.F.		13 (4,9)	25 (8,17)	49 (16,33)	97 (32,65)	8 (4,4)	16 (8,8)	32 (16,16)	64 (32,32)
Mode	1	1	1	1	1	1	1	1	1
Λ^c	6.580	6.581	6.581	6.581	6.581	6.581	6.581	6.581	6.581
A_1^{1c}	-6.580	-6.577	-6.577	-6.577	-6.577	-6.577	-6.577	-6.577	-6.577
A_{11}^{oc}	-1.000	-0.999	-0.999	-0.999	-0.999	-0.999	-0.999	-0.999	-0.999
A_{111}^{c}	-9.870 (1.000)	-9.858 (0.999)	-9.858 (0.999)	-9.858 (0.999)	-9.858 (0.999)	-9.858 (0.999)	-9.858 (0.999)	-9.858 (0.999)	-9.858 (0.999)

* Results for "inextensible" columns.

can be written in the Lagrangian description:

$$\kappa_x = W_{,xx} \left[1 + W^2_{,x} \right]^{-\frac{3}{2}} \tag{4.2.2}$$

Note its Eulerian representation is previously expressed by Eq. (II-3.2.1). In this dissertation, both the FEM and the SEM make use of the above first approximation of the curvature in Eq. (4.2.1). Then, the axial stress σ_x is assumed to be related to ε_x in terms of the Young's modulus E.

$$\sigma_x = E \, \varepsilon_x \tag{4.2.3}$$

The material of column models behave elastically alone.

Then, the total potential energy function V of perfectly straight column can be obtained by the sum of the internal strain energy and the external work due to the applied load Λ :

$$V(U,W,\Lambda) = \frac{EA}{2} \int_0^L \left(U_{,x} + \frac{1}{2} W^2_{,x} \right)^2 dX + \frac{EI}{2} \int_0^L W^2_{,xx} \, dX + \Lambda \int_0^L U_{,x} \, dX \tag{4.2.4}$$

Under the variational principle in the elasticity theory, equations of equilibrium and some boundary conditions can be obtained as follows:

Equations of equilibrium for $0 < X < L$

$$\left(U_{,x} + \frac{1}{2} W^2_{,x} \right)_{,x} = 0 \tag{4.2.5a}$$

and

$$EI \, W_{,xxxx} - EA \left[\left(U_{,x} + \frac{1}{2} W^2_{,x} \right) W_{,x} \right]_{,x} = 0 \tag{4.2.5b}$$

Boundary conditions at $X = 0$ and $X = L$

$$\Lambda + EA \left(U_{,x} + \frac{1}{2} W^2_{,x} \right) = 0 \quad \text{or} \quad U : \text{specified} \tag{4.2.5c}$$

$$EA \left(U_{,x} + \frac{1}{2} W^2_{,x} \right) W_{,x} - EI \, W_{,xxx} = 0 \quad \text{or} \quad W : \text{specified} \tag{4.2.5d}$$

and

$$EI \, W_{,xx} = 0 \quad \text{or} \quad W_{,x} : \text{specified} \tag{4.2.5e}$$

Now, the axial force N_x on the neutral axis and the bending moment M_x with respect to the axis in the cross section are easily represented by

$$N_x = b \int_{-h/2}^{h/2} \sigma_x \, dZ = EA \left(U_{,x} + \frac{1}{2} W^2_{,x} \right) = EA \, \varepsilon_{ox} \tag{4.2.6a}$$

and

$$M_x = b \int_{-h/2}^{h/2} Z \, \sigma_x \, dZ = - EI \, W_{,xx} = - EI \, \kappa_x \tag{4.2.6b}$$

where b and h refer to the width and the height of the rectangular cross section for simplicity. Using these expression, equations of equilibrium in Eqs. (4.2.5a,b) lead to

$$N_{X,X} = 0 \tag{4.2.7a}$$

$$EI\ W_{,XXXX} - N_X\ W_{,XX} = 0 \tag{4.2.7b}$$

In the case of simply supported column as shown in **Fig. 4.2.1**, all the boundary conditions in Eqs. (4.2.5c,d,e) are completely satisfied. Thus, the left condition of Eq. (4.2.5c) and that of the constant axial force N_X are specified at X=L:

$$N_X = -\Lambda \tag{4.2.8}$$

and Eq. (4.2.7) say that the axial force N_X is always kept constant value of the compressive applied load $-\Lambda$ along the neutral axis X, and also that from Eq. (4.2.6a) the Green's strain tensor ε_{OX} remain constant along the axis throughout deformations. Such a peculiar property plays an important role in an evaluation of extensibility of column.

Therefore, the resultant governing equilibrium equation

$$EI\ W_{,XXXX} + \Lambda\ W_{,XX} = 0 \tag{4.2.9}$$

under

$$\left(U_{,X} + \frac{1}{2}\ W^2_{,X} \right)_{,X} = 0$$

yields only an eigenvalue problem with respect to the well-known Euler buckling of column[8].

On the other hand, Eq. (4.2.9) can be also obtained from the first order approximation in Eq. (II-3.2.4) of **Table II-3.2.1** in the case of columns with the inextensible property of the neutral axis[4].

$$V(W, \Lambda) = \frac{EI}{2} \int_0^L W^2_{,XX}\ dX - \Lambda \int_0^L \frac{1}{2}\ W^2_{,X}\ dX \tag{4.2.10}$$

Hence, for the elastic extensible column, the total potential function of Eq. (4.2.4) under the in-plane condition of Eq. (4.2.5a) is equivalent to that of Eq. (4.2.10) for the elastic inextensible column. Of course, if the condition of inextensibility of column

$$\varepsilon_{OX} = U_{,X} + \frac{1}{2}\ W^2_{,X} = 0 \tag{4.2.11}$$

is substituted into Eq. (4.2.4), then it is apparently that Eq. (4.2.10) can be also obtained.

The use of the strain ε_{OX} and the curvature κ_X in Eq. (4.2.1) provides only the characteristic eigenvalue equation of Eq. (4.2.9), and nonlinear postbuckling equilibrium paths can never be solved from this equation. This aspect is confirmed by the proposed catastrophe analysis specially by the SEM such that the constant Λ leads to no postbuckling reservation in Eq. (4.2.9). Then, in or-

der to precisely evaluate the nonlinear behavior of the extensible columns, it is necessary to formulate the higher order axial strain from geometrical configurations and to use the accurate definition of curvature in Eq. (4.2.2).

In the SEM analyses, the shape functions are adopted to be linear functions of the axis coordinate X for both the in-plane displacement U and the out-of-plane deflection W. Then, the condition Eq. (4.2.5a) of such constant axial force N_x, i.e., the constant Green's strain tensor ε_{ox} along the axis X may be always satisfied for the SEM analyses. Hence, the SEM's results provide no postbuckling prediction for the symmetric bifurcation bucklings. However, in the FEM analyses, one of the adopted shape functions is a linear function for the displacement U and another is a cubic function for the deflection W. So, it is apparently difficult to satisfy completely the in-plane condition of Eq. (4.2.5a) in large deflection range. Especially, the quartic terms of the potential function may be overestimated for the postbuckling which is stable or not.

However, it seems that the present numerical results are almost reasonable within practical large deflection allowing the column to behave elastically. The explicit postbuckling expressions by the FEM are predicted by remarkable small values of the associated postbuckling modes non-dimensionalized by very large column-span length L^*. Furthermore, it is found that, if necessary, the higher order analyses in **Table II-3.2.1** will be required so as to predict the elastic large deformations of inextensible columns or struts in comparison with the results of the Elastica problem, Koiter, Thompson, Zeeman[8,32-34].

4.3 Compressed Plates

4.3.1 General remarks

The fundamental equations for the large deflection of thin flat plate were first derived by von Kármán, and were modified for plates with small initial curvatures by Marguerre. Timoshenko provided the classical mathematical solutions by means of double Fourier series for the deflection and Airy's stress function[8]. The numerical solutions for Marguerre's equations were developed by Coan, Yamaki for various supporting conditions[13,14]. Moreover, Williams and Walker proposed some explicit solutions using a perturbation approach and a finite difference for design purpose[15,16]. Also, Harvey and Fok determined similar simple formula by an energy method[17,18].

The present section is concerned with an application of the catastrophe theory to such initial postbuckling characteristics of thin plate models. In the catastrophe theory, the large deflection nonlinear behavior of the plate either perfect or imperfect can be predicted by knowing the stability characteristics of the critical buckling point without recourse to solving nonlinear equations[1,2].

4.3.2 Formulation of potential function A

Consider a distinct primary bifurcation problem of the compressed rectangular plates. Thus, m=1 and ℓ =1+1=2 in Eq. (II-1.2.19), so that the essential state variable representing the primary buckling mode of the plate is designated as v_1, and the control parameters consist of both the deviation $\lambda_o = \lambda$ of the loading parameter Λ from the critical value Λ^c and the initial imperfection parameter $\varepsilon_1 = \varepsilon$ in the same mode of buckling, respectively.

* From the FEM results with 32 elements(**Table 4.2.1**), Λ / Λ^c =1.0037 and Λ / Λ^c =1.0931 at w/L=1/100 and 1/20, respectively, on the postbuckling parabolic equilibrium path.

Particularly, in the case of compressed rectangular unstiffened plates, all asymmetric cubic terms may disappear in the original form of the potential function considered in Eq. (I-1.2.1), (II-1.2.4) or (II-1.3.10) since $K_{ij}^{S} = 0$ and $K_{ijk}^{SS} = 0$. The reduced potential function can be explicitly defined by the Taylor expansion about the distinct critical origin $(v_1, \lambda, \varepsilon)=(0,0,0)$ from Eq. (II-1.3.21):

$$A(v_1, \lambda, \varepsilon) = \frac{1}{24} A_{1111}^{c} v_1^4 + \frac{1}{6} A_{111}^{1c} \varepsilon v_1^3 + \frac{1}{6} A_{111}^{c} v_1^3 + \frac{1}{2} A_{11}^{c} v_1^2 + \frac{1}{2} A_{11}^{oc} \lambda v_1^2 + \frac{1}{2} A_{11}^{1c} \varepsilon v_1^2 + A_{1}^{1c} \varepsilon v_1 \tag{4.3.1}$$

where

$$A_{1111}^{c} = 3 (\hat{K}_{1111}^{BB} - \hat{K}_{1111}^{BPB}) = A_{111}^{1c} ,$$

$$A_{111}^{c} = 3 (\hat{K}_{111}^{SS} - \hat{K}_{111}^{SPB}) = 0 ,$$

$$A_{11}^{1c} = 2 (\hat{K}_{111}^{SS} - \hat{K}_{111}^{SPB}) = 0 ,$$

$$A_{11}^{oc} = - \hat{K}_{11}^{G} , \qquad A_{1}^{1c} = - \Lambda^{c} \hat{K}_{11}^{G} ,$$

$$A_{11}^{c} = \hat{K}_{11}^{B} - \Lambda^{c} \hat{K}_{11}^{G} = 0 \quad (K_{11}^{SP} = 0)$$

Then, the last equation provides the critical load Λ^{c} for the primary bifurcation buckling v_1. Moreover, it is rewritten as

$$A(v_1, \lambda, \varepsilon) = \frac{1}{24} A_{1111}^{c} v_1^4 + \frac{1}{6} A_{111}^{1c} \varepsilon v_1^3 + \frac{1}{2} A_{11}^{oc} \lambda v_1^2 + A_{1}^{1c} \varepsilon v_1 \tag{4.3.2}$$

Now, in order to eliminate the term εv_1^3, a linear transform

$$x = v_1 + \varepsilon \tag{4.3.3}$$

is introduced herein. Then, Eq. (4.3.2) leads to

$$A(x, \lambda, \varepsilon) = \frac{1}{24} A_{1111}^{c} x^4 + \frac{1}{2} A_{11}^{oc} \lambda x^2 + A_{1}^{1} \varepsilon x \tag{4.3.4}$$

in which, such terms as ε^2 and $\lambda\varepsilon$ with respect to the control parameters are neglected as mentioned in the chapter II-1. Of course, each Taylor coefficient is evaluated at the critical point $(x, \lambda, \varepsilon)=(0,0,0)$. As a result, the variable x in Eq. (4.3.3) denotes the "total" amplitude of the deflection mode of the plate considered.

Here, an equilibrium equation in a neighborhood of the critical point for a compressed plate is obtained from Eq. (4.3.4)

$$\frac{\partial A}{\partial x} = \frac{1}{6} A^{c}_{1111} x^3 + A^{oc}_{11} \lambda x + A^{1c}_{1} \varepsilon = 0 \tag{4.3.5}$$

This equation yields both the trivial equilibrium solution for the perfect plate ($\varepsilon = 0$) and the typical nonlinear large deflection equilibrium solution for the imperfect plate ($\varepsilon \neq 0$). The latter solution includes the canonical parabolic postbuckling equilibrium solution in the particular case of the perfect plate. That is,

$$x = 0 \quad \text{or} \quad \frac{\Lambda}{\Lambda^c} = 1 + C_{\ell} x^2 + C_{\varepsilon} \frac{\varepsilon}{x} \tag{4.3.6}$$

where

$$C_{\ell} \equiv \frac{-A^{c}_{1111}}{6A^{oc}_{11}\Lambda^c} \quad , \quad C_{\varepsilon} \equiv \frac{-A^{1c}_{1}}{A^{oc}_{11}\Lambda^c}$$

The equations provide the common nonlinear equilibrium solution for a compressed rectangular plate under the load-control as discussed in the previous chapter II-1.

4.3.3 Formulation for plate edge conditions

In this dissertation, the two controls are mainly discussed on by the existence of the equivalent nodal forces due to some constrained in-plane displacements as mentioned in Eqs. (II-1.3.5) and (II-1.3.8). Then, the total load on the compressed edge under the displacement-control type can be determined by summation of reaction nodal forces on the constrained edge. Let P designate as the total load in the compressive axial direction. It is apparently shown that physical meanings of the total load P for both the load control(A) and the displacement control(B) have significant difference as follows. The total load on the compressive edge is obtained by either of

$$P = n \Lambda \tag{4.3.7a}$$

for the load-control type (A) or

$$P = - \sum_{m=1}^{M_b} \Lambda P_{om} - \sum_{\alpha=1}^{M_c} P_{\alpha}(\Lambda) \tag{4.3.7b}$$

for the displacement-control type (B) as discussed in the chapter II-1. In which, n refers to the number of partition of the plate in the y-direction as shown in **Fig. 4.3.1** below. In the latter case, as a result, the compressive total load P is determined from Eqs. (II-1.3.5) and (II-1.3.8).

$$P = - \sum_{m=1}^{M_b} \Lambda \left(P_{om} - \sum_{\alpha=1}^{M_c} G_{\alpha m} P_{om} \right) - \frac{1}{2} \sum_{\alpha=1}^{M_c} G_{\alpha k} K^{PB}_{k\ell m} w_{\ell} w_m - \sum_{\alpha=1}^{M_c} G_{\alpha k} K^{PB}_{k\ell m} w_{\ell} \bar{w}_m \tag{4.3.8}$$

Then, upon adopting the modal transforms of Eq. (II-1.3.12) and (II-1.3.13), and writing as $\varepsilon_1 = \varepsilon$ and $v_1 + \varepsilon = x$, the first term in the above equation is reasonably equivalent to Λ in the theoretical and numerical manners. This condition is satisfied at the critical point $(x, \lambda, \varepsilon) = (0,0,0)$. Thus,

$$P = n\Lambda - C'_d x^2 + C'_d \varepsilon^2 \qquad (4.3.9)$$

where

$$C'_d = \frac{1}{2} \sum_{\alpha=1}^{M_c} G_{\alpha k} K^{PB}_{k\ell m} \Phi_{\ell 1} \Phi_{m1}$$

In which, upon elimination of the higher term ε^2 from Eqs. (4.3.6) and (4.3.9), the resultant nonlinear equilibrium path including the complete postbuckling parabolic one can be expressed in terms of both the total deflection x and the initial imperfection ε.

$$\frac{P}{P^c} = 1 + C x^2 + C_\varepsilon \frac{\varepsilon}{x} \qquad (4.3.10)$$

where

$$P^c = n \Lambda^c$$

$$C = C_\ell - C_d , \qquad C_d = \frac{C'_d}{n\Lambda^c}$$

The path represents a typical equilibrium solution for the displacement-control type (B), and furthermore, the same form of solutions in the case of another load-control type (A) can be given by replacing F_{jm} in Eqs. (II-1.3.9) and (II-1.3.10) for F^*_{jm}. Also, this solution can be determined from denoting Λ and Λ^c in Eq. (4.3.6) as P and P^c, and letting $C_d = 0$ in Eq. (4.3.10). Therefore, finally, Eq. (4.3.10) involves both types of controls of (A) and (B).

Then, in the displacement-control type(B), the potential function A in Eq. (4.3.4) should be also modified as follows: Substituting directly Eq. (4.3.9) into Eq. (4.3.5) and eliminating Λ, the modified equilibrium equation corresponding to Eq. (4.3.5) can be obtained by

$$\frac{1}{6}(nA^c_{111} + 6A^{oc}_{11}C'_d)v_1^3 + A^{oc}_{11}v_1(P - P^c) + nA^{1c}_1 \varepsilon_1 = 0 \qquad (4.3.11)$$

Therefore, the modified potential function due to the control of the constrained displacements may be written as

$$B(v_1, P, \varepsilon_1) = \frac{1}{24} B^c_{1111} v_1^4 + \frac{1}{2} B^{oc}_{11} v_1 (P - P^c) + B^{1c}_1 v_1 \varepsilon_1 \qquad (4.3.12)$$

where

$$B^c_{1111} = nA^c_{1111} + 6A^{oc}_{11}C'_d , \quad B^{oc}_{11} = A^{oc}_1 , \quad B^{1c}_1 = A^{1c}_1$$

and, P and P^c refer to the total load on the constrained edge and its critical buckling value, respectively. From this potential function, the equilibrium equation can be obtained identically to be Eq. (4.3.10). Of course, in the case of the load-control type, Eq. (4.3.12) leads to Eq. (4.3.4).

However, the difference of the type of controls of (A) and (B) as discussed above may be found to be insignificant in view of the numerical realization. Hence, several demonstrations of computations will be made under mainly the load-control type(A) as discussed in the section **4.3.5.**

4.3.4 Numerical illustrations

The numerical procedure formulated as stated above is applied to predict the postbuckling behavior of compressed steel rectangular flat plates. **Fig. 4.3.1** illustrates the compressed plate model and its Cartesian coordinate system considered herein. The model is assumed to behave only in the elastic range. The applied compressive load is assumed to be in the longitudinal and uniaxial direction under the two types of (A) load and (B) displacement controls for the in-plane displacements on loaded edges. Also, the in-plane transverse displacements on unloaded edges are assumed to be freely deformable throughout. Moreover, the following four types of the out-of-plane supporting conditions are considered: (i) all edges simply supported, (ii) loaded edges simply supported and unloaded edges clamped, (iii) loaded edges clamped and unloaded edges simply supported, and (iv) all edges clamped. Then, the geometrical and material properties considered hereafter in some numerical illustrations are constants as follow (See, **Fig. 4.3.1**):

$\alpha = \frac{a}{b} = 1$: aspect ratio ,

$\nu = \frac{1}{3}$: Poisson's ratio ,

$\beta = \frac{b}{t} = 100$: width-thickness ratio ,

$\zeta = \frac{E}{\sigma_Y} = 875$: ratio of Young's modulus to yield stress ,

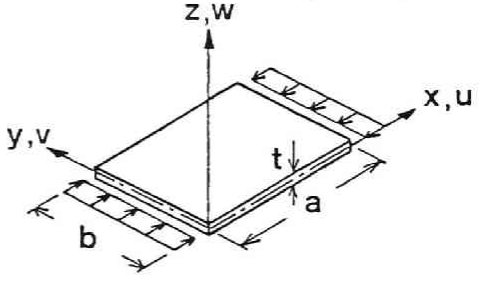

Fig. 4.3.1 Plate Model in Compression.

and

$$R = \frac{b}{t}\sqrt{\frac{12(1-\nu^2)}{\pi^2 k}\frac{\sigma_Y}{E}} = 1.757 \ (k=4) \ : \quad \text{generalized width-thickness ratio} \qquad (4.3.13)$$

The calculations are performed for the plates using the non-dimensionalized potential function in Eq. (4.3.1) through the FEM with the ACM cubic shape function and the SEM developed by Watanabe et al. in APPENDIX [26-29].

The parabolic postbuckling equilibrium paths for the perfect plate ($\varepsilon = 0$) and the canonical general nonlinear large deflection equilibrium solutions for the imperfect plate ($\varepsilon \neq 0$) can be evaluated under four supporting conditions.

4.3.5 Discussions

Tables 4.3.1, 4.3.2, 4.3.3 and **4.3.4** show the numerical results by the FEM analysis for square plates in the cases of four supporting conditions. Each table includes two results of (a) and (b) under the load-control type(A) and the displacement-control type(B), respectively. In these tables, the first row refers to the mesh of discrete elements of the plates. The FEM analyses are calculated from 3x3=9 elements to 8x8=64 elements. Also, the similar results using the SEM are summarized in **Tables 4.3.5, 4.3.6, 4.3.7** and **4.3.8.** The analyses for the SEM are computed up to 10x10=100 elements.

From these sixteen tables, the convergence of the elastic buckling coefficient k and the 4th stability curvature C with respect to the number of elements will be discussed firstly. **Figs. 4.3.2, 4.3.3, 4.3.4** and **4.3.5** show such convergence for square plates in the case of (i), (ii), (iii) and (iv), respectively, under the displacement control(B). In each figure, the abscissa denotes the number of elements; the left and the right ordinates represent the stability curvature C in Eq. (4.3.10) and the ratio of the obtained buckling coefficient k to the Timoshenko's elastic buckling coefficient k_c, respectively. Furthermore, under the load-control type(B), the similar characteristics of the convergence of the buckling coefficient k and the stability curvature C are also realized in above tables.

It is found that for any supported conditions the calculated buckling coefficients tend to converge asymptotically to Timoshenko's results as if they are upper bound values, with increase of the number of elements. For comparison of the SEM results with the FEM ones, the former have slower convergence than the latter except for the case of (i). In the case of (i), the former provide more accurate values than the latter regardless of the number of elements. For any supporting conditions, all the coefficients calculated by both the SEM and the FEM lie in the range of error of about 8 percent to Timoshenko's results for the maximum number of elements.

Furthermore, it is also shown that each stability curvature C may approach to certain appropriate lower-bound value for each supporting condition. For any supporting conditions, the SEM provides more rapid convergence of the stability curvatures than the FEM. Each stability curvature is calculated for the primary buckling mode v_1, which is added to the initial deflection w_o/t, and whose total is rewritten as $\bar{w}/t$. In which, t refers to the plate-thickness considered. In all the computations, herein, the maximum amplitude of the corresponding generalized out-of-plane nodal displacement is assumed to be unity. Similarly, the initial deflection mode is redesignated as w_o/t. Here, Coan and Yamaki postulated the maximum amplitude of the out-of-plane deflection to be unity, so that the present results hereafter may correspond to Coan's and Yamaki's works only for even number partitions of the discrete elements of the plate. Finally, the convergence of the stability curvatures can be clarified more excellently.

The postbuckling parabolic and the general nonlinear large deflection equilibrium paths using Eqs. (4.3.6) and (4.3.10) will be compared with the previous investigations by Coan, Yamaki, Williams and Rhodes et al. **Figs. 4.3.6, 4.3.7, 4.3.8** and **4.3.9** illustrate the nonlinear solutions of compressed square plates with the supporting conditions of (i), (ii), (iii) and (iv), respectively. Here, the initial out-of-plane deflection is assumed to be the same mode that the primary buckling mode calculated, and the maximum amplitude is given by $w_o/t = 0.1$, In these figures, Coan's and Yamaki's works include the first order solutions consisting of only the primary buckling mode and the second order solutions involving

Table 4.3.1(a) Stability Curvatures of Compressed Square Plates. (i) All Edges Simply Supported. Load Control using the FEM.

	3 X 3	4 X 4	5 X 5	6 X 6	7 X 7	8 X 8
D.O.F.	47 (27,20)	83 (44,39)	129 (65,64)	185 (90,95)	251 (119,132)	327 (152,175)
P_{cr}	29.188	30.421	31.072	31.450	31.612	31.840
Λ_{cr}	9.729	7.605	6.214	5.243	4.527	3.980
k	3.605	3.757	3.838	3.884	3.914	3.933
mode	(1,1)	(1,1)	(1,1)	(1,1)	(1,1)	(1,1)
A_{11}^{oc}	-0.129	-0.098	-0.150	-0.148	-0.191	-0.197
A_1^{1c}	-1.257	-0.750	-0.934	-0.774	-0.864	-0.785
A_{1111}^{c}	5.674	1.473	1.999	1.304	1.657	1.491
C_ε	-1.000	-1.000	-1.000	-1.000	-1.000	-1.000
C	0.752	0.329	0.357	0.280	0.319	0.317

Table 4.3.1(b) Stability Curvatures of Compressed Square Plates. (i) All Edges Simply Supported. Displacement Control using the FEM.

	3 X 3	4 X 4	5 X 5	6 X 6	7 X 7	8 X 8
D.O.F.	47 (27,20)	83 (44,39)	129 (65,64)	185 (90,95)	251 (119,132)	327 (152,175)
P_{cr}	29.188	30.421	31.072	31.450	31.686	31.834
Λ_{cr}	9.729	7.605	6.214	5.242	4.527	3.979
k	3.605	3.757	3.838	3.884	3.914	3.932
mode	(1,1)	(1,1)	(1,1)	(1,1)	(1,1)	(1,1)
A_{11}^{oc}	-0.129	-0.098	-0.150	-0.148	-0.191	-0.197
A_1^{1c}	-1.257	-0.750	-0.934	-0.774	-0.864	-0.785
A_{1111}^{c}	7.344	2.133	3.005	1.959	2.427	2.093
C_ℓ	0.974	0.477	0.536	0.421	0.468	0.444
C_d	0.204	0.129	0.152	0.116	0.120	0.101
C_ε	-1.000	-1.000	-1.000	-1.000	-1.000	-1.000
C	0.770	0.348	0.384	0.305	0.348	0.343

Table 4.3.2(a) **Stability Curvatures of Compressed Square Plates. (ii) Loaded Edges Simply Supported and Unloaded Edges Clamped. Load Control using the FEM.**

	3 X 3	4 X 4	5 X 5	6 X 6	7 X 7	8 X 8
D.O.F.	43 (27,16)	77 (44,33)	121 (65,56)	175 (90,85)	239 (119,120)	313 (152,161)
P_{cr}	52.221	54.737	56.746	58.130	59.083	59.752
Λ_{cr}	17.407	13.684	11.349	9.688	8.440	7.469
k	6.450	6.761	7.009	7.180	7.298	7.380
mode	(2,1)	(2,1)	(2,1)	(2,1)	(2,1)	(2,1)
A_{11}^{oc}	-0.476	-0.322	-0.526	-0.661	-0.658	-0.664
A_1^{1c}	-8.286	-4.409	-5.971	-6.407	-5.554	-4.960
A_{1111}^{c}	99.219	24.143	27.710	27.174	18.258	13.484
C_ϵ	-1.000	-1.000	-1.000	-1.000	-1.000	-1.000
C	1.996	0.913	0.773	0.707	0.548	0.453

Table 4.3.2(b) **Stability Curvatures of Compressed Square Plates. (ii) Loaded Edges Simply Supported and Unloaded Edges Clamped. Displacement Control using the FEM.**

	3 X 3	4 X 4	5 X 5	6 X 6	7 X 7	8 X 8
D.O.F.	43 (27,16)	77 (44,33)	121 (65,56)	175 (90,85)	239 (119,120)	313 (152,161)
P_{cr}	52.221	54.738	56.748	58.130	59.082	59.748
Λ_{cr}	17.407	13.684	11.350	9.688	8.440	7.469
k	6.450	6.761	7.009	7.180	7.297	7.380
mode	(2,1)	(2,1)	(2,1)	(2,1)	(2,1)	(2,1)
A_{11}^{oc}	-0.476	-0.322	-0.526	-0.661	-0.658	-0.664
A_1^{1c}	-8.286	-4.409	-5.971	-6.407	-5.554	-4.961
A_{1111}^{c}	160.866	44.712	63.061	65.464	45.739	34.651
C_ℓ	3.236	1.690	1.760	1.703	1.373	1.164
C_d	1.029	0.638	0.799	0.799	0.657	0.563
C_ϵ	-1.000	-1.000	-1.000	-1.000	-1.000	-1.000
C	2.206	1.052	0.961	0.904	0.716	0.601

Table 4.3.3(a) Stability Curvatures of Compressed Square Plates. (iii) Loaded Edges Clamped and Unloaded Edges Simply Supported. Load Control using the FEM.

	3 X 3	4 X 4	5 X 5	6 X 6	7 X 7	8 X 8
D.O.F.	43 (27,16)	77 (44,33)	121 (65,56)	175 (90,85)	239 (119,120)	313 (152,161)
P_{cr}	49.289	50.658	51.752	52.484	52.983	53.321
Λ_{cr}	16.430	12.664	10.350	8.747	7.569	6.665
k	6.088	6.257	6.392	6.483	6.544	6.586
mode	(1,1)	(1,1)	(1,1)	(1,1)	(1,1)	(1,1)
A_{11}^{oc}	-0.161	-0.096	-0.166	-0.148	-0.202	-0.198
A_1^{1c}	-2.641	-1.214	-1.722	-1.292	-1.529	-1.319
A_{1111}^{c}	13.598	2.618	3.744	1.933	2.594	1.941
C_ε	-1.000	-1.000	-1.000	-1.000	-1.000	-1.000
C	0.858	0.359	0.362	0.249	0.283	0.245

Table 4.3.3(b) Stability Curvatures of Compressed Square Plates. (iii) Loaded Edges Clamped and Unloaded Edges Simply Supported. Displacement Control using the FEM.

	3 X 3	4 X 4	5 X 5	6 X 6	7 X 7	8 X 8
D.O.F.	43 (27,16)	77 (44,33)	121 (65,56)	175 (90,85)	239 (119,120)	313 (152,161)
P_{cr}	49.289	50.658	51.752	52.484	52.979	53.316
Λ_{cr}	16.430	12.664	10.350	8.747	7.568	6.664
k	6.088	6.257	6.392	6.483	6.544	6.585
mode	(1,1)	(1,1)	(1,1)	(1,1)	(1,1)	(1,1)
A_{11}^{oc}	-0.161	-0.096	-0.166	-0.148	-0.202	-0.198
A_1^{1c}	-2.641	-1.214	-1.722	-1.292	-1.529	-1.319
A_{1111}^{c}	15.775	3.010	4.639	2.466	3.359	2.516
C_ℓ	0.996	0.413	0.582	0.318	0.366	0.318
C_d	0.128	0.048	0.077	0.061	0.073	0.064
C_ε	-1.000	-1.000	-1.000	-1.000	-1.000	-1.000
C	0.868	0.365	0.504	0.257	0.259	0.254

Table 4.3.4(a) Stability Curvatures of Compressed Square Plates. (iv) All Edges Clamped. Load Control using the FEM.

	3 X 3	4 X 4	5 X 5	6 X 6	7 X 7	8 X 8
D.O.F.	39 (27,12)	71 (44,27)	113 (65,48)	165 (90,75)	227 (119,108)	299 (152,147)
P_{cr}	73.884	74.603	76.250	77.494	78.390	79.029
Λ_{cr}	24.628	18.651	15.250	12.916	11.199	9.879
k	9.126	9.214	9.418	9.572	9.682	9.761
mode	(1,1)	(1,1)	(1,1)	(1,1)	(1,1)	(1,1)
A_{11}^{oc}	-0.172	-0.081	-0.156	-0.126	-0.181	-0.169
A_1^{1c}	-4.244	-1.506	-2.382	-1.625	-2.028	-1.668
A_{1111}^{c}	30.077	3.494	6.155	2.714	3.929	2.581
C_ε	-1.000	-1.000	-1.000	-1.000	-1.000	-1.000
C	1.181	0.387	0.431	0.278	0.323	0.258

Table 4.3.4(b) Stability Curvatures of Compressed Square Plates. (iv) All Edges Clamped. Displacement Control using the FEM.

	3 X 3	4 X 4	5 X 5	6 X 6	7 X 7	8 X 8
D.O.F.	39 (27,12)	71 (44,27)	113 (65,48)	165 (90,75)	227 (119,108)	299 (152,147)
P_{cr}	73.884	74.604	76.250	77.494	78.385	79.023
Λ_{cr}	24.628	18.651	15.250	12.916	11.198	9.878
k	9.126	9.214	9.418	9.572	9.682	9.761
mode	(1,1)	(1,1)	(1,1)	(1,1)	(1,1)	(1,1)
A_{11}^{oc}	-0.172	-0.081	-0.156	-0.126	-0.181	-0.169
A_1^{1c}	-4.244	-1.506	-2.382	-1.625	-2.028	-1.668
A_{1111}^{c}	34.316	3.872	7.107	3.133	4.550	2.984
C_ℓ	1.348	0.429	0.497	0.321	0.374	0.298
C_d	0.149	0.038	0.060	0.038	0.044	0.035
C_ε	-1.000	-1.000	-1.000	-1.000	-1.000	-1.000
C	1.199	0.391	0.437	0.283	0.329	0.263

Table 4.3.5(a) Stability Curvatures of Compressed Square Plates. (i) All Edges Simply Supported. Load Control using the SEM.

	3 X 3	4 X 4	5 X 5	6 X 6	7 X 7	8 X 8	9 X 9	10 X 10
D.O.F.	31 (27,4)	53 (44,9)	81 (65,16)	115 (90,25)	155 (119,36)	201 (152,49)	253 (189,64)	311 (220,81)
P_{cr}	31.008	31.585	31.864	32.021	32.117	32.183	32.228	32.257
Λ_{cr}	10.336	7.896	6.373	5.337	4.588	4.023	3.581	3.226
k	3.830	3.901	3.936	3.955	3.967	3.975	3.980	3.984
mode	(1,1)	(1,1)	(1,1)	(1,1)	(1,1)	(1,1)	(1,1)	(1,1)
A_{11}^{oc}	-0.100	-0.084	-0.137	-0.138	-0.182	-0.190	-0.229	-0.241
A_{1}^{1c}	-1.034	-0.668	-0.871	-0.738	-0.834	-0.764	-0.820	-0.776
A_{1111}^{c}	2.996	0.938	1.412	0.951	1.170	0.957	1.080	0.955
C_{ε}	-1.000	-1.000	-1.000	-1.000	-1.000	-1.000	-1.000	-1.000
C	0.483	0.234	0.270	0.214	0.234	0.209	0.220	0.205

Table 4.3.5(b) Stability Curvatures of Compressed Square Plates. (i) All Edges Simply Supported. Displacement Control using the SEM.

	3 X 3	4 X 4	5 X 5	6 X 6	7 X 7	8 X 8	9 X 9	10 X 10
D.O.F.	31 (27.4)	53 (44.9)	81 (65,16)	115 (90,25)	155 (119,36)	201 (152,49)	253 (189,64)	311 (220,81)
P_{cr}	31.008	31.585	31.864	32.021	32.117	32.179	32.264	32.248
Λ_{cr}	10.336	7.896	6.373	5.337	4.588	4.022	3.580	3.224
k	3.830	3.902	3.936	3.955	3.967	3.974	3.979	3.983
mode	(1,1)	(1,1)	(1,1)	(1,1)	(1,1)	(1,1)	(1,1)	(1,1)
A_{11}^{oc}	-0.100	-0.084	-0.137	-0.138	-0.182	-0.190	-0.229	-0.241
A_{1}^{1c}	-1.034	-0.668	-0.871	-0.738	-0.834	-0.764	-0.820	-0.776
A_{1111}^{c}	4.189	1.476	2.293	1.548	1.890	1.527	1.707	1.491
C_{ℓ}	0.675	0.368	0.439	0.350	0.378	0.333	0.347	0.320
C_{d}	0.175	0.116	0.141	0.110	0.115	0.098	0.099	0.088
C_{ε}	-1.000	-1.000	-1.000	-1.000	-1.000	-1.000	-1.000	-1.000
C	0.500	0.252	0.298	0.239	0.262	0.235	0.249	0.232

Table 4.3.6(a) Stability Curvatures of Compressed Square Plates. (ii) Loaded Edges Simply Supported and Unloaded Edges Clamped. Load Control using the SEM.

	3 X 3	4 X 4	5 X 5	6 X 6	7 X 7	8 X 8	9 X 9	10 X 10
D.O.F.	31 (27,4)	53 (44,9)	81 (65,16)	115 (90,25)	155 (119,36)	201 (152,49)	253 (189,64)	311 (220,81)
P_{cr}	39.867	46.651	50.881	53.657	55.564	56.921	57.917	58.666
Λ_{cr}	13.289	11.663	10.176	8.943	7.938	7.115	6.435	5.867
k	4.924	5.762	6.284	6.627	6.863	7.031	7.154	7.246
mode	(2,1)	(2,1)	(2,1)	(2,1)	(2,1)	(2,1)	(2,1)	(2,1)
A_{11}^{oc}	-0.300	-0.273	-0.465	-0.619	-0.624	-0.642	-0.783	-0.899
A_{1}^{1c}	-3.987	-3.184	-4.732	-5.540	-4.949	-4.564	-5.037	-5.273
A_{1111}^{c}	18.541	6.542	11.006	13.711	10.270	8.579	10.238	11.060
C_{ϵ}	-1.000	-1.000	-1.000	-1.000	-1.000	-1.000	-1.000	-1.000
C	0.775	0.342	0.388	0.413	0.350	0.313	0.339	0.350

Table 4.3.6(b) Stability Curvatures of Compressed Square Plates. (ii) Loaded Edges Simply Supported and Unloaded Edges Clamped. Displacement Control using the SEM.

	3 X 3	4 X 4	5 X 5	6 X 6	7 X 7	8 X 8	9 X 9	10 X 10
D.O.F.	31 (27,4)	53 (44,9)	81 (65,16)	115 (90,25)	155 (119,36)	201 (152,49)	253 (189,64)	311 (220,81)
P_{cr}	39.867	46.651	50.880	53.656	55.562	56.916	57.943	58.653
Λ_{cr}	13.289	11.663	10.176	8.943	7.937	7.114	6.434	5.865
k	4.924	5.762	6.284	6.627	6.863	7.030	7.152	7.244
mode	(2,1)	(2,1)	(2,1)	(2,1)	(2,1)	(2,1)	(2,1)	(2,1)
A_{11}^{oc}	-0.300	-0.273	-0.465	-0.619	-0.624	-0.642	-0.783	-0.899
A_{1}^{1c}	-3.986	-3.184	-4.732	-5.540	-4.949	-4.564	-5.036	-5.274
A_{1111}^{c}	36.538	18.864	35.284	44.276	33.359	27.252	32.204	34.520
C_{ℓ}	1.528	0.988	1.243	1.332	1.123	0.995	1.066	1.091
C_{d}	0.651	0.540	0.706	0.751	0.625	0.547	0.580	0.588
C_{ϵ}	-1.000	-1.000	-1.000	-1.000	-1.000	-1.000	-1.000	-1.000
C	0.877	0.447	0.537	0.582	0.498	0.448	0.486	0.503

Table 4.3.7(a) Stability Curvatures of Compressed Square Plates. (iii) Loaded Edges Clamped and Unloaded Edges Simply Supported. Load Control using the SEM.

	3 X 3	4 X 4	5 X 5	6 X 6	7 X 7	8 X 8	9 X 9	10 X 10
D.O.F.	31 (27,4)	53 (44,9)	81 (65,16)	115 (90,25)	155 (119,36)	201 (152,49)	253 (189,64)	311 (220,81)
P_{cr}	42.821	47.800	50.044	51.358	52.183	52.736	53.120	53.394
Λ_{cr}	14.274	11.950	10.009	8.560	7.454	6.592	5.902	5.339
k	5.289	5.904	6.181	6.344	6.446	6.514	6.561	6.595
mode	(2,1)	(1,1)	(1,1)	(1,1)	(1,1)	(1,1)	(1,1)	(1,1)
A_{11}^{oc}	-0.300	-0.073	-0.142	-0.131	-0.185	-0.184	-0.232	-0.237
A_{1}^{1c}	-4.282	-0.876	-1.421	-1.122	-1.382	-1.218	-1.369	-1.265
A_{1111}^{c}	18.539	1.159	2.252	1.242	1.757	1.304	1.596	1.332
C_{ε}	-1.000	-1.000	-1.000	-1.000	-1.000	-1.000	-1.000	-1.000
C	0.722	0.221	0.264	0.184	0.212	0.178	0.194	0.175

Table 4.3.7(b) Stability Curvatures of Compressed Square Plates. (iii) Loaded Edges Clamped and Unloaded Edges Simply Supported. Displacement Control using the SEM.

	3 X 3	4 X 4	5 X 5	6 X 6	7 X 7	8 X 8	9 X 9	10 X 10
D.O.F.	31 (27,4)	53 (44,9)	81 (65,16)	115 (90,25)	155 (119,36)	201 (152,49)	253 (189,64)	311 (220,81)
P_{cr}	42.820	47.800	50.043	51.358	52.183	52.730	53.107	53.382
Λ_{cr}	14.273	11.950	10.009	8.560	7.454	6.591	5.901	5.338
k	5.289	5.904	6.181	6.343	6.445	6.513	6.560	6.594
mode	(2,1)	(1,1)	(1,1)	(1,1)	(1,1)	(1,1)	(1,1)	(1,1)
A_{11}^{oc}	-0.300	-0.073	-0.142	-0.131	-0.185	-0.184	-0.232	-0.237
A_{1}^{1c}	-4.281	-0.876	-1.421	-1.122	-1.382	-1.218	-1.369	-1.265
A_{1111}^{c}	36.526	1.450	3.039	1.724	2.474	1.851	2.278	1.906
C_{ε}	1.422	0.276	0.354	0.256	0.298	0.253	0.277	0.251
C_{d}	0.606	0.050	0.083	0.063	0.077	0.066	0.073	0.066
C_{ε}	-1.000	-1.000	-1.000	-1.000	-1.000	-1.000	-1.000	-1.000
C	0.817	0.226	0.271	0.192	0.222	0.187	0.204	0.185

Table 4.3.8(a) Stability Curvatures of Compressed Square Plates. (iv) All Edges Clamped. Load Control using the SEM.

	3 X 3	4 X 4	5 X 5	6 X 6	7 X 7	8 X 8	9 X 9	10 X 10
D.O.F.	31 (27,4)	53 (44,9)	81 (65,16)	115 (90,25)	155 (119,36)	201 (152,49)	253 (189,64)	311 (220,81)
P_{cr}	44.297	58.470	65.467	69.650	72.411	74.332	75.717	76.744
Λ_{cr}	14.766	14.617	13.093	11.608	10.344	9.291	8.413	7.674
k	5.471	7.222	8.086	8.603	8.944	9.180	9.352	9.479
mode	(2,1)	(1,1)	(1,1)	(1,1)	(1,1)	(1,1)	(1,1)	(1,1)
A_{11}^{oc}	-0.300	-0.101	-0.174	-0.130	-0.185	-0.171	-0.217	-0.212
A_{1}^{1c}	-4.430	-1.483	-2.284	-1.504	-1.915	-1.584	-1.824	-1.629
A_{1111}^{c}	18.541	2.276	3.988	1.692	2.677	1.802	2.362	1.867
C_{ε}	-1.000	-1.000	-1.000	-1.000	-1.000	-1.000	-1.000	-1.000
C	0.698	0.256	0.291	0.188	0.233	0.190	0.216	0.191

Table 4.3.8(b) Stability Curvatures of Compressed Square Plates. (iv) All Edges Clamped. Displacement Control using the SEM.

	3 X 3	4 X 4	5 X 5	6 X 6	7 X 7	8 X 8	9 X 9	10 X 10
D.O.F.	31 (27,4)	53 (44,9)	81 (65,16)	115 (90,25)	155 (119,36)	201 (152,49)	253 (189,64)	311 (220,81)
P_{cr}	44.297	58.470	65.467	69.450	72.409	74.324	75.702	76.727
Λ_{cr}	14.765	14.617	13.093	11.608	10.344	9.291	8.411	7.673
k	5.471	7.223	8.086	8.603	8.944	9.180	9.350	9.477
mode	(2,1)	(1,1)	(1,1)	(1,1)	(1,1)	(1,1)	(1,1)	(1,1)
A_{11}^{oc}	-0.300	-0.101	-0.174	-0.130	-0.185	-0.171	-0.217	-0.212
A_{1}^{1c}	-4.430	-1.483	-2.284	-1.504	-1.915	-1.584	-1.824	-1.629
A_{1111}^{c}	36.541	3.096	5.571	2.254	3.468	2.290	2.960	2.314
C_{ℓ}	1.374	0.348	0.407	0.250	0.302	0.241	0.270	0.237
C_{d}	0.586	0.084	0.105	0.056	0.062	0.046	0.048	0.040
C_{ε}	-1.000	-1.000	-1.000	-1.000	-1.000	-1.000	-1.000	-1.000
C	0.789	0.264	0.301	0.193	0.240	0.195	0.222	0.197

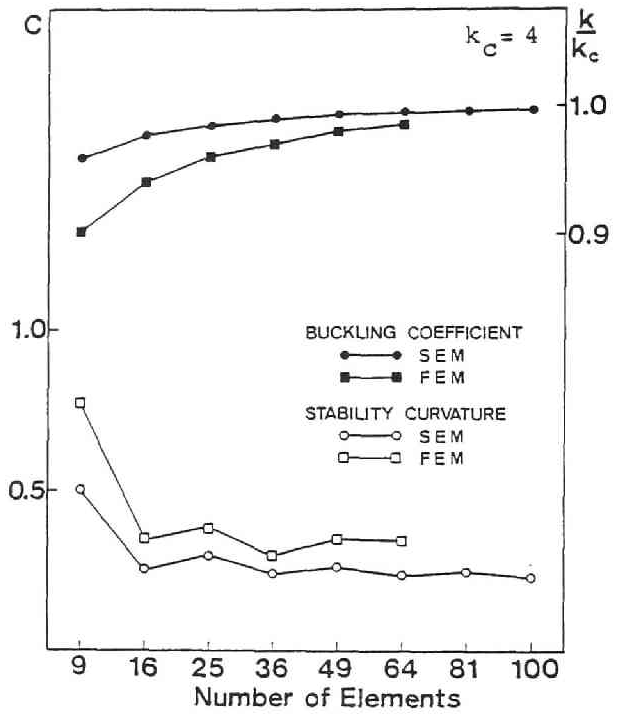

Fig. 4.3.2 Convergence of Buckling Strengths and Stability Curvatures. (i) All Edges Simply Supported. Displacement Control.

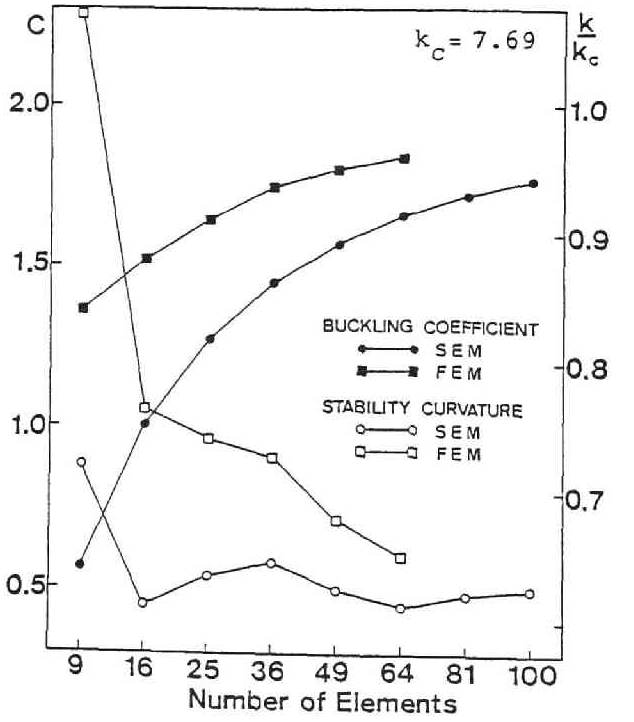

Fig. 4.3.3 Convergence of Buckling Strengths and Stability Curvatures. (ii) Loaded Edges Simply Supported and Unloaded Edges Clamped. Displacement Control.

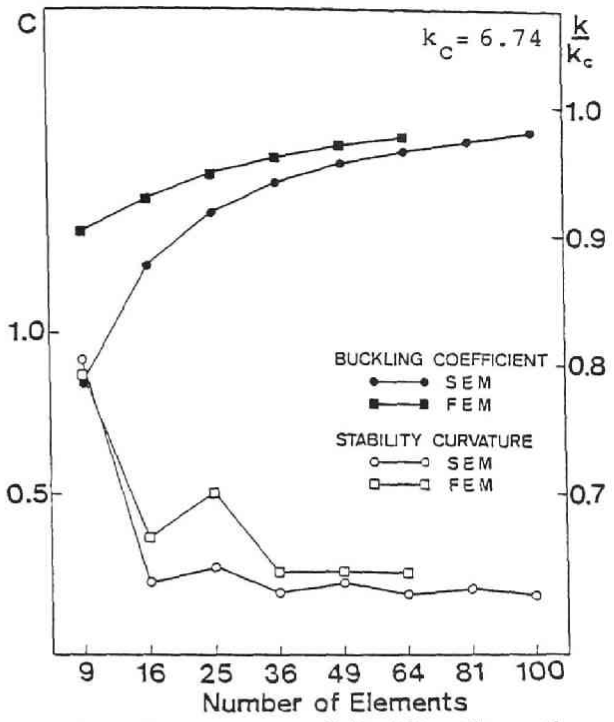

Fig. 4.3.4 Convergence of Buckling Strengths and Stability Curvatures. (iii) Loaded Edges Clamped and Unloaded Edges Simply Supported. Displacement Control.

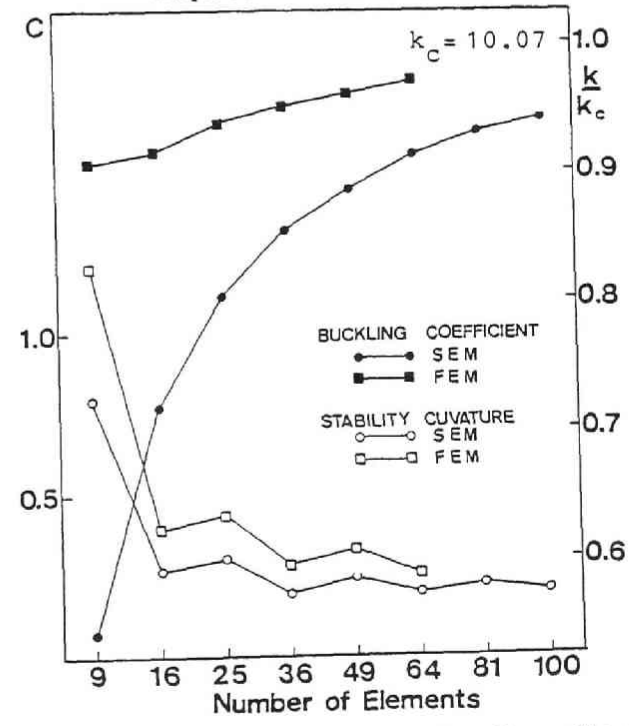

Fig. 4.3.5 Convergence of Buckling Strengths and Stability Curvatures. (iii) All Edges Clamped. Displacement Control.

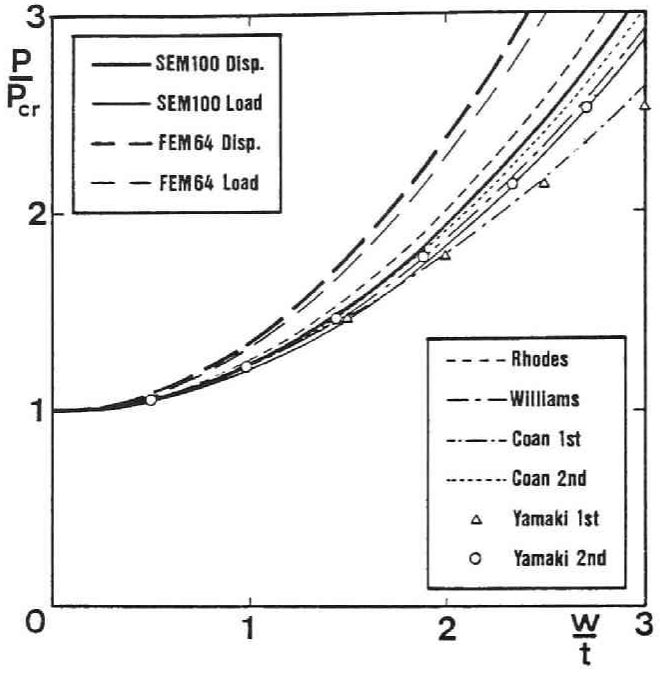

Fig. 4.3.6(a) Postbuckling Equilibrium Paths of Compressed Plate.
(i) All Edges Simply Supported.

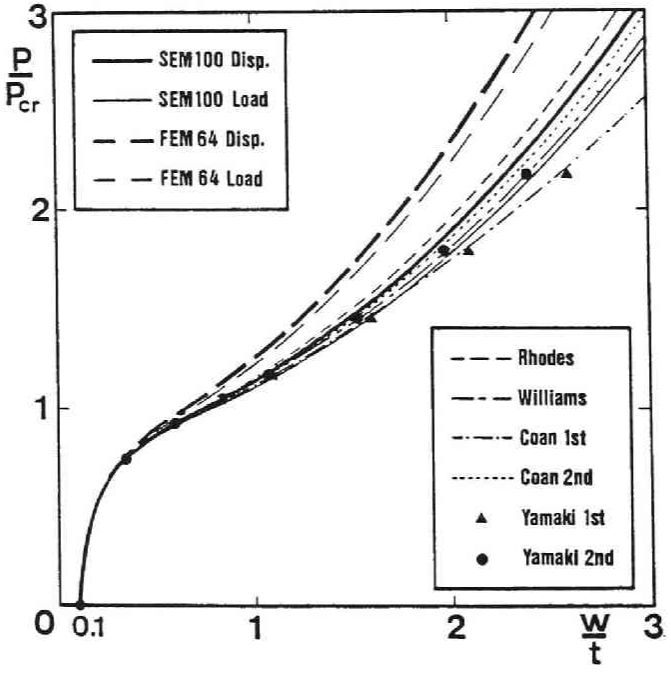

Fig. 4.3.6(b) Nonlinear Equilibrium Paths of Compressed Plate.
(i) All Edges Simply Supported.

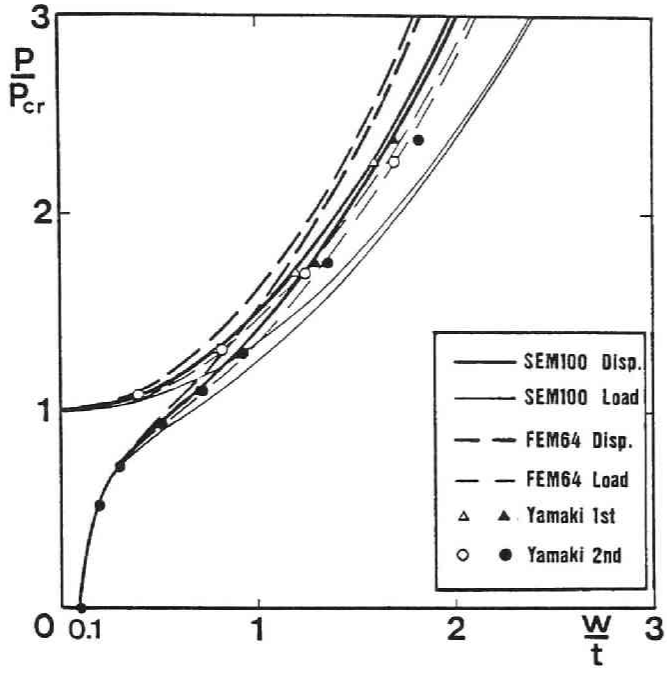

Fig. 4.3.7 Postbuckling and Nonlinear Equilibrium Paths of Compressed Plate. (ii) Loaded Edges Simply Supported and Unloaded Edges Clamped.

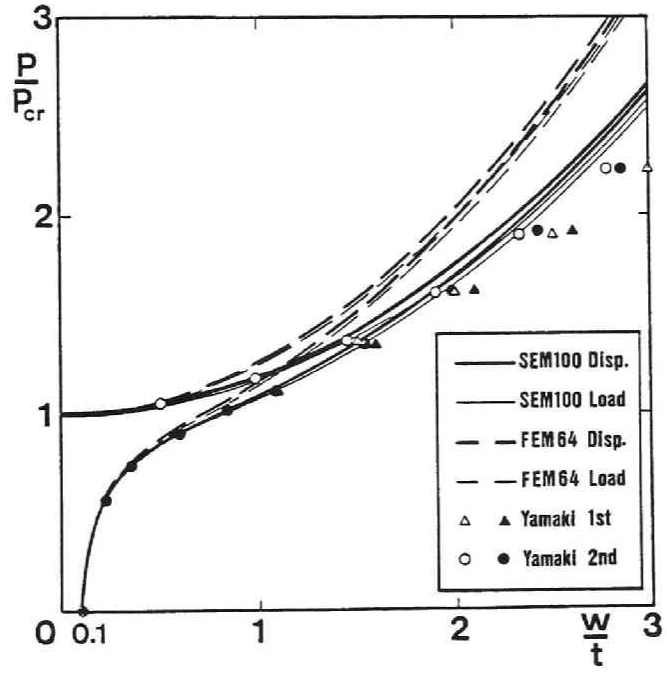

Fig. 4.3.8 Postbuckling and Nonlinear Equilibrium Paths of Compressed Plate. (iii) Loaded Edges Clamped and Unloaded Edges Simply Supported.

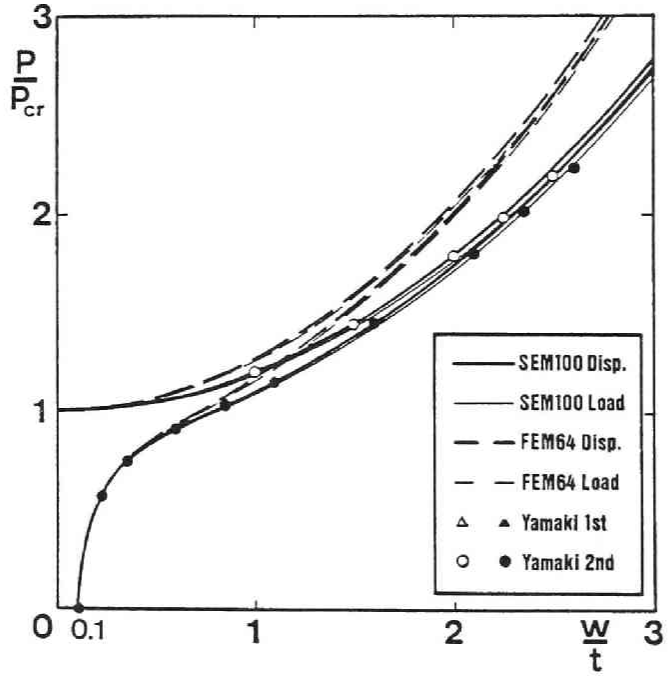

Fig. 4.3.9 **Postbuckling and Nonlinear Equilibrium Paths of Compressed Plate. (iv) All Edges Clamped.**

the higher order buckling modes.

For smaller out-of-plane deflection w/t < 1.5, the proposed solutions are shown to be in good agreement with Coan, Yamaki, Williams, Rhodes et al. Throughout larger deflection, the results obtained by the SEM may be in more excellent agreement with the above previous investigations than those by the FEM. The latter method may be found to slightly overestimate the stability curvatures in comparison with the former because the latter results are in the middle of convergence as shown in **Figs. 4.3.2-4.3.5**, previously. This tendency confirmed the catastrophe analysis of column structures in the chapter II-3.

The main objective of the proposed catastrophe analysis is to predict a nonlinear behavior of slender structure in terms of evaluation of only the stability characteristics at the associated critical point. So far at the critical point, the in-plane displacements constrained on loaded edges satisfy their condition to remain straight, regardless of control types of (A) and (B). The load-control type (A) says that all the axial in-plane displacement components are linearly distributed in the axial direction at the critical point, and that the resultant formulation provides the first order approximation to actual postbuckling behavior of the compressed plate. Of course, the displacement-control type (B) should give more accurate values of the stability curvatures.

Then, it is found that the proposed results under the two control types of (A) and (B) approximate the Yamaki's solutions for larger deflection w/t > 1.5 and for smaller deflection w/t < 1.5, respectively. This is satisfied for any out-of-plane supporting condition except for the second one (ii) in **Fig. 4.3.7.** Especially, in the case of condition (ii), the results under the type (B) may approach to the Yamaki's ones in the whole deflection field. Also, for the plate with all edges simply supported (i), the results by the load-control type (A) are shown to be rather slightly reasonable than those by the displacement one (B). Both the control types of (A) and (B) may approximate the previous works with an appropriate accuracy for smaller deflection considered herein. That is, in engineering practice, a difference between two control types may become little significant quantitatively and qualitatively within the range of deflection allowing to apply the elastic theory of stability to such problems. Therefore, the effect of control types on the stability of structural members may be secondary since the difference of controls never change the essential characteristics of the instability phenomena.

Thus, in the proceeding section, some numerical illustrations for compressed rectangular stiffened plates will be performed under mainly the load-control type (A) because of a simple expression of numerical formulation.

4.4 Compressed Stiffened Plates

4.4.1 General remarks

Instability phenomena of rectangular stiffened plates with longitudinal stiffeners under uniaxial in-plane compression involve the following prototypes of bifurcation problems. One of them is a global instability when the stiffened plate overally buckles with an Euler-type mode of a stiffener like a simple column. Another type is a local buckling of an isolated plate panel between stiffeners which form nodal lines of the associated buckling mode. The former type of buckling may appear in general for a compressed stiffened plate with smaller

flexural rigidities of its stiffeners. Whereas, the latter type of buckling may occur for the stiffened plate with the larger flexural rigidities. Then, there exist their simultaneous bucklings with the two-fold bifurcation. The compound buckling point may be characterized by the complex umbilic catastrophes identified by Thompson, Hunt and Tvergaard [7,12, 19,21,22]. Also, the distinct or the compound bifurcations are characterized by the symmetry of the stiffener itself with respect to the plate panel of stiffened plate.

4.4.2 Numerical illustrations

Figs. 4.4.1 show square plates subjected to in-plane uniaxial compression. Each stiffened plate has only one longitudinal stiffener on the center line at equal distance from both unloaded edges. All edges of the stiffened plate are simply supported with respect to the out-of-plane deflections under the load-control type (A) or the displacement-control type(B) as discussed previously. The geometrical and material properties are similar to those of the unstiffened plates in **Fig. 4.3.1** as follows:

$$\alpha = \frac{a}{b} = 1 , \quad \nu = \frac{1}{3} , \quad \beta = \frac{b}{t} = 200 , \quad \zeta = \frac{E}{\sigma_Y} = 875 ,$$

and

$$R = \frac{b}{t}\sqrt{\frac{12(1-\nu^2)}{\pi^2 k_\ell}\frac{\sigma_Y}{E}} = 1.757 \qquad (k_\ell = 16) \qquad (4.4.1)$$

Moreover, the major parameters of a stiffener are

$$\gamma = \frac{E_s I_s}{bD} , \quad \delta = \frac{A_s}{bt} , \quad D = \frac{Et^3}{12(1-\nu^2)} \qquad (4.4.2)$$

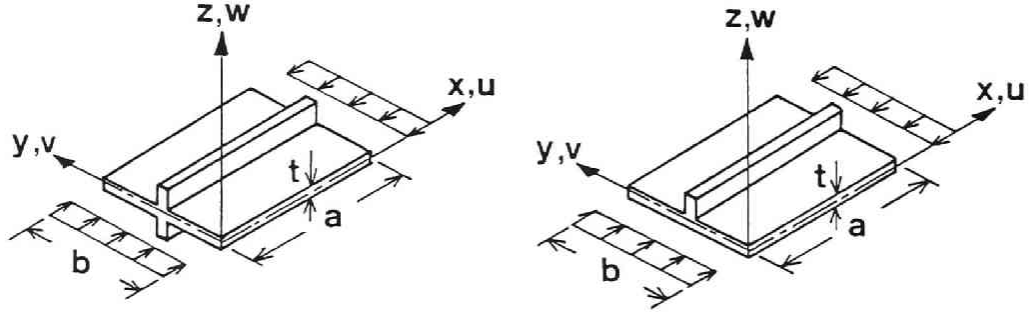

Fig. 4.4.1 Compressed Stiffened Plate Models.
(a) Symmetric Stiffener (b) Eccentric Stiffener

where γ and δ refer to the ratios of the flexural rigidities and of the cross-sectional areas between a stiffener and its plate panel, respectively. Also, E_s, I_s and A_s denote the Young's modulus, the moment of inertia and the are of the stiffener, respectively. The torsional rigidities of the stiffener are assumed to be negligible in this dissertation. It seems that the first parameter γ is superior to the second one δ on effects of the stability properties of stiffened plates. Thus, the numerical calculations are performed for several values of the flexural rigidity γ under a constant cross-sectional ratio of $\delta = 0.1$. Then, the typical bifurcation bucklings may appear discontinuously as the parameter γ changes smoothly. Herein, all the numerical calculations are illustrated through the SEM analyses for several partitions of their discrete elements.

4.4.3 Discussions

Stiffened plate with symmetric stiffener

This model as shown in **Fig. 4.4.1**(a) is called a symmetric-stiffened plate only in the dissertation. **Tables 4.4.1, 4.4.2, 4.4.3** and **4.4.4** show the results and relations of some coefficients for the prototypes of bucklings of square symmetric-stiffened plates with the number of the discrete elements of 4x4=16, 6x6=36, 8x8=64 and 10x10=100, respectively. Their total degrees of freedom are (44,9), (90,25), (152,49) and (220,81), respectively, where each has summation of the in-plane displacement components and the out-of-plane deflections. The computations are performed under the displacement control (B) for all partitions. In these tables, the subscripts of "1" and "2" correspond to the first and the second bucklings of the parameterized stiffened plates by the flexural rigidity γ . Thus, case by case, each buckling mode of v_1 or v_2 may have either of the global or the local one.

The symbols of G(m,n) and L(m,n) on the rows of the mode 1 and 2 in each table are designated as follows: G(m,n) denotes the Euler-column mode of a central stiffener for the global buckling of stiffened plate with m and n half-wave numbers in the longitudinal and transverse directions. Also, L(m,n) denotes the local-plate mode of overall stiffened plates for the local buckling of stiffened plates with m and n half-wave forms.

The primary instability has the **stable symmetric** bifurcation point, characterized by the **cups** catastrophe, without regard to values of the flexural rigidities. The symmetric-stiffened plate at a smaller flexural rigidity buckles with the global mode; while it buckles with the local mode of the plate panel at a larger flexural rigidity. This is shown in above four tables. In the case of 4x4 elements, however, the local mode is different from that in other cases of the greater elements. The results of 4x4 elements may be unreasonable in comparison with those of other elements because of insufficient partition of the stiffened plate. The forms of buckling modes are referred to the next type of the stiffened plate as shown in **Fig. 4.4.1**(b).

It is clearly found that the buckling coefficient and the stability curvature may converge to the well-known value of 16 by Timoshenko and an unknown appropriate value, respectively, as the number of discrete elements increases. The characteristics of such convergence may be drawn similarly to the unstiffened plates as shown in the previous section.

Table 4.4.1

Stability Curvatures of Compressed Square Symmetric-Stiffened Plates. Displacement Control using the SEM4x4.

Case	1	2	3	4
Y	5.0	10.0	15.0	20.0
Λ_1^c	85.990	115.140	115.737	115.737
Λ_2^c	111.800	115.737	115.904	116.285
k_1	10.621	14.222	14.295	14.295
k_2	13.809	14.295	14.316	14.363
mode 1	G(1,1)	L(3,3)	L(3,2)	L(3,2)
mode 2	L(3,2)	L(3,2)	L(3,3)	L(3,3)
A_{11}^{oc}	-0.142	-0.372	-0.363	-0.364
A_{22}^{oc}	-0.243	-0.364	-0.368	-0.368
A_1^{1c}	-12.222	-42.822	-41.992	-42.108
A_2^{2c}	-20.905	-41.891	-42.597	-42.558
A_{1111}^c	11.436	184.592	183.947	185.020
C_ℓ	0.156	0.718	0.730	0.732
C_d	0.0545	0.0138	0.0034	0.0044
C_ε	-1.000	-1.000	-1.000	-1.000
C	0.101	0.704	0.726	0.728
Type	STABLE SYMMETRIC BUCKLING			
Catastrophe	CUSP CATASTROPHE			

Table 4.4.2

Stability Curvatures of Compressed Square Symmetric-Stiffened Plates. Displacement Control using the SEM6x6.

Case	1	2	3	4
Y	5.0	10.0	15.0	20.0
Λ_1^c	58.199	82.686	82.686	82.686
Λ_2^c	82.686	88.094	88.593	88.593
k_1	10.783	15.320	15.320	15.320
k_2	15.320	16.321	16.414	16.414
mode 1	G(1,1)	L(2,2)	L(2,2)	L(2,2)
mode 2	L(2,2)	G(1,1)	L(3,2)	L(3,2)
A_{11}^{oc}	-0.201	-0.800	-0.800	-0.800
A_{22}^{oc}	-0.799	-0.188	-1.199	-1.199
A_1^{1c}	-9.169	-66.118	-66.121	-66.122
A_2^{2c}	-46.509	-15.517	-99.134	-99.144
A_{1111}^c	8.728	288.668	288.696	288.710
C_ℓ	0.124	0.728	0.728	0.728
C_d	0.0528	0.139	0.139	0.139
C_ε	-1.000	-1.000	-1.000	-1.000
C	0.0716	0.588	0.588	0.588
Type	STABLE SYMMETRIC BUCKLING			
Catastrophe	CUSP CATASTROPHE			

Table 4.4.3

Stability Curvatures of Compressed Square Symmetric-Stiffened Plates. Displacement Control using the SEM8x8.

Case	1	2	3	4
Y	5.0	10.0	15.0	20.0
Λ_1^c	44.042	63.167	63.167	63.168
Λ_2^c	63.167	67.564	70.323	70.324
k_1	10.880	15.604	15.604	15.604
k_2	15.604	16.690	17.372	17.372
mode 1	G(1,1)	L(2,2)	L(2,2)	L(2,2)
mode 2	L(2,2)	G(1,1)	G(1,1)	L(3,2)
A_{11}^{oc}	-0.270	-0.676	-0.676	-0.676
A_{22}^{oc}	-0.676	-0.279	-1.426	-1.426
A_1^{1c}	-11.911	-42.716	-42.714	-42.716
A_2^{2c}	-29.770	-17.632	-90.063	-90.067
A_{1111}^c	8.211	103.265	103.261	103.276
C_ℓ	0.115	0.403	0.403	0.403
C_d	0.0475	0.0915	0.0915	0.0915
C_ϵ	-1.000	-1.000	-1.000	-1.000
C	0.0674	0.311	0.311	0.311
Type	STABLE SYMMETRIC BUCKLING			
Catastrophe	CUSP CATASTROPHE			

Table 4.4.4

Stability Curvatures of Compressed Square Symmetric-Stiffened Plates. Displacement Control using the SEM10x10.

Case	1	2	3	4
Y	5.0	10.0	15.0	20.0
Λ_1^c	35.390	50.978	50.978	50.978
Λ_2^c	50.978	54.698	57.820	57.820
k_1	10.928	15.742	15.742	15.742
k_2	15.742	16.890	17.854	17.854
mode 1	G(1,1)	L(2,2)	L(2,2)	L(2,2)
mode 2	L(2,2)	G(1,1)	G(1,1)	L(3,2)
A_{11}^{oc}	-0.342	-1.092	-1.092	-1.092
A_{22}^{oc}	-1.092	-0.349	-2.133	-2.134
A_1^{1c}	-13.209	-55.660	-55.660	-55.660
A_2^{2c}	-38.622	-17.797	-108.758	-108.767
A_{1111}^c	7.913	161.194	161.199	161.206
C_ℓ	0.109	0.483	0.483	0.483
C_d	0.0426	0.107	0.107	0.107
C_ϵ	-1.000	-1.000	-1.000	-1.000
C	0.0664	0.376	0.376	0.376
Type	STABLE SYMMETRIC BUCKLING			
Catastrophe	CUSP CATASTROPHE			

Stiffened plate with eccentric stiffener

This model as shown in **Fig. 4.4.1**(b) is called an eccentric-stiffened plate only in the dissertation. **Tables 4.4.5, 4.4.6, 4.4.7** and **4.4.8** show the numerical results of compressed square eccentric-stiffened plates with the number of the discrete elements of 4x4=16, 6x6=36, 8x8=64 and 10x10=100, respectively. All the computations are demonstrated under the load-control type (A). The same notations in the symmetric-stiffened plate are also used herein. Then, for smaller flexural rigidity γ, the global buckling tends to occur with the asymmetric point of bifurcation. Adversely, for larger rigidity γ, the local-plate buckling may appear with the symmetric bifurcation point. Of course, there exist the simultaneous bifurcations at a particular value of γ.

Firstly, the case 1 in the first column shows the results of a distinct primary global buckling v_1 prior to the local buckling v_2. The typical buckling mode of **Table 4.4.8** is drawn spatially for the SEM10x10 in **Fig. 4.4.2.** It is found that the instability has an **asymmetric** point of bifurcation, i.e., the **fold** catastrophe characteristics since $A_{111} \neq 0$. The global buckling mode v_1 is **symmetric** with respect to the stiffener in an opposite meaning of the **asymmetric** buckling due to eccentricity of the stiffener. Then, the form of the total potential function can be expressed in Eq. (II-3.2.19), and the nonlinear equilibrium solutions are obtained from Eqs. (II-3.2.20) and (II-3.2.21). Furthermore, its significant imperfection sensitivity curve can be explicitly expanded by Eq. (II-3.2.22), and also the detail algorithm to evaluate the bifurcation set of the imperfection sensitivity was presented in the chapter II-2. **Fig. 4.4.3** shows the imperfection sensitivity of the **fold** catastrophe in the case 1 of **Table 4.4.8** by the SEM. When the stiffened plate with the eccentric stiffener in the upper side as shown in **Fig. 4.4.1**(b) has the downward global buckling mode in **Fig. 4.4.2**, the stability coefficient A_{111} is negative. Then, it is reasonable to be $\varepsilon_1 > 0$ for evaluating the load-carrying capacity. Therefore, the eccentric-stiffened plate is sensitive to the downward global initial deflection since the corresponding buckling mode is negative itself. While the stiffened plate may be rather stable for the upward global initial deflection. Herein, the plus sign of ε_1 says that the global initial deflection is in the downward direction as shown in **Fig. 4.4.2.** For example, the numerical results of 10x10 elements are illustrated herein. If the downward global initial deflection non-dimensionalized by the plate-panel thickness is prescribed as $\varepsilon_1 = 0.1$, then the load-carrying capacity will be reduced by 15% from the buckling load; $\Lambda/\Lambda^C = 0.850$.

Secondly, the case 4 on the last column in each table shows the results of a distinct primary local buckling v_1 of isolated plates prior to the previous global buckling v_2. The typical buckling mode is drawn spatially for the SEM10x10 in **Fig. 4.4.4.** This bifurcation is identical with that for the unstiffened plates as discussed in the previous section, and indicates a **stable symmetric** point of bifurcation as the **cusp** catastrophe since $A^C_{111} \cong 0$ and $A^C_{1111} > 0$. The local buckling mode v_1 is **asymmetric** with respect to the stiffener in an opposite meaning of the **symmetric** buckling as the local-plate panel. So far as the local buckling mode of L(2,2) is concerned, the stability may be regarded to realize the equivalent behavior of the simply supported one-fourth plate panel of the overall stiffened plate. Then, the nonlinear solutions can be presented similarly by Eqs. (II-3.2.6-8). Since equilibrium paths are essential stable in such cases within the elastic range, the prediction of strength of stiffened plates requires further elasto-plastic analyses. They are beyond in this chapter, but one of them will be proposed to be a simple prediction approach of elasto-plastic strength of stiffened plates in the proceeding chapters of PART III.

Table 4.4.5 Stability Curvatures of Compressed Square Eccentric-Stiffened Plates. Load Control using the SEM4x4.

Case	1	2	3	4
Y	10.0	14.2	15.0	20.0
Λ_1^c	94.498	115.657	115.737	115.737
Λ_2^c	114.747	115.737	115.763	116.210
k_1	11.672	14.285	14.295	14.295
k_2	14.173	14.295	14.590	14.354
mode 1	G(1,1)	L(3,1)	L(3,2)	L(3,2)
mode 2	L(3,2)	L(3,2)	L(3,1)	L(3,1)
A_{11}^{oc}	-0.133	-0.334	-0.348	-0.363
A_{22}^{oc}	-0.343	-0.359	-0.333	-0.362
A_1^{1c}	-12.606	-38.579	-40.272	-42.054
A_2^{2c}	-32.389	-41.552	-38.597	-41.873
A_{111}^c	-0.291	-0.736	-0.0098	-0.000068
A_{112}^c	0.143	-0.0019	-0.136	-0.0130
A_{122}^c	-8.147	-0.240	-0.0042	-0.000031
A_{222}^c	0.0354	-0.0046	-0.438	-0.0571
a*	—	-1.216	—	—
a'**	—	—	-1.310	—
$A_{111}^c \cdot A_{122}^c$	—	0.177	—	—
$A_{222}^c \cdot A_{112}^c$	—	—	0.060	—
A_{1111}^c	7.334	151.436	167.702	182.471
C_s***	0.0115	0.0095	0.00012	0.00000081
C	0.0970	0.654	0.694	0.723
Type of Buckling	ASYMM.	MONO-CLINAL	MONO-CLINAL	STABLE SYMM.
Catastrophe	FOLD	HYPERB. UMBILIC	HYPERB. UMBILIC	CUSP

* $a = \frac{2A_{11}^{oc}}{A_{22}^{oc}} \frac{A_{111}^c}{A_{122}^c}$ ** $a' \frac{2A_{22}^{oc}}{A_{11}^{oc}} - \frac{A_{222}^c}{A_{112}^c}$ *** $C_s \frac{A_{111}^c}{2A_{11}^{oc}\Lambda_1^c}$

Table 4.4.6 Stability Curvatures of Compressed Square Eccentric-Stiffened Plates. Load Control using the SEM6x6.

Case	1	2	3	4
γ	10.0	13.8	14.2	20.0
Λ_1^c	58.534	82.448	82.688	82.688
Λ_2^c	81.888	82.688	84.513	88.595
k_1	10.845	15.275	15.320	15.320
k_2	15.172	15.320	15.658	16.414
mode 1	G(1,1)	G(1,1)	L(2,2)	L(2,2)
mode 2	G(2,1)	L(2,2)	G(1,1)	L(3,2)
A_{11}^{oc}	-0.203	-0.199	-0.799	-0.799
A_{22}^{oc}	-0.490	-0.791	-0.200	-1.198
A_1^{1c}	-11.906	-16.390	-66.040	-66.103
A_2^{2c}	-37.442	-65.249	-16.556	-99.058
A_{111}^c	-0.550	-2.233	0.0142	-0.00028
A_{112}^c	-3.307	0.0116	-8.051	-0.0010
A_{122}^c	6.306	-8.227	-0.00032	-0.0016
A_{222}^c	-5.277	-0.144	-2.694	0.00071
a *	—	0.231	—	—
a' **	—	—	0.167	—
$A_{111}^c \cdot A_{122}^c$	—	18.371	—	—
$A_{222}^c \cdot A_{112}^c$	—	—	21.689	—
A_{1111}^c	4.797	6.187	226.990	227.426
C_s***	0.0113	0.0681	0.00011	0.0000021
C	0.0671	0.0629	0.573	0.573
Type of Buckling	ASYMM.	HOMEO-CLINAL	HOMEO-CLINAL	STABLE SYMM.
Catastrophe	FOLD	HYPERB. UMBILIC	HYPERB. UMBILIC	CUSP

* $a = \frac{2A_{11}^{oc}}{A_{22}^{oc}} - \frac{A_{111}^c}{A_{122}^c}$ ** $a' = \frac{2A_{22}^{oc}}{A_{11}^{oc}} - \frac{A_{222}^c}{A_{112}^c}$ *** $C_s = \frac{A_{111}^c}{2A_{11}^{oc}\Lambda_1^c}$

Table 4.4.7 Stability Curvatures of Compressed Square Eccentric-Stiffened Plates. Load Control using the SEM8x8.

Case	1	2	3	4
γ	10.0	13.8	14.4	20.0
Λ_1^c	41.674	61.559	63.173	63.173
Λ_2^c	59.634	63.173	64.209	70.329
k_1	10.294	15.207	15.606	15.606
k_2	14.732	15.606	15.862	17.373
mode 1	G(1,1)	G(1,1)	L(2,2)	L(2,2)
mode 2	G(2,1)	L(2,2)	G(1,1)	L(3,2)
A_{11}^{oc}	-0.277	-0.283	-0.674	-0.676
A_{22}^{oc}	-0.664	-0.674	-0.288	-1.424
A_1^{1c}	-11.554	-17.391	-42.602	-42.698
A_2^{2c}	-27.679	-41.537	-18.162	-89.958
A_{111}^c	-0.891	-1.469	-0.0028	-0.00021
A_{112}^c	-3.488	-0.0052	-5.582	-0.0011
A_{122}^c	5.569	-5.664	0.0041	0.0023
A_{222}^c	2.998	0.0241	-1.964	0.0019
a *	—	0.578	—	—
a' **	—	—	0.501	—
$A_{111}^c \cdot A_{122}^c$	—	8.320	0.000011	—
$A_{222}^c \cdot A_{112}^c$	—	0.00013	10.963	—
A_{1111}^c	4.540	5.237	76.082	76.236
C_s ***	0.0389	0.151	0.00032	0.0000025
C	0.0654	0.0502	0.298	0.298
Type of Buckling	ASYMM.	HOMEO-CLINAL	HOMEO-CLINAL	STABLE SYMM.
Catastrophe	FOLD	HYPERB. UMBILIC	HYPERB. UMBILIC	CUSP

* $a = \dfrac{2A_{11}^{oc}}{A_{22}^{oc}} \dfrac{A_{111}^c}{A_{122}^c}$ ** $a' = \dfrac{2A_{22}^{oc}}{A_{11}^{oc}} \dfrac{A_{222}^c}{A_{112}^c}$ *** $C_s = \dfrac{A_{111}^c}{2A_{11}^{oc}\Lambda_1^c}$

Table 4.4.8 Stability Curvatures of Compressed Square Eccentric-Stiffened Plates. Load Control using the SEM10x10.

Case	1	2	3	4
γ	10.0	14.2	14.4	20.0
Λ_1^c	32.091	50.622	50.987	50.987
Λ_2^c	42.856	50.987	51.360	57.830
k_1	9.909	15.632	15.744	15.744
k_2	13.233	15.744	15.859	17.857
mode 1	G(1,1)	G(1,1)	L(2,2)	L(2,2)
mode 2	G(2,1)	L(2,2)	G(1,1)	L(3,2)
A_{11}^{oc}	-0.337	-0.350	-1.080	-1.091
A_{22}^{oc}	-0.913	-1.081	-0.349	-2.130
A_1^{1c}	-10.802	-17.742	-55.059	-55.633
A_2^{2c}	-29.309	-54.722	-17.777	-108.586
A_{111}^c	-0.950	-1.247	0.133	-0.00030
A_{112}^c	-3.074	0.0243	-7.164	0.0019
A_{122}^c	5.180	-7.231	-0.0197	-0.0054
A_{222}^c	-2.912	-0.150	-1.362	-0.0053
a *	—	0.476	—	—
a' **	—	—	0.456	—
$A_{111}^c \cdot A_{122}^c$	—	9.017	-0.0026	—
$A_{222}^c \cdot A_{112}^c$	—	-0.0036	9.757	—
A_{1111}^c	4.141	4.747	116.377	118.817
C_s ***	0.0440	0.0351	0.0012	2.702×10^{-10}
C	0.0639	0.0446	0.352	0.356
Type of Buckling	ASYMM.	HOMEO-CLINAL	HOMEO-CLINAL	STABLE SYMM.
Catastrophe	FOLD	HYPERB. UMBILIC	HYPERB. UMBILIC	CUSP

* $a = \frac{2A_{11}^{oc}}{A_{22}^{oc}} \frac{A_{111}^c}{A_{122}^c}$ ** $a' = \frac{2A_{22}^{oc}}{A_{11}^{oc}} - \frac{A_{222}^c}{A_{112}^c}$ *** $C_s = \frac{A_{111}^c}{2A_{11}^{oc}\Lambda_1^c}$

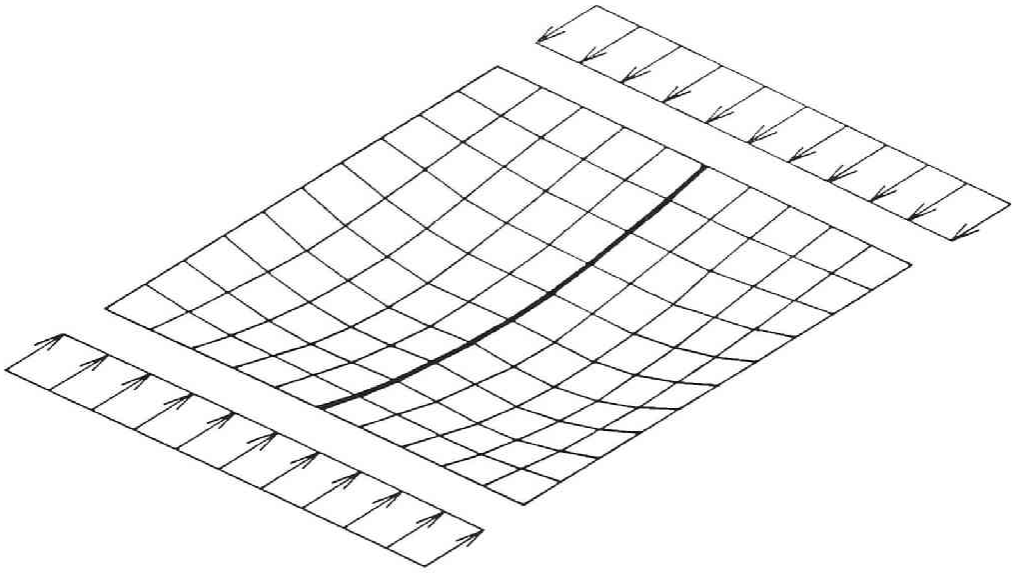

Fig. 4.4.2 Typical Global Buckling Mode G(1,1). SEM10 x 10 (Case 1).

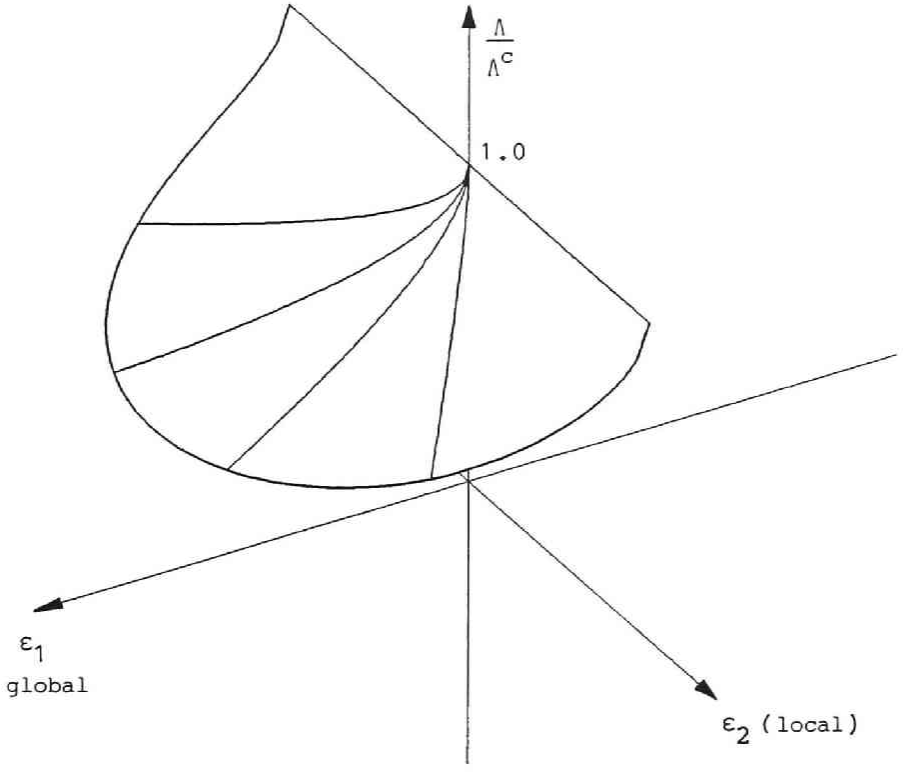

Fig. 4.4.3 Imperfection Sensitivity of FOLD Catastrophe for Global Buckling. SEM10 x 10 (Case 1).

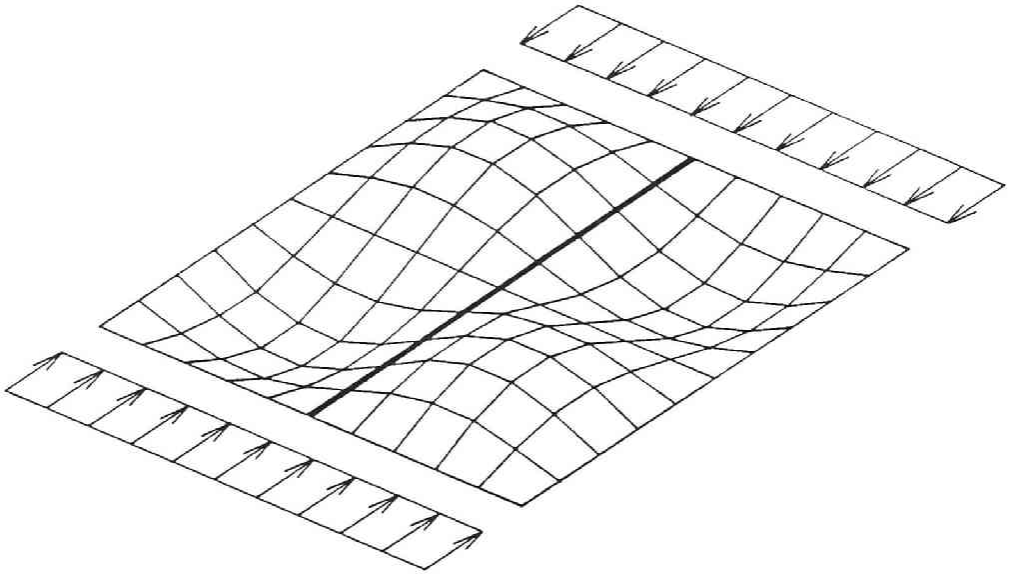

Fig. 4.4.4 Typical Local Buckling Mode L(2,2). SEM10 x 10 (Case 4).

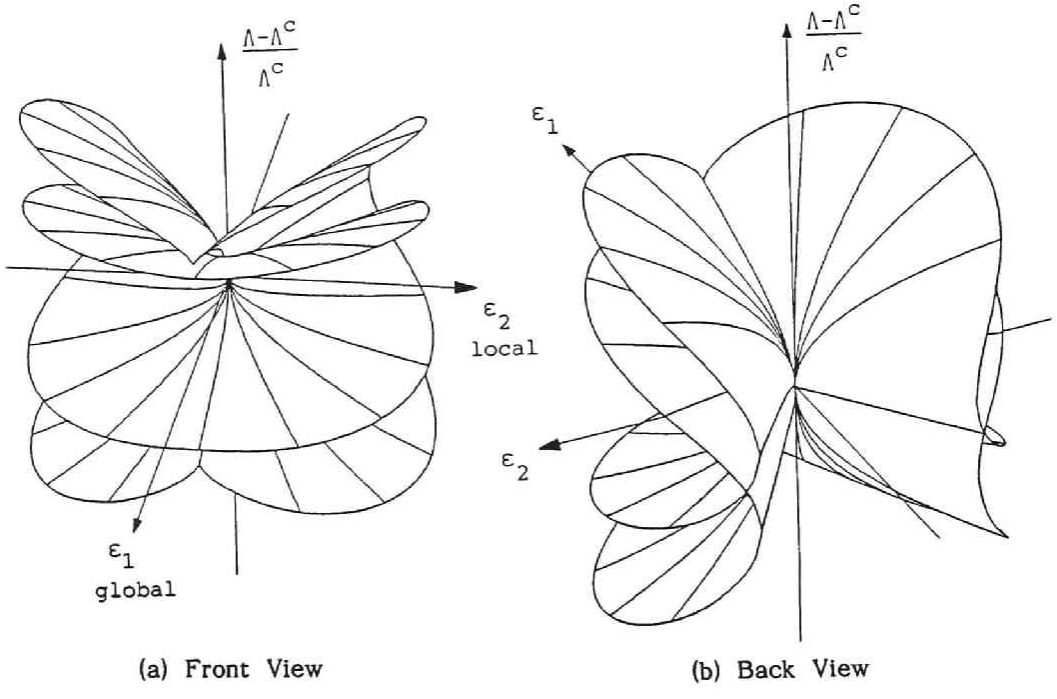

(a) Front View (b) Back View

Fig. 4.4.5 Imperfection Sensitivity of HYPERBOLIC UMBILIC Catastrophe for Homeoclinal Buckling. SEM10 x 10 (Case 2).

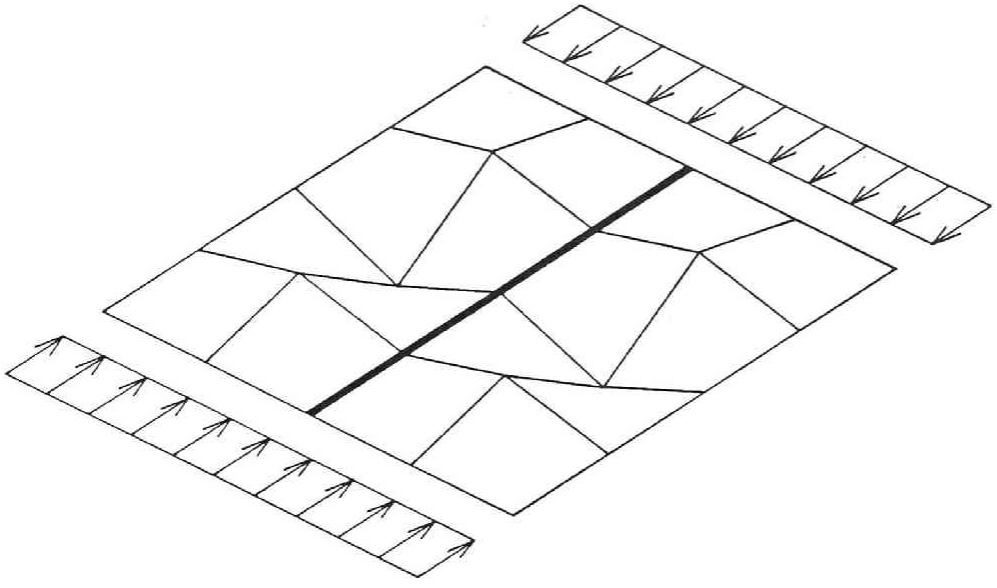

Fig. 4.4.6 Symmetric Local Buckling Mode L(3,1). SEM4x4.

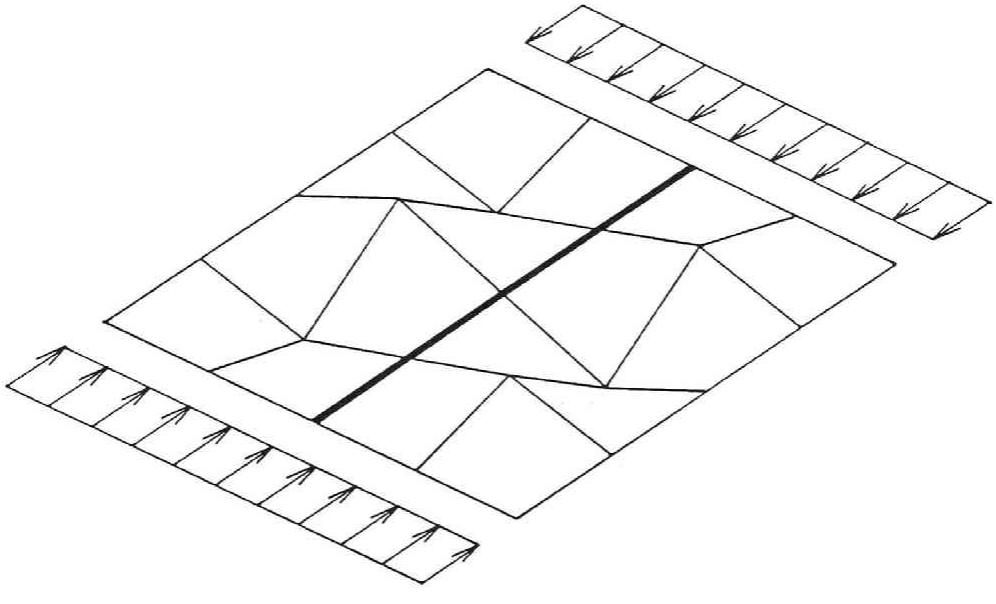

Fig. 4.4.7 Asymmetric Local Buckling Mode L(3,2). SEM4x4.

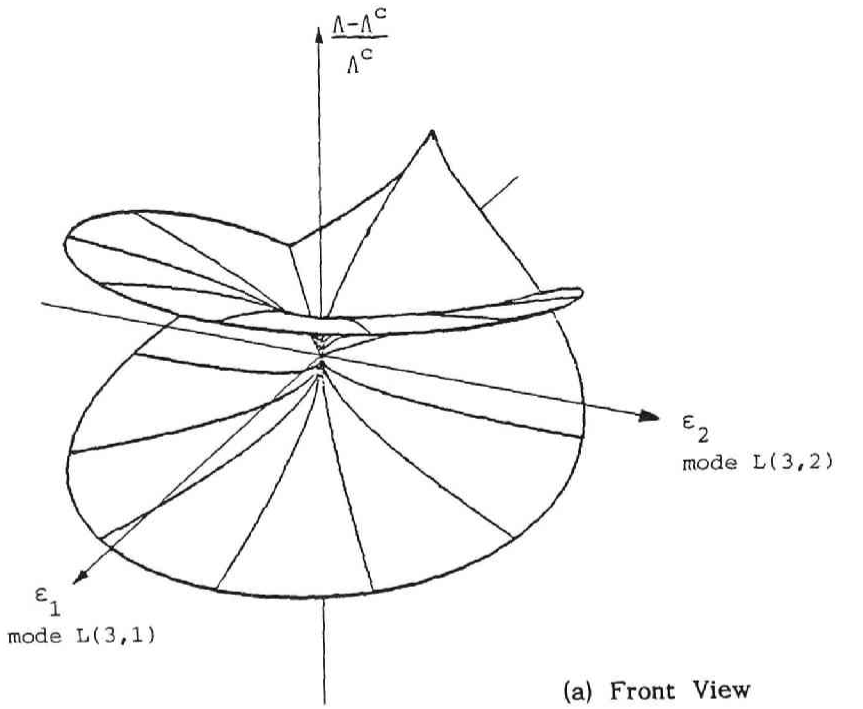

(a) Front View

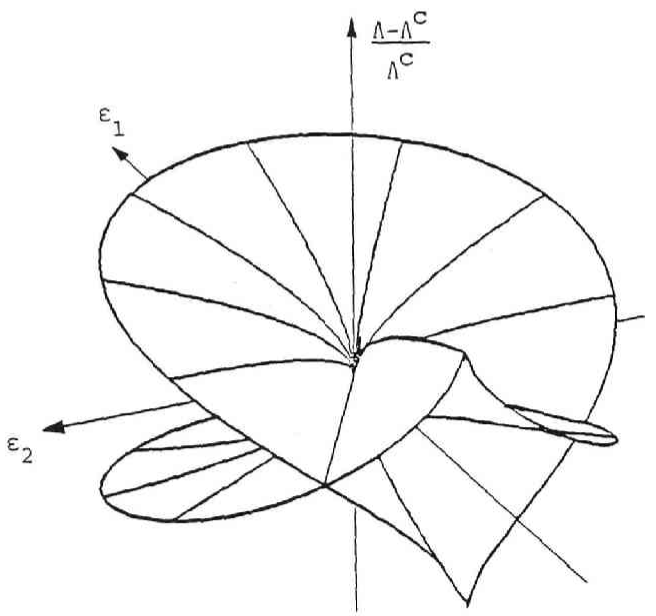

(b) Back View

Fig. 4.4.8 Imperfection Sensitivity of HYPERBOLIC UMBILIC Catastrophe for Monoclinal Buckling. SEM4x4 (Case 2).

Finally, the cases 2 and 3 in the middle two columns of each table show the results of near-coincident bucklings between the global and the local modes as mentioned and drawn in **Figs. 4.4.2** and **4.4.4.** In a numerical sense, it is rather difficult to realize the complete coincidence of above two bifurcations, so that the near-compound cases are considered in the present dissertation. The simultaneous bucklings are characterized by the **hyperbolic umbilic** catastrophe with the **homeoclinal** point of bifurcation proposed by Thompson and Hunt from relationships between the coefficients of the potential function. Then, the total potential function is expressed in the form similar to Eq. (II-3.2.23). The nonlinear equilibrium solutions of Eqs. (II-3.2.24) can not be easily analyzed with the aid of any nonlinear process of calculations, but the imperfection sensitivity surfaces can be obtained as the bifurcation sets in the catastrophe theory, using a powerful manipulation as stated in the chapter II-2 . **Figs. 4.4.5**(a) and (b) show the imperfection sensitivity surfaces and their back views of the hyperbolic umbilic catastrophe.

For example, the numerical results in the case 2 of 10x10 elements are demonstrated herein. When the initial deflections non-dimensionalized by the plate-panel thickness are prescribed, the elastic load-carrying capacity can be determined from the lowest cusp-type sheet with respect to the local initial deflection ε_2, as shown in **Fig. 4.4.5.** The imperfection surfaces are symmetric with respect to the ε_2=0 plane, and the sign of the local initial deflection mode will never affect the load-carrying capacity. Of course, since $A_{111} < 0$, the plus sign of the global initial deflection ε_1 is downward similarly to the distinct asymmetric case 1. If there exists only the downward global initial deflection, i.e., ε_1=0.1 and ε_2=0, then the load-carrying capacity will be reduced by 13.4% as Λ / Λ^c =0.866. Also, if there exists only the local initial deflection; ε_1=0, ε_2=0.1, then the capacity will be reduced by 21.1% as Λ / Λ^c =0.783. Moreover, if there exist both the downward global and local initial deflections; $\varepsilon_1=\varepsilon_2$=0.1, then Λ / Λ^c =0.783 by 21.7%. At the compound bifurcation, the load-carrying capacity is more sensitive to the local initial deflection ε_2 than to the global mode ε_1 for their magnitudes being the same. While, as shown in **Fig. 4.4.5**(b), the upward global initial deflection with $\varepsilon_1<0$ may also reduce the capacity, differently from the case 1 of the distinct asymmetric buckling.

In the special case of 4x4 elements, it is found that, as the flexural rigidity changes continuously, two typical buckling modes of v_1 and v_2 may approach each other under keeping the **symmetry** and **asymmetry** of each mode. Therefore, the coincidence of two local modes in **Figs. 4.4.6** and **4.4.7** lead to the similar **hyperbolic umbilic** catastrophe but with the **monoclinal** point of bifurcation(See, **Figs. 4.4.8**). It seems that the numerical results of 4x4 elements may be more unreasonable than those of other partitions of elements. This may provide an example at the coincidence of two local buckling modes of stiffened plates.

4.5 Conclusions

Several applications of the catastrophe analysis were made in order to predict the nonlinear behavior of structural models such as columns and compressed plates with or without stiffeners by discretization and modal transforms. This chapter particularly asserts that the catastrophe analysis accompanies with the static condensation procedure under the certain control types of loads and displacements in the initial postbuckling range. The main conclusions are:

(1) For an extensible column with the first-order approximations of the axial strain and the curvature, the 4th order terms of the buckling mode in the total potential function always disappear, and the potential function leads to only an eigenvalue problem for the ideal buckling load. Then, the column model has no postbuckling strength.

(2) The present numerical results analyzed by the SEM confirm such a theoretical prediction of the first-order approximate extensible column. However, the results by the FEM may tend to slightly overestimate the nonlinear characteristics. This quantitative difference depends on the kind of the shape function adopted in each discrete method.

(3) An extensibility of the neutral axis of column will not affect the cubic terms of the potential function, and the terms completely equal to those in the case of the inextensible column as the number of the discrete elements increases. Thus, the dual cusp, hyperbolic umbilic and fold catastrophes for the asymmetric buckling model can be realized, and the imperfection sensitivity surfaces of extensible columns are drawn spatially as the bifurcation sets in the catastrophe theory.

(4) The nonlinear solutions of elastic large deflection for compressed rectangular plates are predicted by the proposed numerical formulation. In the case of square unstiffened plates, the numerical results are found to be in excellent agreement with those by Timoshenko, Coan, Yamaki, Williams and Rhodes under various supporting conditions and the two control types.

(5) From the numerical results of compressed square plates, the difference between two control types of load and displacement may become little significant quantitatively and qualitatively within the accessible range of elastic large deflection.

(6) The compressed stiffened plate with the symmetric stiffener has the stable symmetric bifurcation point, **cusp**, for both the global and the local buckling modes at smaller and larger flexural rigidities, respectively.

(7) The present analysis is applied to both distinct and simultaneous bifurcation phenomena between the global and the local bucklings of compressed rectangular stiffened plate with the eccentric stiffener. For the distinct global buckling, the load-carrying capacity can be determined from the asymmetric buckling, **fold**, for the downward mode of the global initial deflection.

(8) Whereas, the distinct local buckling of the stiffened plate has the stable symmetric point of bifurcation, **cusp**, and the load-carrying capacity can never predicted in the stability and the catastrophe theories of elastic structures.

(9) At their coincident bifurcation for the stiffened plate, the imperfection sensitivity surfaces are expressed in the form of the **hyperbolic umbilic** catastrophe with the **homeoclinal** bifurcation. The load-carrying capacity is commonly more sensitive to the global initial mode than to the local initial mode for the same magnitudes.

(10) However, an insufficient partition of elements by the SEM may lead to the coincident of symmetric and asymmetric local modes, and its imperfection sensitivity is in the **hyperbolic umbilic** catastrophe with the **monoclinal** bifurcation.

Bibliographies of chapter 4 in PART II

1) Niwa,Y., E.Watanabe and H.Isami, Catastrophe analysis of structures by discretization and modal transforms. Memoirs of the Faculty of Engineering, Kyoto University, Vol. 43, pp. 67-87, 1981.
2) Niwa,Y., E.Watanabe and H.Isami, On prediction of large deflection of compressed rectangular plates. Proceedings of Structural Mechanics, Vol. 31A, pp. 25-35, 1985 (in Japanese).
3) Niwa,Y., E.Watanabe and N.Nakagawa, Catastrophe and imperfection sensitivity of two-degree-of-freedom systems. Proceedings of the Japan Society of Civil Engineers, No. 307, pp. 99-111, 1981.
4) Niwa,Y., E.Watanabe and H.Isami, Catastrophes of elastic column structures. Memoirs of the Faculty of Engineering, Kyoto University. Vol. 45, pp. 71-97, 1983.
5) Thompson,J.M.T. and G.W.Hunt, A General Theory of Elastic Stability. John Wiley & Sons, 1975.
6) Thompson,J.M.T., Instability and Catastrophes in Science and Engineering. John Wiley & Sons, 1982.
7) Thompson,J.M.T. and G.W.Hunt, Elastic Instability Phenomena. John Wiley & Sons, 1984.
8) Timoshenko,S.P. and J.M.Gere, Theory of Elastic Stability, 2nd Edition. McGraw-Hill, 1961.
9) Dym,C.L. and I.H.Shames, Solid Mechanics: A Variational Approach. McGraw-Hill, 1973.
10) Isami,H., A topological aspect of imperfection sensitivity of structures. Bulletin of Kohchi Technical College, No. 20, pp. 85-94, 1984.
11) Thompson,J.M.T., J.K.Y.Tan and K.C.Lim, On the topological classification of postbuckling phenomena. Journal of Structural Mechanics, Vol. 6, pp. 383-414, 1978.
12) Hunt,G.W., An algorithm for the nonlinear analysis of compound bifurcation. Philosophical Transactions of the Royal Society of London, Series A, Vol. 300, pp. 443-471, 1981.
13) Coan,J.M., Large-deflection theory for plates with small initial curvatures loaded in edge compression. Journal of Applied Mechanics, Transactions of American Society of Mechanical Engineers, Vol. 18, pp. 143-151, 1951.
14) Yamaki,N., Postbuckling behavior of rectangular plates with small initial curvatures loaded in edge compression. Journal of Applied Mechanics, Transactions of American Society of Mechanical Engineers, Vol. 26, pp. 407-414, 1959.
15) Williams,D.G. and A.C.Walker, Explicit solutions for the design of initially deformed plates subject to compression. Proceedings of the Institution of Civil Engineers, Part 2, Vol. 59, pp. 763-787, 1975.
16) Williams,D.G. and A.C.Walker, Explicit solutions for plate buckling analysis. Journal of the Engineering Mechanics Division, Proc. ASCE, Vol. 103, No. EM4, pp. 545-568, 1977.
17) Rhode,J., J.M.Harvey and W.C.Fok, The load-carrying capacity of initially imperfect eccentrically loaded plates. International Journal of Mechanical Sciences, Vol. 17, pp. 161-175, 1975.

18) Rhodes,J. and J.M.Harvey, Examination of plate post-buckling behavior. Journal of the Engineering Mechanics Division, Proc. ASCE, Vol. 103, No. EM3, pp. 461-473, 1977.
19) Hunt,G.W., Symmetries of elastic buckling. Engineering Structures, Vol. 14, pp. 21-28, 1982.
20) Hui,D. and J.S.Hansen, Two-mode buckling of an elastically supported plate and its relation to catastrophe theory. Journal of Applied Mechanics, Transactions of American Society of Mechanical Engineers, Vol. 47, pp. 607-612, 1980.
21) Tvergaard,V., Imperfection-sensitivity of a wide integrally stiffened panel under compression. International Journal of Solids and Structures, Vol. 9, pp. 177-192, 1973.
22) Tvergaard,V., Influence of post-buckling behavior on optimum design of stiffened panels. International Journal of Solids and Structures, Vol. 9, pp. 1519-1534, 1973.
23) Murray,N.W., Introduction to the Theory of Thin-Walled Structures. Oxford University Press, 1984.
24) Walker,A.C., A brief review of plate buckling research. Behavior of Thin-Walled Structures (Eds. J.Rhodes and J.Spense), Elsevier Applied Science Pub., pp. 375-398, 1984.
25) Thompson,J.M.T. and G.W.Hunt, Towards a unified bifurcation theory. Journal of Applied Mathematics and Physics (Zeitschrift für Angewandte Mathematik und Mechanik), Vol. 26, pp. 581-603, 1975.
26) Watanabe,E. and Y.Yamada, On the behaviour and ultimate strength of longitudinally stiffened flanges of steel box girders. Proceedings of the Japan Society of Civil Engineers, No. 252, pp. 127-142, 1976.
27) Yamada,Y., E.Watanabe and R.Ito, Compressive strength of plates with cross-sectional ribs. Proceedings of the Japan Society of Civil Engineers, No. 278, pp. 133-147, 1978.
28) Tateishi,A., A Study on the Utilization of Static Instability Analysis by a Discretization Method. Thesis presented to the Faculty of Engineering of Kyoto University in partial fulfillment of the requirements for the degree of Master of Engineering, 1980 (in Japanese).
29) Kageyama,M., A Study on the Utilization of Geometrical and Material Nonlinear Analysis. Thesis presented to the Faculty of Engineering of Kyoto University in partial fulfillment of the requirements for the degree of Master of Engineering, 1980 (in Japanese).
30) Gilmore,R., Catastrophe Theory for Scientists and Engineers. John Wiley & Sons, 1981.
31) Poston,T. and I.Stewart, Catastrophe Theory and Its Applications. Pitman, 1981.
32) Koiter,W.T., Over de Stabiliteit van het Elastische Evenwicht. Thesis, Delft, 1945 (English translations: On the Stability of Elastic Equilibrium. NASA Technical Transactions, F10, 833, National Aeronautics and Space Administration, 1967 and Technical Report AFFDL-TR-70-25, Air Force Flight Dynamics Laboratory, 1970).
33) Thompson,J.M.T. and G.W.Hunt, Comparative perturbation studies of the Elastica. International Journal of Mechanical Sciences, Vol. 11, pp. 999-1014, 1969.
34) Zeeman,E.C., Euler buckling. Structural Stability, the Theory of Catastrophes, and Applications in the Sciences. Lecture Notes in Mathematics, Vol. 525, Springer-Verlag, pp. 373-395, 1976.

APPENDIX A for PART II

SIMPLIFIED ELEMENT METHODS

A simplified element method (abbreviated as SEM) was firstly proposed by Yamada and Watanabe in order to reduce degrees of freedom of deformations at each discrete nodal point[1-4]. The adopted shape functions in each discrete element are linear or bi-linear ones of the reference coordinates. Then, the total strain energy stored in an element can be divided into two parts; one is the membrane strain energy due to stretching deformations of the element itself associated with the so-called Green's strain tensors; and another is the flexural strain energy due to bending deformations associated with the curvatures. Using some constitutive equation in the elastic range of the material, the former is derived from integration throughout an element, while the latter is replaced for the bending and twisting strain energies of equivalent flexural and twisting linear springs about the relevant coordinates between two adjacent elements.

A brief introduction of such a manipulation of the simplified element method will be provided for a discrete column or rectangular isotropic plate model[5-11]:

A.1 Column Model

Element coordinates

Fig. A.1.1 shows the Cartesian coordinate system (x,z) defined locally in an discrete element with four nodal generalized displacements; u_1 and u_2 are in-plane nodal displacements, w_1 and w_2 are out-of-plane nodal displacements. Each node has two degrees of freedom of deformations.

Shape function

The deformation of the column element can be described in terms of the displacement vector $(u,w,\bar{w})$, which denotes the axial displacement, the lateral deflection and the initial lateral deflection on the neutral axis z=0, respectively. Then, geometry of the column element is defined by

$$u(\xi) = a_{ij}\,\xi^{j-1}u_i\ , \qquad w(\xi) = a_{ij}\,\xi^{j-1}w_i\ , \qquad x = L\,\xi \qquad (i,j=1,2) \tag{A.1.1}$$

using four nodal displacements (u_1,u_2,w_1,w_2). In which, L denotes the axial length of the element, and components of coefficient a_{ij} (i,j=1,2) are listed:

i\j	1	2
1	1	-1
2	0	1

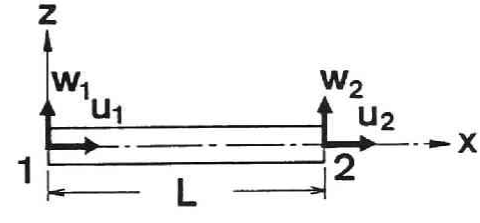

Fig. A.1.1 Column Model.

Strain-displacement relationship

$$\varepsilon_x = \varepsilon_{ox} - Z\,\kappa_x \tag{A.1.2}$$

where

$$\varepsilon_{ox} = \frac{dU}{dx} + \frac{1}{2}\left(\frac{dw}{dx}\right)^2 + \frac{d\bar{w}}{dx}\frac{dw}{dx}\ , \qquad \kappa_x = \frac{d^2w}{dx^2}$$

Furthermore, Eq. (A.1.2) is written in terms of the shape function of Eq. (A.1.1).

$$\varepsilon_{ox} = B_i^P u_i + \frac{1}{2} B_{ij}^{BB} w_i w_j + B_{ij}^{BB} \bar{w}_i w_j \qquad \text{(A.1.3)}$$

where B_i^P and B_{ij}^{BB} denote difference operators easily derived from Eq. (A.1.2).

Constitutive equation

$$\sigma_x = E \varepsilon_x \qquad \text{(A.1.4)}$$

where σ_x and E refer to the Euler's stress in the axial x-direction and the constant Young's modulus, respectively. This PART II treats with only the material to behave elastically.

Total strain energy

$$U^e = \int_V \int_\varepsilon \sigma_x \varepsilon_x \, d\varepsilon_x \, dV = \frac{1}{2} \int_V E \varepsilon_x^2 \, dV \qquad \text{(A.1.5)}$$

is stored in one element, and it can be clearly divided into two parts:

$$U^e = U_M^e + U_B^e \qquad \text{(A.1.6)}$$

where

$$U_M^e = \frac{1}{2} \int_V E \varepsilon_{ox}^2 \, dV , \qquad U_B^e = \frac{1}{2} \int_V E Z^2 \kappa_x^2 \, dV$$

using Eq. (A.1.2). The symbol $\int_V$ means the integral on the total volume of the element.

Total membrane strain energy due to stretching deformation

The membrane part of the total stored in one element is expressed by

$$U_M^e = \frac{1}{2} K_{ij}^P u_i u_j + K_{kij}^{PB} u_k \bar{w}_i w_j + \frac{1}{2} K_{kij}^{PB} u_k w_i w_j$$
$$+ \frac{1}{2} K_{ijk\ell}^{BB} \bar{w}_i \bar{w}_j w_k w_\ell + \frac{1}{2} K_{ijk\ell}^{BB} \bar{w}_i w_j w_k w_\ell + \frac{1}{8} K_{ijk\ell}^{BB} w_i w_j w_k w_\ell \qquad \text{(A.1.7)}$$

where

$$K_{ij}^B = \int_V E B_i^P B_j^P \, dV \qquad (i,j=1,2)$$

$$K_{kij}^{PB} = \int_V E B_k^P B_{ij}^{BB} \, dV \qquad (i,j,k=1,2)$$

$$K^{BB}_{ijk\ell} = \int_V E\, B^{BB}_{ij}\, B^{BB}_{k\ell}\, dV \qquad (i,j,k,\ell=1,2)$$

Then, the total membrane strain energy due to stretching deformations throughout the column model can be determined by

$$U_M = \sum_e U^e_M \qquad (A.1.8)$$

where $\sum_e$ denotes the summation over all discrete elements.

Total bending strain energy due to flexural spring

Consider a linear flexural spring with the constant k between two adjacent elements as shown in **Fig. A.1.2** and replace the bending strain energy stored in the second part of Eq. (A.1.6) for an equivalent strain energy stored in one flexural spring. The bending moment M_x at the node 2 is

$$M_x = - k\, d\theta \qquad (A.1.9)$$

where k and $d\theta$ indicate the spring constant and the relative rotation between two adjacent elements.

$$d\theta = \frac{1}{L} B^B_i w_i \quad (i=1,2,3) \qquad (A.1.10)$$

where

$$\{ B^B \} = (1 \;\; -2 \;\; 1)$$

On the other hand, the well-known differential equation for elastic beams is expressed in the finite difference form.

$$\frac{d^2 w}{dx^2} \cong \frac{d\theta}{L} = - \frac{M_x}{EI} \qquad (A.1.11)$$

where EI denotes the flexural rigidity of the column model. Then, the spring constant can be defined by

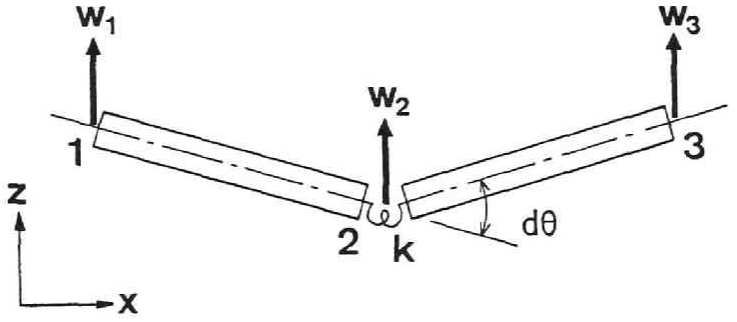

Fig. A.1.2 Flexural Spring between Two Adjacent Elements for Column Model.

$$k = \frac{EI}{L} \qquad \text{(A.1.12)}$$

so that the moment of the flexural spring in Eq. (A.1.9) is completely equivalent to the bending moment in Eq. (A.1.11). Therefore, the flexural strain energy in the second part U_B^e of Eq. (A.1.6) stored in one element can be determined as

$$U_B^e = \frac{1}{2} k (d\theta)^2 = \frac{1}{2} K_{ij}^B w_i w_j \qquad \text{(A.1.13)}$$

where

$$K_{ij}^B = \frac{EI}{L^3} k_{ij}^B , \qquad k_{ij}^B = B_i^B B_j^B \qquad (i,j=1,2,3)$$

$$[\, k^B \,] = \begin{bmatrix} 1 & -2 & 1 \\ -2 & 4 & -2 \\ 1 & -2 & 1 \end{bmatrix}$$

This can be evaluated directly without integration process over one element, differing from other stiffness matrices in Eq. (A.1.7). Then, the total bending strain energy throughout the column model can be determined by

$$U_B = \sum_s U_B^e \qquad \text{(A.1.14)}$$

where $\sum_s$ refers to the summation over all flexural springs.

Therefore, the total strain energy stored in the column model is obtained by the sum of U_M and U_B in Eqs. (A.1.8) and (A.1.14).

A.2 Rectangular Plate Model

Element coordinates

Fig. A.2.1 shows the Cartesian coordinate system (x,y,z) defined locally in an discrete element with twelve nodal generalized displacements; u_i (i=1,2,3,4) and v_j (i=1,2,3,4) are in-plane nodal displacements in the x- and y-directions, respectively, and w_i (i=1,2,3,4) are out-of-plane nodal displacements. Each node has three degrees of freedom of deformations.

Shape functions

The deformation of the rectangular plate element can be described by the displacement vector $(u,v,w,\bar{w})$, which denotes the in-plane displacements in the x- and y-directions, the lateral deflection in the z-direction, and the initial lateral deflection, respectively. This vector is defined on the neutral plane z=0 at any coordinate (x,y). Then, the geometry of the plate element is expressed by

$$u(\xi,\eta) = b_{kij}\, \xi^{i-1} \eta^{j-1} u_k , \qquad v(\xi,\eta) = b_{kij}\, \xi^{i-1} \eta^{j-1} u_{k+4}$$

$$w(\xi,\eta) = b_{kij}\, \xi^{i-1} \eta^{j-1} w_k \qquad (k=1,2,3,4) \qquad \text{(A.2.1)}$$

using twelve nodal displacements $(u_1,..,u_4,v_1,...,v_4,w_1,...,w_4)$. In which,

$$x = a\xi \quad , \quad y - b\eta \quad , \quad u_{k+4} = v_k \qquad (k=1,2,3,4)$$

and, a and b refer to the longitudinal length and the width of the rectangular plate element. The components of coeffi-cient b_{kij} (k=1,2,3,4; i,j=1,2) are listed:

	k=1	k=2	k=3	k=4
k11	1	0	0	0
k12	-1	0	0	1
k21	-1	1	0	0
k22	1	-1	1	-1

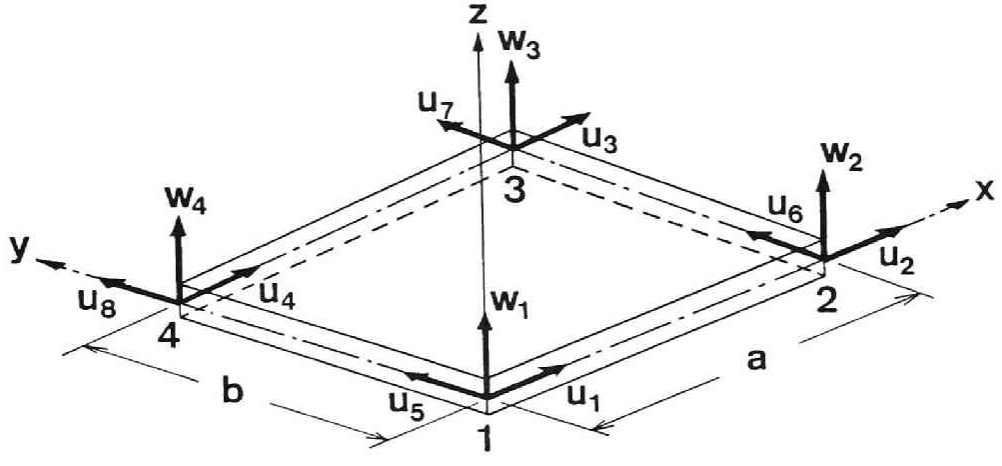

Fig. A.2.1 Plate Model.

Strain-displacement relationship

$$\varepsilon_i = \varepsilon_{oi} - z\kappa_i \qquad (i=1,2,3) \qquad (A.2.2)$$

where

$$\begin{Bmatrix} \varepsilon_{o1} \\ \varepsilon_{o2} \\ \varepsilon_{o3} \end{Bmatrix} = \begin{Bmatrix} \varepsilon_{ox} \\ \varepsilon_{oy} \\ \varepsilon_{oxy} \end{Bmatrix} = \begin{Bmatrix} \frac{\partial u}{\partial x} \\ \frac{\partial v}{\partial y} \\ \frac{\partial u}{\partial y} + \frac{\partial v}{\partial x} \end{Bmatrix} + \frac{1}{2} \begin{Bmatrix} (\frac{\partial w}{\partial y})^2 \\ (\frac{\partial w}{\partial y})^2 \\ 2\frac{\partial w}{\partial x}\frac{\partial w}{\partial y} \end{Bmatrix} + \begin{Bmatrix} \frac{\partial \bar{w}}{\partial x}\frac{\partial w}{\partial x} \\ \frac{\partial \bar{w}}{\partial y}\frac{\partial w}{\partial y} \\ \frac{\partial \bar{w}}{\partial x}\frac{\partial w}{\partial y} + \frac{\partial w}{\partial x}\frac{\partial \bar{w}}{\partial y} \end{Bmatrix}$$

$$\begin{Bmatrix} \kappa_1 \\ \kappa_2 \\ \kappa_3 \end{Bmatrix} = \begin{Bmatrix} \kappa_x \\ \kappa_x \\ \kappa_{xy} \end{Bmatrix} = \begin{Bmatrix} -\frac{\partial^2 w}{\partial x^2} \\ -\frac{\partial^2 w}{\partial y^2} \\ -\frac{\partial^2 w}{\partial x \partial y} \end{Bmatrix}$$

Furthermore, Eq. (A.2.2) is rewritten in terms of the shape functions

$$\varepsilon_{oi} = B^{P}_{ij} u_j + \frac{1}{2} B^{BB}_{ijk} w_j w_k + B^{BB}_{ijk} \bar{w}_j w_k \qquad \text{(A.2.3)}$$

where B^{P}_{ij} and B^{BB}_{ijk} denote difference operators easily derived from Eq. (A.2.1).

Constitutive equations

$$\sigma_i = D_{ij} \varepsilon_j \qquad \text{(A.2.4)}$$

where

$$[\, D_{ij} \,] = \frac{E}{1 - \nu^2} \begin{bmatrix} 1 & \nu & 0 \\ \nu & 1 & 0 \\ 0 & 0 & \frac{1-\nu}{2} \end{bmatrix}$$

in the case of a plane stress parallel to the x-y plane of the isotropic plate model. In which, ν refers to the Poisson's ration, and the coordinates x, y and z are redesignated as x_1, x_2 and x_3. Hereafter, the quantities such as stresses and strains are subscripted by 1, 2 and 3 in the x-, y- and z-directions, respectively.

Total strain energy

$$U^e = \int_V \int_{\{\varepsilon\}} \sigma_i \varepsilon_i \, d\{\varepsilon\} \, dV = \frac{1}{2} \int_V D_{ij} \varepsilon_i \varepsilon_j \, dV \qquad \text{(A.2.5)}$$

is stored in one element, and it can be clearly divided into two parts:

$$U^e = U^e_M + U^e_B \qquad \text{(A.2.6)}$$

where

$$U^e_M = \frac{1}{2} \int_V D_{ij} \varepsilon_{oi} \varepsilon_{oj} \, dV \,, \qquad U^e_B = \frac{1}{2} \int_V D_{ij} z^2 \kappa_i \kappa_j \, dV$$

using Eq. (A.2.2). The symbol $\int_V$ denotes the integral on the total volume of the element.

Total membrane strain energy due to stretching deformations

The membrane part of the total strain energy stored in one element can be redescribed by

$$U^e_M = \frac{1}{2} K^{P}_{ij} u_i u_j + K^{PB}_{kij} u_k \bar{w}_i w_j + \frac{1}{2} K^{PB}_{kij} u_k w_i w_j$$

$$+ \frac{1}{2} K^{BB}_{ijk\ell} \bar{w}_i \bar{w}_j w_k w_\ell + \frac{1}{2} K^{BB}_{ijk\ell} \bar{w}_i w_j w_k w_\ell + \frac{1}{8} K^{BB}_{ijk\ell} w_i w_j w_k w_\ell \qquad \text{(A.2.7)}$$

where

$$K^{P}_{ij} = \int_{V} D_{mn} B^{P}_{mi} B^{P}_{nj} \, dV \qquad (i,j=1,\ldots,8;\ m,n=1,2,3)$$

$$K^{PB}_{kij} = \int_{V} D_{mn} B^{P}_{mk} B^{BB}_{nij} \, dV \qquad (k=1,\ldots,8;\ i,j=1,\ldots,4;\ m,n=1,2,3)$$

$$K^{BB}_{ijk\ell} = \int_{V} D_{mn} B^{BB}_{mij} B^{BB}_{nk\ell} \, dV \qquad (i,j,k,\ell=1,\ldots,4;\ m,n=1,2,3)$$

Then, the total membrane strain energy due to stretching deformations throughout the plate model can be determined by

$$U_M = \sum_{e} U^{e}_{M} \qquad (A.2.8)$$

where $\sum_{e}$ denotes the summation over all discrete elements.

Total bending and twisting strain energies of springs

Under Eqs. (A.2.2) and (A.2.4), the energy can be further divided into three sub-parts:

$$U^{e}_{B} = U^{e}_{B1} + U^{e}_{B2} + U^{e}_{B3} \qquad (A.2.9)$$

where

$$U^{e}_{B1} = \frac{D}{2} \int_{0}^{a} \int_{0}^{b} (\kappa^{2}_{x} + \kappa^{2}_{y}) \, dx \, dy$$

$$U^{e}_{B2} = \frac{D}{2} \int_{0}^{a} \int_{0}^{b} 2 \kappa^{2}_{xy} \, dx \, dy$$

$$U^{e}_{B3} = \frac{D}{2} \int_{0}^{a} \int_{0}^{b} [2 (\kappa_{x} \kappa_{y} - \kappa^{2}_{xy})] \, dx \, dy$$

$$D = \frac{E t^{3}}{12(1-\nu^{2})}$$

in which, D, t, a and b indicate the flexural rigidity, the constant thickness, the longitudinal length and the width of the isotropic rectangular plate element, respectively, as shown in **Fig. A.2.1.** The energy can not be measured so far as the shape functions of Eqs. (A.2.1) are used herein. Hence, the following concepts of two types of elastic linear spring will be introduced:

(a) Flexural spring

Consider a linear flexural spring between two adjacent elements, and assume the spring to have both flexural and twisting rigidities. For instance, such a spring at the center on the boundary between elements in the x-direction as shown in **Fig. A.2.2.** Then, using the finite difference process, the bending moment m_x about the y-direction per unit length acting perpendicular to the boundary 25 is replaced as follows:

$$m_x = D (\kappa_x + \nu \kappa_y) \cong D \kappa_x \cong D \frac{d\theta_x}{a} \qquad (A.2.10)$$

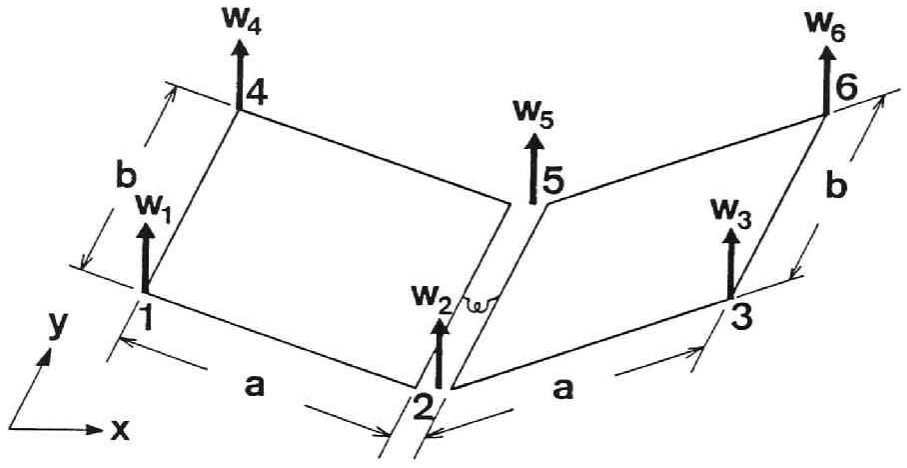

Fig. A.2.2 Flexural/Torsional Spring between Two Adjacent Elements in x-direction for Plate Model.

where the relative rotation $d\theta_x$ between two adjacent elements in the x-direction

$$d\theta_x = \frac{1}{2a} B''_{xi} w_i \qquad (i=1,\ldots,6)$$

$$\{ B''_x \} = (1 \quad -2 \quad 1 \quad 1 \quad -2 \quad 1)$$

The total bending moment M_x about the y-axis on the boundary 25 is

$$M_x = b\, m_x = k_x\, d\theta_x \qquad (A.2.11)$$

where the flexural spring constant k_x leads to

$$k_x = \frac{b}{a} D$$

In a similar manner, the total bending moment M_y about the x-axis between two adjacent elements in the y-direction can be finally obtained as

$$M_y = k_y\, d\theta_y \qquad (A.2.12)$$

where

$$k_y = \frac{a}{b} D$$

and $d\theta_y$ denotes the relative rotation in the y-direction

$$d\theta_y = \frac{1}{2b} B''_{yi} w_i \qquad (i=1,..,6)$$

$$\{ B''_y \} = (1 \quad -2 \quad 1 \quad 1 \quad -2 \quad 1)$$

(b) Torsional Spring

The twisting moment m_{xy} per unit length acting on the boundary 25 in **Fig. A.2.2** is replaced by

$$m_{xy} = D (1 - \nu) \kappa_{xy} \cong D \kappa_{xy} \cong D \, d\phi_{xy} \qquad (A.2.13)$$

where

$$d\phi_{xy} = \frac{1}{ab} (w_1 - w_2 + w_5 - w_4)$$

is equivalently computed by the shape function of Eq. (A.2.1) in one element. Then, the torsional strain energy stored is defined in one element and can be determined as the sum of equal four torsional springs on four element boundaries

$$U^e_{B2} = 4 \times \frac{1}{2} k_t ab (d\phi_{xy})^2 \qquad (A.2.14)$$

where the torsional spring constant is

$$k_t = \frac{D}{2}$$

The energy is equivalently proposed by the definition of a twisting moment m^*_{xy} per unit length for one torsional spring on a boundary in one element

$$m^*_{xy} = \frac{D}{2} d\phi_{xy} \qquad (A.2.15)$$

For convenience, the torsional spring is rewritten

$$t_x = \frac{D}{2b} d\phi_x \qquad \text{in the x-direction} \qquad (A.2.16)$$

where

$$d\phi_x = \frac{1}{a} B''_{xi} w_i \qquad (i=1,\ldots,4)$$

$$\{ B''_x \} = (1 \quad -1 \quad 1 \quad -1)$$

and

$$t_y = \frac{D}{2a} d\phi_y \qquad \text{in the y-direction} \qquad (A.2.17)$$

where

$$d\phi_y = \frac{1}{b} B''^{t}_{yi} w_i \qquad (i=1,\ldots,4)$$

$$\{ B''^{t}_{y} \} = (1 \quad -1 \quad 1 \quad -1)$$

(c) Total strain energy due to flexural and torsional springs

Fig. A.2.3 shows the typical adjacent two elements and the flexural/ torsional spring on their boundary in the x-direction similarly to **Fig. A.2.2.** In which, the symbols "L" and "R" denote the left and right elements with respect to the relevant spring. Then, as discussed above, the bending and the twisting moments per unit length on the boundary 25 are rewritten in terms of six nodal out-of-plane displacements

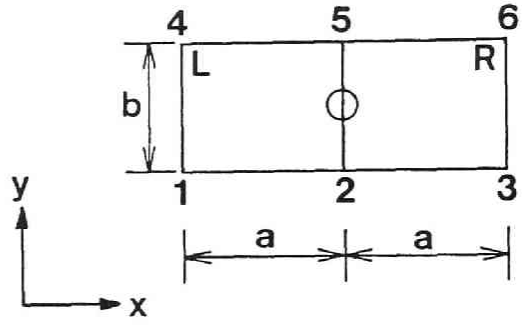

Fig. A.2.3 Two Adjacent Elements in x-direction.

$$m_x = \frac{D}{a} d\phi_x , \qquad t_x^L = \frac{D}{2b} d\phi_x^L , \qquad t_x^R = \frac{D}{2b} d\phi_x^R \qquad (A.2.18)$$

where

$$d\theta_x = (B'_x) \{ w \} , \qquad (B'_x) = \frac{1}{2a} (1 \quad -2 \quad 1 \quad 1 \quad -2 \quad 1)$$

$$d\phi_x^L = (B'^{L}_x) \{ w \} , \qquad (B'^{L}_x) = \frac{1}{a} (1 \quad -1 \quad 0 \quad -1 \quad 1 \quad 0)$$

$$d\phi_x^R = (B'^{R}_x) \{ w \} , \qquad (B'^{R}_x) = \frac{1}{a} (0 \quad 1 \quad -1 \quad 0 \quad -1 \quad 1)$$

$$\{ w \}^T = (w_1 \quad w_2 \quad w_3 \quad w_4 \quad w_5 \quad w_6)$$

The total bending and twisting moments are

$$M_x = b\, m_x = \left(\frac{b}{a} D \right) d\theta_x = \left(\frac{b}{a} D \right) (B'_x) \{ w \}$$

$$T_x^L = b\, t_x^L = \left(\frac{1}{2} D \right) d\phi_x^L = \left(\frac{1}{2} D \right) (B'^{L}_x) \{ w \}$$

$$T_x^T = b\, t_x^R = \left(\frac{1}{2} D \right) d\phi_x^R = \left(\frac{1}{2} D \right)\left(B_x'^R \right)\{ w \} \tag{A.2.19}$$

Therefore, the bending strain energy of the flexural spring in the x-direction is obtained from Eqs. (A.2.10), (A.2.11) and (A.2.19)

$$\begin{aligned} U_{Bx} &= \frac{1}{2} \left(\frac{b}{a} D \right)(d\theta_x)^2 \\ &= \frac{1}{2} \{ w \}^T \left[\left(\frac{b}{a} D \right)\left(B_x' \right)^T \left(B_x' \right) \right]\{ w \} \\ &= \frac{1}{2} K_{ij}^{Bx} w_i w_j \end{aligned} \tag{A.2.20}$$

where the bending stiffness matrix is explicitly presented

$$K_{ij}^{Bx} = \frac{1}{4a^2} \left(\frac{b}{a} D \right) k_{ij}^{Bx} \qquad (i,j=1,\ldots,6)$$

$$[\, k_{ij}^{Bx} \,] = \left[\begin{array}{rrr|rrr} 1 & -2 & 1 & 1 & -2 & 1 \\ -2 & 4 & -2 & -2 & 4 & -2 \\ 1 & -2 & 1 & 1 & -2 & 1 \\ \hline 1 & -2 & 1 & 1 & -2 & 1 \\ -2 & 4 & -2 & -2 & 4 & -2 \\ 1 & -2 & 1 & 1 & -2 & 1 \end{array}\right]$$

It is apparently found that the energy is equivalent to the first term of the first sub-part in Eq. (A.2.9). Furthermore, the twisting strain energy of the torsional spring is defined in each element, that is, in the left element

$$\begin{aligned} U_x^{tL} &= \frac{1}{2} \left(\frac{D}{2} \right)(d\phi_x^L)^2 \\ &= \frac{1}{2} \{ w \}^T \left[\left(\frac{D}{2} \right)\left(B_x'^L \right)^T \left(B_x'^L \right) \right] \{ w \} \\ &= \frac{1}{2} K_{ij}^{txL} w_i w_j \end{aligned} \tag{A.2.21}$$

where

$$K_{ij}^{txL} = \frac{1}{a^2} \left(\frac{D}{2} \right) k_{ij}^{txL} \qquad (i,j=1,\ldots,6)$$

$$[\, k_{ij}^{txL} \,] = \left[\begin{array}{ccc|ccc} 1 & -1 & 0 & -1 & 1 & 0 \\ -1 & 1 & 0 & 1 & -1 & 0 \\ 0 & 0 & 0 & 0 & 0 & 0 \\ \hline -1 & 1 & 0 & 1 & -1 & 0 \\ 1 & -1 & 0 & -1 & 1 & 0 \\ 0 & 0 & 0 & 0 & 0 & 0 \end{array}\right]$$

Similarly, in the right element

$$U_x^{tR} = \frac{1}{2}\left(\frac{D}{2}\right)(d\,\phi_x^R)^2$$

$$= \frac{1}{2}\{w\}^T \left[\left(\frac{D}{2}\right)(B_x'^R)^T(B_x'^R)\right]\{w\}$$

$$= \frac{1}{2} K_{ij}^{txR} w_i w_j \qquad \text{(A.2.22)}$$

where

$$K_{ij}^{txR} = \frac{1}{a^2}\left(\frac{D}{2}\right) k_{ij}^{txR} \qquad (i,j=1,\ldots,6)$$

$$[\, k_{ij}^{txR} \,] = \left[\begin{array}{ccc|ccc} 0 & 0 & 0 & 0 & 0 & 0 \\ 0 & 1 & -1 & 0 & -1 & 1 \\ 0 & -1 & 1 & 0 & 1 & -1 \\ \hline 0 & 0 & 0 & 0 & 0 & 0 \\ 0 & -1 & 1 & 0 & 1 & -1 \\ 0 & 1 & -1 & 0 & -1 & 1 \end{array}\right]$$

The above two energies are equivalent to the second sub-part in Eq. (A.2.9). Using the spring constants of Eqs. (A.2.12) and (A.2.13), the flexural/torsional spring between adjacent two elements in the y-direction can be defined in the similar manner. Finally, the total strain energies of the spring in the y-direction are provided by the equivalent forms to the sum of both the second term of the first sub-part and the second sub-part in Eq. (A.2.9).

It is apparently found that the third sub-part U_{B3}^e in Eq. (A.2.9) may vanish throughout the rectangular plate model when its four edges simply supported or clamped, and this part is neglected in the SEM analysis.

Therefore, the total bending and twisting strain energy can be obtained by

$$U_B = \sum_{sx}\left(U_{Bx} + U_x^{tR} + U_x^{tL}\right) + \sum_{sy}\left(U_{By} + U_y^{tR} + U_y^{tL}\right) \qquad \text{(A.2.23)}$$

where $\sum_{sx}$ and $\sum_{sy}$ refer to the summations of the flexural/torsional springs in the x- and y-direction, respectively. Then, the overall bending/torsional stiffness matrix is defined as

$$U_B = \frac{1}{2} K_{ij}^B w_i w_j \qquad \text{(A.2.24)}$$

As a result, the total strain energy stored in the plate model is given in the form of the sum of two parts (A.2.8) and (A.2.24).

Bibliographies of APPENDIX A in PART II

1) Yamada,Y. and E.Watanabe, On the behavior and ultimate of longitudinally stiffened flanges of steel box girders. Proceedings of the Japan Society of Civil Engineers, No. 252, pp. 127-142, 1976.
2) Yamada,Y., E.Watanabe and R.Itoh, Compressive strength of plates with closed-sectional ribs. Proceedings of the Japan Society of Civil Engineers, No. 278, pp. 133-147, 1978.
3) Niwa,Y. and E.Watanabe, Applications of subspace iteration method to the analysis of finite deformations. Proceedings of the Annual Meeting of the Japan Society of Civil Engineering, I-951, 1977.
4) Niwa,Y. and E.Watanabe, On reduction of degrees of freedom in nonlinear structural analysis. Proceedings of the 33rd Annual Meeting of the Japan Society of Civil Engineering, I-31, 1978.
5) Tateishi,A., A Study on the Utilization of Static Instability Analysis by a Discretization Method. Thesis presented to the Faculty of Engineering of Kyoto University in partial fulfillment of the requirements for the degree of Master of Engineering, 1980 (in Japanese).
6) Kageyama,M., A Study on the Utilization of Geometrical and Material Non linear Analysis. Thesis presented to the Faculty of Engineering of Kyoto University in partial fulfillment of the requirements for the degree of Master of Engineering, 1980 (in Japanese).
7) Isami,H., Applications of Catastrophe Theory to Static Instabilities by Discretization and Modal Transforms. Thesis presented to the Faculty of Engineering of Kyoto University in partial fulfillment of the requirements for the degree of Master of Engineering, 1980 (in Japanese).
8) Niwa,Y., E.Watanabe and H.Isami, Catastrophe analysis of structures by discretization and modal transforms. Memoirs of the Faculty of Engineering, Kyoto University, Vol. 43, pp. 67-87, 1981.
9) Niwa,Y., E.Watanabe and H.Isami, Catastrophes of elastic column structures. Memoirs of the Faculty of Engineering, Kyoto University, Vol. 45, pp. 71-97, 1983.
10) Nomura,T., A Study on the Utilization of Elasto-Plastic Large Deflection Analysis of Plated Structures. Thesis presented to the Faculty of Engineering of Kyoto University in partial fulfillment of the requirements for the degree of Master of Engineering, 1985 (in Japanese).
11) Watanabe,E., A Study on the Catastrophe and Static Load-Carrying Capacity of Structures. Thesis presented to the Graduate Faculty of Engineering of Kyoto University in partial fulfillment of the requirements for the degree of Doctor of Engineering, 1986.

APPENDIX B for PART II

STANDARD FORM OF STRUCTURAL POTENTIAL FUNCTION

The canonical form of the structural potential function defined by the Taylor's expansion near the distinct or compound critical point can be transformed to the Thom's unfolding of the corresponding elementary catastrophe. The diffeomorphic transformation is briefly discussed for the **fold, cusp** and **umbilics** in this dissertation. Hereafter, the notations of A and F refer to the structural potential function and the Thom's unfolding, respectively.

B.1 Fold Catastrophe

$$A(v_1,\lambda,\varepsilon_1) = \frac{1}{6} A^{c}_{111} v_1^3 + \frac{1}{2} A^{oc}_{11} v_1^2 \lambda + A^{1c}_{1} v_1 \varepsilon_1$$

$$F(x,\alpha) = x^3 + \alpha x$$

Then,

$$F(x,\alpha) \simeq A(v_1,\lambda,\varepsilon_1) + G(\lambda,\varepsilon_1)$$

under the diffeomorphic transformations: $(v_1,\lambda,\varepsilon_1) \rightarrow (x,\alpha)$

$$x = \left(\frac{A^{c}_{111}}{6}\right)^{\frac{1}{3}} v_1 + \frac{A^{oc}_{11}}{6}\left(\frac{6}{A^{c}_{111}}\right)^{\frac{2}{3}} \lambda$$

$$\alpha = A^{1c}_{1}\left(\frac{6}{A^{c}_{111}}\right)^{\frac{1}{3}} \varepsilon_1 - \frac{(A^{oc}_{11})^2}{12}\left(\frac{6}{A^{c}_{111}}\right)^{\frac{4}{3}} \lambda^2$$

where

$$G(\lambda,\varepsilon_1) = \left(\frac{A^{oc}_{11} A^{1c}_{1}}{A^{c}_{111}}\right) \varepsilon_1 - \frac{(A^{oc}_{11})^3}{3(A^{c}_{111})^2} \lambda^3$$

B.2 Cusp or Dual Cusp Catastrophe

$$A(v_1,\lambda,\varepsilon_1) = \frac{1}{24} A^{c}_{1111} v_1^4 + \frac{1}{2} A^{oc}_{11} v_1^2 \lambda + A^{1c}_{1} v_1 \varepsilon_1$$

$$F(x,\alpha,\beta) = \pm x^4 + \alpha x^2 + \beta x$$

Then,

$$F(x,\alpha,\beta) \simeq A(v_1,\lambda,\varepsilon_1)$$

under the diffeomorphic transformations: $(v_1,\lambda,\varepsilon_1) \to (x,\alpha,\beta)$

$$x = \left|\frac{A^c_{1111}}{24}\right|^{\frac{1}{4}} v_1 \ , \quad \alpha = \frac{A^{oc}_{11}}{2}\left|\frac{24}{A^c_{1111}}\right|^{\frac{1}{2}} \lambda \ , \quad \beta = A^{1c}_1\left|\frac{24}{A^c_{1111}}\right|^{\frac{1}{4}} \varepsilon_1$$

B.3 Umbilic Catastrophes

$$A(v_1,v_2,\lambda,\varepsilon_1,\varepsilon_2) = \frac{1}{6} A^c_{111} v_1^3 + \frac{1}{2} A^c_{122} v_1 v_2^2 + \frac{\lambda}{2}(A^{oc}_{11} v_1^2 + A^{oc}_{22} v_2^2) + A^{1c}_1 v_1 \varepsilon_1 + A^{2c}_2 v_2 \varepsilon_2$$

$$F(x,y,\alpha,\beta,\gamma) = x^3 \pm a\,x\,y^2 + \alpha(x^2 + y^2) + \beta x + \gamma y$$

Then,

$$F(x,y,\alpha,\beta,\gamma) \simeq A(v_1,v_2,\lambda,\varepsilon_1,\varepsilon_2)$$

under the diffeomorphic transformations: $(v_1,v_2,\lambda,\varepsilon_1,\varepsilon_2) \to (x,y,\alpha,\beta,\gamma)$

$$x = \left(\frac{A^c_{111}}{6}\right)^{\frac{1}{3}} v_1 \ , \quad y = \left(\frac{A^{oc}_{22}}{A^{oc}_{11}}\right)^{\frac{1}{2}} \left(\frac{A^c_{111}}{6}\right)^{\frac{1}{3}} v_2 \ ,$$

$$\alpha = \frac{A^{oc}_{11}}{2}\left(\frac{6}{A^c_{111}}\right)^{\frac{1}{3}} \lambda \ , \quad \beta = A^{1c}_1\left(\frac{6}{A^c_{111}}\right)^{\frac{1}{3}} \varepsilon_1 \ , \quad \gamma = A^{2c}_2\left(\frac{A^{oc}_{11}}{A^{oc}_{22}}\right)^{\frac{1}{2}}\left(\frac{6}{A^c_{111}}\right)^{\frac{1}{3}} \varepsilon_2 \ ,$$

where

$$a = \left|\frac{3A^{oc}_{11}A^c_{122}}{A^{oc}_{22}A^c_{111}}\right|$$

PART III

CATASTROPHE ANALYSIS OF ELASTO-PLASTIC STRUCTURES

CHAPTER 1

A NEW UNIFIED APPROACH TO PREDICT THE STRENGTH OF STEEL STRUCTURES

1.1 General Remarks

The stability and the strength of steel slender members in the elasto-plastic range have been among the most important research interests in the field of civil engineering. A great number of investigations have been performed through analytical and numerical procedures on their initial bucklings, the postbucklings and the load-carrying capacities. Recently, the incremental materially and geometrically nonlinear numerical calculations are being increasingly adopted within the framework of discretization methods such as finite differences, finite element methods and boundary element methods. Their main objective is to predict the elasto-plastic strength of slender structural members for certain set of parameters such as the material properties, the geometrical dimensions and the imperfections[1-4].

Niwa, Watanabe and Isami have been concerned with a unified approach to evaluate the load-carrying capacity of structural members in the elasto-plastic range[5-10]. The effects of above parameters on the elasto-plastic strength can be explicitly expressed in terms of the bifurcation set in a closed-form expression without resort to solving the nonlinear simultaneous equilibrium equations.

This chapter unifies an evaluation of the elasto-plastic buckling load, the postbuckling equilibrium path, the plastic failure mechanism curve and the imperfection sensitivity curve. Herein, the proposed approach is demonstrated in detail to predict the elasto-plastic ultimate strength of axially compressed columns. Furthermore, applications of the approach to other types of members such as laterally unsupported beam-columns, compressed rectangular plates with or without stiffeners, and compressed cylindrical shells will be discussed in the subsequent chapters of this PART.

1.2. Basic Formulations

1.2.1 Elasto-plastic buckling strength

An appropriate presence of residual stress distribution is considered in the cross section of the perfect structural model without any geometrical imperfections. The distribution of residual stress is assumed to be assigned in a proper form satisfying the initial self-equilibrium. Then, the strength can be obtained directly from the reduction ratio k of the elastic portion to the total cross section[11,12].

For each prescribed form of residual stress distribution and its maximum magnitude σ_r, the effective ratio k of the elastic portion to the total cross section is defined by the tangent modulus E_t and the secant modulus E_s[9]:

$$E_t \equiv \frac{d\sigma}{d\varepsilon} = kE \quad \text{and} \quad E_s \equiv \frac{\sigma}{\varepsilon} \tag{1.2.1}$$

where

$\sigma = \sigma(k)$ *and* $\varepsilon = \varepsilon(k)$,

E : Young's modulus,

σ : generalized stress, ε : generalized strain.

Two functions of $\sigma(k)$ and $\varepsilon(k)$ depend on the type and the magnitude of the distribution of residual stress for each member.

The associated buckling mode and its corresponding initial imperfection mode in the elasto-plastic range are assumed reasonably for given boundary conditions. Their magnitudes are designated as the generalized displacements of w and w_o, non-dimensionalized by the column-span length ℓ or the thickness t. Then, on the basis of the ordinary differential equations of equilibrium, a modified eigenvalue equation is obtained in a neighborhood of the critical buckling point[9]

$$f\sigma_E w - \sigma w = 0 \tag{1.2.2}$$

where σ_E denotes the well-known elastic Euler buckling strength, which is a deterministic function of the capital symbol "R", designating as the generalized slenderness ratio for columns, the generalized width-thickness ratio for plated structures or the generalized radius-thickness ratio of cylindrical shells. Also, f represents the coefficient due to the elasto-plasticity. Since it is quite difficult to estimate the coefficient f exactly, it is approximated by a simple function of k using the elasto-plastic moment-curvature relation or the nonlinear equilibrium equations for each member considered. Herein, f is assumed to be invariant to prescribed geometrical initial imperfection w_o[5].

For columns and unstiffened plates, only the primary elasto-plastic buckling mode corresponding to the least elasto-plastic buckling strength is taken into account as the generalized displacement w. In the case of stiffened plates, two primary modes of their global and local bucklings are treated independently. Moreover, for cylindrical shells, two types of interactive analyses are provided: one-mode analysis with only an asymmetric buckling mode and two-mode analysis with both an asymmetric and an axi-symmetric buckling modes.

Therefore, for given generalized slenderness R and several parameters, the elasto-plastic buckling strength σ_{cr} can be determined as[9]

$$\sigma_{cr} = f^c \sigma_E \tag{1.2.3}$$

where f^c designates the critical value of f when the perfect member buckles elasto-plastically, and is expressed by an explicit function of the critical value k_c of the ratio k. When $k_c = 1$, i.e., $f^c = 1$, Eq. (1.2.3) of course leads to the elastic Euler strength σ_E.

1.2.2 Postbuckling path

It is well known that the plated members generally have the stable postbuckling strength in the elastic range[12,13]. However, an exact prediction of such significant post-bifurcation equilibrium path in the closed form is extremely difficult in the elasto-plastic range as well as in the elastic range. Herein, a modification of the von Kármán's equations will result in the following path[7,10]

$$\sigma = \sigma_{cr} - C_s w + C_p w^2 \qquad (1.2.4)$$

where C_s and C_p designates coefficients depending on the generalized slenderness R, the critical elastic factor k_c and the secant modulus defined by $E_s = \sigma / \varepsilon$ in Eq. (1.2.1). If C_s=0 and C_p=0 as in the case of columns, Eq. (1.2.4) becomes a horizontal line $\sigma = \sigma_{cr}$ in the σ-w space, with no postbuckling strength. If C_s=0 and C_p>0 for plated members, the equation leads to a normal stable postbuckling in the parabolic form. Moreover, shell members have an unstable asymmetric postbuckling when C_s>0 and C_p=0, using the one-mode analysis. In the case of the shells' two-mode analysis, the initial postbuckling path can be obtained directly from solving two nonlinear equilibrium equations with no consideration of the failure mechanism.

1.2.3 Failure mechanism

Load-carrying capacity of the actual slender members can not be determined by evaluating only the elasto-plastic buckling strength due to the residual stress. It is not only affected by the elasto-plastic postbuckling behavior, but by the initial geometrical imperfection and the plastic failure mechanism[14,15,16].

A pathological plastic failure mechanism curve corresponding to the ultimate state of each member can be defined approximately by

$$\sigma = \sigma_p(w) \quad or \quad w = w_p(\sigma) \qquad (1.2.5)$$

where σ_p and w_p refer to explicit functions derived from the failure mechanism and the interaction criterion adopted; for example, a relationship between axial stress and the corresponding bending moment.

1.2.4 Ultimate strength

Now, consider an **equivalent bifurcation point** as the intersection of the elasto-plastic postbuckling path AC, Eq. (1.2.4), with the plastic failure mechanism curve BCD, Eq. (1.2.5) in **Fig. 1.2.1.** The point is designated as the point C(w^*, σ^*). In a neighborhood of the point C, a pseudo-potential function, V, is assumed to exist so that its equilibrium equation near the point C is[9]

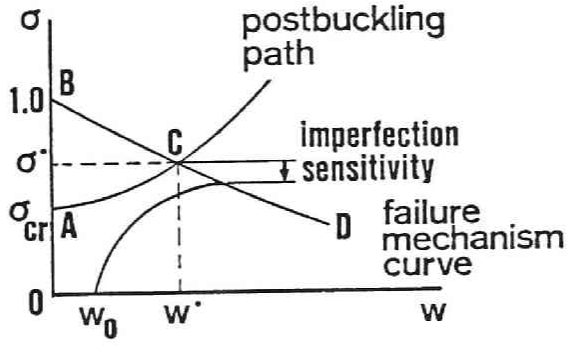

Fig. 1.2.1 Equivalent Bifurcation Point.

$$V' \equiv \frac{\partial V}{\partial w} = g\,\sigma_E w_d - \sigma\,(w_d + w_o) = 0 \tag{1.2.6}$$

where

$$g(w_d) = g^c + \frac{1}{2} g_t'^c w_d \ , \quad w_d = w - w_o - w^*$$

and when $w_o=0$ and $w_d=0$,

$$\sigma^* = g^c \sigma_E \tag{1.2.7}$$

in which, the factors on g are analogous to those on f. However, as shown in **Fig. 1.2.1**, g is evaluated at the equivalent bifurcation point $C(w^*,\sigma^*)$, f is not at the elasto-plastic buckling point $A(0,\sigma_{cr})$. The spatial drawings of the equilibrium surface from Eq. (1.2.6) and its projections to three orthogonal planes are shown in **Fig. 1.2.2.**

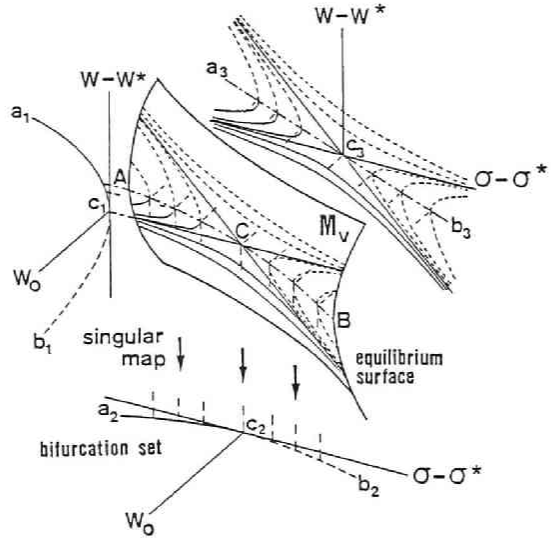

Fig. 1.2.2 Equilibrium Surface and Bifurcation Set.

Then, the ultimate strength σ_m of the general imperfect member can be predicted by the imperfection sensitivity curve. The curve a_2c_2 is regarded as one projecting vertically the set AC of singular points on the equilibrium surface M_V. It takes the form[9]:

$$\frac{\sigma_m}{\sigma^*} = 1 + \alpha^* w_0 - \sqrt{2\,\alpha^* w_0 \left(1 + \frac{1}{2}\,\alpha^* w_0\right)} \tag{1.2.8}$$

where

$$\alpha^* \equiv -\frac{g_t'^c}{g^c}$$

A precise determination of g'^{C}_{t} may be quite difficult, so the factor α^* is approximated by the slope of the plastic unloading curve at the equivalent bifurcation point C:

$$\alpha^* \equiv -\frac{1}{\sigma^*}\frac{d\sigma_p}{dw}\Big|_{(w^*,\sigma^*)} \quad or \quad \alpha^* \equiv -\frac{1}{\sigma^*}\left(\frac{dw_p}{d\sigma}\Big|_{(w^*,\sigma^*)}\right)^{-1} \tag{1.2.9}$$

This asserts that the general nonlinear equilibrium path of the imperfect member may reach the local maximum of the strength on the plastic failure mechanism curve BCD in **Fig. 1.2.1** as if the curve is a set of singular points, AC, in **Fig. 1.2.2.** For column and plate structures, the ultimate strength can be predicted by Eq. (1.2.8). However, for cylindrical shells, the equivalent bifurcation point C is taken to be the normal elasto-plastic bifurcation point A since the point A is unstable itself. Then, the ultimate strength can be obtained in the chapter 3 of this PART.

1.2.5 Modification of imperfection

Furthermore, the equivalent initial imperfection is introduced so as to describe the actual strength behavior of the member concerned

$$w_0^* \equiv \mu(R) w_0 \tag{1.2.10}$$

where

$$\mu(R) \equiv \mu_c \left(\frac{R}{R_p}\right)^{\beta}$$

and R_p refers to the slenderness value R at which the ordinary buckling point changes from elasto-plastic to elastic. The value and the form of μ_c and β can be determined so that the effect of the imperfection w^*_o may diminish for two limits of $R \to 0$ and $R \to \infty$, i.e., for extremely stocky and extremely slender members. Furthermore, this takes into account observations on many previous strength curves in design practice[11,12].

Finally, the imperfection sensitivity on the load-carrying capacity for column and plate members can be determined by Eq. (1.2.8); however, with the slope α^* of Eq. (1.2.9) and the equivalent imperfection w^*_o of Eq. (1.2.10).

1.3. Applicability

The proposed unified approach will be applied to the strength prediction for such axially compressed members as columns, rectangular plates, rectangular stiffened plates and cylindrical shells, and its flow chart is illustrated in **Fig. 1.3.1. Table 1.3.1** summarizes applicability of the approach to such structures.

In this table, the generalized stress σ is taken to be the average axial stress, which is non-dimensionalized by the yielding stress of the material. Also, the generalized displacement w is the magnitude of the assumed buckling mode, non-dimensionalized by the column-span length ℓ of column or the thickness t of plate/shell members.

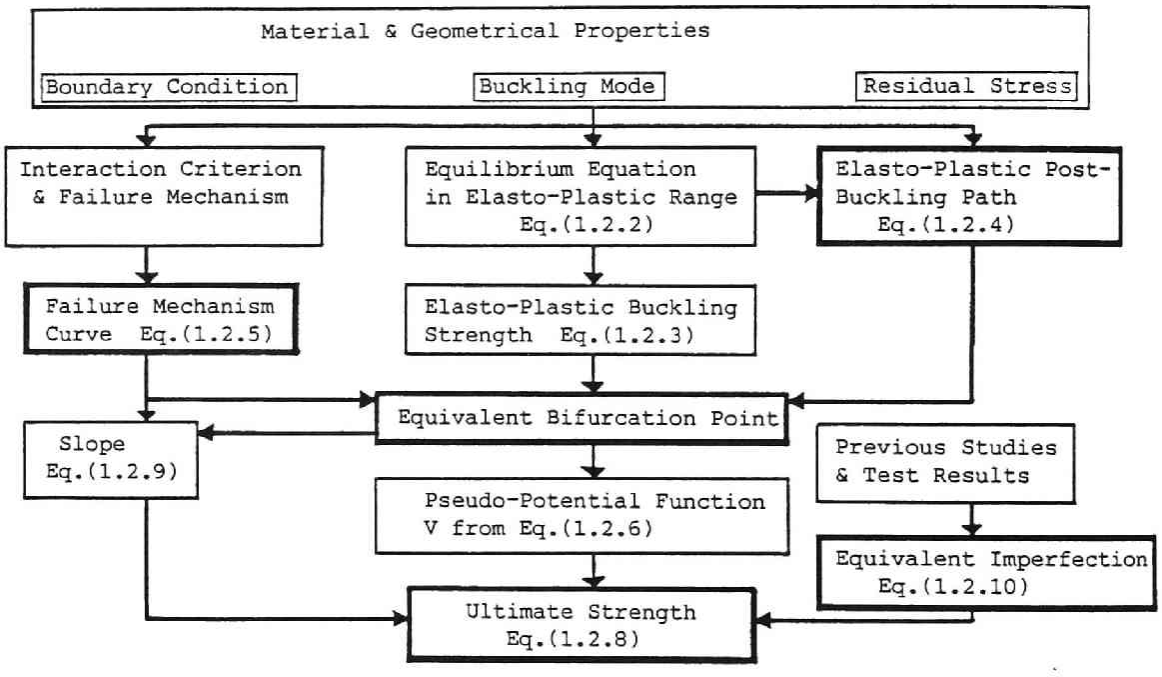

Fig. 1.3.1 Flow Chart of the Proposed Unified Approach to Elasto-Plastic Ultimate Strength.

Table 1.3.1 Applications of the Present Approach to Structural Members.

	COLUMN (Weak Axis)	PLATE PANEL & ST. PLATE	SHELL 1-MODE	SHELL 2-MODE
APPLIED LOAD	axial compression			
GENERALIZED STRENGTH σ	$\frac{\bar{\sigma}}{\sigma_Y}$ ($\bar{\sigma}$: average axial stress, σ_Y yielding stress)			
GENERALIZED DISPLACEMENT w	w/ ℓ ℓ: column length	w/t t : plate-thickness		t : shell-thickness
EULER BUCKLING STRENGTH σ_E	R: generalized slenderness ratio	$\frac{1}{R^2}$ R: generalized width-thickness ratio		R: generalized radius-thickness ratio
ELASTO-PLASTIC BUCKLING STRENGTH $\sigma_{cr} = f^c\sigma_E$, f^c	$(k_c)^3$	$\sqrt{k_c}$	asymmetric $\frac{\sqrt{k_c+1}}{2}\sqrt{\frac{E_s}{E}}$	+ axi-symmetric $\sqrt{k_c}\sqrt{\frac{E_s}{E}}$
POSTBUCKLING PATH	no postbuckling $\sigma = \sigma_{cr}$	stable parabola $\sigma = \sigma_{cr} + c_p w^2$	asym. line $\sigma = \sigma_{cr} - c_s w$	solutions of equilibrium in 2-mode analysis
FAILURE CONDITION	$m=c_2(1-\sigma)\{2-c_2'(1-\sigma)\}$	$m + \sigma^2 = 1$	———	
FAILURE MECHANISM CURVE	$w=A_p'\frac{1-\sigma}{\sigma}\{2-c_2'(1-\sigma)\}$	$w=A_p\frac{1-\sigma^2}{\sigma}$	———	
SLOPE α^*	$\frac{A_p'\sigma^*}{2-c_2'(1-\sigma^*)}$	$\frac{\sigma^*}{A_p(1+\sigma^{*2})}$	* shell; direct evaluation from pseudo-potential	
INITIAL DEFLECTION w_o	JSHB: $\ell/1000$	JSHB: b/150 , a/1000 b: width, a: length	ECCS: $\ell_r/100$ ℓ_r: gauge length	
MODIFICATION $\mu(R)=\mu_c(\frac{R}{R_p})^\beta$	$\mu_c = \frac{1}{2}$	$\mu_c \frac{1}{8}$	μ_c 1	
	$\beta = 2(1 - \frac{R}{R_p})$			

Table 1.4.1 Buckling Parameters for Numerical Demonstrations of Compreesed Steel Columns.

	$\delta \equiv \frac{A_w}{A_f}$	$\frac{\sigma_{Yw}}{\sigma_Y}$	Res. Stress	Initial Def. w_o/l	R_p	Strength Curves Parabolic Residual Stress	Strength Curves Triangular Residual Stress
Strong-Axis	0.5	1.0	0.2	1/1000	1.118	Fig. 1.4.3	Fig. 1.4.4
	1.0					Fig. 1.4.5	Fig. 1.4.6
Weak-Axis	0.5	1.0	0.4		1.291	Fig. 1.4.7	Fig. 1.4.8
	1.0					Fig. 1.4.9	Fig. 1.4.10

Furthermore, two interaction criteria are adopted herein, and their corresponding plastic failure mechanism curves are obtained respectively in the table. Herein, m designates the bending moment along the fold-line of the failure mechanism considered. Given a coefficient A_p for each member, the slopes α^* can be explicitly at the equivalent bifurcation point $C(w^*, \sigma^*)$ for column and plate members. Whereas, for cylindrical shells, the slope can be determined directly from evaluating the elasto-plastic postbuckling equilibrium near the elasto-plastic bifurcation point being equal to the equivalent bifurcation point.

Finally, the factor β is identically taken to be a linear form of the generalized slenderness R without regard to a type of members. While, the form μ_c is explicitly provided in the table. It must be stated that proposed bifurcation sets of Eq. (1.2.8) are found to have good correlation with several design strength curves and those by many researchers.

1.4 Numerical Illustrations

This chapter provides numerical results of axially compressed steel columns using the proposed approach. Their detailed descriptions have been discussed in references[5-10]. For all computations, the maximum magnitude in compression of each residual stress is restricted to be $0.4\,\sigma_Y$ and $0.2\,\sigma_Y$. Also, each initial deflection is the allowable value of tolerance in the JRA Highway Specifications[19].

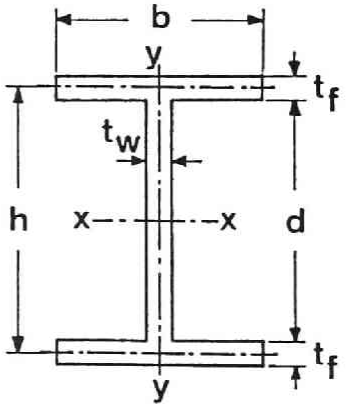

Fig. 1.4.1 I-Sectional Steel Column Model.

Table 1.4.1 summarizes typical values of buckling parameters for numerical computations of axi-symmetric I-sectional steel compressed columns(See, **Fig.1.4.1**). When both the material properties

$$E/\sigma_{Yf}=875,\ \sigma_{Yw}/\sigma_Y=1 \qquad \sigma_Y \text{ and } \sigma_{Yw}: \text{yielding stress of the flange plate and of the web} \tag{1.4.1}$$

remain constant, eight numerical demonstrations will be illustrated in two cases of web-flanges area-ratios δ and two forms of residual stress distributions for two types of strong- and weak-axis bucklings.

The present elasto-plastic load-carrying capacity curves are obtained from the bifurcation sets in Eq. (1.2.8) using Eqs. (1.2.9), and (1.2.10). The results are shown as the relationship between the non-dimensionalized strength on the ordinate and the generalized slenderness ratio on the abscissa. Herein, several strength curves such as the beam-column interaction curve[1,11,12,19,25-27], the Perry-Robertson curve, the JRA Specification basic column strength curve[19] and the ECCS column curves[1,11,12,28-31] are compared with the proposed numerical results. These curves were provided in details as explicit forms in the references[5,6].

Considering these analytical and experimental investigations, the **equivalent imperfection** in Eq. (1.2.10) is taken to be

$$\mu_c = \frac{1}{2} \quad , \quad \beta = 2\left(1 - \frac{R}{R_P}\right) \qquad (1.4.2)^*$$

in which, the form of $\mu(R)$ is also taken into account further test data[34]: **Fig. 1.4.2**(a) shows the column test results reviewed by L.Tall in the CRC and SSRC; **Fig. 1.4.2**(b) provides the envelopes of 112 experimental maximum strength curves when the initial deflections at the center span is prescribed by $w_0/l = 1/1000$.

Figs. 1.4.3 to **1.4.10** shows the numerical demonstrations corresponding to eight column types in **Table 1.4.1.** It is found that the bifurcation sets with the equivalent imperfection give appropriate strength predictions within the intermediate elasto-plastic range of R. So far as the slenderness ratio R and the area-ratio δ are concerned in this dissertation, the present strength curves may be insignificantly affected by the area-ratio δ and the type of residual stress distributions with respect to the strong- and weak-axis. For given slenderness ratios, the proposed strength by Eq. (1.2.8) can be explicitly drawn as the imperfection sensitivity curves. **Figs. 1.4.11** and **1.4.12** illustrate families of imperfection sensitivity curves corresponding to the case of **Figs. 1.4.3** and **1.4.7**, respectively. It is apparently shown that the maximum load-carrying capacity is remarkably sensitive to the initial imperfection within the slenderness ratio R ranging 0.75 to 1.25, including the critical slenderness ratio R_p. Moreover, such sensitivities can be clarified by the following reduction rate of the proposed strength to the **equivalent bifurcation** σ^* as shown in **Figs. 1.4.13** and **1.4.14** for the strong and weak axis. The former is more imperfection-sensitive than the latter, without regard to the invariant forms of the equivalent imperfection.

Through some numerical demonstrations of compressed columns, it was made apparent that the proposed method of approach does not rely on the nonlinear numerical analysis, but is based on the explicit representation of the imperfection sensitivity formula in the light of the catastrophe theory. That is, the unified expression of compressed strength of steel columns can be made in terms of Eq. (1.2.8) using Eqs. (1.2.9) and (1.2.10). In other words, Eq. (1.2.8) presents an explicit representation of the imperfection sensitivity for specified generalized slenderness ratio R.

---

* The generalized slenderness ratio R for columns is chosen as

$$R = \frac{\ell}{\pi r_x}\sqrt{\frac{\sigma_Y}{E}} \quad \text{about strong axis} \quad \text{or} \quad R = \frac{\ell}{\pi r_y}\sqrt{\frac{\sigma_Y}{E}} \quad \text{about weak axis}$$

where r_x and r_y refers to the radius of gyration with respect to the strong and weak axis, respectively.

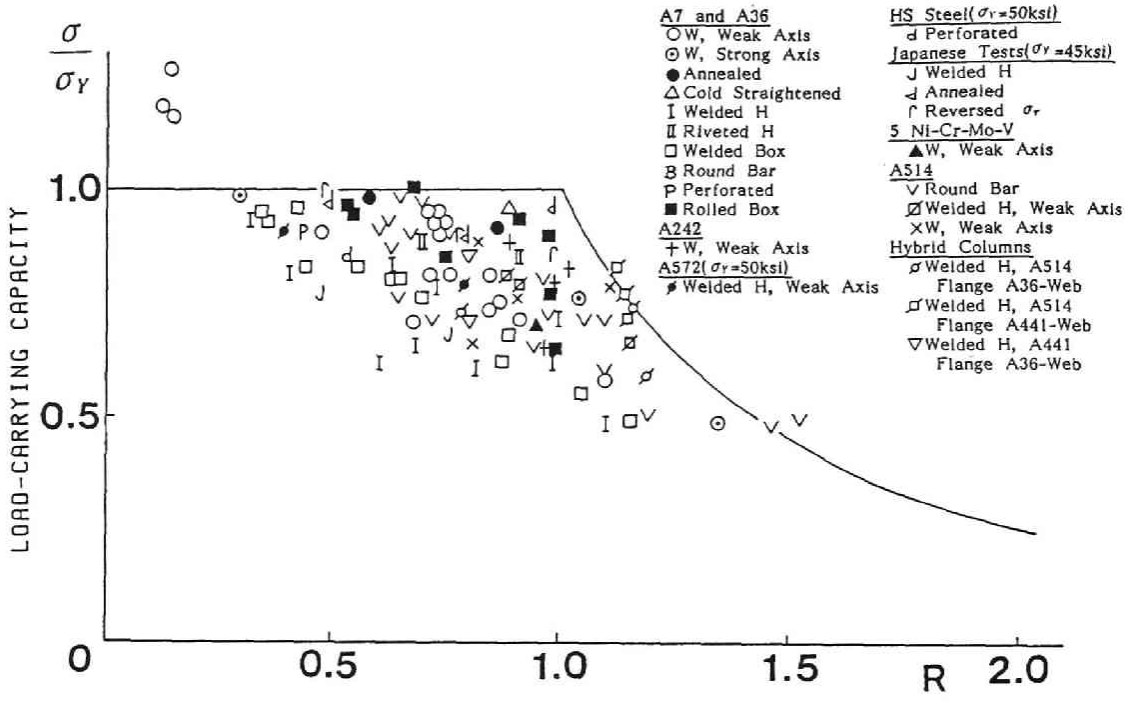

Fig. 1.4.2(a) Column Test Results summarized by L.Tall. [34]

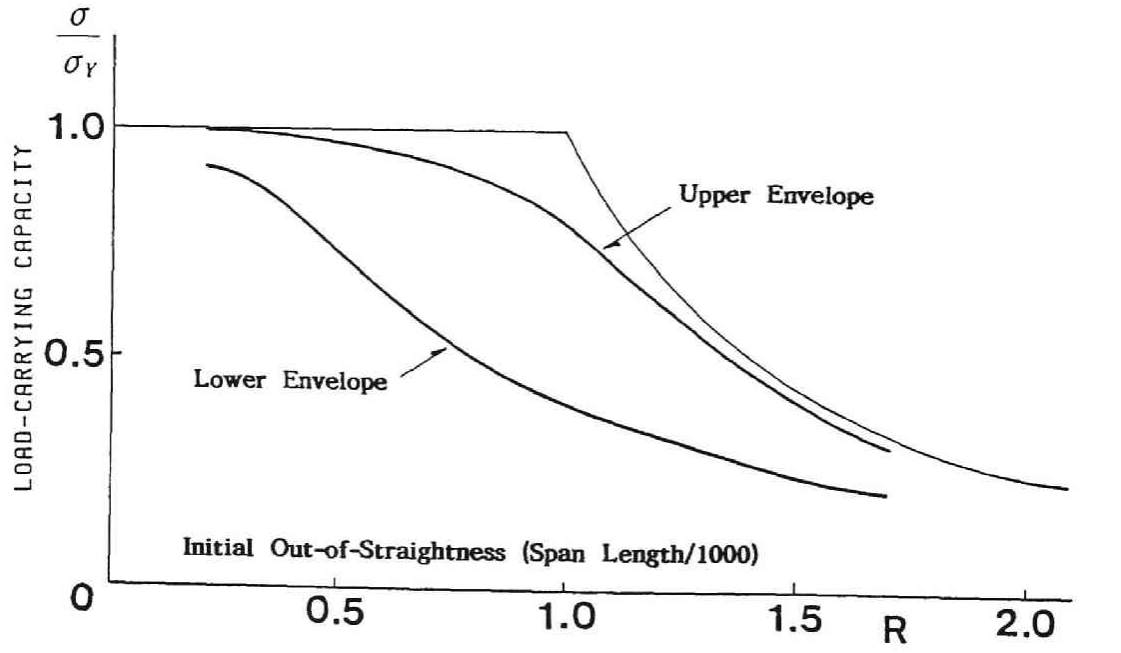

Fig. 1.4.2(b) Envelope of 112 Ultimate Strength Curves. [34]

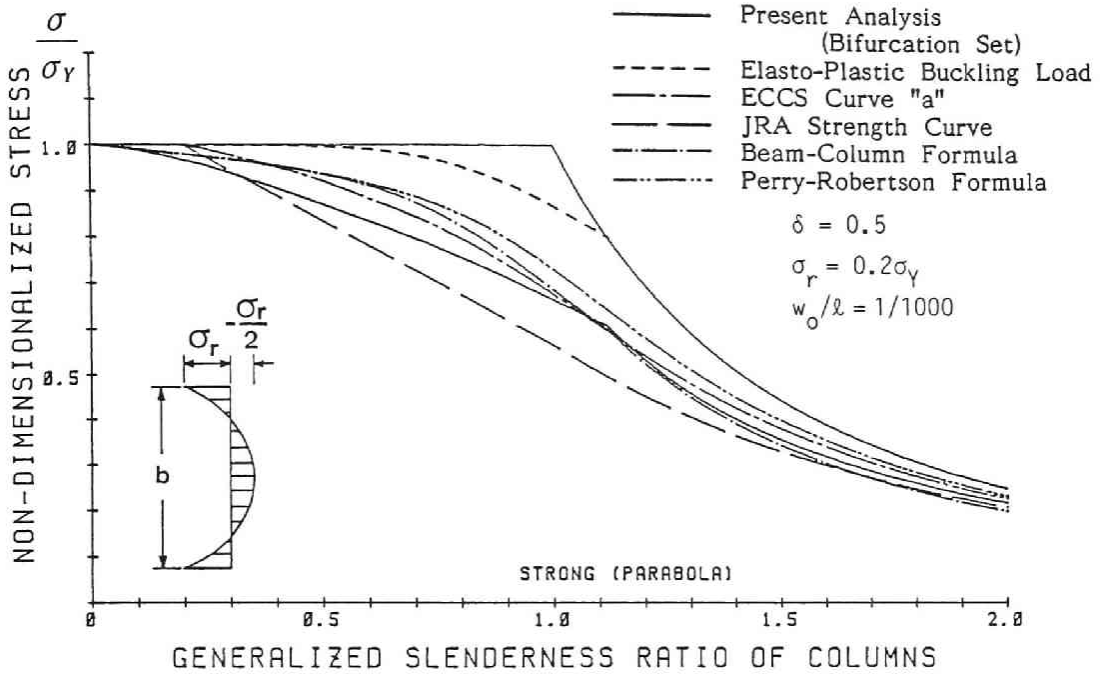

Fig. 1.4.3 Ultimate Strength Curves for the Strong-Axis Buckling of Columns with Parabolic Distribution of Residual Stress.

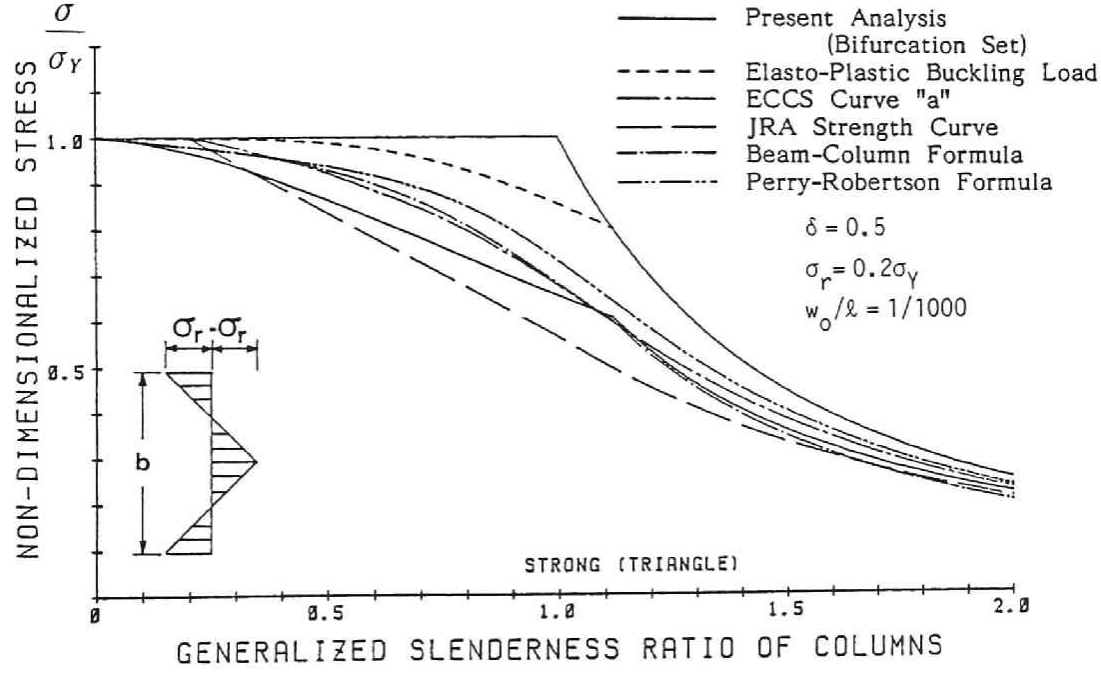

Fig. 1.4.4 Ultimate Strength Curves for the Strong-Axis Buckling of Columns with Triangular Distribution of Residual Stress.

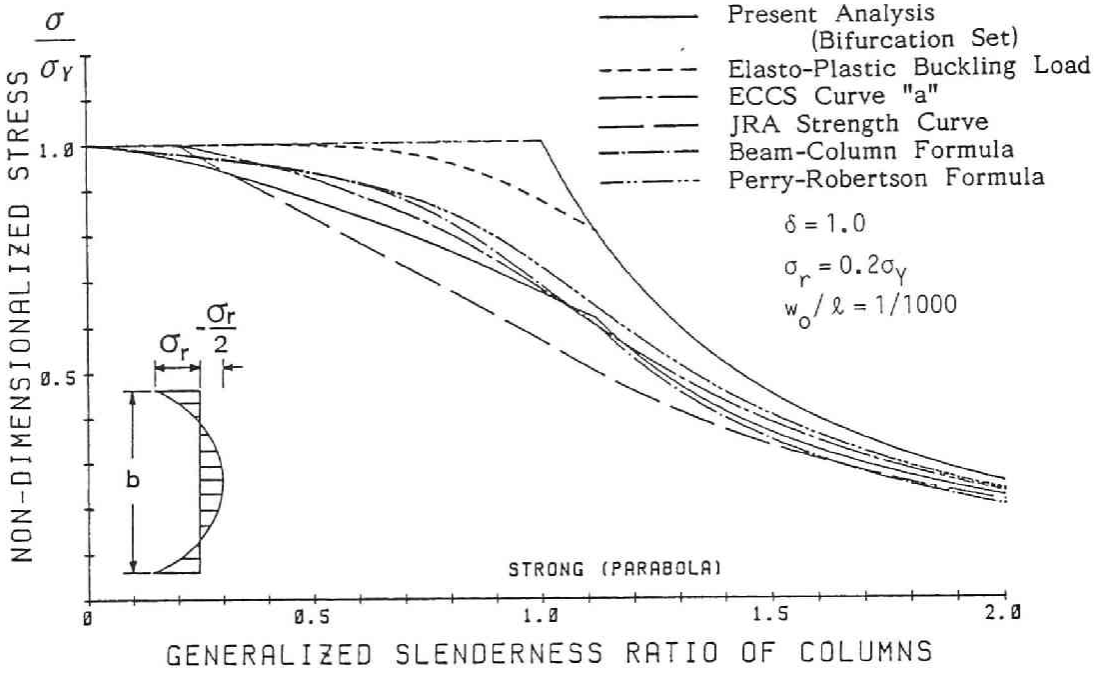

Fig. 1.4.5 **Ultimate Strength Curves for the Strong-Axis Buckling of Columns with Parabolic Distribution of Residual Stress.**

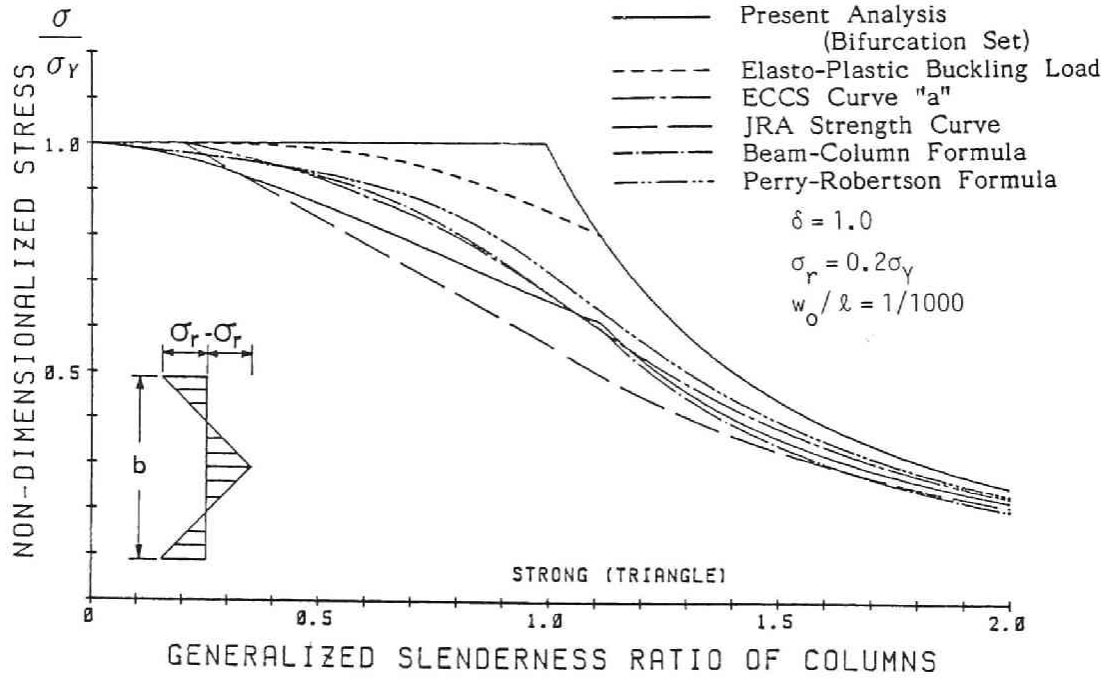

Fig. 1.4.6 **Ultimate Strength Curves for the Strong-Axis Buckling of Columns with Triangular Distribution of Residual Stress.**

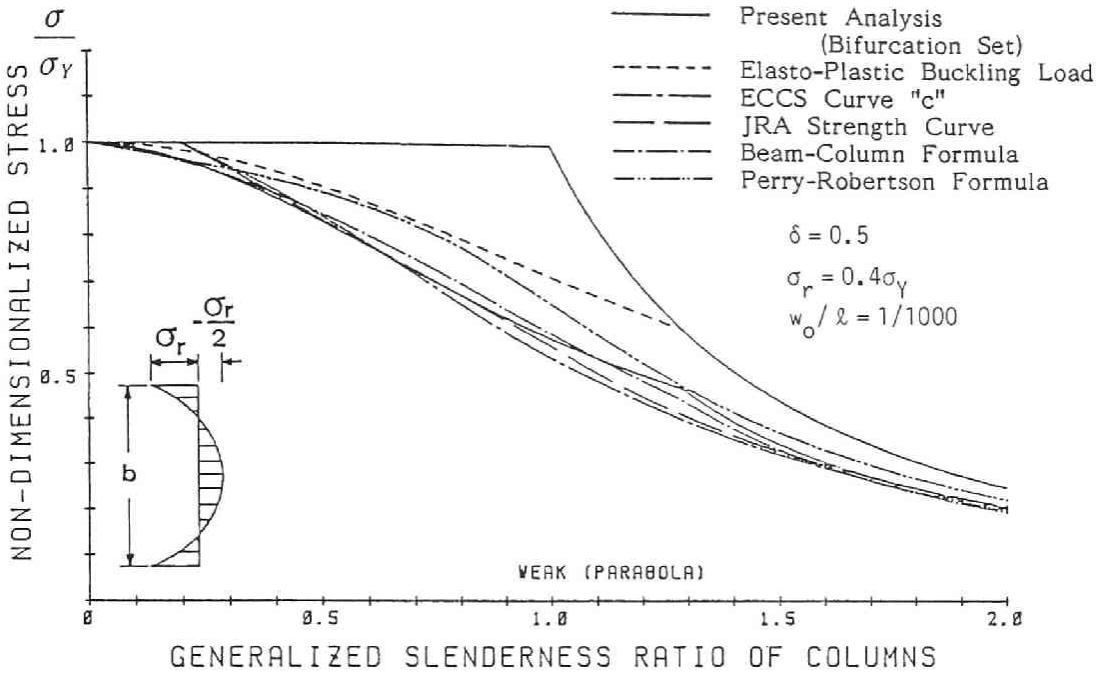

Fig. 1.4.7 **Ultimate Strength Curves for the Weak-Axis Buckling of Columns with Parabolic Distribution of Residual Stress.**

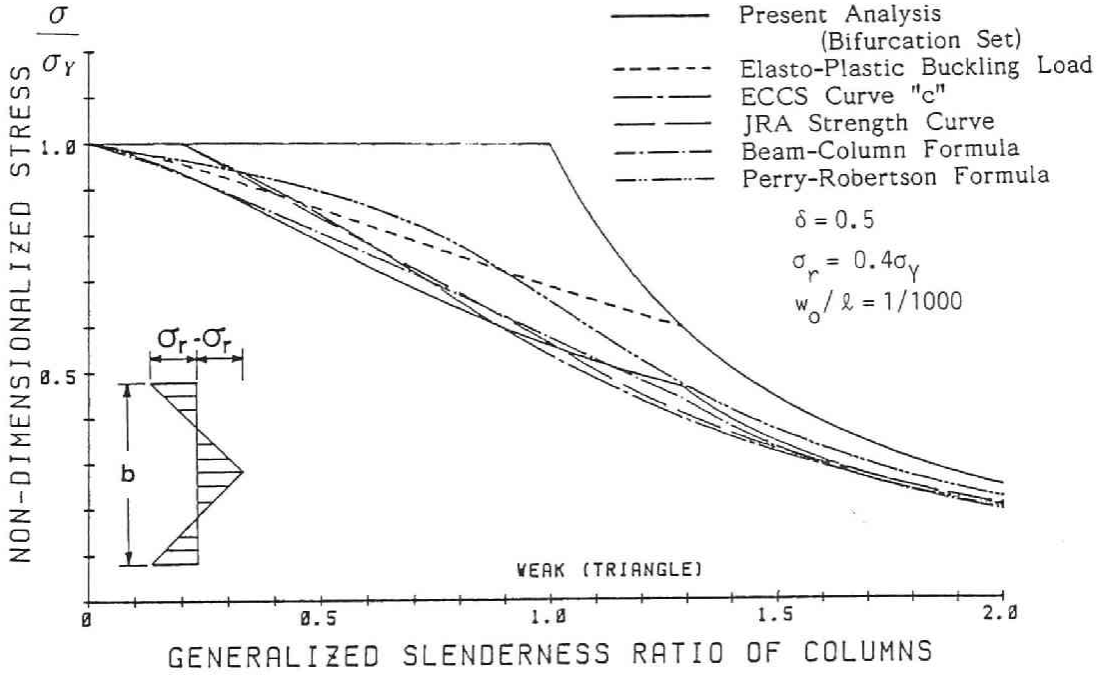

Fig. 1.4.8 **Ultimate Strength Curves for the Weak-Axis Buckling of Columns with Triangular Distribution of Residual Stress.**

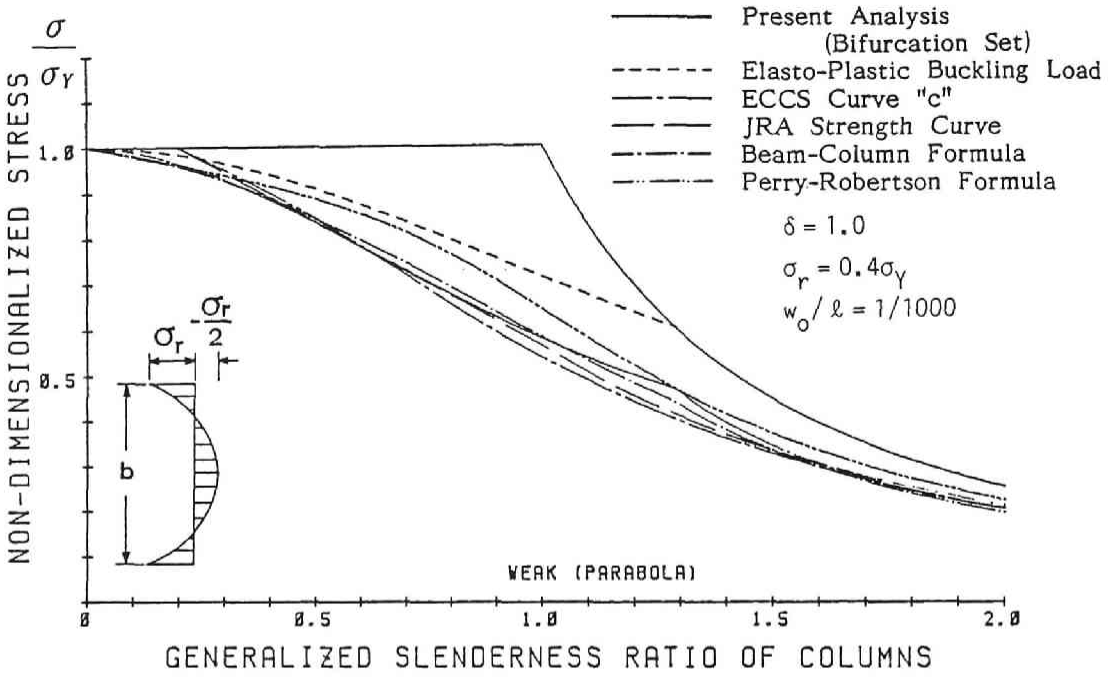

Fig. 1.4.9 Ultimate Strength Curves for the Weak-Axis Buckling of Columns with Parabolic Distribution of Residual Stress.

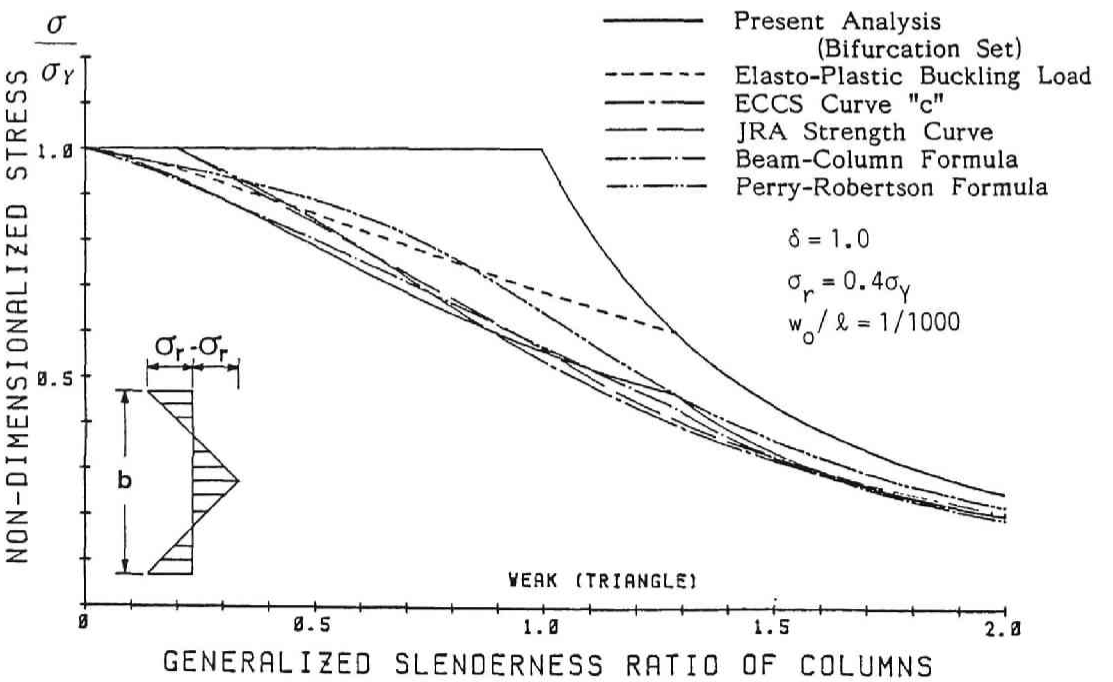

Fig. 1.4.10 Ultimate Strength Curves for the Weak-Axis Buckling of Columns with Triangular Distribution of Residual Stress.

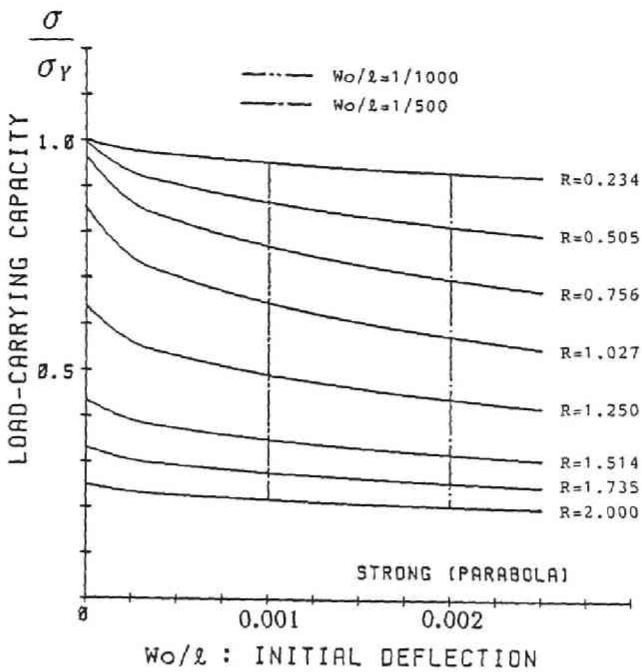

Fig. 1.4.11 Family of Imperfection Sensitivity Curves for Typical Strong-Axis Buckling.

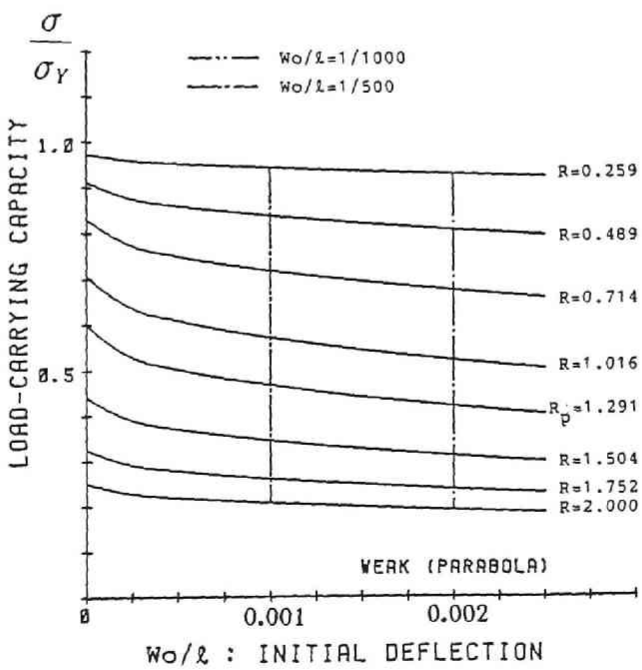

Fig. 1.4.12 Family of Imperfection Sensitivity Curves for Typical Weak-Axis Buckling.

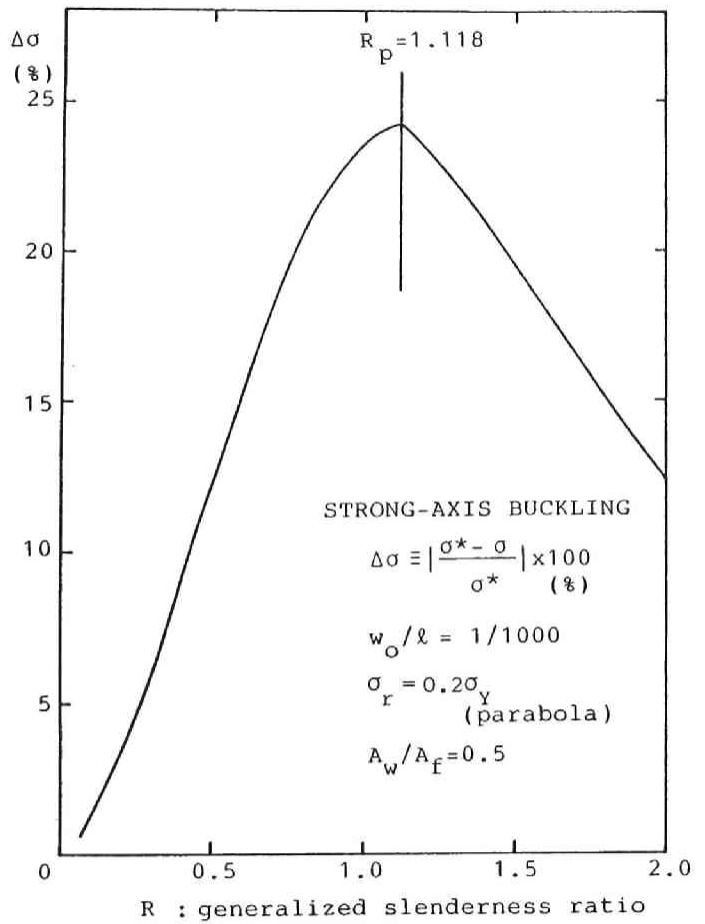

Fig. 1.4.13 Reduction Rate of Ultimate Strength to Equivalent Bifurcation Point for Typical Strong-Axis Buckling.

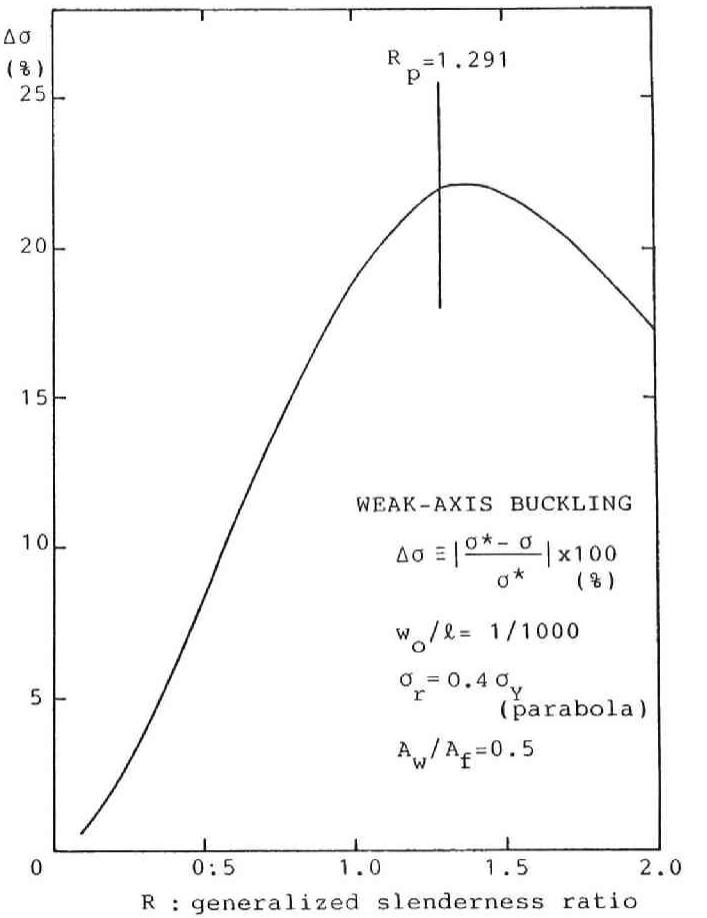

Fig. 1.4.14 Reduction Rate of Ultimate Strength to Equivalent Bifurcation Point for Typical Weak-Axis Buckling.

1.5 Conclusions

This chapter unifies a new simplified approach for evaluation of the strength of slender steel structural members such as columns, plates and shells. The main conclusions are:

(1) The residual stresses and the initial deflections may affect the evaluation of the elasto-plastic buckling stress and the form of the explicit imperfection sensitivity formula, respectively.

(2) The inelastic strength prediction of the members may be explicitly evaluated in terms of the bifurcation sets or the imperfection sensitivity curves.

(3) The bifurcation set can be defined explicitly near the equivalent bifurcation point being the intersection point of the elasto-plastic postbuckling path with the plastic failure mechanism curve for typical members with neutral and stable postbuckling equilibria.

(4) In the case of members with unstable postbuckling equilibria like cylindrical shells, their normal elasto-plastic bifurcation point is taken to be the equivalent bifurcation point. Then, the bifurcation set can be determined from evaluating stability characteristics at the point.

(5) The actual initial geometrical imperfections are modified in the form of the proposed equivalent imperfections. The equivalent imperfection can be determined in a unified form on the basis of the previous strength curves and practical design curves.

(6) All the computations can be easily performed using a small microcomputer.

(7) Several numerical illustrations for axially compressed columns are calculated using appropriate form of the equivalent initial deflections. The results are compared with some design curves and analytical results.

(8) The demonstrations are found to be in good correlation with those by such various investigations and experimental results.

(9) The form of distribution of residual stress assumed herein may insignificantly affect the present results.

(10) The proposed unified approach may be applicable to other types of steel structures such as beams, rigid frames and trusses in civil engineering field.

Bibliographies of Chapter1 in PART III

1) SSRC, IABSE, ECCS, JCRC, FABSE, Stability of Metal Structures. Proceedings of the 3rd International Colloquium on Stability of Metal Structures, Preliminary Report, Centre Technique de la Construction Metallique, Paris, 16-17 Nov., 1983.
2) Rockey, K.C. and H.R. Evans (eds.), The Design of Steel Bridges. Granada Publishing, 1981.

3) Morris, L.J. (ed.), Instability and Plastic Collapse of Steel Structures. Granada Publishing, 1983.
4) Rhodes, J. and J. Spence (eds.), Behaviour of Thin-Walled Structures. Elsevier Applied Science Publishers, 1984.
5) Niwa, Y., E. Watanabe and H. Isami, A new approach to predict the strength of steel columns. Proceedings of Japan Society of Civil Engineers, No. 341, pp. 13-21, 1984.
6) Isami, H., E. Watanabe and Y. Niwa, Strength of I-sectional steel columns predicted by catastrophe theory. Bulletin of Kohchi Technical College, pp. 127-135, 1984 (in Japanese).
7) Niwa, Y., E. Watanabe, H. Isami and Y. Fukumori, A new approach to predict the strength of compressed steel plates. Proceedings of Japan Society of Civil Engineers, No. 341, pp. 23-31, 1984.
8) Niwa, Y., E. Watanabe and S. Suzuki, A new approach to the elasto-plastic lateral buckling strength of beams. Proceedings of Japan Society of Civil Engineers, Structural Engineering/Earthquake Engineering, Vol. 1, No. 1, pp. 41s-49s, 1984.
9) Niwa, Y., E. Watanabe and H. Isami, A unified view of the strength of columns, beams and compressed plates through catastrophe theory. Proceedings of the 3rd International Colloquium on Stability of Metal Structures, Preliminary Report, Centre Technique Industriel de la Construction Metallique, pp. 313-317, 1983.
10) Niwa, Y. E. Watanabe and H. Isami, A new approach to predict the strength of steel stiffened plates. Proceeding of Japan Society of Civil Engineers, Structural Engineering/Earthquake Engineering, Vol. 2, No.2, pp. 281s-290s, 1985.
11) Johnston, B.G., Guide to Stability Design Criterion for Metal Structures, Third Edition. Structural Stability Research Council, John Wiley & Sons, 1976.
12) Allen, H.G. and P.S. Bulson, Background to Buckling, McGraw-Hill, 1980.
13) Timoshenko, S.P. and J.M. Gere, Theory of Elastic Stability, Second Edition. McGraw-Hill, 1961.
14) Horne, M.R. and L.J. Morris, Plastic Design of Low-Rise Frames. Granada Publishing, 1981.
15) Murray, N.W., Introduction to the Theory of Thin-Walled Structures. Oxford University Press, 1984.
16) Korol, R.M. and A.N. Sherbourne, Strength prediction of plates in uniaxial compression. J. Struct. Div., Proc. ASCE, Vol. 98, No. ST9, pp. 1965-1986, 1972.
17) Thompson, J.M.T., Instabilities and Catastrophes in Science and Engineering. John Wiley & Sons, 1982.
18) Thom, R., Structural Stability and Morphogenesis. Benjamin, 1975.
19) Japan Road Association, Specifications of Highway Bridges. 1980.
20) Bradfield, C.D., An evaluation of the elasto-plastic analyses of steel plates loaded by uniaxial in-plane compression. Int. J. Mech. Sci., Vol. 24, pp. 127-146, 1982.
21) Fukumoto, Y., Numerical data bank for the ultimate strength of steel structures. Der Stahlbau, Vol. 51, pp. 21-27, 1982.
22) Komatsu, S., S. Nara and T. Kitada, Elasto-plastic analysis of orthogonally stiffened plates with initial imperfections under uniaxial compression. Computer & Structures, Vol. 11, pp. 429-437, 1980.
23) ECCS, European Recommendations for Steel Construction: Buckling of Shells, 2nd Edition. European Convention for Constructional Steelwork, Publication No. 29, 1983.

24) Niwa, Y., E. Watanabe, H. Isami and N. Taniguchi, An evaluation of elasto-plastic ultimate strength of compressed cylindrical shells. Proceedings of the 40th Annual Meeting of Japan Society of Civil Engineers, I-95, 1985 (in Japanese).
25) Brockenbrough, R.L. and B.G. Johnston, Steel Design Manual. United States Steel Construction, 1968.
26) Tall, L., L.S. Beedle and T.V. Galambos (eds.), Structural Steel Design. Ronald Press, 1964.
27) Trahair, N.S., The Behavior and Design of Steel Structures. Chapman and Hall, 1977.
28) SSRC, ECCS, CRCJ, CMEA, Stability of Metal Structures A World View (Part I). Engineering Journal, AISC, 3rd Quarter, Vol. 18, No.13, 1981.
29) SSRC, ECCS, CRCJ, CMEA, Stability of Metal Structures A World View. Engineering Journal, AISC, 2nd Quarter, Vol. 19, No. 2, 1982.
30) Ito, K. and M. Naruoka, Ultimate strength of centrally compressed structural elements with consideration of their imperfections (translated from the original paper of H. Beer and G. Schulz), Bridge and Foundation Engineering, No. 73-5, pp. 31-40, 1973 (in Japanese).
31) Ito, K. and A. Nishimura, New ECCS column strength curves. Bridge and Foundation Engineering, No. 80-2, pp. 36-39, 1980 (in Japanese).
32) Maquoi, R. and J. Rondal, Analytical formulation of the new European curves. Acier-Stahl-Steel, Vol. 43, pp. 23-28, 1978.
33) Rondal, J. and R. Maquoi, Single equation for SSRC column-strength curves. Journal of the Structural Division, Proc. ASCE, Vol. 105, pp. 247-250, 1979.
34) Tall, L, Centrally compressed members. Axially Compressed Structures: Stability and Strength (ed. R.Narayanan), Applied Science Publishers, pp. 1-40, 1982.

CHAPTER 2

APPLICATIONS TO ELASTO-PLASTIC PLATE STRUCTURES

2.1 General Remarks

The stability and the strength of steel plates and stiffened plates in the elasto-plastic range have been one of the subjects of the greatest concern of civil engineers[1-4]. They are being used for such members as plate and box girders, chords of trusses and arches, bridge piers and towers. Each member is known to buckle locally and may fail prematurely before reaching the yielding point. However, they do not generally fail by the elastic buckling strength but have significant reservation of the postbuckling strength. This is known as one of the major differences between plates and bars.

The early attempts of the elasto-plastic buckling analysis of plates have been seemingly made by Bijlaard, Ilyushin, Stowell, Pearson and Bleich[5-8]. They have derived the fundamental differential equations of the plates, and obtained explicitly the closed-form solutions under various edge conditions and various loading conditions. These classical methods of approach are summarized by Okumura et al.[9].

Recently, in both the elastic and inelastic ranges, the prime research interests are shifting to the evaluation of the elasto-plastic strengths of imperfect plates with different width-thickness ratios by means of discretization methods and the procedures of solving sets of nonlinear simultaneous equations[10-23].

This chapter especially concentrates on the problems of ultimate strength of stiffened plates: Several theoretical and numerical procedures have been proposed so far on problems of the initial buckling, the postbuckling and the ultimate strength of stiffened plates[24]. They can be classified with respect to the method of approach: firstly, the orthotropic plate approach; secondly, the beam-column analysis using the concept of the "effective width"; thirdly, discretization methods such as finite strip method, finite difference method, finite element adopting the incremental energy-approach; and, finally, the nonlinear bifurcation approach based on the hypoelasticity and the topological considerations.

The first or orthotropic approach for stiffened plates was initiated by Huffington et al.[25]. They determined four orthogonal rigidities of **equivalent** elastic homogeneous orthotropic plates. Improvements of the procedure for flat plates in the inelastic region beyond elastic limit were made by Stowell[26] and Bleich [27] using some reduction factors of orthogonal rigidities. Attempts have been made to evaluate the elasto-plastic buckling stress of stiffened plates. Mikami et al.[24] studied the inelastic buckling stress of continuous orthogonal stiffened plates through the Bleich's factors.

The second beam-column approach have been developed by Faulkner[28], Little [29], Carlsen[30], Horne et al.[31] and Rhodes[21]. They derived fundamental relationships between the average axial stress and the corresponding strain in the theoretical and numerical form, and compared the results with available experimental results. Also, Moolani et al.[32] discussed on the parametric study of the behavior of eccentrically stiffened plates.

The third approach of discretization is now being widely accepted as reasonably accurate. The early researches in Japanese civil engineering field on the numerical elasto-plastic buckling stress of stiffened plates were accomplished by Usami[33], Hasegawa et al.[34] and Yoshida et al.[35] using finite strip methods. Furthermore, the large-deflection elasto-plastic analyses of compressed stiffened plates have been developed by many researchers in the world such as Crisfield [11], Komatsu et al.[36], Marchesi[37] and Webb et al.[38] through finite element methods and finite difference methods in order to solve the relevant nonlinear simultaneous equations.

The final group of approach is based on the concept of nonlinear bifurcation. Tvergaard et al.[17,39] investigated the elasto-plastic bifurcation behavior, the initial postbuckling behavior and the imperfection sensitivity of eccentrically stiffened plates. They employed an incremental linearized Rayleigh-Ritz method for the stiffened plates regarding as hypoelastic plates neglecting the effect of elastic unloading. They also discussed the stability and the imperfection sensitivity of the elastic simultaneous interaction among the global buckling of the panels as a wide Euler column and the local buckling of the plates between the stiffeners[40]. Some powerful contributions on such interaction problems of stiffened plates have been also provided by Koiter[41] and van der Neut[42].

These theoretical and numerical analyses allow for the maximum ultimate strength of stiffened plate models to be determined in an isolated form for a selected set of geometrical and material parameters.

Niwa, Watanabe and Isami have proposed a new simplified approach to evaluate the ultimate strength of slender steel structures such as columns, beam-columns and unstiffened plates in the elasto-plastic range[43-49]. The approach does not require a nonlinear process of simultaneous equations concerned, and means a simplified prediction of the imperfection sensitivity of structures in view of the singular bifurcation set through the catastrophe theory. This chapter formulates the procedure for the elasto-plastic strength of compressed rectangular plates with longitudinal stiffeners. Both their global and local bucklings are taken into account herein.

Other applications of the approach to compressed plates are discussed and demonstrated in detail[44,48,49]. Especially, this chapter also provides comparative investigations of the present procedure in the case of both unstiffened and stiffened plates.

2.2 Basic Formulations

2.2.1 Residual stress distributions

A rectangular stiffened plate with four edges simply supported under uniaxial compression as shown in **Fig. 2.2.1** is analyzed as a typical basic model. The stiffened plate has only several longitudinal stiffeners with equal area and equal flexural rigidity arranged in certain equal distance. The residual stress is assumed to be distributed in an appropriate form in the local plate panel, with the magnitude σ_r and σ_{rt} in compression and tension, respectively, and to be uniform in the stiffener cross section with the magnitude σ_{rs} in tension.

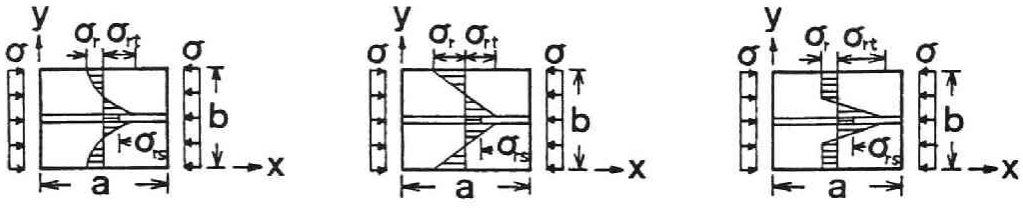

Fig. 2.2.1 Distributions of Residual Stresses of Compressed Rectangular Stiffened Plates.
(a) Parabola (b) Triangle (c) Trapezoid

In view of the self-equilibrium of the residual stress distribution over the entire stiffened plate, the equivalent tensile residual stress $\overline{\sigma}_{rs}$ may be assumed to be distributed uniformly in the global orthotropic plate in addition to the residual stress distribution of the plate panel alone. Hence, the magnitudes of σ_r and σ_{rt} can be replaced for the corresponding "prime" value, respectively:

$$\sigma'_r=\sigma_r-\overline{\sigma}_{rs} \text{ and } \sigma'_{rt}=\sigma_{rt}+\overline{\sigma}_{rs} \tag{2.2.1}$$

where

$$\overline{\sigma}_{rs}\equiv\frac{N\delta}{1+N\delta}\,\sigma_{rs}$$

and δ refers to the ratio of a stiffener area A_s to the plate panel area bt, and N denotes the number of stiffeners defined below. The relationship between σ'_r and σ'_{rt} can be determined from the initial self-equilibrium condition of each distribution of residual stress.

The distribution of residual stress with the maximum compressive stress σ_r is assumed to be in either parabolic, triangular or trapezoidal form as shown in **Figs. 2.2.1**(a)-(c)[43,44,47]. The relationships among the tangent modulus E_t, the secant modulus E_s, the average axial strain ε and the average axial stress σ can be obtained as:

$$E_t\equiv\frac{d\sigma}{d\varepsilon}=kE \text{ and } E_s\equiv\frac{\sigma}{\varepsilon} \tag{2.2.2a}$$

and for parabolic distribution ($0 \le k \le 1$),

$$\sigma=\sigma_Y-(3-2k)k^2\sigma'_r$$
$$\varepsilon=\frac{1}{E}[\sigma_Y+3(1-k)^2\sigma'_r-\sigma'_r] \tag{2.2.2b}$$

for triangle distribution ($0 \le k \le 1$),

$$\sigma=\sigma_Y-k^2\sigma'_r$$
$$\varepsilon=\frac{1}{E}[\sigma_Y-(2k-1)\sigma'_r] \tag{2.2.2c}$$

and, for trapezoidal distribution ($0 \le k \le \frac{2\sigma_r'}{\sigma_r'+\sigma_Y}$)

$$\sigma=\sigma_Y-k^2\frac{(\sigma_r'+\sigma_Y)^2}{4\sigma_r'}$$

$$\varepsilon=\frac{1}{E}\left[2\sigma_Y-k\frac{(\sigma_r'+\sigma_Y)^2}{2\sigma_r'}\right] \qquad (2.2.2d)$$

where E and σ_Y refers to the Young's modulus and the yielding stress of the material, respectively. Furthermore, k denotes the ratio of the elastic portion of the cross section to the total section of the plate, namely, it indicates the global tangent modulus factor of the orthotropic plate section.

In the case of unstiffened plates, that is, when the cross-sectional ratio δ =0, σ_{rs} =0, analogous equations to Eq. (2.2.2) are obtained for appropriate distribution of residual stress[44].

2.2.2 Elasto-plastic buckling strength

From the boundary condition, the buckling mode and the initial imperfection mode of the equivalent global orthotropic plate are assumed in both elastic and elasto-plastic ranges as follows:

$$W=wY(y)\sin\frac{m\pi x}{a},\quad W_0=w_0Y(y)\sin\frac{m\pi x}{a},\quad Y(y)=\sin\frac{n\pi y}{b} \qquad (2.2.3)$$

for all edges simply supported.

in the coordinate system as shown in **Figs. 2.2.1.** In which, w, w_0, Y(y), m and n designate the magnitude of the total out-of-plane deflection, that of initial out-of-plane deflection, mode of deflection in y-direction, number of the half waves in x- and y-direction, respectively.

Consider the compressed rectangular stiffened plates with N longitudinal stiffeners with stiffener parameters[65]:

$$\delta\equiv\frac{A_s}{bt}\ \text{and}\ \gamma\equiv\frac{EI_s}{bD_e} \qquad (2.2.4)$$

where b, t and D_e refer to the total width, the net thickness and the elastic flexural rigidity of the plate panel, respectively. Also, A_s and I_s denote the cross-sectional area and the moment of inertia of a stiffener, respectively. The torsional rigidity of stiffener itself is not considered in this dissertation. Through the classical orthotropic approach using partial differential equations, the basic equation of equilibrium of the stiffened plate can be written as[24,65]:

$$D_e\nabla_p^4W+\sigma t_0\frac{\partial^2W}{\partial x^2}=0 \qquad (2.2.5)$$

where

$$D_e\equiv\frac{Et^3}{12(1-\nu^2)},\quad t_0\equiv t[1+(N+1)\delta],$$

$$\nabla_p^4 \equiv k_1 \frac{\partial^4}{\partial x^4} + 2(k_2 + 2k_4) \frac{\partial^4}{\partial x^2 \partial y^2} + k_3 \frac{\partial^4}{\partial y^4}$$

in which, ν, t_0 and k_j (j=1,2,3,4) refer to the Poisson's ratio, the equivalent thickness and the constants to designate flexural and torsional rigidities of the orthotropic plate in the elasto-plastic range.

Upon substitution of W in Eq. (2.2.3) into Eq. (2.2.5) and through the Galerkin's method, the critical stress σ_{cr} can be defined in the following form [44,47]:

$$\sigma_{cr} = \frac{D_e \int_0^b Y Y_1 dy}{t_0 \int_0^b \left(\frac{m\pi}{a}\right)^2 Y^2 dy} \tag{2.2.6}$$

where

$$Y_1(y) \equiv k_1 \left(\frac{m\pi}{a}\right)^4 Y(y) - 2(k_2 + 2k_4) \left(\frac{m\pi}{a}\right)^2 \frac{d^2 Y}{dy^2} + k_3 \frac{d^4 Y}{dy^4}$$

The buckling coefficient K_s can be given by

$$K_s = \frac{\sigma_{cr}}{\sigma_0} \tag{2.2.7}$$

where

$$\sigma_0 \equiv \frac{\pi^2 D_e}{b^2 t}$$

thus, K_s can be obtained as

$$K_s \equiv \frac{\left(\frac{n\phi}{m}\right)^2}{1 + (N+1)\delta} \left[k_1 \left(\frac{m}{n\phi}\right)^4 + 2(k_2 + 2k_4) \left(\frac{m}{n\phi}\right)^2 + k_3 \right] \tag{2.2.8}$$

where

$$\phi \equiv \frac{a}{b} : \text{aspect ratio}$$

Let us define a factor f by

$$f = \frac{K_s}{K_{SE}} \tag{2.2.9}$$

where K_{SE} refers to the minimum elastic buckling coefficient. Thus,

$$f = \frac{\sigma_{cr}}{\sigma_0} \frac{1}{K_{SE}} = \frac{\sigma_{cr}}{\sigma_E} \tag{2.2.10}$$

where

$$\sigma_E \equiv K_{SE}\sigma_0 = K_{SE}\frac{\pi^2 D_e}{b^2 t}$$

$$K_{SE} \equiv \frac{2[1+\sqrt{1+(N+1)\gamma}\,]}{1+(N+1)\delta}$$

that is, σ_E refers to the elastic Euler buckling stress for the global buckling of the stiffened plate.

Then, the non-dimensionalized equation of equilibrium in the elasto-plastic range can be written as[44,47]:

$$f\tilde{\sigma}_E\tilde{w} - \tilde{\sigma}\tilde{w} = 0 \qquad (2.2.11)$$

where

$$\tilde{\sigma}_E \equiv \frac{\sigma_E}{\sigma_Y} = \frac{1}{R_{SE}^2},\quad \tilde{w} \equiv \frac{w}{t},\quad \tilde{\sigma} \equiv \frac{\sigma}{\sigma_Y},\quad R_{SE} \equiv \frac{b}{t}\sqrt{\frac{12(1-\nu^2)}{\pi^2 K_{SE}}\frac{\sigma_Y}{E}}$$

in which, the symbol "$\sim$" designates the non-dimensionalization in terms of the yielding strength σ_Y and the thickness t for the stress and the displacement, respectively. R_{SE} and K_{SE} refer to the generalized width-thickness ratio for the buckling of the global stiffened plate and the corresponding elastic buckling coefficient, respectively.

In this chapter, however, numerical examples are demonstrated using only the Bleich's approach[27] to evaluate the elasto-plastic buckling stress. Therefore, using the Bleich's factor τ, the coefficients k_j in Eq. (2.2.5) are defined in the elasto-plastic range as follows[24-28]:

$$k_1 \equiv \tau[1+(N+1)\gamma],\quad k_2 \equiv \nu\sqrt{\tau},\quad k_3 \equiv 1,\quad k_4 \equiv \frac{1-\nu}{2}\sqrt{\tau} \qquad (2.2.12)$$

In order to take into account the effects of residual stress on the elasto-plastic buckling stress, the factor τ is set to be equal to the tangent modulus k in Eq. (2.2.2). Upon substitution of Eq. (2.2.12) into Eqs. (2.2.8) and (2.2.9), the factor f can be obtained by

$$f = \frac{1}{[1+(N+1)\delta]n^2 K_{SE}}\left\{\left[\sqrt{k_c}\sqrt{1+(N+1)\gamma}\left(\frac{m}{\phi}\right) - n^2\left(\frac{\phi}{m}\right)\right]^2 + 2n^2\sqrt{k_c}\,[1+\sqrt{1+(N+1)\gamma}\,]\right\} \qquad (2.2.13)$$

where k_c refers to the value of the factor k in Eq. (2.2.2) at the elasto-plastic buckling point. **Table 2.2.1** provides several possible classical expressions for the factor f, based on the methods by Bleich, Chwalla, Stowell, Bijlaard and Pearson for compressed plates. In this dissertation, numerical examples are demonstrated using only Bleich's method so as to evaluate the elasto-plastic buckling stress as stated above.

Table 2.2.1 Comparison of Buckling Coefficients of Elasto-Plastic Plates.

Type	Theory	Buckling Coefficient: K K = f K_E	Comments
Elastic	Hooke	4	
Plastic	Bleich	$4\sqrt{\tau}$ *	analogous to elastic
	Chwalla	$4\tau_r$****	
	Stowell	$4\tau_t\left(\frac{1}{2}+\frac{1}{2}\sqrt{\frac{1}{4}+\frac{3}{4}\tau}\right)$**	Deformation Theory
	Bijlaard	$2(1-\nu^2)(\sqrt{k_1 k_3}+k_2+2k_4)$***	
	Pearson	$2\left[1+\frac{1}{2}\sqrt{1+3\tau}\right]$.	Flow Theory

* $\tau \equiv E_t/E$: tangent modulus factor

** $\tau_t \equiv E_s/E$: secant modulus factor

*** $k_1=[1+3(1+e)\tau]/d$, $k_2=[2-(2-4\nu)\tau]/d$, $k_3=4/d$, $k_4=1/d'$; $d \equiv 5-4\nu-(1-2\nu)^2\tau+3e$, $d' \equiv 2+2\nu+3e$, $e \equiv 1/\tau_s-1$, ν: Poisson's ratio

**** $\tau_r \equiv 4\tau/(1+\sqrt{\tau})^2$: reduced modulus factor

Now, by evaluating the minimum value of K_s, the value of f can be obtained simply as

$$f=f^c=\sqrt{k_c} \tag{2.2.14}$$

since, for the elasto-plastic buckling,

$$(K_s)_{\min}\equiv\frac{2\sqrt{k_c}\,[1+\sqrt{1+(N+1)\gamma}\,]}{1+(N+1)\delta} \tag{2.2.15}$$

at

$$n=1 \text{ and } \phi=m\sqrt[4]{k_c[1+(N+1)\gamma]}$$

Thus, using Eqs. (2.2.7), (2.2.8), (2.2.11), (2.2.14) and (2.2.15), the elasto-plastic buckling stress σ_{cr} can be given by

$$\tilde{\sigma}_{cr}=f^c\tilde{\sigma}_E \tag{2.2.16}$$

where

$$\tilde{\sigma}_{cr}\equiv\frac{\sigma_{cr}}{\sigma_Y}$$

It implies that the elasto-plastic buckling stress of the stiffened plates can be expressed in the unified form similar to that of columns, beam-columns and compressed plates. Of course, $\tilde{\sigma}_{cr}=\tilde{\sigma}_E$ with $f^c=1$ and $k_c=1$.

2.2.3 Postbuckling path

The rigorous prediction of the significant postbuckling behavior of stiffened plate in a closed form is entirely difficult even in the elastic range. Thus, for simplicity, a modification on the von Kármán's equations is made in order to evaluate such postbuckling reservation using the analogous orthotropic plate approach. The modified von Kármán's equations for such orthotropic plates in the elasto-plastic range lead to the following postbuckling path[47]:

$$\tilde{\sigma}=\tilde{\sigma}_{cr}+\tilde{C}_p\tilde{w}^2 \tag{2.2.17}$$

at

$$n=1 \text{ and } \phi=m\sqrt[4]{k_c[1+(N+1)\gamma]}$$

where

$$\tilde{C}_p\equiv\frac{3(1-\nu^2)}{4\,K_{SE}}\frac{1}{R_{SE}^2}\frac{E_s}{E}\frac{1+k_c[1+(N+1)\gamma]}{\sqrt{k_c[1+(N+1)\gamma]}},$$

$$R_{SE}=R\sqrt{\frac{K}{K_{SE}}},\quad R\equiv\frac{b}{t}\sqrt{\frac{12(1-\nu^2)}{\pi^2K}\frac{\sigma_Y}{E}},\quad K\equiv4(N+1)^2$$

and R denotes the generalized width-thickness ratio for the local buckling of the plate-panel. It is clear seen that Eq. (2.2.17) provides the elastic postbuckling path if $E_s = E$ and $k_c = 1$.

2.2.4 Ultimate strength

Ultimate strength of the actual stiffened plates can not be determined by evaluating only the elasto-plastic buckling strength. It is further affected by the initial lateral deflection and the plastic unloading curve as well as by both the residual stress and the elasto-plastic postbuckling path. The plastic unloading curve is obtained from the failure mechanism corresponding the ultimate state of the stiffened plate. Many investigations have been performed on the failure mechanism curve in the last two decades. Their mechanism curves for compressed square plates are compared in **Fig. 2.2.2.** Detailed discussions on the plastic unloading curve have been made by Sherbourne, Murray, Fujita and Davies[57-62], but here in this chapter, the following intersection formula is assumed for simplicity between the in-plane axial compressive load and the bending moment[47]. The failure mechanism of the plate under uniaxial pure compression is assumed to consist of fold lines for the global buckling mode as shown in **Fig. 2.2.4.**

$$\bar{\sigma}^2+\bar{m}=1. \tag{2.2.18}$$

where

$$\bar{m}\equiv\frac{M}{M_p}$$

in which M and M_P refers to the bending moment perpendicular to the corresponding fold line and the full plastic moment, respectively. **Fig. 2.2.3** shows a comparison of the interaction curves by many researchers for compressed square plates.

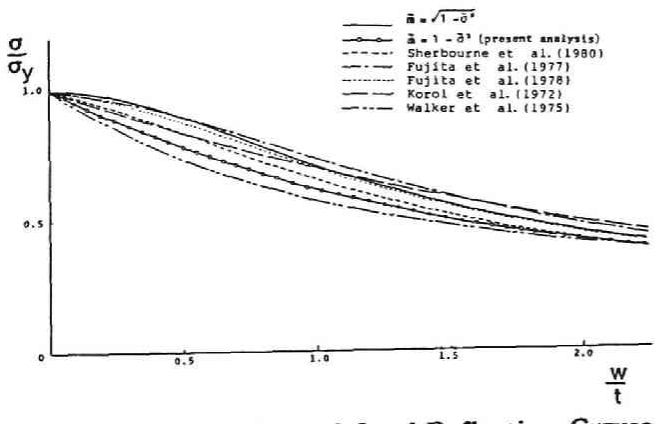

Fig. 2.2.2 **Comparison of Load-Deflection Curves in Plastic Failure Mechanisms of Compressed Square Plates:** $\phi = 1;\ \theta = 45^\circ$.

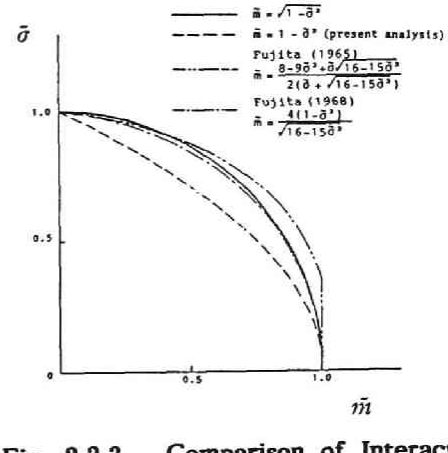

Fig. 2.2.3 **Comparison of Interaction Curves for Compressed Square Plates:** $\phi = 1;\ \theta = 45^\circ$.

Then, for the global buckling mode of the stiffened plate, the plastic unloading curve can be approximately predicted by:

$$\bar{w}=\bar{w}_p\equiv A\frac{1-\bar{\sigma}^2}{\bar{\sigma}} \tag{2.2.19}$$

where, for $\phi^* \equiv \phi/m \geqq \cot\theta$,

$$A=\frac{1}{2}\frac{1+\phi^*\cot\theta+N\delta\dfrac{h_s}{t}}{1+\dfrac{N(N+2)}{N+1}\delta} \quad (N:\text{even})$$

$$A=\frac{1}{2}\frac{1+\phi^*\cot\theta+N\delta\dfrac{h_s}{t}}{1+(N+1)\delta} \quad (N:\text{odd})$$

for $\phi^* < \cot\theta \leqq 1$,

$$A=\frac{1}{2}\frac{1+\phi^*\cot\theta+N\delta\dfrac{h_s}{t}}{2-\phi^*\tan\theta+2N_I\delta+\dfrac{N_{II}(N_{II}+2)}{N+1}\delta\dfrac{\cot\theta}{\phi^*}} \quad (N=N_I+N_{II})$$

in which θ denotes the angle of the yielding fold line as shown in **Fig. 2.2.4**. In the second types in **Fig. 2.2.4**(b), N_I and N_{II} refers to the numbers of longitudinal stiffeners on the fold lines of (I) and (II), respectively. Moreover, h_s designates the height of a stiffener from the surface of the plate panel, and the factor h_s/t can be given as a function of the stiffener parameters.

Now, let us consider the **equivalent bifurcation point** as the intersection of the elasto-plastic postbuckling path, Eq. (2.2.17), with the plastic unloading curve, Eq. (2.2.19). The point can be obtained by solving the following quartic polynomial equation:

$$\tilde{C}_p A^2\tilde{\sigma}^4-\tilde{\sigma}^3-(2\tilde{C}_p A^2-\tilde{\sigma}_{cr})\tilde{\sigma}^2+\tilde{C}_p A^2=0 \qquad (2.2.20)$$

Let $\tilde{\sigma}^*$ and $\tilde{w}^*$ designates a proper real root of the equation and the corresponding deflection calculated by Eq. (2.2.17) or (2.2.19). Hence, the equivalent bifurcation point can be given by the point $C(\tilde{w}^*, \tilde{\sigma}^*)$ in **Fig. 2.2.5.**

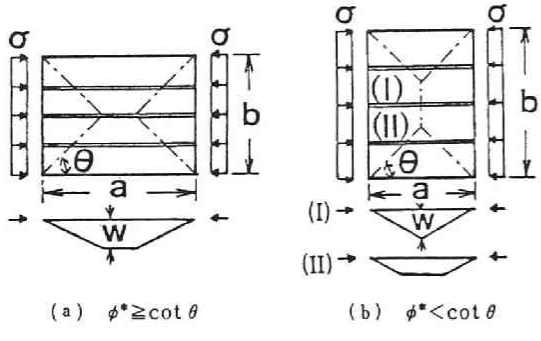

Fig. 2.2.4 **Plastic Fold Lines of Failure Mechanisms for Global Buckling Mode.**

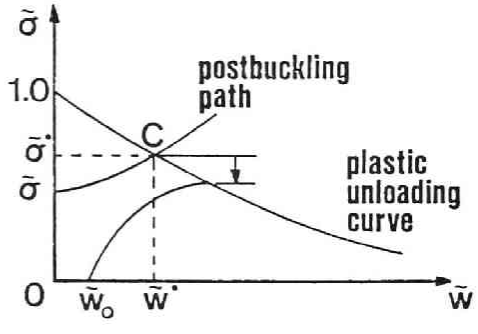

Fig. 2.2.5 **Postbuckling Path and Failure Mechanism Curve.**

In order to evaluate the ultimate strength of the imperfect plate, a pseudo-potential may also be defined near the equivalent bifurcation point C. Then, the ultimate strength $\tilde{\sigma}_m$ of the imperfect stiffened plate can be predicted in terms of the bifurcation set through the catastrophe theory. It can be defined by a set of singular points[43-49]:

$$\frac{\tilde{\sigma}_m}{\tilde{\sigma}^*}=1+\alpha^*\tilde{w}_0-\sqrt{2\,\alpha^*\tilde{w}_0\left(1+\frac{1}{2}\,\alpha^*\tilde{w}_0\right)} \tag{2.2.21}$$

where

$$\tilde{\sigma}_m\equiv\frac{\sigma_m}{\sigma_Y}$$

and α^* can be approximated by the slope of the plastic unloading curve at the equivalent bifurcation point C, that is,

$$\alpha^*=-\frac{1}{\tilde{\sigma}^*}\frac{1}{d\tilde{w}_p/d\tilde{\sigma}}\Bigg|_{\tilde{\sigma}=\tilde{\sigma}^*}=\frac{\tilde{\sigma}^*}{A(1+\tilde{\sigma}^{*2})} \tag{2.2.22}$$

2.2.5 Modification of imperfection

Furthermore, the concept of the **equivalent initial imperfection** is adopted herein in order to describe the actual strength behavior of the plates considered:

$$\tilde{w}_0^*\equiv\mu(R)\tilde{w}_0 \tag{2.2.23}$$

where

$$\mu(R)\equiv\mu_c\left(\frac{R}{R_p}\right)^{\beta}$$

μ_c is a constant specified below, and R_p refers to the value of the generalized width-thickness ratio, R, for the local plate buckling between stiffeners, at which the buckling point changes from the elasto-plastic to purely elastic, and R is alternatively used as the generalized width-thickness ratio R_{SE} for the global stiffened plate buckling.

Explicit forms of μ_c and β will be presented below in the numerical demonstrations with some design curves and the numerical results by many investigators. Their determination takes into reasonable account the unified expression for both unstiffened and stiffened plates. As a result, the form of $\mu(R)$ can be presented to be

$$\mu_c\equiv\frac{1}{8},\quad \beta\equiv 2\left(1-\frac{R}{R_p}\right) \tag{2.2.24}$$

This form has been also applied to a unified formulation of strength prediction for both local and global bucklings of stiffened plates. Finally, the imperfection sensitivity or the load-carrying capacity can be determined by Eq. (2.2.21); however, with the slope α^* of Eq. (2.2.22) and the equivalent imperfection of Eq. (2.2.23) and (2.2.24)[43-49].

On the other hand, the ultimate strength for the local buckling of plate panel between stiffeners may be also evaluated as four edges simply supported rectangular plate with the width spacing stiffeners[44,47].

It is apparently shown that discussions in this section are identically equal to those for unstiffened plates when the stiffener's parameter N=0, δ =0 and γ =0, i.e., $t=t_0$, $R=R_{SE}$ and $K=K_{SE}$[44] for n=1 and $\phi = m\sqrt[4]{k_c}$.

2.3 Compressed Plates

Now, as the first numerical illustrations, let us examine the simply supported plates under uniaxial compression. The type of the distribution of the residual stress considered herein is either of a parabola, a triangle or a trapezoid as shown in **Figs. 2.3.1**(a)-(c), respectively. The magnitude of the maximum compressive residual stress is restricted for practical reason to 0.4 σ_Y, for all types. Also, the magnitude of the initial deflections of the plates considered herein is taken to be whether b/200 or b/150, with consideration of the tolerance of b/150 as allowed by the JRA Specification for Highway Bridges[50], where b represents the width of the loaded edge of the plate.

In order to make a comparison with the present numerical illustrations, the following four types of strength curves are used herein: **Fig. 2.3.2** shows the basic design strength curves adopted in Japan, USA and Europe[1,3,4,50] and several "effective width formula" by von Kármán, Winter, Lind, Yoshiki, Grave Smith, Komatsu and Fukumoto[51,52]; **Fig. 2.3.3** shows the numerical computations by Crisfield, Little, Harding, Dawson and Horne[11-16,20]; **Fig. 2.3.4** provides the typical test data[53], including repetitive loading results by automated microcomputer testing at Kyoto University in 1981-84 with reference to [54-57]; and **Fig. 2.3.5** also shows the design curves by Fokumoto-Itoh data-base approach[64], who summarize a great number of experimental data for buckling steel plates in the world.

The numerical results of plates are illustrated in **Figs. 2.3.6**(a)-(c) for the residual stress distribution of the parabola, the triangle and the trapezoid, respectively. The abscissa indicates the generalized width-thickness ratio ratio R and the ordinate indicates the non-dimensionalized ultimate strength with respect to the yield stress. It must be mentioned that all of the bifurcation sets for the rectangular plates are obtained for such aspect ratio ϕ that the least buckling coefficients are obtained both in the elastic and in the elasto-plastic range, that is, for n=1 and $\phi = m\sqrt[4]{k_c}$. Then, all the calculations are made taking into account the basic ultimate strength formula, the theoretical/numerical results and experimental curves. Therefore, the form of $\mu(R)$ is also given by Eq. (2.2.24), similarly to the case of stiffened plates.

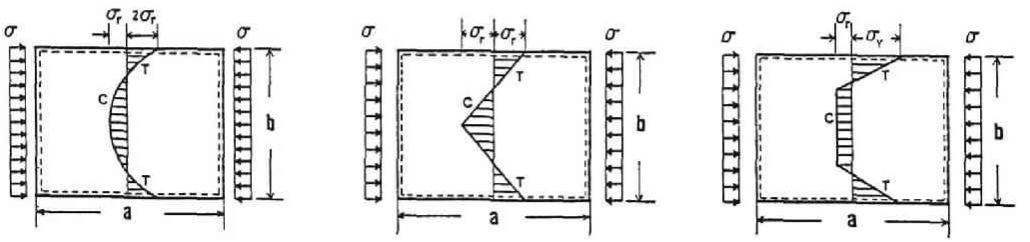

Fig. 2.3.1 Distributions of Residual Stresses of Compressed Rectangular Plates.
(a) Parabola (b) Triangle (c) Trapezoid

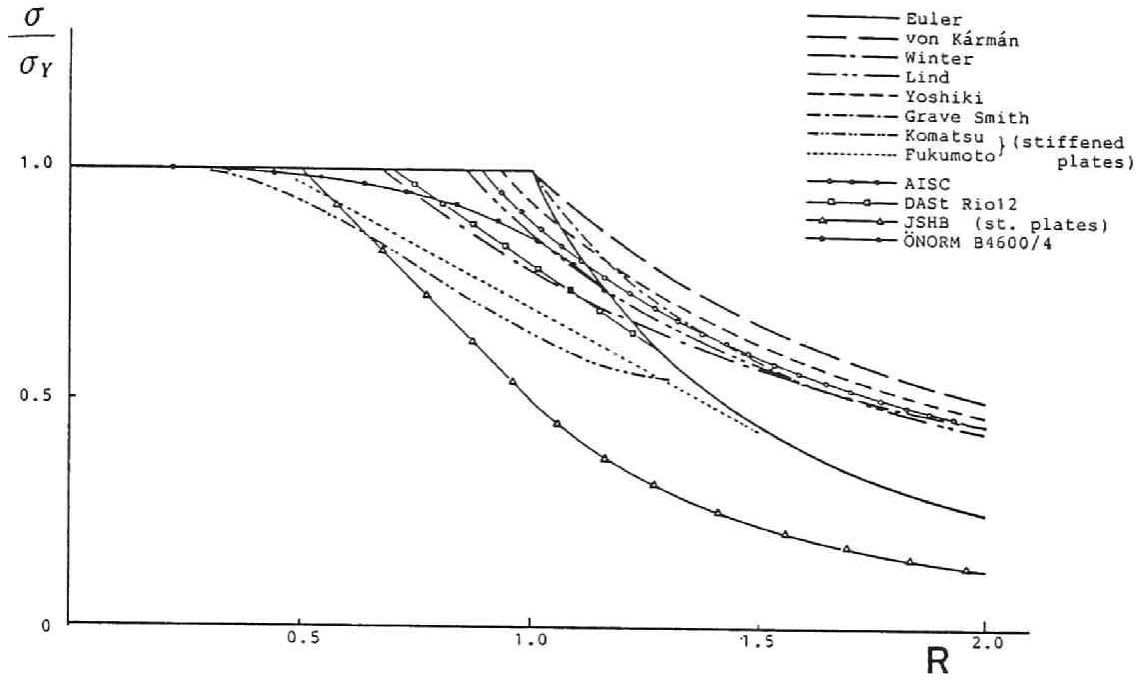

Fig. 2.3.2 Basic Design Strength Curves and Effective Width Formula.

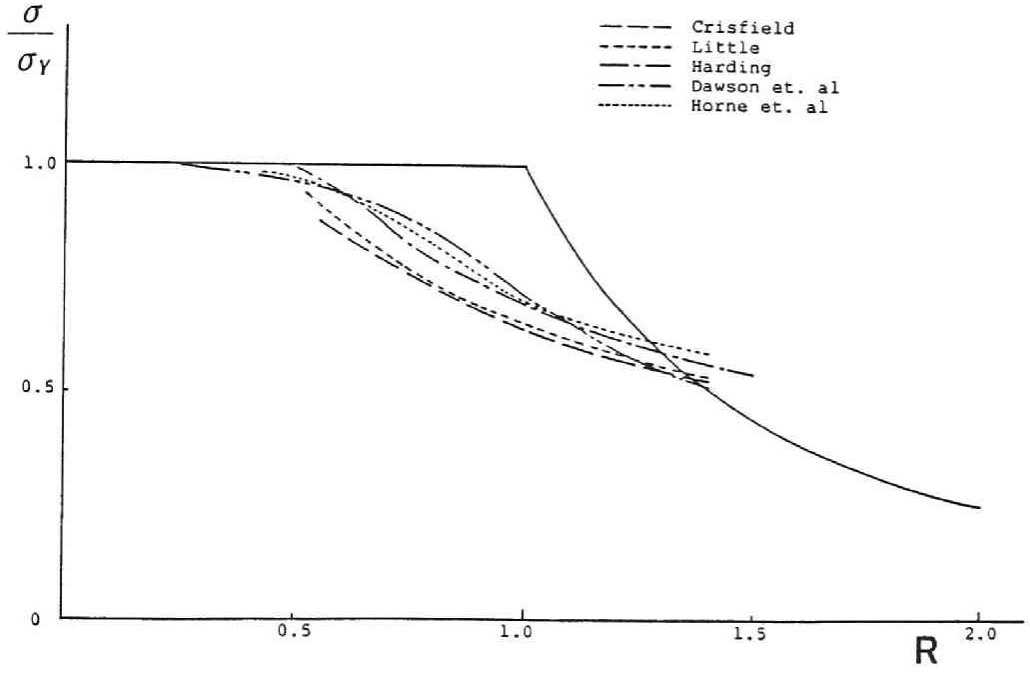

Fig. 2.3.3 Ultimate Strength Curves by Several Numerical Analyses.

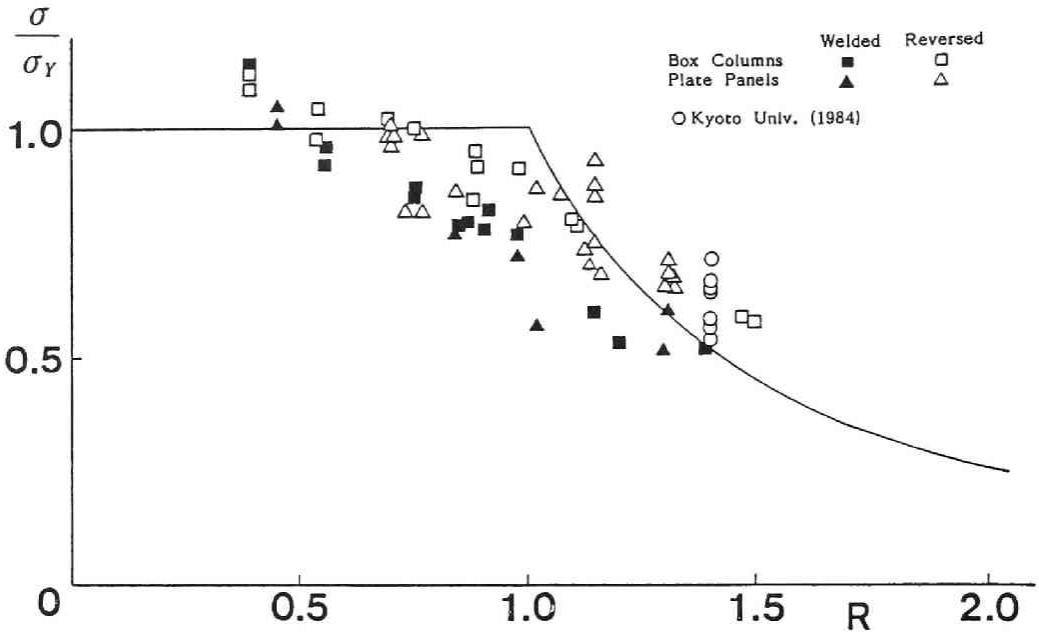

Fig. 2.3.4 Experimental Results of Compressed Plates. [53]

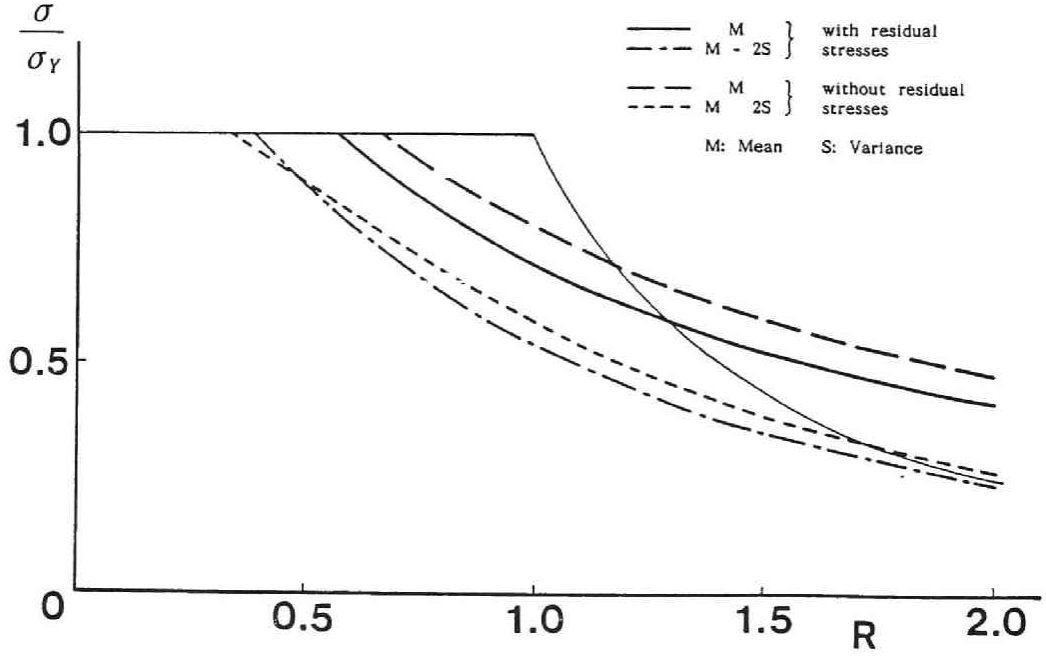

Fig. 2.3.5 Fukumoto-Itoh Data-Base Approach of Compressed Plates. [66]

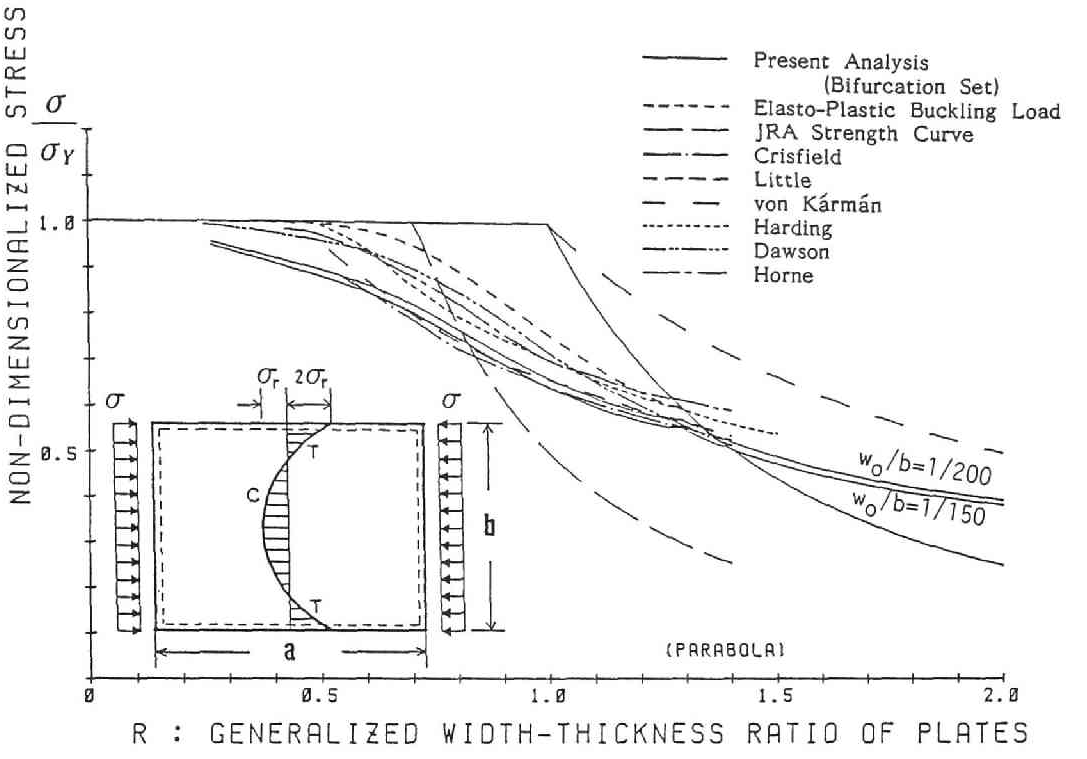

Fig. 2.3.6(a) Ultimate Strength Curves for Compressed Rectangular Plates with Parabolic Distribution of Residual Stress.

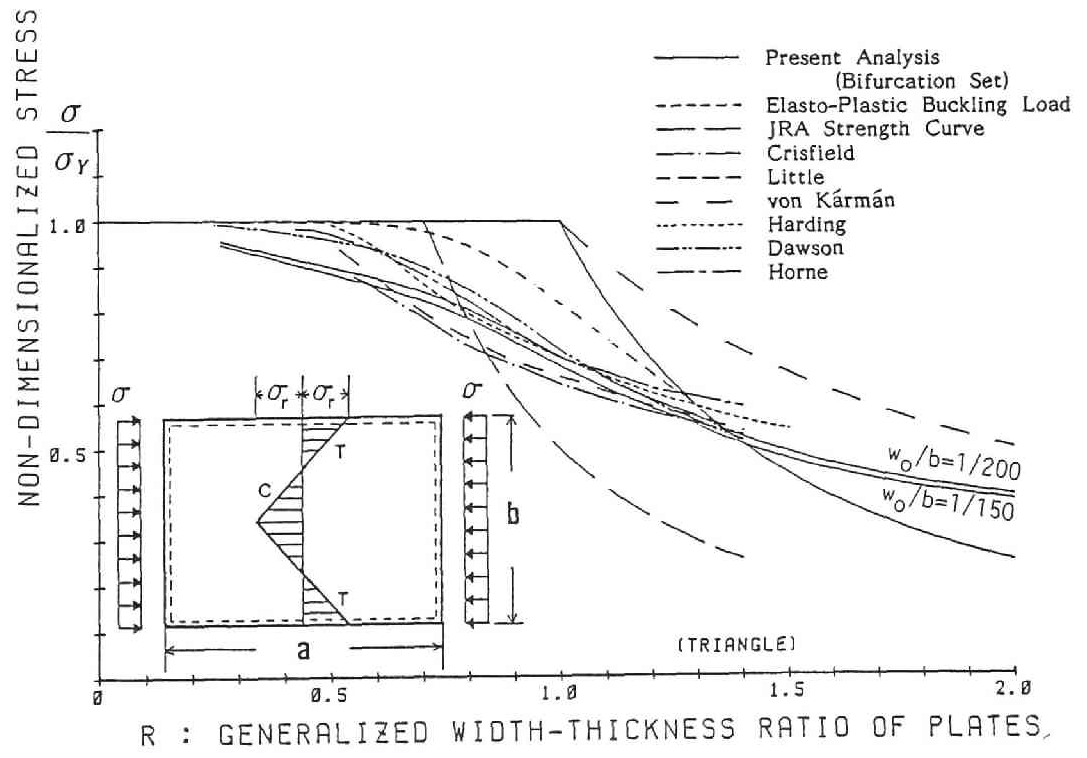

Fig. 2.3.6(b) Ultimate Strength Curves for Compressed Rectangular Plates with Triangular Distribution of Residual Stress.

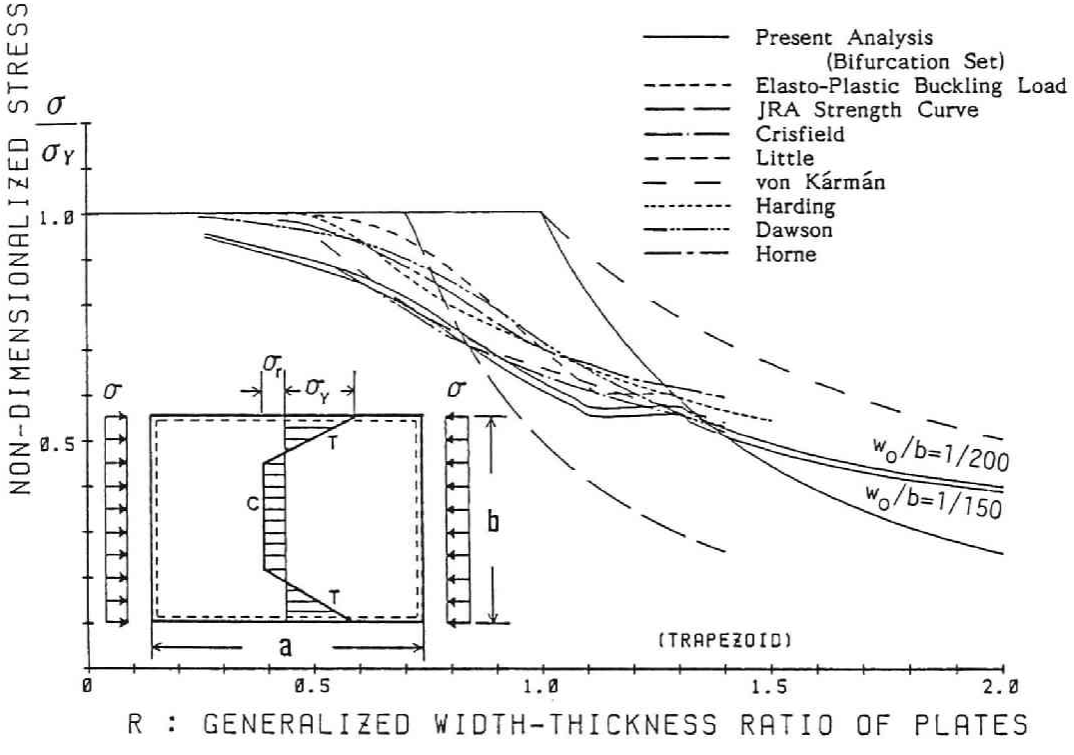

Fig. 2.3.6(c) Ultimate Strength Curves for Compressed Rectangular Plates with Trapezoidal Distribution of Residual Stress.

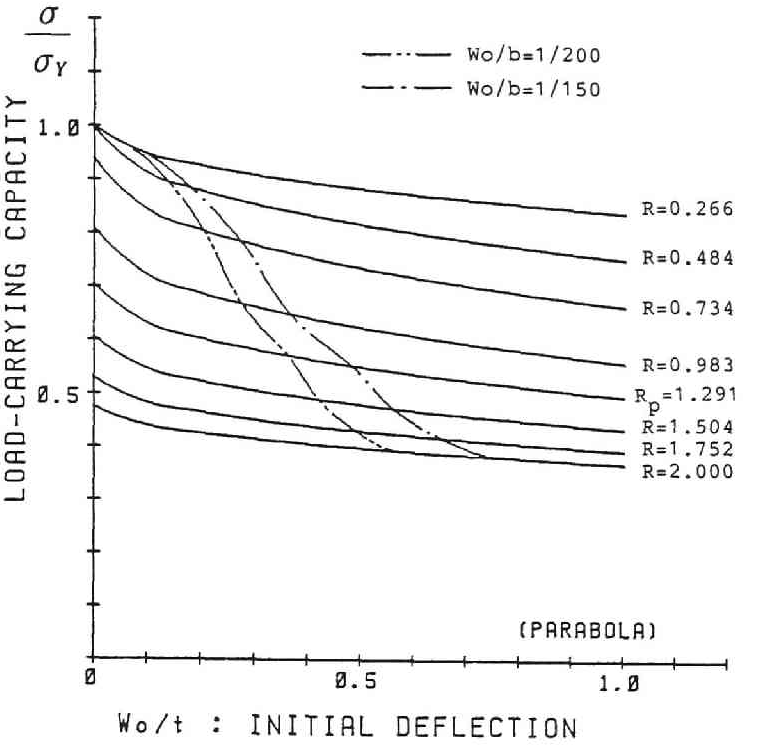

Fig. 2.3.7 **Family of Imperfection Sensitivity Curves for Elasto-Plastic Buckling of Compressed Plates with Parabolic residual Stress.**

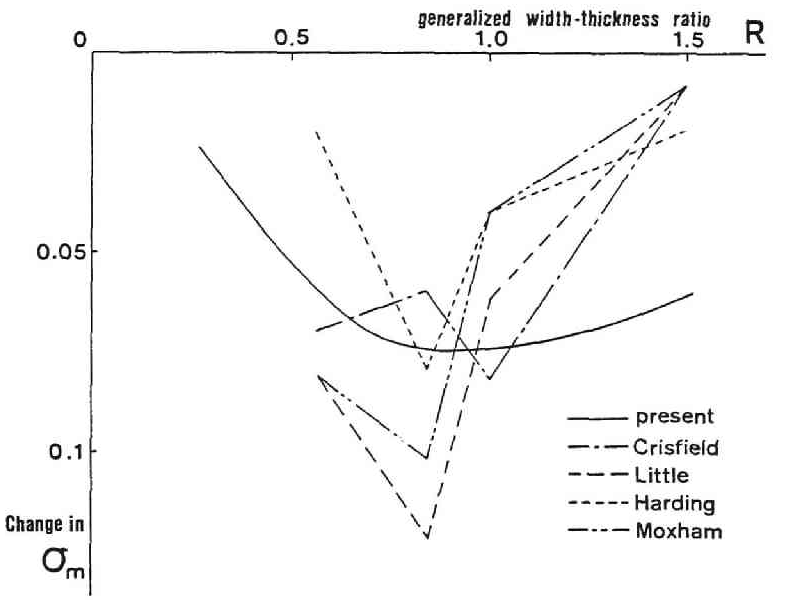

Fig. 2.3.8 **Relationship between Change in the Ultimate Strengths and the Generalized Width-Thickness Ratio.**

The proposed bifurcation sets are compared with six ultimate strength curves herein: by von Kármán, Crisfield's finite element large deflection elasto-plastic buckling analysis[11], Little's energy minimization[16], Harding's finite difference analysis with a dynamic relaxation[12], Dawson's simplified elastic large deflection perturbation analysis[58] and by Horne's effective width approach [13,14,15]. These strength curves were drawn for simply supported rectangular plates with ϕ = 0.7 ~ 1.0, w_o/b = 1/200 and the rectangular band width at 3t of the residual yield tensile stress[20].

The ultimate strength curves in the elastic range for the slender plates are throughout the same regardless of the residual stress types. But, in the elasto-plastic range for intermediate values of R, the ultimate strengths in the case of the trapezoidal distribution are found to be the lowest, and those of the triangular distribution are the highest, independently of the magnitude of the imperfections. However, the present ultimate strength curves are found to be affected insignificantly by the difference of the types of residual stress distributions, similarly to the case of compressed columns. Of course, the unified bifurcation set with the equivalent imperfection gives the unified ultimate strength curve to be excellent correlation with many strength curves as mentioned above.

For given width-thickness ratios, the present strength can be explicitly drawn as the imperfection sensitivity curve. **Fig. 2.3.7** illustrates a family of imperfection sensitivity curves in the case of compressed plates with the parabolic residual stress distribution. The ultimate strength may be shown to be remarkably sensitive to the initial imperfection especially at the intermediate width-thickness ratios.

Bradfield reviewed the numerical evaluation of strength curves of compressed plates by Crisfield, Little, Harding, Dawson and Horne[20]. In order to compare the present curves with his results, the imperfection sensitivity curve is replaced for the change in the non-dimensionalized strength $\bar{\sigma}_m$ between smaller and larger magnitudes of the initial deflections, i.e., w_o/b = 1/1000 and 1/200 (b is the plate-edge width). **Fig. 2.3.8** shows the relationship between the change in the ultimate strength and the generalized width-thickness ratio. It is seemed that the present reductions provide relatively middle strength among other investigations except for the case of elastic buckling region. Within large width-thickness R corresponding to the purely elastic buckling, the proposed results may overestimate the imperfection sensitivity greater than the others. This is caused by the form of the **equivalent imperfection** $\mu(R)$ using peculiar limit condition of $R \to \infty$.

2.4 Compressed Stiffened Plates

Several numerical illustrations are provided on the strength of the simply supported stiffened plates under in-plane uniaxial compression. A single longitudinal stiffener is assumed to be spliced with equal interval and can be characterized by the geometrical and material parameters such as N, δ and γ, E/σ_Y . Moreover, torsional rigidities of the stiffener are assumed to be neglected. The type of residual stress distribution of the local plate panel is assumed to be either of a parabola, a triangle or a trapezoid as shown in **Figs. 2.2.1**(a)-(c), and that of the stiffener to be tensile uniformly distributed in its cross section. For all the distribution types, the magnitude of the maximum compressive residual stress σ_r in the local plate panel and that of the uniform tensile residual stress σ_{rs} in the stiffener are restricted to 0.4 σ_Y and 0.2 σ_Y, respectively. Moreover, the magnitude of initial deflection of the stiffened plates

are assumed to be a/1000 and b/300 with its global and local modes, respectively. The values are prescribed on the basis of the tolerances allowed by the JRA Specifications for Highway Bridges[50], which "a" denotes the half-wave length of the stiffened plate for the global buckling and "b/2" indicates the width of the loaded edge of the plate panel for the local buckling.

For given parameters such as N, δ, γ and E/σ_Y, all of the bifurcation sets or the ultimate strength curves can be calculated under the following condition: the **equivalent** orthotropic plates have such aspect ratio ϕ to take the least buckling strengths in the elasto-plastic ranges. That is,

$$n=1 \text{ and } \phi=m\sqrt[4]{k_c[1+(N+1)\gamma]} \tag{2.4.1}$$

Herein, for a comparison with the difference of residual stress types, the numerical results are presented for three types of distributions of residual stresses: parabola, triangle and trapezoid for the buckling. **Figs. 2.4.1**(a), (b), (c) illustrate the proposed bifurcation sets of compressed stiffened plates with parabolic, triangular and trapezoidal distributions of residual stresses for the global buckling. In these figures, the generalized width-thickness ratio R of the local plate panel is chosen as the abscissa without regard to the types of bucklings; whereas the ordinate designates the non-dimensionalized ultimate strength with respect to the yielding stress σ_Y. The ultimate strength curves of stiffened plates are found to be affected only insignificantly by the difference of the types of distribution of the residual stress, similarly to the cases of compressed columns and plates as discussed previously. Hereafter, the numerical results are provided for only the parabolic residual stress distribution. On the other hand, for the local buckling of the plate panel, **Fig. 2.4.2** typically shows the present results of the compressed stiffened plate.

For a comparison with the proposed strength prediction, the following ultimate strength curves and some test results are presented herein: von Kármán, Fukumoto's data-base approach[64], Komatsu's large-deflection elasto-plastic finite element analysis[11,36], and practical design formulations such as JRA, DASt and ÖNORM[63]. **Fig. 2.4.3** shows several Japanese experimental results of stiffened plates[63,64], including the test data by automated microcomputer testing at Kyoto University in 1981-84[54-57].

The present ultimate strength curves in the elastic range for the slender stiffened plates are throughout the same without regard of the residual stress types. However, in the intermediate width-thickness ratio of R, the ultimate strength curve for the trapezoidal distribution of residual stress is found to be the lowest, and that in the case of the triangular is the highest, not related with the magnitudes of initial deflections.

Especially, in the case of the local buckling corresponding to **Fig. 2.4.2, Fig. 2.4.4** compares the same results with the numerical calculations by Crisfield, Little, Harding, Dawson, Horne and the JRA Specifications for compressed unstiffened plate panels[44,47].

For both the global buckling of the stiffened plate as a wide Euler column and the local buckling of the local plate, it may be found that the present imperfection sensitivity curve in Eq. (2.2.21) using Eqs. (2.2.22), (2.2.23) and (2.2.24) gives a unified strength prediction of the stiffened plate. Moreover, this unified equation has been applicable to the cases of columns, beams and compressed unstiffened plates as well[43-49].

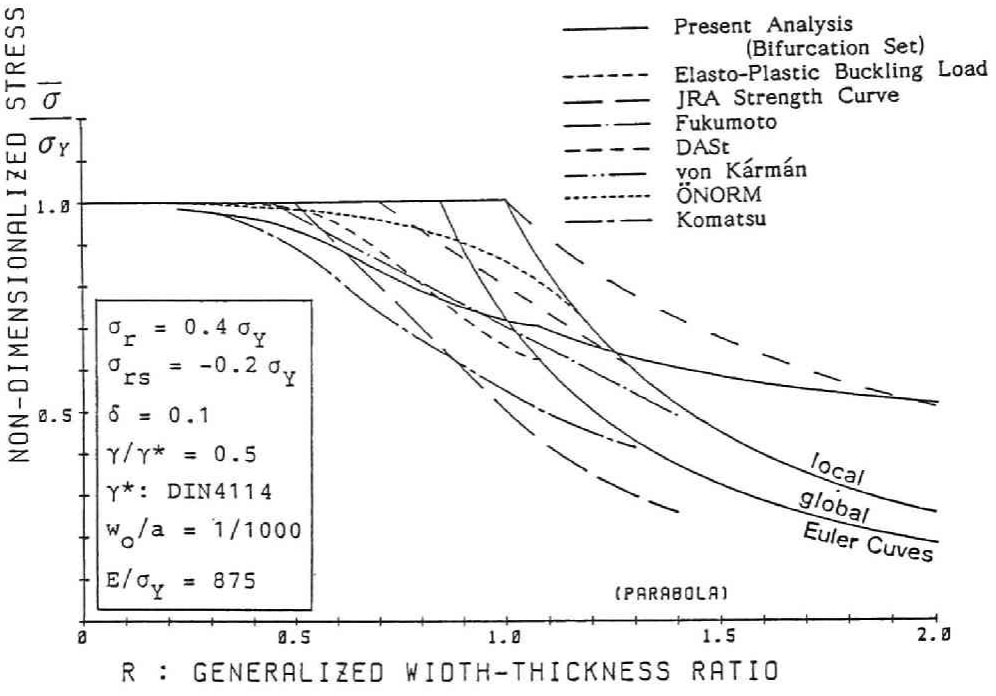

Fig. 2.4.1(a) Ultimate Strength Curves of Compressed Rectangular Stiffened Plates with Parabolic Residual Stress for Global Buckling.

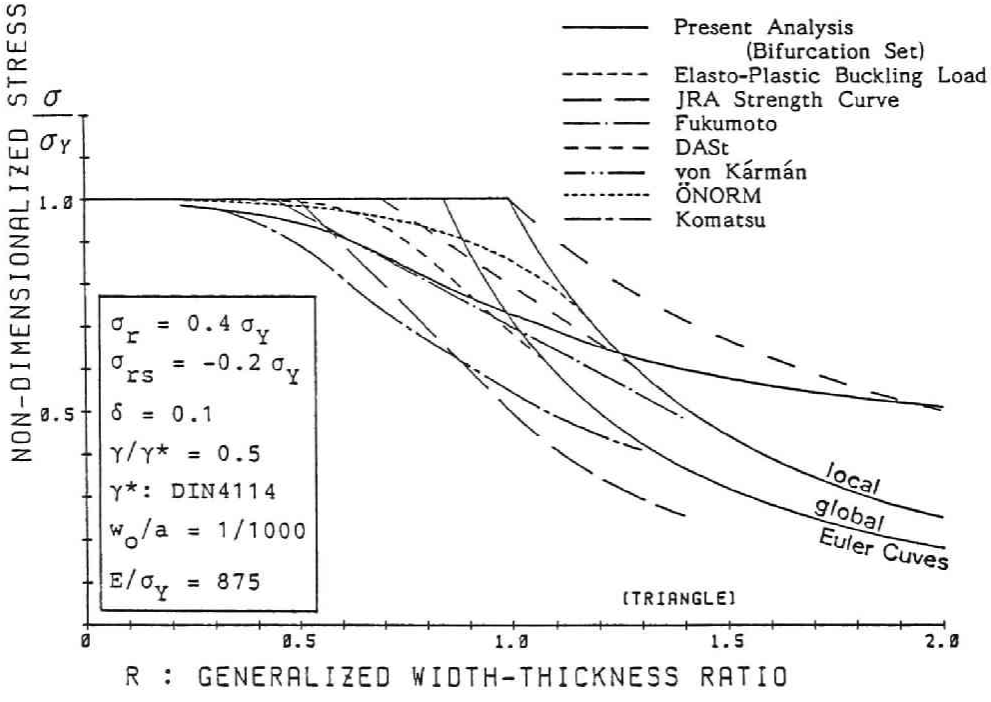

Fig. 2.4.1(b) Ultimate Strength Curves of Compressed Rectangular Stiffened Plates with Triangular Residual Stress for Global Buckling.

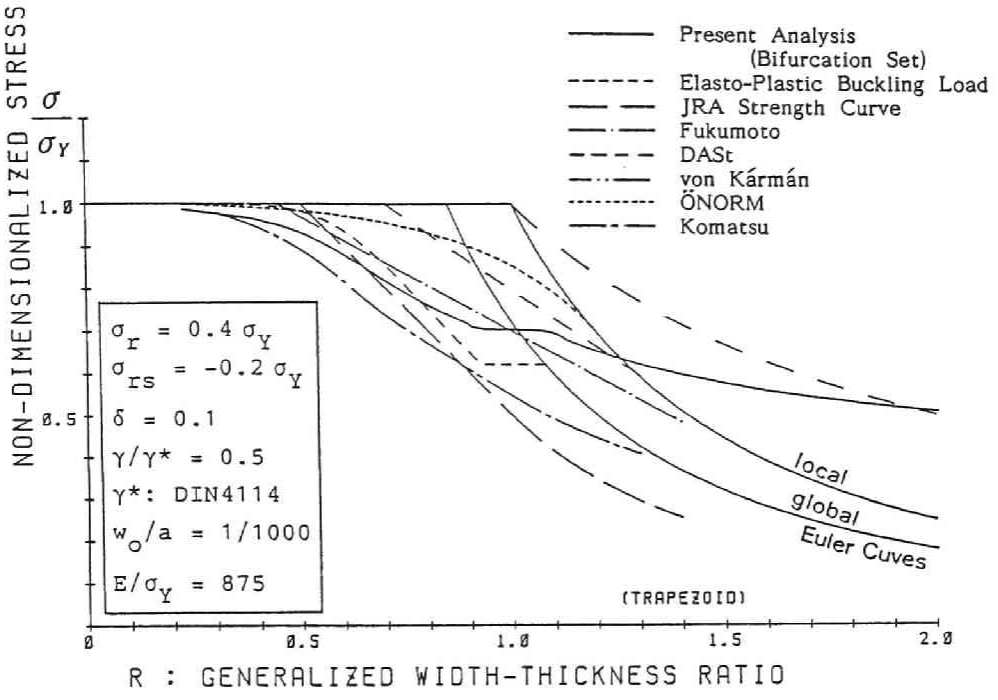

Fig. 2.4.1(c) Ultimate Strength Curves of Compressed Rectangular Stiffened Plates with Trapezoidal Residual Stress for Global Buckling.

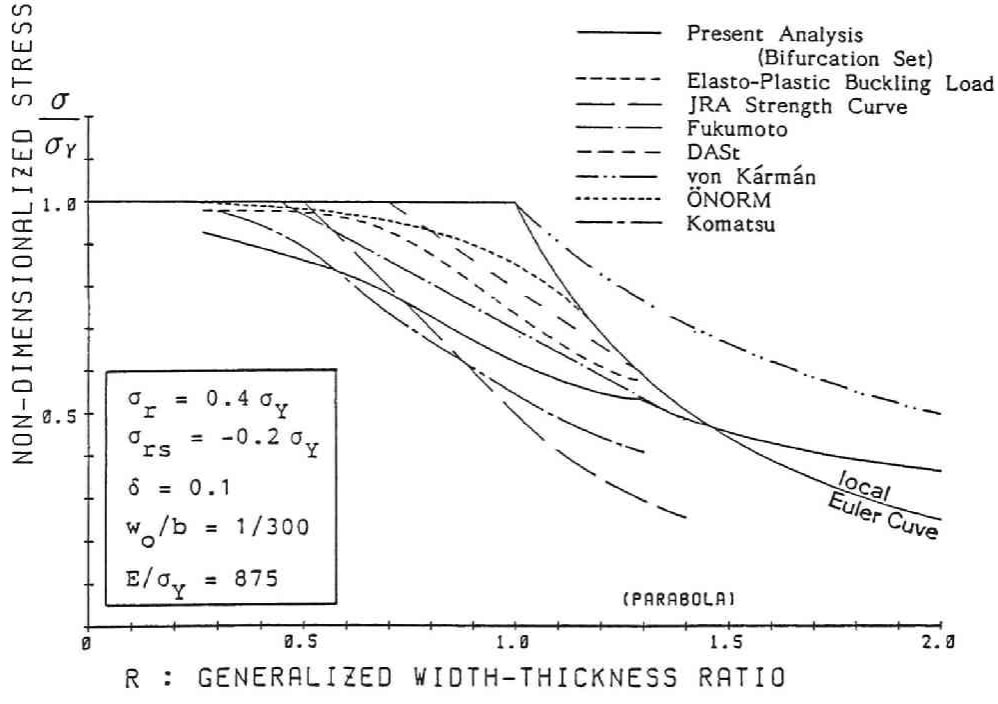

Fig. 2.4.2 Ultimate Strength Curves of Compressed Rectangular Stiffened Plates with Parabolic Residual Stress for Local Buckling.

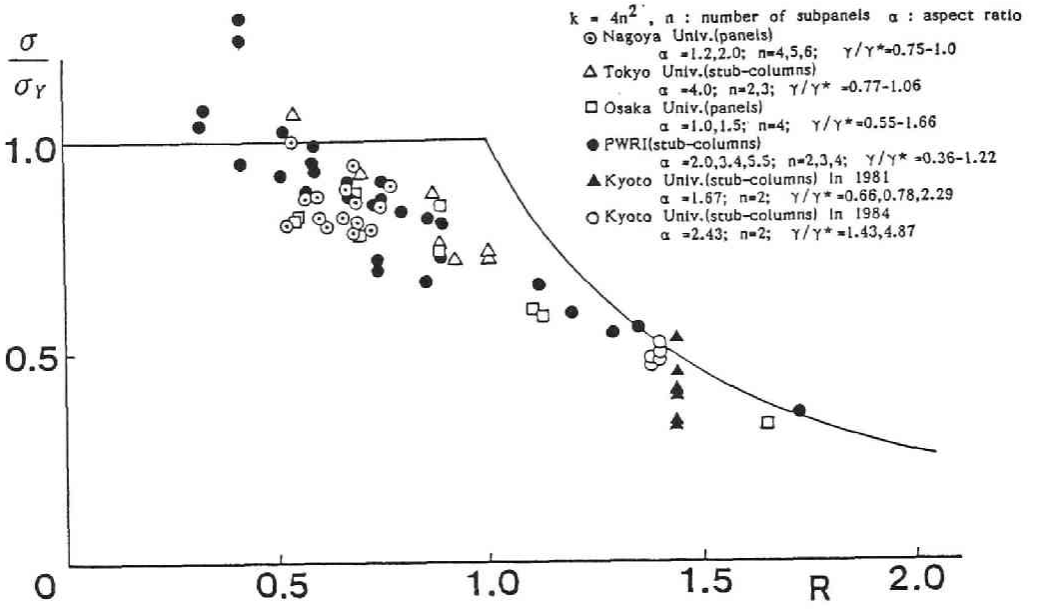

Fig. 2.4.3 Japanese Test Results of Stiffened Plates. [54-56, 63, 64]

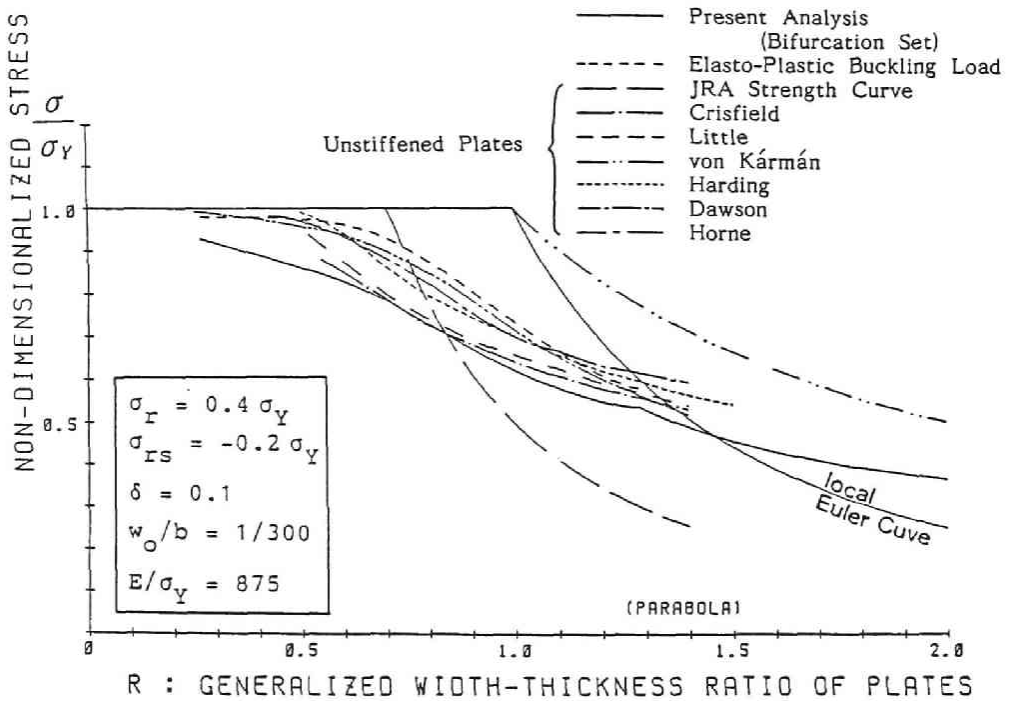

Fig. 2.4.4 Ultimate Strength Curves of Compressed Rectangular Stiffened Plates with Parabolic Residual Stress for Local Buckling. (Comparison of the Present Results with Several Strength Curves of Compressed Unstiffened Local-Plate Panel.)

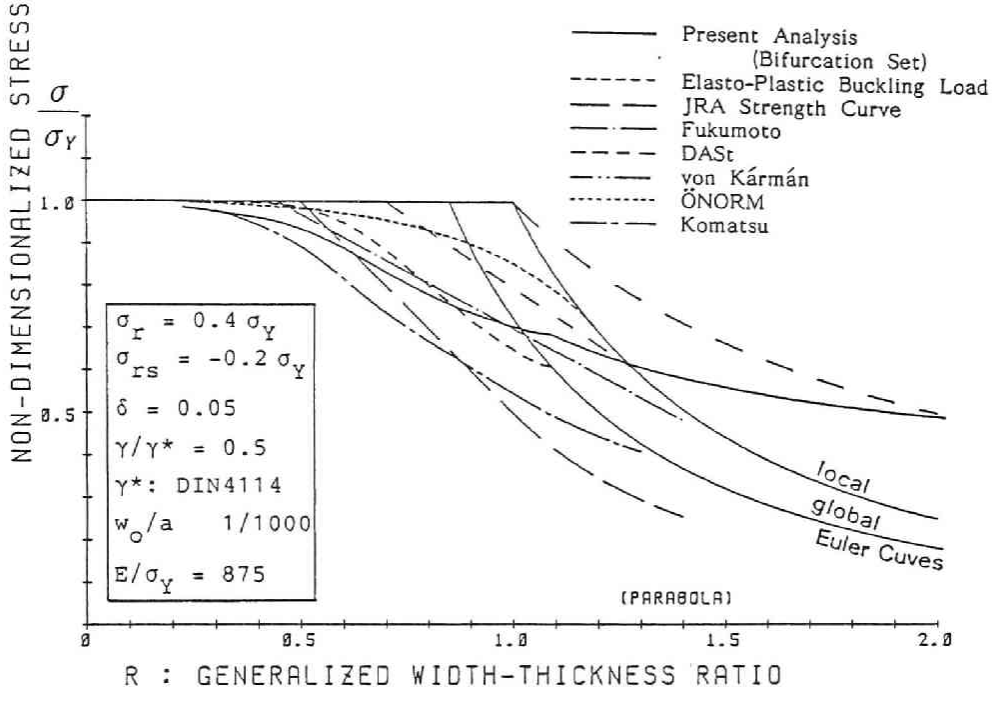

Fig. 2.4.5 **Ultimate Strength Curves of Compressed Rectangular Stiffened Plates with Parabolic Residual Stress for Global Buckling.**

In this chapter, all the calculations on the ultimate strength of stiffened plates are made for only typical values of parameters; N, δ, γ and E/σ_Y as shown in these figures. For various values of such parameters, the similar strength prediction may be explicitly determined by Eq. (2.2.21) through Eqs. (2.2.22), (2.2.23) and (2.2.24). For example, **Fig. 2.4.5** shows the results of the stiffened plates with the parabolic residual stress and the area-parameter δ =0.05. Then, the effect of such area-parameter δ on the ultimate strength may be shown to be insignificant, so far as the values are considered herein, similarly to the effect of the types of residual stress distributions.

2.5 Application to Statistical Simulations

2.5.1 General remarks

The present approach allows us to predict the unified ultimate strength formula of steel structures in elasto-plastic range. Especially, the effects of the residual stresses and the initial displacements on the strength are explicitly expressed in Eq. (2.2.21). This formula is so effective that it can be used in order to evaluate the statistical strengths of steel rectangular plate members with or without stiffeners. Through a great number of statistical surveys on the initial imperfections of the actual structural members and typical tested specimens, a Monte Carlo simulation is performed herein. In this section, the imperfections are taken to be the initial displacements and the residual stresses, and are generated from their proper statistical form of probability density functions. The distributions of the initial displacements and of the residual stresses are normalized into two-way normal distributions, and their three-dimensional view is visually drawn with the contour lines representing constant strength levels. Hence, the most frequent combinations of such imperfections are determined with respect to the 5%-fractile strengths for a prescribed generalized slenderness.

2.5.2 Statistical distributions of initial imperfections

Initial deflections The statistical distribution of initial deflections is well known to follow the Weibull or the Erlang(Gamma) distribution from many experimental data for compressed plates with the plate-bending mode(I)[63]. Then, herein, the magnitude of initial deflections non-dimensionalized by the total width "b" of plate member is assumed to be the Erlang distribution with the mean value of 5.97×10^{-3} and the standard deviation of 8.76×10^{-6}.

Residual stresses The statistical distribution of the magnitude of the maximum compressive residual stress is assumed to be the normal distribution with the mean value of $0.23\ \sigma_Y$ and the standard deviation of $0.145\ \sigma_Y$[66].

2.5.3 Monte Carlo simulations

For each specified generalized width-thickness ratio R for 0.6 to 1.4 with interval 0.2, a Monte Carlo simulation is made:

[i] Generate random numbers following the normal and the Erlang distributions for the residual stresses and the initial deflections, respectively. Their methods of generations are briefly discussed in the papers[49,67].

[ii] Substitute the pair of these values of imperfections into the imperfection sensitivity formula in Eq. (2.2.21). Then, the ultimate strengths are scattered in an unknown form of distribution.

[iii] Repeat steps [i] to [ii] as many times if necessary.

[iv] Normalize the variables in order to take two-way normal distribution with both the residual stresses and the initial deflections[49,67].

[v] Plot the contour lines representing the constant strength levels.

[vi] Find the most frequent combinations of the imperfections with respect to the 5%-fractile ultimate strengths in Eq. (2.2.21).

Herein, the simulation tests are made for compressed plates with typical three types of residual stress distributions[44,47]. Also, in the case of stiffened plates with only the parabolic distribution of residual stress, the tests are performed for three prototypes of flexural rigidities γ/γ^*=0.5, 0.75 and 1.0 in the global buckling modes.

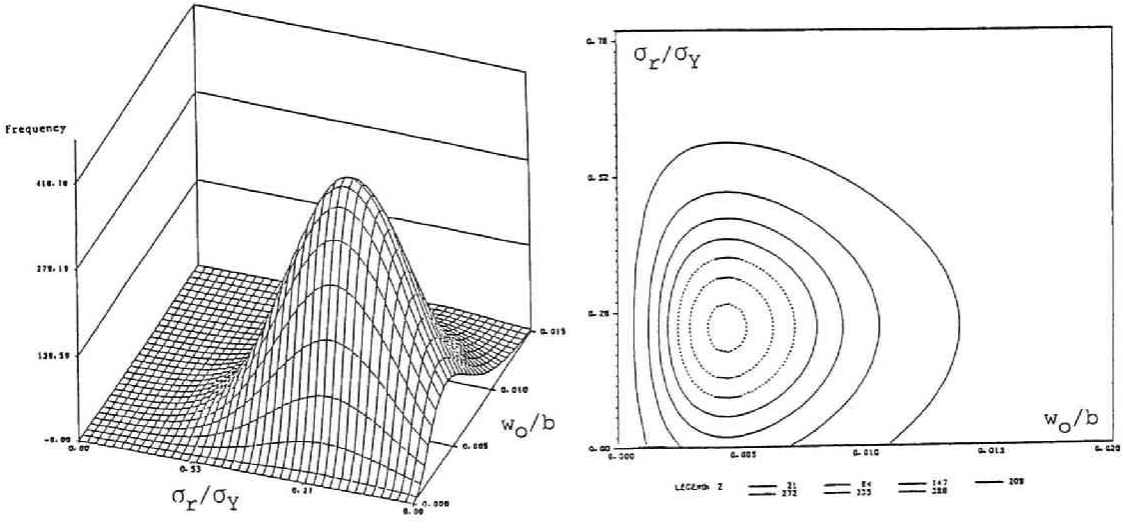

Fig. 2.5.1 Joint Probability Density Function of Residual Stresses and Initial Deflections.

2.5.4 Numerical illustrations

Assume two variables of the residual stresses and the initial deflections to be independent one another, their joint distribution can be obtained easily. **Figs. 2.5.1** show a 3-dimensional drawing of the joint probability density function and the contour lines in the imperfection space.

In order to search for the most frequent combination of the residual stresses and the initial deflections for prescribed generalized width-thickness ratio R, their variables are transformed to take the two-way normal distribution. The transformation procedure is confirmed in the papers[49,67].

Compressed plates The generalized width-thickness ratio R is chosen as

$$R \equiv \frac{b}{\pi t}\sqrt{\frac{12(1-\nu^2)\sigma_Y}{K_E E}} \qquad K_E : \text{Euler buckling coefficient} \qquad (2.5.1)$$

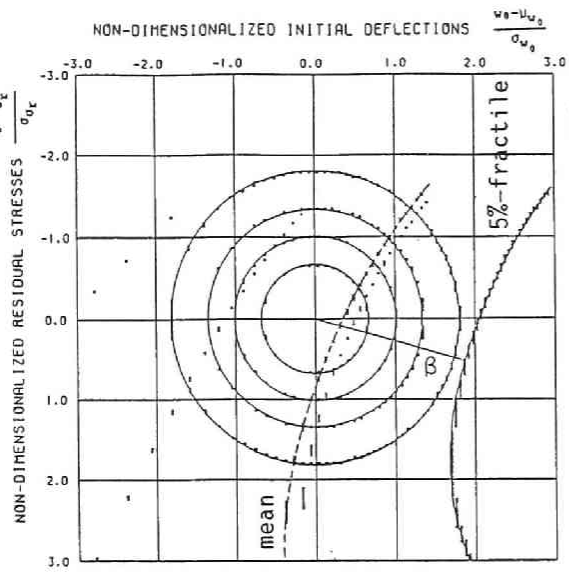

Fig. 2.5.2 **Contour Lines of Strength for Compressed Plates:** R=0.8

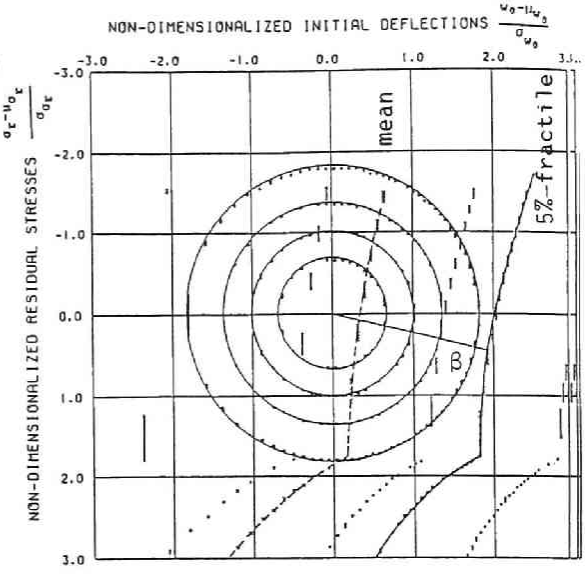

Fig. 2.5.3 **Contour Lines of Strength for Compressed Plates:** R=1.4

The discrete value of R varies from 0.6 to 1.4 with interval 0.2. For instance, **Fig. 2.5.2** presents the 2-dimensional contour lines of the joint probability density function, together with each constant level of ultimate strengths. The broken line and the thick solid line denotes the mean and the 5%-fractile values of strengths, respectively. A foot of the perpendicular from the origin of the joint function to the 5%-fractile strength level specifies the pair of the most frequent combination of the residual stresses and the initial deflections, denoted as an index β . Also, **Fig. 2.5.3** shows the results for R=1.4, and the similar figures are obtained for each generalized width-thickness ratio R and for each type of distribution of residual stress.

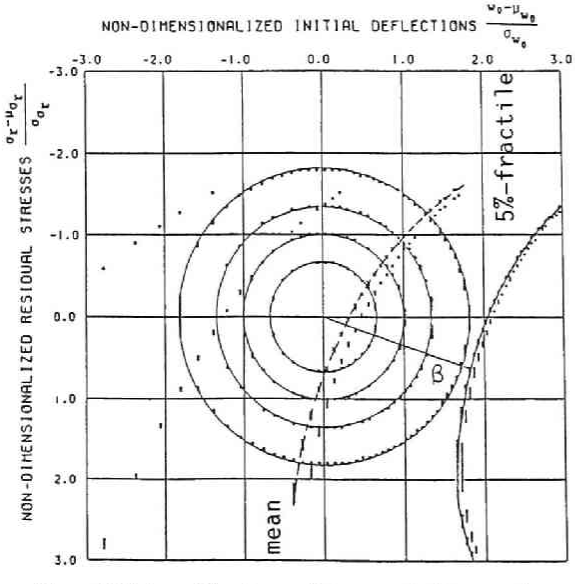

Fig. 2.5.4 **Contour Lines of Strength for Compressed Stiffened Plates:** R=0.6, $\gamma/\gamma^* = 0.5$

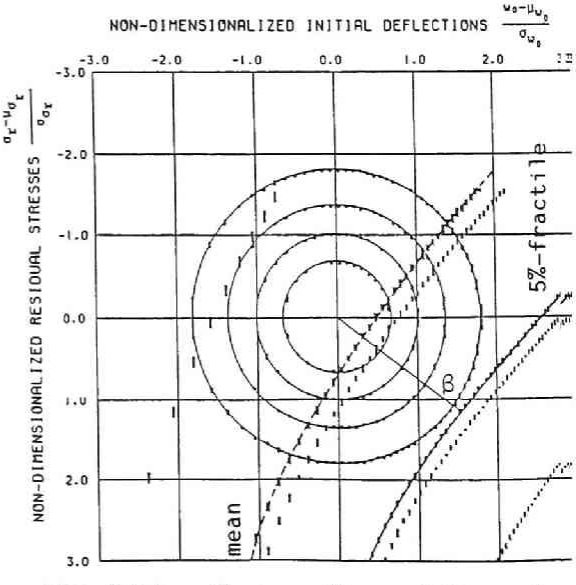

Fig. 2.5.5 **Contour Lines of Strength for Compressed Stiffened Plates:** R=1.4, $\gamma/\gamma^* = 0.5$

Compressed stiffened plates The generalized width-thickness ratio R is selected for the local-plate panel of stiffened plate, similarly to Eq. (2.5.1). **Figs. 2.5.4** and **2.5.5** show the results of models with the rigidities $\gamma/\gamma^* = 0.5$ at R=0.6 and R=1.4, respectively, in the global buckling mode. The residual stress distribution is restricted to be parabola for all the computations.

Fig. 2.5.6 provides the numerical results of compressed plates with parabolic distribution of residual stress. For discrete values of R from 0.6 to 1.4, this figure shows the changes of the most frequent combinations of the residual stresses, the initial deflections and the index β of the corresponding probability of appearance. They are designated as the chain line, the thin broken line and the solid line, respectively. Also, an another broken line indicates the 5%-fractile value of initial deflections. The effect of the residual stresses decreases as R increases upto 1.2, since the allowance of the residual stresses increases. While the opposite tendency appears for R>1.2. Furthermore, the effect of the initial deflections slightly increases for R<1.2, since the allowance of the initial deflections decreases. For R>1.2, however, the effect decreases. In other words, it may be found that the ultimate strength is relatively sensitive to the initial deflections for R<1.2, and is more sensitive to the residual stresses for R>1.2. In the other hand, the index β is not scattered throughout the whole ranges of R, so that the probability of the most frequent combination of the residual stresses and the initial deflections is approximately constant with slight tendency to decrease as R increases.

Fig. 2.5.7 shows the similar results of stiffened plates with $\gamma/\gamma^* = 0.5$ for their global bucklings. The effect of the residual stresses slightly decrease with increase of R; While that of the initial deflections slightly increases as R increases. Also, the index β becomes the minimum for R=1.2, representing the maximum value of the joint probability.

2.6 Conclusions

A simple unified approach to the ultimate strength of compressed steel plates with and without stiffeners is presented on the basis of the concept of the catastrophe theory. The main conclusions are:

(1) The residual stresses and the initial deflections may affect the evaluation of the elasto-plastic buckling stress and the form of the explicit imperfection sensitivity formula, respectively.

(2) The inelastic strength prediction of the plate members may be explicitly determined in the form of the bifurcation sets or the imperfection sensitivity curves for both global and local bucklings.

(3) The bifurcation sets can be defined explicitly near the **equivalent bifurcation point** being the intersection point of the elasto-plastic postbuckling path with the plastic mechanism curve.

(4) The initial imperfections are modified and replaced by the **equivalent imperfections** proposed herein.

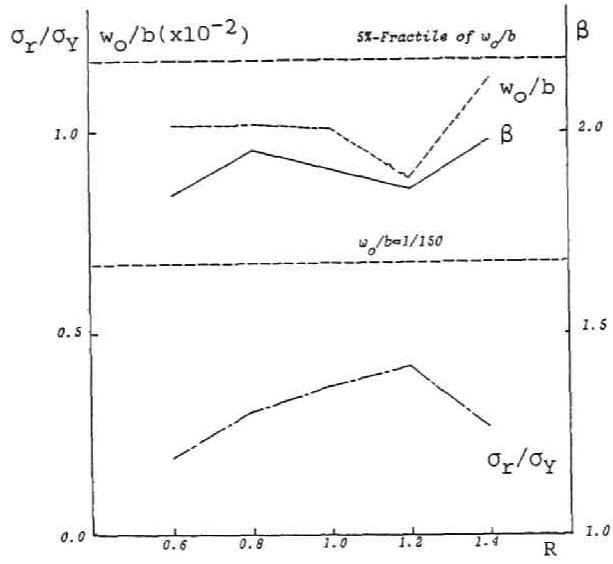

Fig. 2.5.6 Most Frequent Combinations of Residual Stresses and Initial Deflections for Compressed Plates.

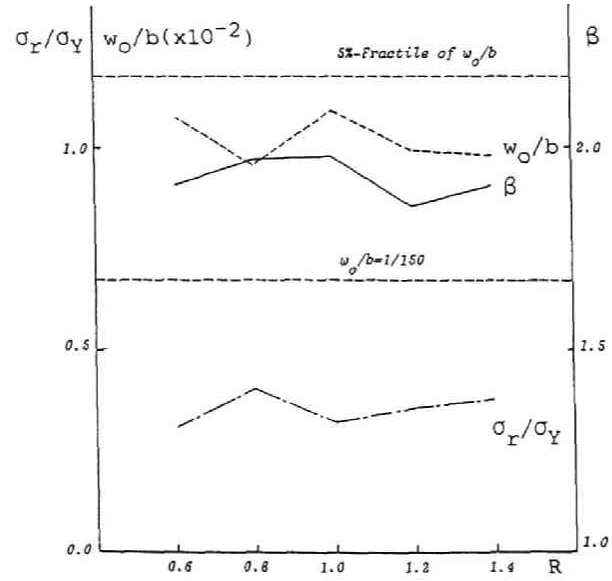

Fig. 2.5.7 Most Frequent Combinations of Residual Stresses and Initial Deflections for Compreesed Stiffened Plates: $\gamma/\gamma^* = 0.5$.

(5) The proposed approach can be applied to the strength prediction of unstiffened and stiffened plates in in-plane compression, and these numerical results are demonstrated for typical plate models.

(6) Using the proposed strength formula expressed as the imperfection sensitivity, a Monte Carlo simulation is performed on appropriate statistical distributions of the residual stresses and the initial deflections for compressed plates and stiffened plates. Then, the most frequent combinations of such imperfections can be explicitly determined from both their joint probability density function and the 5%-fractile ultimate strengths.

(7) All the calculations herein can be made using mainly a microcomputer with small memory storage.

(8) The form of distribution of residual stress assumed herein may insignificantly affect the present results.

(9) The general philosophy adopted in this chapter may also be applicable to other type of engineering structures such as rigid frames, arches, trusses and shells as well as columns, beam-columns and compressed plate panels.

Bibliographies of Chapter 2 in PART 3

1) Johnston, B.G., Guide to Stability Design Criteria for Metal Structures, 3rd Edition. Structural Stability Research Council, John Wiley & Sons, 1976.
2) Trahair, N.S., The Behaviour and Design of Steel Structures. John Wiley & Sons, 1977.
3) SSRC, ECCS, CRCJ, CMEA, Stability of metal structures - A world view (Part 2). Engineering Journal, AISC, 4th Quarterly, Vol. 18, No. 4, 1981.
4) SSRC, ECCS, CRCJ, CMEA, Stability of metal structures - A world view. Engineering Journal, AISC, 3rd Quarterly, Vol. 19, No. 2, 1982.
5) Stowell, E.Z., A Unified Theory of Plastic Buckling of Columns and Plates. NACA Technical Note 1556, National Advisory Committee on Aeronautics, 1948.
6) Bleich, F., Buckling Strength of Metal Structures. McGraw-Hill, 1952.
7) Bijlaard, P.P., Theory and tests on plastic stability of plates and shells. Journal of the Aerospace Sciences., Vol. 16, pp. 529-541, 1949.
8) Pearson, C.E., Bifurcation criterion and plastic buckling of plates and columns. Journal of the Aeronautical Sciences, Vol. 17, pp. 417-455, 1950.
9) Okumura, T., F. Nishino and A. Hasegawa, Relation and buckling coefficient in uniaxial compression. Proceedings of the Japan Society of Civil Engineers, No. 205, pp. 19-30, 1972.
10) Dwight, J.B. and K.E. Moxham, Welded steel plates in compression. The Structural Engineer, Vol. 47, No. 2, pp. 49-66, 1969.
11) Crisfield, M.A., Full-range analysis of steel plates and stiffened plating under uniaxial compression. Proceedings of the Institution of Civil Engineers, Part2, Vol. 59, pp. 595-624, 1975.
12) Harding, J.E., R.E. Hobbs and B.G. Neal, The elastoplastic analysis of imperfect square plates under in-plane loading. Proceedings of the Institution of Civil Engineers, Part 2, Vol. 63, pp. 137-158, 1977.
13) Horne, M.R. and R. Narayanan, An approximate method for the design of stiffened steel compression panels. Proceedings of the Institution of Civil Engineers, Part 2, Vol. 59, pp. 501-514, 1975.

14) Horne, M.R. and R. Narayanan, Strength of axially loaded stiffened panels. Publications, International Association for Bridges and Structural Engineering, Vol. 36, pp. 125-157, 1976.
15) Narayanan, R. and N.E. Shanmugam, Effective widths of axially loaded plates. Journal of Civil Engineering Design, Vol. 1, pp. 253-272, 1979.
16) Little, G.H., The collapse of rectangular steel plates under uniaxial compression. The Structural Engineer. Vol. 58B, pp. 45-61, 1980.
17) Tvergaard, V. and A. Needleman, Structural collapse due to plastic in stability. Trans. Int. Conf. Struct. Mech. React. Technol., 5th, L1/3*, pp. 1-10, 1979.
18) Ueda, Y. and T. Yao, Ultimate strength of a rectangular plate under thrust - with consideration of the effects of initial imperfections due to welding -. Trans. JWRI, Welding Research Institute of Osaka University, Vol. 8, pp. 97-104, 1979.
19) Chatterjee, S. and P.J. Dowling, The design of box girder, compression flange. Steel Plated Structures (ed. by P.J. Dowling et al.), Crosby Lockwood Staples, pp. 196-228, 1977.
20) Bradfield, C.D., An evaluation of the elastic-plastic analyses of steel plates loaded by uniaxial in-plane compression. International Journal of Mechanical Sciences, Vol. 24, No. 3, pp. 127-146, 1982.
21) Rhodes, J., On the approximate prediction of elasto-plastic plate behaviour. Proceedings of the Institution of Civil Engineers, Part 2, Vol. 71, pp. 165-183, 1981.
22) Usami, T., Post-buckling of plates in compression and bending. Journal of the Structural Division, Proc. ASCE, Vol. 108, pp. 591-609, 1982.
23) Maquoi, R. and J. Rondal, Towards a unified approach to main stability problems of steel structures. Staveb. Cas., Vol. 28, pp. 883-892, 1980.
24) Mikami, I., M. Dogaki and H. Yonezawa, Inelastic buckling of continuous stiffened plates under compression. Proceedings of the japan Society of Civil Engineers, No. 298, pp. 17-30, 1980 (in Japanese).
25) Huffington, Jr., N.J. and VA. Blackburg, Theoretical determination of rigidity properties of orthogonally stiffened plates. Journal of Applied Mechanics, Transactions of American Society of Mechanical Engineers, Vol. 23, pp. 15-20, 1956.
26) Stowell, E.Z., A Unified Theory of Plastic Buckling of Columns and Plates. NACA Technical Note 1556, National Advisory Committee on Aeronautics, 1948.
27) Bleich, F., Buckling Strength of Metal Structures. McGraw-Hill, 1952.
28) Faulkner, D., A review of effective plating for use in the analysis of stiffened plating in bending and compression. Journal of Ship Research, Vol. 19, No. 1, pp. 1-17, 1975.
29) Little, G.H., Stiffened steel compression panels - theoretical failure analysis. The Structural Engineer, Vol. 54, No. 12, pp. 489-500, 1976.
30) Carlsen, C.A., Simplified collapse analysis of stiffened plates. Norwegian Maritime Research, Vol. 5, No. 4, pp. 20-36, 1977.
31) Horne, M.R. and R. Narayanan, Design of axially loaded stiffened plates. Journal of the Structural Division, Proc. ASCE, Vol. 103, No. ST11, pp. 2243-2257, 1977.
32) Moolani, F.M. and P.J. Dowling, Ultimate load behaviour of stiffened plates in compression. Steel Plated Structures (eds. P.J. Dowling, J.E. Harding and P.A. Frieze), pp. 51-88, 1977.
33) Usami, T., Elastic and inelastic buckling strength of stiffened plates in compression. Proceedings of the Japan Society of Civil Engineers, No. 288, pp. 13-28, 1974 (in Japanese).

34) Hasegawa, A., K. Ota and F. Nishino, Some considerations on buckling strength of stiffened plates. Proceedings of the Japan Society of Civil Engineers, No. 232, pp. 1-15, 1974 (in Japanese).
35) Yoshida, H. and K. Maegawa, The buckling strength of orthogonally stiffened plates under uniaxial compression. Journal of Structural Mechanics, Vol. 7, No. 2, pp. 161-191, 1979.
36) Komatsu, S., S. Nara and T. Kitada, Elasto-plastic analysis of orthogonally stiffened plates with initial imperfections under uniaxial compression. Computers & Structures, Vol. 11, pp. 429-437, 1980.
37) Marchesi, A. and F. Ziliotto, Post-buckling of stiffened plates: numerical and experimental behavior. Stability of Metal Structures, Preliminary Report, CTICM, Paris, pp. 285-289, 1983.
38) Webb, S.E. and P.J. Dowling, Large-deflection elasto-plastic behaviour of discrete stiffened plates. Proceedings of the Institution of Civil Engineers, Part 2, Vol. 69, pp. 375-401, 1980.
39) Needleman, A. and V. Tvergaard, An analysis of the imperfection sensitivity of square elastic plates under axial compression. International Journal of Solids and Structures, Vol. 12, pp. 185-201, 1976.
40) Tvergaard, V., Imperfection-sensitivity of a wide integrally stiffened panel under compression. International Journal of Solids and Structures, Vol. 9, pp. 177-192, 1973.
41) Koiter, W.T. and M. Pignataro, An alternative approach to the interaction between local and overall buckling in stiffened panels. Buckling of Structures (ed. B. Budiansky), pp. 133-148, 1976.
42) van der Neut, Mode interaction with stiffened plates. Buckling of Structures (ed. B. Budiansky), pp. 117-132, 1976.
43) Niwa, Y., E. Watanabe and H. Isami, A new approach to predict the strength of steel columns. Proceedings of the Japan Society of Civil Engineers, No. 341, pp. 13-21, 1984.
44) Niwa, Y., E. Watanabe, H. Isami and Y. Fukumori, A new approach to predict the strength of compressed steel plates. Proceedings of the Japan Society of Civil Engineers, No. 341, pp. 23-31, 1984.
45) Niwa, Y., E. Watanabe and S. Suzuki, A new approach to the elasto-plastic lateral buckling strength of beams. Proceedings of the Japan Society of Civil Engineers, No. 344/I-1, pp. 79-87, 1984.
46) Niwa, Y., E. Watanabe and H. Isami, A unified view on the strength of columns, beams and compressed plates through catastrophe theory. Stability of Metal Structures, Preliminary Report, CTICM, Paris, pp. 313-317, 1983.
47) Niwa, Y., E. Watanabe and H. Isami, A new approach to predict the strength of compressed steel stiffened plates. Proceedings of Japan Society of Civil Engineers, Structural Engineering/Earthquake Engineering, Vol. 2 No. 2, pp. 281s-290s, 1985.
48) Niwa, Y. E. Watanabe and H. Isami, A new unified approach to predict the strength of steel structures. Proceedings of National Theoretical and Applied Mechanics, Vol. 34, 1985 (printing).
49) Watanabe, E., A Study on the Catastrophe and Static Load-Carrying Capacity of Structures. These presented to the Graduate Faculty of Kyoto University in partial fulfillment of the requirements for the degree of Doctor of Engineering, 1986.
50) Japan Road Association, Specifications for Highway Bridges, 1980.
51) Faulker, D., A review of effective plating for use in the analysis of stiffened plating in bending and compression. Journal of Ship Research, Vol. 19, pp. 1-17, 1975.

52) Usami, T., Y. Fukumoto and T. Aoki, Interaction between local and overall buckling of welded box columns. Proceedings of the Japan Society of Civil Engineers, No. 308, pp. 47-58, 1981 (in Japanese).
53) Kitada, T., A Study on Ultimate Strength of Steel Plates and Stiffened Plates under Compression. Thesis presented to the Faculty of Engineering of Osaka University in partial fulfillment of the requirements for the degree of Doctor of Engineering, 1980 (in Japanese).
54) Iwashimizu, Y., A Statistical Study on the Initial Imperfections and Their Relations to the Strength of Webs of Steel Bridges. Thesis presented to the Faculty of Engineering of Kyoto University in partial fulfillment of the requirements for the degree of Master of Engineering, 1981 (in Japanese).
55) Asano, T., Load-Carrying Capacity of Thin-Walled Box Columns under Repetitive Loading in Compression and Tension. Thesis presented to the Faculty of Engineering of Kyoto University in partial fulfillment of the requirements for the degree of Master of Engineering, 1984 (in Japanese).
56) Yamanouchi, T., A Study on the Ultimate Strength of Steel Beam-Columns under Repetitive Bending. Thesis presented to the Faculty of Engineering of Kyoto University in partial fulfillment of the requirements for the degree of the Master of Engineering, 1985 (in Japanese).
57) Niwa, Y., E. Watanabe and H. Isami, Automated structural testing using microcomputer system. Proceedings of the Japan Society of Civil Engineers, No. 332, pp. 145-158, 1983.
58) Dawson, R.G. and A.C. Walker, Post-buckling of geometrically imperfect plates. Journal of the Structural Div., Proc. ASCE, Vol. 98, No. ST1, pp. 75-94, 1971.
59) Korol, R.M. and A.N. Sherbourne, Strength predictions of plates in uniaxial compression. Journal of the Structural Division, Proc. ASCE, Vol. 98, No. ST9, pp. 1965-1986, 1972.
60) Walker, A.C. and N.W. Murray, A plastic collapse mechanism for compressed plates. Publications, International Association for Bridges and Structural Engineering, Vol. 34, pp. 217-236, 1975.
61) Fujita, Y., T. Nomoto and O. Niho, Ultimate strength of stiffened plates subjected to compression. Journal of the Society of the Naval Architect of Japan, No. 141, pp. 191-197, 1977 (in Japanese).
62) Davies, P.K., O. Kemp and A.C. Walker, An analysis of the failure mechanism of an axially loaded simply supported plate. Proceedings of the Institution of Civil Engineers, Part 2, Vol. 59, pp. 645-658, 1975.
63) IDMC, Statistical study on the initial deformations and the ultimate strength of steel bridge members. Committee of Initial Deflection Measurement, Journal of Society of Steel Construction of Japan, Vol. 16, No. 179, pp. 10-43, 1980 (in Japanese).
64) Fukumoto, Y., Numerical data bank for the ultimate strength of steel structures. Der Stahlbau, Vol. 51, No. 1, pp. 21-27, 1982.
65) Timoshenko, S.P. and J.M. Gere, Theory of Elastic Stability, 2nd Edition. McGraw-Hill, 1961.
66) Fukumoto, Y. and Y. Itoh, Basic compression strength of steel plates from test data. Proceedings of Japan Society of Civil Engineers, No. 344, pp. 129-139, 1984.
67) Fukuda, A., A Study on the Strength Evaluation of Compressed Plates and Stiffened Plates through a Monte Carlo Simulation and the Catastrophe Theory. Thesis presented to the Faculty of Engineering of Kyoto University in partial fulfillment of the degree for the Bachelor of Engineering, 1985 (in Japanese).

CHAPTER 3

APPLICATIONS TO COMPRESSED CYLINDRICAL SHELLS

3.1 General Remarks

Nowadays, cylindrical shells have been used in many civil engineering structures such as offshore constructions, nuclear power supplies, pipe lines and storage oil tanks. These cylindrical shell members are often subjected to uniaxial compression as independent or combined loadings together with hydraulic pressure or torsion. Then, the load-carrying capacity of the compressed shell is known to be very sensitive to even a few initial imperfections, and they may yield the global collapse of the cylinder. Therefore, problems on the stability and the strength of cylindrical shells are significantly important for our civil engineers to analyze and evaluate them.

Studies on the strength of cylindrical shells were initiated in the later nineteenth century[1]. Lorenz, von Kármán and Flüge obtained the buckling loads of cylinders, subjected to axially compression, uniform external pressure and their combinations, respectively[2]. Especially, Donnell derived the fundamental equations of equilibrium for shell structures under torsion[3]. However, the analytical or theoretical investigations had been remarkably inconsistent with the corresponding experimental results by Flüge, Donnell and et al.[4] These inconsistency between theory and experiments was tried to clearly interpret using the so-called **imperfection sensitivity** by von Kármán and Tsien, who solved the nonlinear equilibrium equations[5]. Moreover, Donnell and Wan clarified the post-bifurcation and the general equilibrium paths of compressed cylindrical shells[6].

Koiter discussed the stability and the imperfection sensitivity of cylinders on the basis of the potential energy function using his general theory of elastic stability[7]. He also analyzed the imperfection sensitivity curves of compressed cylindrical shells with axi-symmetric modes of initial deflections[8]. Arbocz and Babcock reported on relationships between initial deflection modes and the buckling configuration modes from many test data[9]. Similarly, Hutchinson, Hansen and Croll focused on the imperfection sensitivity of axially loaded cylindrical shells[10-12].

The shell members are being designed so that they may fail commonly in the elasto-plastic range. Then, in order to examine their inelastic strengths, the incremental materially and geometrically nonlinear numerical procedures are performed in recent trends. These time-consuming analyses of compressed cylindrical shells may provide us the ultimate strength, which is determined in an isolated form for a specified set of material and geometrical several parameters. On the other hand, advanced studies on the inelastic strength of cylinders have been vigorously performed by Batterman, Hutchinson and Croll[13-15].

This chapter formulates the unified approach of the elasto-plastic ultimate strength for compressed cylindrical shell members. Then, the effects of initial imperfections such as residual stresses and initial deflections are explicitly defined by a unified strength formula[16-20]. The cylindrical shells are known to have unstable postbuckling characteristics with asymmetries, which yield the sensitivity of initial imperfections on the ultimate strength. This is generally different from the cases of columns, beams and plates with neutral or stable symmetric postbuckling reservations. Therefore, from the instability of the elastic

and the similar elasto-plastic buckling points, a strength prediction of the compressed cylinders is proposed by the direct evaluation of an **elastic** pseudo-potential energy, considering the **elasto-plastic** behaviors near the elasto-plastic buckling point. Then, the **equivalent bifurcation point** introduced in the previous chapter of this PART is the ordinal elasto-plastic buckling point itself, what is summarized in the chapter III-1.

3.2 Basic Formulations

3.2.1 Residual stress distributions

A cylindrical shell model under uniaxial compression as shown in **Figs. 3.2.1** is analyzed herein. The cylinder behavior is commonly affected by the end conditions in **Fig. 3.2.1** since the out-of-plane deflections in the radius direction are constrained on both edges. However, neglecting the effects of the end constraints, the center part of the cylinder model with the length "L" is treated hereafter.

As shown in **Figs. 3.2.2**, the cylinder is welded on a longitudinal line and possesses an appropriate form of residual stress distribution uniformly in the longitudinal direction. The form of residual stress distribution with the maximum compressive stress σ_r is assumed to be either a parabola, a triangle or a trapezoid in the circumferential direction as shown in **Figs. 3.2.2**(a)-(c), respectively. These figures develop the distributions of residual stresses in the half-circumferential direction. Then, the relationships among the tangent modulus E_t, the Secant modulus E_s, the average axial stress σ and the average axial stress ε can be obtained as[21]:

$$E_t = \frac{d\sigma}{d\varepsilon} = k\,E \quad \text{and} \quad E_s = \frac{\sigma}{\varepsilon} \tag{3.2.1a}$$

and, for parabolic distribution,

$$\sigma = \sigma_Y + (2k - 3)\, k^2\, \sigma_r$$

$$\varepsilon = \frac{1}{E}[\, \sigma_Y - \sigma_r + 3(1 - k)^2\, \sigma_r]$$

$$(0 \le k \le 1) \tag{3.2.1b}$$

for triangular distribution,

$$\sigma = \sigma_Y - \frac{1}{2}\,\sigma_r[\, \frac{\sigma_Y\ \sigma_r}{\sigma_Y} + \frac{\sigma_Y + \sigma_r}{\sigma_Y}\, k^2\,]$$

$$\varepsilon = \frac{1}{E}\,[\ 2\sigma_Y \quad (\sigma_Y + \sigma_r)(\frac{\sigma_Y - \sigma_r}{\sigma_Y} + \frac{\sigma_r}{\sigma_Y}\, k\ )]$$

$$(\frac{\sigma_r}{\sigma_Y + \sigma_r} \le k \le 1)$$

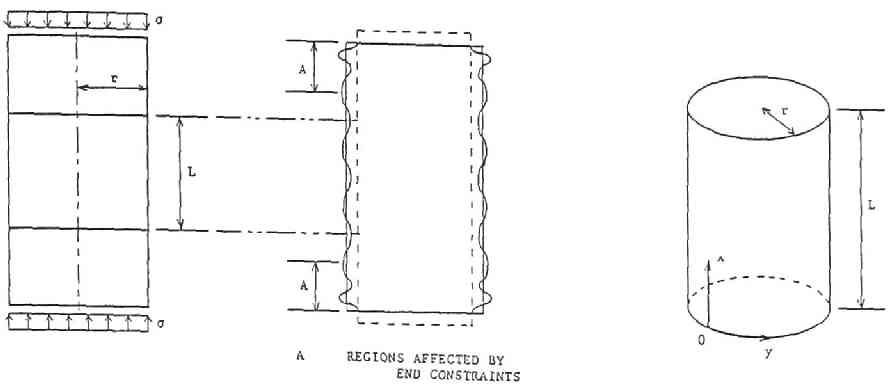

Fig. 3.2.1 Cylindrical Shell Models.

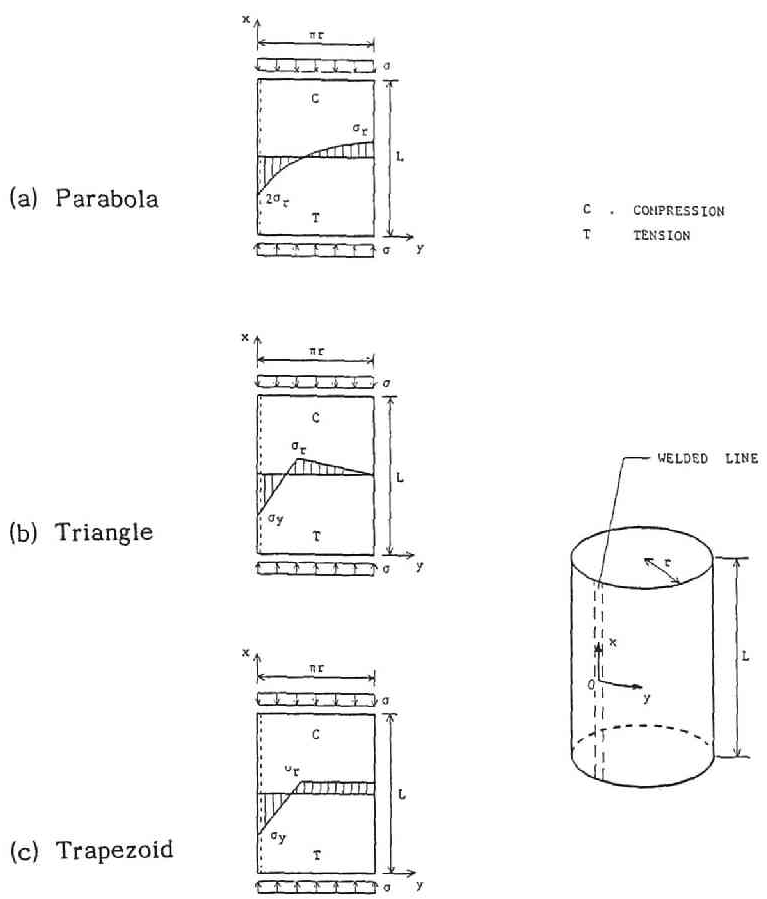

Fig. 3.2.2 Distributions of Residual Stresses of Compressed Cylindrical Shells.

$$\sigma = \sigma_Y - \frac{1}{2}\sigma_Y \frac{\sigma_Y + \sigma_r}{\sigma_r} k^2$$

$$\varepsilon = \frac{1}{E}\left[2\sigma_Y - \sigma_Y \frac{\sigma_Y + \sigma_r}{\sigma_r} k \right] \qquad \left(0 \le k \le \frac{\sigma_r}{\sigma_Y + \sigma_r} \right)$$

(3.2.1c)

and for trapezoidal distribution,

$$\sigma = \sigma_Y - \frac{(\sigma_Y + \sigma_r)^2}{4\sigma_r} k^2$$

$$\varepsilon = \frac{1}{E}\left[2\sigma_Y - \frac{(\sigma_Y + \sigma_r)^2}{2\sigma_r} k \right] \qquad \left(0 \le k \le \frac{2\sigma_r}{\sigma_Y + \sigma_r} \right) \qquad (3.2.1d)$$

where E and σ_Y refer to the elastic Young's modulus and the yielding stress of the material considered, respectively. Also, the factor k indicates the ratio of the elastic portion of the cross section to the total section of the compressed cylindrical shell, that is, it clearly denotes the so-called tangent modulus factor of the global axial behavior of the cylinder.

3.2.2 Elasto-plastic buckling strength

As mentioned above, the effects of supporting conditions of compressed cylinders are not taken into account in this dissertation. Then, two types of analytical procedures are performed with respect to the numbers of associated buckling modes. The buckling modes are assumed in the elastic and the elasto-plastic ranges as follows[8,9]:

1-mode analysis: only an asymmetric buckling mode

$$W = w_1 \sin \frac{m\pi x}{L} \cos \frac{ny}{r} \qquad (3.2.2a)$$

2-mode analysis: both an asymmetric and an axi-symmetric buckling modes

$$W = w_1 \sin \frac{m\pi x}{L} \cos \frac{ny}{r} + w_2 \cos \frac{\ell\pi x}{L} \qquad (3.2.2b)$$

in the coordinate system as shown in **Fig. 3.2.1.** Herein, W, L and r refer to the magnitude of the total out-of-plane deflection, the longitudinal length and the radius of the cylinder considered, respectively. Also, w_1 means the magnitude of the asymmetric buckling mode with m- and n-half wave numbers in the longitudinal and the circumferential directions, respectively, in both analyses. In the latter analysis, an axi-symmetric buckling mode is further considered, and the magnitude is designated as w_2 with ℓ-half wave number uniformly in the longitudinal axial direction. Moreover, the magnitudes of the corresponding initial out-of-plane deflections to W, w_1 and w_2 are denoted as W_o, w_{o1} and w_{o2}, respectively.

From the classical Donnell's equations of equilibrium and the classical orthotropic theory, modified fundamental equations of equilibrium in the elasto-plastic range can be written as

$$\nabla^4 F + E_s t \left[\frac{1}{r} \frac{\partial^2 W}{\partial x^2} + \frac{\partial^2 W}{\partial x^2} \frac{\partial^2 W}{\partial y^2} - \left(\frac{\partial^2 W}{\partial x \partial y} \right)^2 \right.$$

$$\left. + \frac{\partial^2 W}{\partial x^2} \frac{\partial^2 W_o}{\partial y^2} + \frac{\partial^2 W_o}{\partial x^2} \frac{\partial^2 W}{\partial y^2} - 2 \left(\frac{\partial^2 W}{\partial x \partial y} \right) \left(\frac{\partial^2 W_o}{\partial x \partial y} \right) \right] = 0 \qquad (3.2.3a)$$

and

$$\frac{D_e}{t} \nabla_p^4 W - \frac{1}{t} \left[\frac{1}{r} \frac{\partial^2 F}{\partial x^2} + \frac{\partial^2 F}{\partial x^2} \frac{\partial^2 (W + W_o)}{\partial y^2} \right.$$

$$\left. - 2 \frac{\partial^2 F}{\partial x \partial y} \frac{\partial^2 (W + W_o)}{\partial x \partial y} + \frac{\partial^2 F}{\partial y^2} \frac{\partial^2 (W + W_o)}{\partial x^2} \right] = 0 \qquad (3.2.3b)$$

where

$$\nabla^4 F = \frac{\partial^4 F}{\partial x^4} + 2 \frac{\partial^4 F}{\partial x^2 \partial y^2} + \frac{\partial^4 F}{\partial y^4} \quad , \quad D_e = \frac{E t^3}{12(1 - \nu^2)} \quad ,$$

$$\nabla_p^4 W = k_1 \frac{\partial^4 W}{\partial x^4} + 2 (k_2 + 2k_4) \frac{\partial^4 W}{\partial x^2 \partial y^2} + k_3 \frac{\partial^4 W}{\partial y^4}$$

and F, ν, t and k_j (j=1,2,3,4) refer to a proper stress function, the Poisson's ratio, the thickness and the constants to designate flexural and torsional rigidities of the cylinder in the elasto-plastic range. For examples, using the Bleich's theory[22], the factors k_j follow

$$k_1 = \tau, \quad k_2 = \nu \sqrt{\tau}, \quad k_3 = 1 \quad \text{and} \quad k_4 = \frac{1 - \nu}{2} \sqrt{\tau} \qquad (3.2.4)$$

where τ refer to the tangent modulus of the cylinder.

Upon substitution of W in Eq. (3.2.2a) or (3.2.2b) into Eqs. (3.2.3) and through the Galerkin's method, the elasto-plastic buckling stress σ_{cr} can be obtained in each analysis:

1-mode analysis: The elasto-plastic buckling stress is

$$\tilde{\sigma}_{cr1} = f^c \tilde{\sigma}_E \qquad (3.2.5a)$$

where

$$\tilde{\sigma}_{cr1} = \frac{\sigma_{cr1}}{\sigma_Y} \quad , \quad \tilde{\sigma}_E = \frac{\sigma_E}{\sigma_Y} = \frac{1}{R^2} \quad , \quad \sigma_E = \frac{E}{\sqrt{3(1 - \nu^2)}} \frac{t}{r}$$

$$R = \sqrt{\frac{r}{t} \frac{\sigma_Y}{E} \sqrt{3(1 - \nu^2)}} \quad , \quad f^c = \frac{\sqrt{k_c} + 1}{2} \sqrt{\frac{E_s}{E}}$$

and

$$\tilde{\sigma}_{cr} = \tilde{\sigma}_{cr1}$$

with the square asymmetric buckling mode:

$$(\frac{m\pi}{L})^2 = (\frac{n}{r})^2 = \frac{\sqrt{3(1-\nu^2)}}{tr} \frac{1}{\sqrt{k_c + 1}} \sqrt{\frac{E_s}{E}} \qquad (3.2.5b)$$

in which, σ_E and R refer to the fundamental Euler buckling stress and the generalized radius-thickness ratio for the compressed cylindrical shell, respectively.

In order to consider the effect of residual stress on the elasto-plastic buckling stress σ_{cr}, the Bleich's factor τ in Eq. (3.2.4) is herein taken to be equal to the tangent modulus k in Eq. (3.2.1). Then, in Eq. (3.2.5a), k_c means the critical value of the factor k, evaluated at the elasto-plastic buckling point. Moreover, f^c refer to the factor being the ratio of the elasto-plastic buckling stress to the elastic Euler buckling stress, so as to provide the unified expression of $\tilde{\sigma}_{cr}$, similarly to the cases of columns, beams and plates.

2-mode analysis: The elasto-plastic buckling stress $\tilde{\sigma}_{cr1}$ for the asymmetric mode of buckling can be previously obtained by Eq. (3.2.5). Furthermore, for the axi-symmetric mode of buckling, the elasto-plastic buckling stress $\tilde{\sigma}_{cr2}$ is independently determined by

$$\left.\begin{aligned} \tilde{\sigma}_{cr2} &= f_2^c \tilde{\sigma}_E \\ \text{where} \quad f_2^c &= \sqrt{k_c}\sqrt{\frac{E_s}{E}}, \qquad \tilde{\sigma}_{cr2} = \frac{\sigma_{cr2}}{\sigma_Y} \end{aligned}\right\} \qquad (3.2.6a)$$

with the axi-symmetric buckling mode:

$$(\frac{\ell\pi}{L})^2 = \frac{2\sqrt{3(1-\nu^2)}}{\sqrt{k_c}\, t\, r} \sqrt{\frac{E_s}{E}} \qquad \text{at} \quad \frac{\ell\pi}{L} = 2(\frac{m\pi}{L}) \qquad (3.2.6b)$$

However, taking into account the interactive behaviors of both asymmetric and axi-symmetric modes, the form of the elasto-plastic buckling mode is taken to be

$$(\frac{\ell\pi}{L})^2 = \frac{2\sqrt{3(1-\nu^2)}}{\sqrt{k_c}\, t\, r} \sqrt{\frac{E_s}{E}} \qquad \text{and} \quad \frac{\ell\pi}{L} = 2(\frac{m\pi}{L}) = 2(\frac{n}{r}) \qquad (3.2.6c)$$

This buckling mode means the interaction of both the square asymmetric mode w_1 and the axi-symmetric mode w_2 with twice as half-wave lengths as w_1.

Therefore, the elasto-plastic buckling stresses, $\tilde{\sigma}_{cr1}$ and $\tilde{\sigma}_{cr2}$, for the asymmetric and the axi-symmetric bucklings of compressed cylindrical shells, can be rewritten as

$$\tilde{\sigma}_{cr1} = f_1^c \tilde{\sigma}_E \quad \text{and} \quad \tilde{\sigma}_{cr2} = f_2^c \tilde{\sigma}_E \tag{3.2.7}$$

where

$$\tilde{\sigma}_{cr1} = \frac{\sigma_{cr1}}{\sigma_Y} , \quad \tilde{\sigma}_{cr2} = \frac{\sigma_{cr2}}{\sigma_Y} , \quad f_1^c = \beta f_2^c ,$$

$$f_2^c = \sqrt{k_c}\sqrt{\frac{E_s}{E}} , \quad \beta = \frac{(\sqrt{k_c}+1)^2}{8k^c} + \frac{1}{2} = \frac{\tilde{\sigma}_{cr1}}{\tilde{\sigma}_{cr2}}$$

Then, since $0 < k_c \leq 1$, $\beta \geq 1$. In this chapter, the least elasto-plastic buckling stress $\tilde{\sigma}_{cr}$ is taken to be $\tilde{\sigma}_{cr2}$ for the axi-symmetric mode w_2 of buckling, considering the compound characteristics together with the asymmetric mode w_1. It is needless to say that in Eq. (3.2.7) $\tilde{\sigma}_{cr2}$ is equal to $\tilde{\sigma}_{cr1}$ when $\beta = 1$, i.e., $k_c = 1$ in the purely elastic range. Then, the complete compound bifurcations for two modes may occur at the elastic buckling point.

3.2.3 Postbuckling path

Furthermore, substituting the elasto-plastic buckling modes in Eq. (3.2.2) into the fundamental equations in Eq. (3.2.3), the elasto-plastic postbuckling equilibrium paths can be also obtained:

1-mode analysis: The elasto-plastic postbuckling equilibrium equation is

$$-\frac{\alpha_s}{2}x^2 + (1-\lambda)x - \lambda\varepsilon_1 = 0 \tag{3.2.8}$$

where

$$\alpha_s \equiv \frac{10}{3\pi^2}\frac{4}{\sqrt{k_c}+1}\sqrt{3(1-\nu^2)}\sqrt{\frac{E_s}{E}} , \quad \lambda \equiv \frac{\tilde{\sigma}}{\tilde{\sigma}_{cr}} , \quad \tilde{\sigma} \equiv \frac{\sigma}{\sigma_Y} ,$$

$$\tilde{\sigma}_{cr} = \tilde{\sigma}_{cr1} , \quad x = \frac{w_1}{t} , \quad \varepsilon_1 = \frac{w_{01}}{t}$$

Herein, an **elastic** pseudo-potential energy A near the **elasto-plastic** buckling point can be defined so that its equilibrium is determined by Eq. (3.2.8):

$$A = -\frac{\alpha_s}{6}x^3 + \frac{1}{2}(1-\lambda)x^2 - \lambda\varepsilon_1 x \tag{3.2.9}$$

It is clearly found that the potential is topologically equivalent to the universal unfolding of the **fold** catastrophe by Thom, and Eq. (3.2.8) or (3.2.9) presents the imperfection sensitivity curve characterized by the well-known 1/2-power rule[23].

2-mode analysis: An **elastic** pseudo-potential energy A, defining two fundamental equilibrium equations with respect to two modes from Eq. (3.2.3), is written

as

$$A = \frac{1}{16}(\beta - \lambda)x^2 - \frac{1}{8}\lambda x\varepsilon_1 + \frac{1}{2}(1-\lambda)y^2 - \lambda y\varepsilon_2 + \alpha'_s x^2 y \tag{3.2.10a}$$

and equilibrium equations

$$\frac{1}{8}(\beta - \lambda)x - \frac{1}{8}\lambda\varepsilon_1 + 2\alpha'_s x y = 0 \tag{3.2.10b}$$

$$(1-\lambda)y - \lambda\varepsilon_2 + \alpha'_s x^2 = 0 \tag{3.2.10c}$$

where

$$\beta \equiv \frac{\tilde{\sigma}_{cr1}}{\tilde{\sigma}_{cr}} = \frac{(\sqrt{k_c}+1)^2}{8k_c} + \frac{1}{2}\ , \qquad \lambda \equiv \frac{\tilde{\sigma}}{\tilde{\sigma}_{cr}}\ , \qquad \tilde{\sigma}_{cr} = \tilde{\sigma}_{cr2}$$

$$\alpha'_s \equiv \frac{3\sqrt{3(1-\nu^2)}}{32\sqrt{k_c}}\sqrt{\frac{E_s}{E}}\ , \quad x = \frac{w_1}{t}\ , \quad \varepsilon_1 = \frac{w_{o1}}{t}\ , \quad y = \frac{w_2}{t}\ , \quad \varepsilon_2 = \frac{w_{o2}}{t}$$

and the corresponding buckling mode is given by Eq. (3.2.6c). The potential is trancated up to the 3rd-order terms of the modes, and yields the incomplete **parabolic umbilic** catastrophe with the paraclinal bifurcation between the hyperbolic umbilic catastrophe with the homeoclinal bifurcation and the elliptic umbilic catastrophe with the anticlinal bifurcation. The elasto- plastic and the elastic bucklings correspond to the near-coincident and completely simultaneous bifurcations concerened, respectively.

3.2.4 Ultimate strength

The elasto-plastic ultimate strength of compressed cylindrical shells is obtained directly from the singularity of the "Hessian" matrix of the **elastic** pseudo-potential energy with considerations of the elasto-plastic characteristics.

1-mode analysis: Both Eq. (3.2.8) and its derivative with respect to x leads to the singular condition of equilibrium surface, and then the load-carrying capacity λ_m in the elasto-plastic range can be explicitly expressed by

$$\lambda_m = 1 + \alpha_s\varepsilon_1 - \sqrt{2\alpha_s\varepsilon_1(1 + \frac{1}{2}\alpha_s\varepsilon_1)} \tag{3.2.11}$$

where

$$\lambda_m \equiv \frac{\tilde{\sigma}_m}{\tilde{\sigma}_{cr}}\ , \qquad \tilde{\sigma}_m \equiv \frac{\sigma_m}{\sigma_Y}$$

The significant factor α_s is specified in Eq. (3.2.8), and corresponds to the slope factor α^* of the similar expression of ultimate strength previously in Eq. (1.2.8) or (2.2.21) of this PART III.

2-mode analysis: Solving simultaneously the nonlinear process of Eqs. (3.2.10 b,c) and the Hessian (their derivatives with respect to the x and y), the elasto-plastic ultimate strength formula λ_m can be obtained as:

$$\frac{16}{3\sqrt{6}\,\alpha'_s}\left[\,2\,\alpha'_s\lambda_m\varepsilon_2+\frac{1}{8}(1-\lambda_m)(\beta-\lambda_m)\right]^{-\frac{3}{2}}=\lambda_m(1-\lambda_m)\varepsilon_1 \tag{3.2.12a}$$

where

$$\lambda_m=\frac{\tilde{\sigma}_m}{\tilde{\sigma}_{cr}}\quad,\quad \tilde{\sigma}_m=\frac{\sigma_m}{\sigma_Y}$$

As special cases,

$$\varepsilon_1=\frac{1}{6\sqrt{3}\alpha'_s}\,\frac{(\beta-\lambda_m)\sqrt{(1-\lambda_m)(\beta-\lambda_m)}}{\lambda_m}\qquad(\varepsilon_2=0) \tag{3.2.12b}$$

$$\varepsilon_2=\frac{-1}{16\alpha'_s}\,\frac{(1-\lambda_m)(\beta-\lambda_m)}{\lambda_m}\qquad(\varepsilon_1=0) \tag{3.2.12c}$$

In the purely elastic range, apparently, Eq. (3.2.12c) is identically equal to the Koiter's imperfection sensitivity formula with finite axi-symmetric mode of initial deflections for compressed cylinders[8](See, **Fig. 3.2.3**).

Hence, for a prescribed generalized radius-thickness ratio R, the elasto-plastic ultimate strength can be obtained by Eq. (3.2.11) with the asymmetric mode of buckling, or by Eq. (3.2.12) with both the asymmetric and axi-symmetric modes.

3.2.5 Modification of imperfection

The concept of the **equivalent initial imperfection** is also adopted herein, similarly to the cases of columns, beams, plate panels and stiffened plates[16-20]. The form is the unified expression as

$$\varepsilon_i^*=\mu(R)\,\varepsilon_i\qquad(i=1\text{ or }i=1,2) \tag{3.2.13}$$

where ε_i^* and ε_i denote the equivalent and the original initial deflections, non-dimensionalized by the shell-thickness. Taking into account many experimental results and the ECCS strength design curves, the form of $\mu(R)$ may be expressed by

$$\mu(R)=\mu_c\left(\frac{R}{R_p}\right)^{\beta} \tag{3.2.14}$$

where

$$\mu_c=1\quad,\quad \beta=2\left(1-\frac{R}{R_p}\right)$$

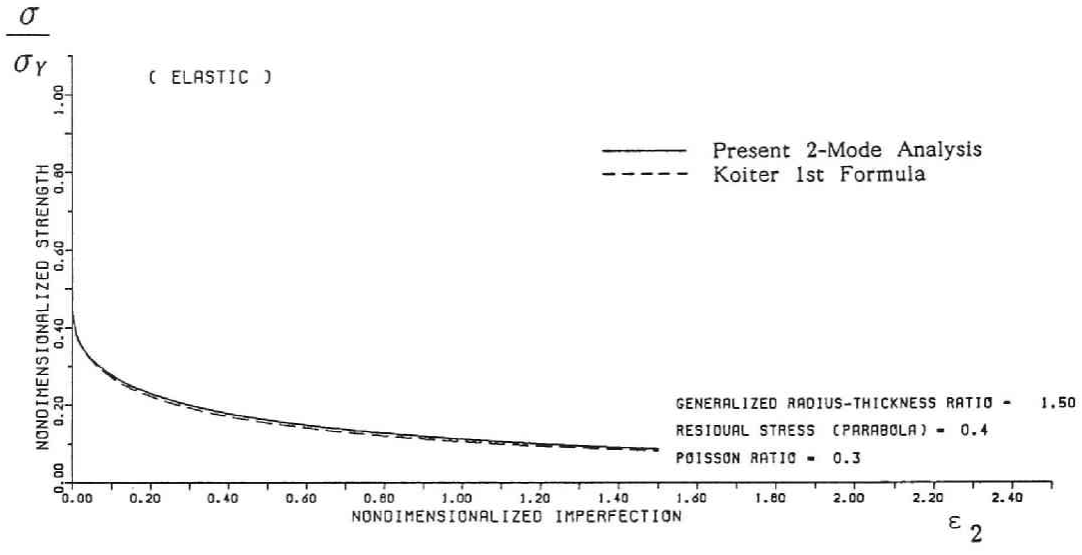

Fig. 3.2.3 **Typical Imperfection Sensitivity Curves in Elastic Range. Compared with the Koiter's Curve. 2-Mode Analysis.**

R = 1.50 $\varepsilon_1 = 0$

and R_p refers to the slenderness value R at which the ordinary buckling point changes from the elasto-plastic to purely elastic.

Finally, the imperfection sensitivity or the load-carrying capacity can be determined by Eq. (3.2.11) or Eqs. (3.2.12) with the equivalent imperfections of Eq. (3.2.13) and (3.2.14)[16-20].

3.3 Numerical Illustrations

3.3.1 General remarks

Several numerical demonstrations are provided on the elasto-plastic strength of the compressed cylindrical shells. The type of residual stress distribution in the circumferential direction of the cylinder is assumed to be in either parabolic, triangle or trapezoidal form as shown in **Figs. 3.2.2**(a)-(c). The magnitude of initial out-of-plane deflection is also assumed to be $\ell_r/100$ with both asymmetric and axi-symmetric modes. The value is prescribed on the basis of the maximum limitation allowed by the ECCS Recommendations, where ℓ_r refers to the gauge length specified as $\ell_r = 4\sqrt{rt}$[24]. Therefore, the magnitudes of the non-dimensionalized initial deflections can be obtained by a constant ε'_{max} as follows:

$$\varepsilon_i = \frac{w_{oi}}{t} = \frac{w_{oi}}{\ell_r}\frac{\ell_r}{t} = \varepsilon'_{max}\sqrt{\frac{r}{t}} = \varepsilon_{max} \qquad (i=1 \text{ or } i=1,2) \tag{3.3.1}$$

where

$$\varepsilon'_{max} = 0.04 \quad \text{and} \quad \frac{w_{oi}}{\ell_r} = \frac{1}{100} \qquad (i=1 \text{ or } i=1,2)$$

3.3.2 One-mode analysis

Figs. 3.3.1(a), (b) and (c) show the present ultimate strength curves in Eq. (3.2.11) with the maximum compressive residual stress $\sigma_r = 0.4\,\sigma_Y$ with the parabolic, triangle and trapezoidal distributions, respectively. In these figures, the abscissa is the generalized radius-thickness ratio R; while the non-dimensionalized ultimate strength by the yielding stress σ_Y is chosen as the ordinate. As shown herein, the results of the strength predictions by the present analysis is compared with the well-known ECCS Recommendation curves: the upper curve at the factor $\alpha = 1$, and the lower at $\alpha = \alpha_o$ for purely compressed cylinders, where the factor α is specified by the ECCS in terms of the generalized radius-thickness ratio R[24]. These notations are adopted in the 2-mode analysis as below. Especially, in the 1-mode analysis, the initial deflection half of the ECCS limiting value is also demonstrated in these figures.

Herein, at about R=0.66 in **Figs. 3.3.1**, the present results may suddenly disappear since the corresponding elasto-plastic buckling stress σ_{cr} reaches the yielding stress σ_Y. For smaller R of the minimum value, the elasto-plastic ultimate strength fails to be predicted in the 1-mode analysis. However, it is needless to say that the results are in good correlation with the lower ECCS curve for the larger values of R in the elasto-plastic and the elastic bucklings. The effect of types of residual stress distributions assumed herein may be found to be insignificant quantitatively throughout the ranges of the generalized radius-

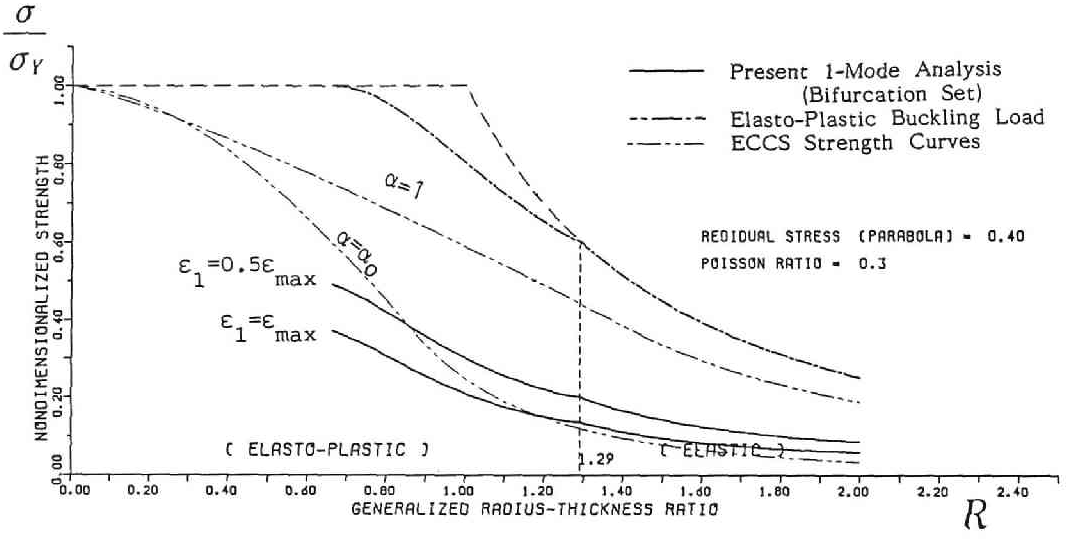

Fig. 3.3.1(a) Ultimate Strength Curves of Compressed Cylindrical Shells with Parabolic Residual Stress. 1-Mode Analysis. σ_r 0.4 σ_Y

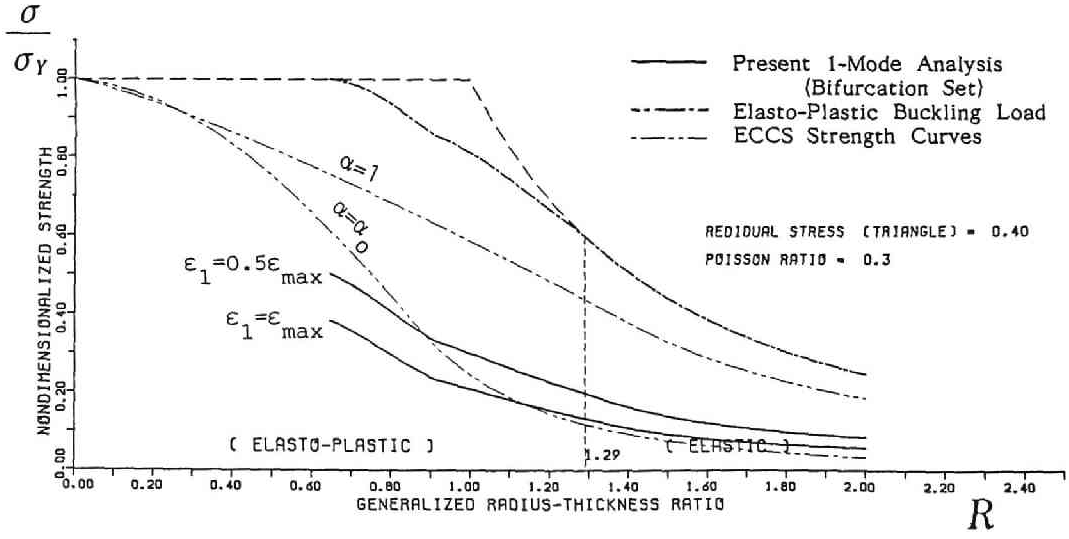

Fig. 3.3.1(b) Ultimate Strength Curves of Compressed Cylindrical Shells with Triangle Residual Stress. 1-Mode Analysis. σ_r 0.4 σ_Y

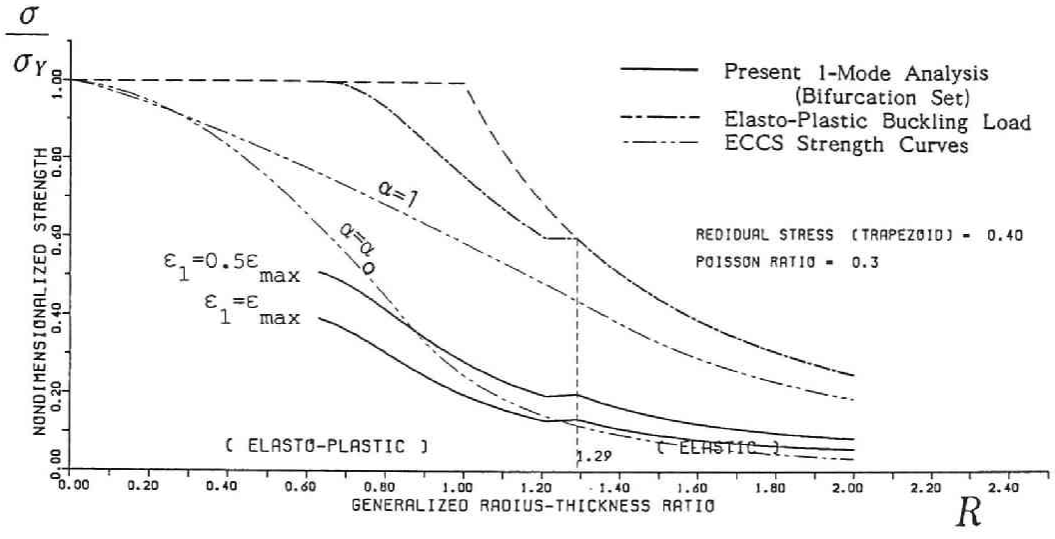

Fig. 3.3.1(c) Ultimate Strength Curves of Compressed Cylindrical Shells with Trapezoidal Residual Stress. 1-Mode Analysis. $\sigma_r = 0.4\ \sigma_Y$

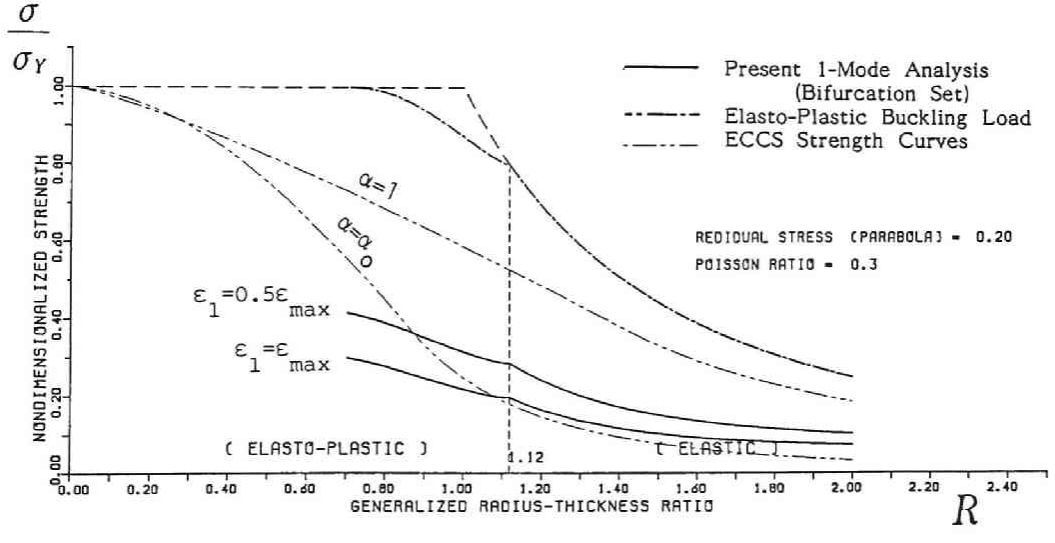

Fig. 3.3.2 Ultimate Strength Curves of Compressed Cylindrical Shells with Parabolic Residual Stress. 1-Mode Analysis. $\sigma_r = 0.2\ \sigma_Y$

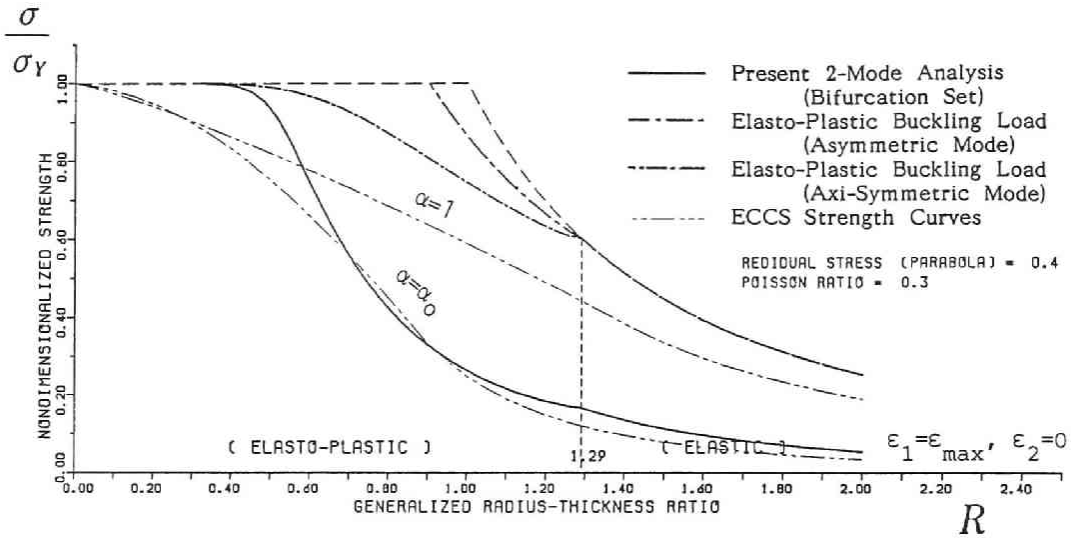

Fig. 3.3.3(a) Ultimate Strength Curves of Compressed Cylindrical Shells with Parabolic Residual Stress for only Asymmetric Initial Deflections. 2-Mode Analysis. σ_r 0.4 σ_Y

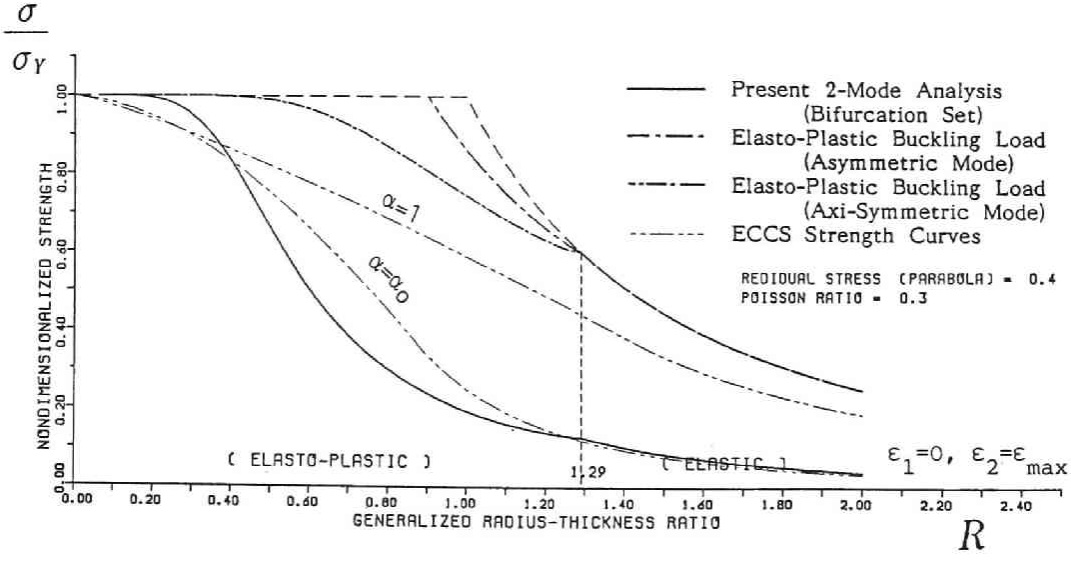

Fig. 3.3.3(b) Ultimate Strength Curves of Compressed Cylindrical Shells with Parabolic Residual Stress for only Axi-Symmetric Initial Deflections. 2-Mode Analysis. σ_r = 0.4 σ_Y

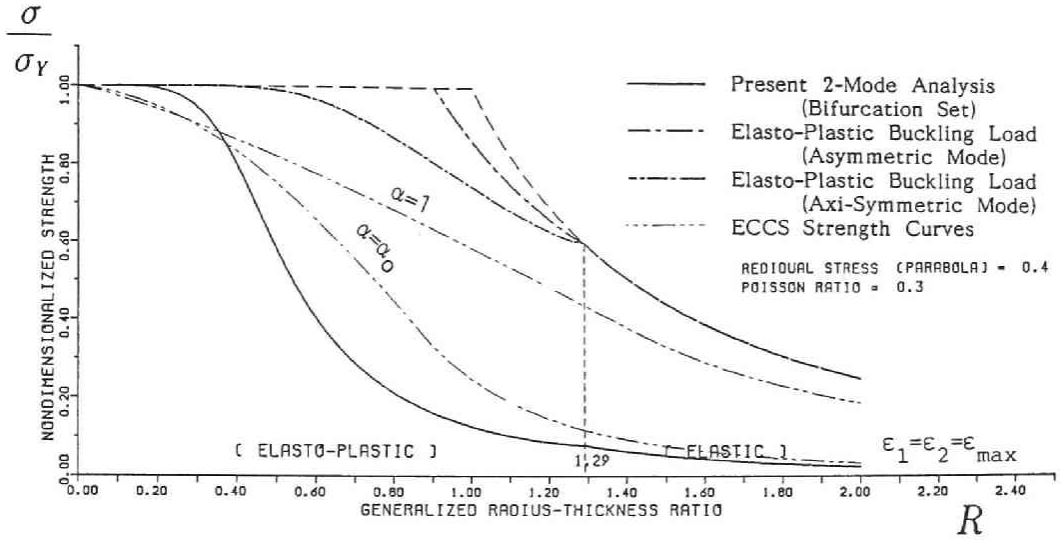

Fig. 3.3.3(c) Ultimate Strength Curves of Compressed Cylindrical Shells with Parabolic Residual Stress for both Asymmetric and Axi-Symmetric Initial Deflections. 2-Mode Analysis. $\sigma_r = 0.4\ \sigma_Y$

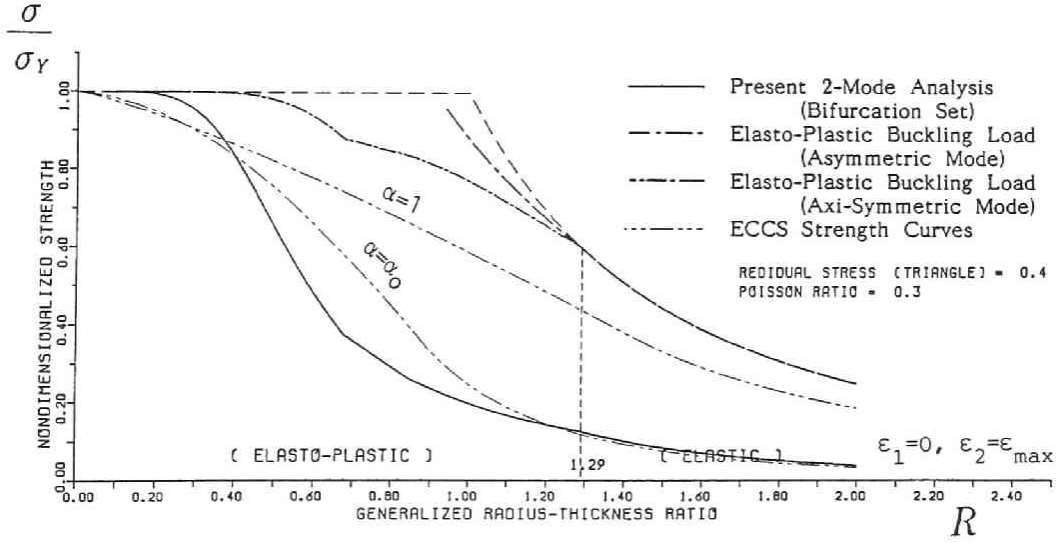

Fig. 3.3.4 Ultimate Strength Curves of Compressed Cylindrical Shells with Triangle Residual Stress for only Axi-Symmetric Initial Deflections. 2-Mode Analysis. $\sigma_r = 0.4\ \sigma_Y$

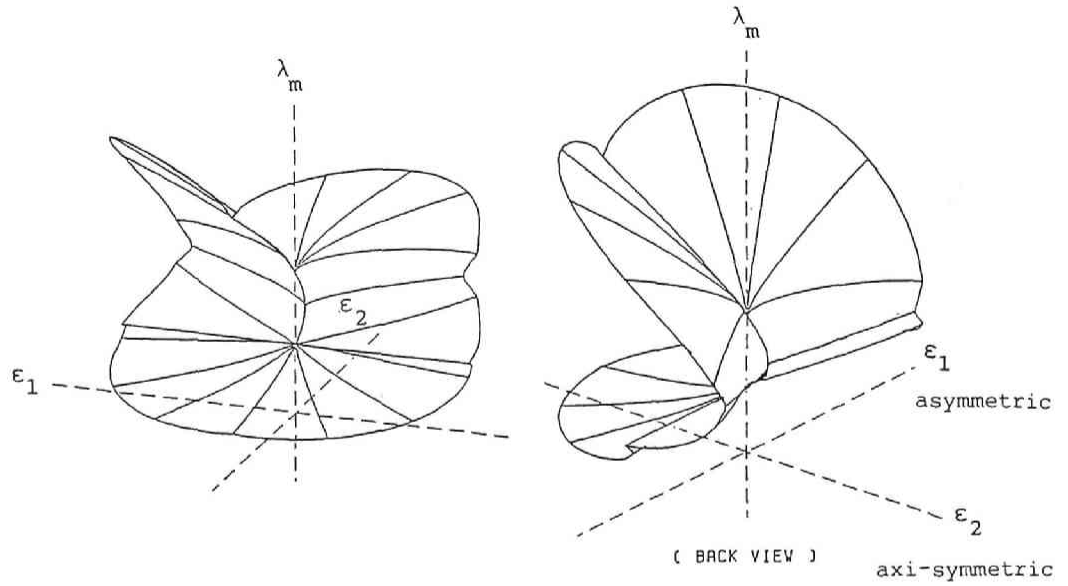

Fig. 3.3.5 **Typical Imperfection Sensitivity Surfaces in Elasto-Plastic Range. 2-Mode Analysis.** R = 0.58

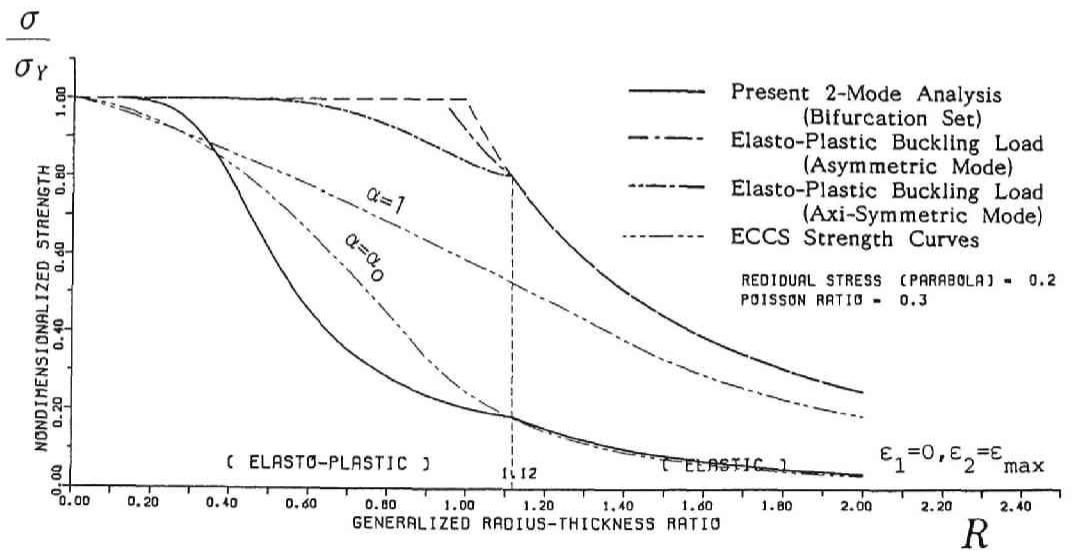

Fig. 3.3.6 **Ultimate Strength Curves of Compressed Cylindrical Shells with Parabolic Residual Stress for only Axi-Symmetric Initial Deflections. 2-Mode Analysis.** $\sigma_r = 0.2\ \sigma_Y$

thickness ratio R, similarly to the cases of columns, beams, plate panels and stiffened plates.

Also, **Fig. 3.3.2** shows the similar results with the parabolic residual stress $\sigma_r = 0.2\,\sigma_Y$, and the results become unreasonable in the smaller values of R than 0.7.

3.3.3 Two-mode analysis

Figs. 3.3.3 show the present ultimate strength curves in Eq. (3.3.12), with the maximum compressive residual stress $\sigma_r = 0.4\,\sigma_Y$ of parabolic distribution. **Fig. 3.3.3**(a), (b) and (c) illustrate the results for three types of initial deflection modes; (a) $\varepsilon_1 = \varepsilon_{max}$, $\varepsilon_2 = 0$ (only asymmetric mode), (b) $\varepsilon_1 = 0$, $\varepsilon_2 = \varepsilon_{max}$ (only axi-symmetric mode) and (c) $\varepsilon_1 = \varepsilon_2 = \varepsilon_{max}$ (both modes), respectively. In which, $\varepsilon'_{max} = 0.04$ in Eq. (3.3.1).

In the cases of other distributions of residual stresses, the similar results can be obtained. For examples, **Fig. 3.3.4** shows the results for the triangle residual stress $\sigma_r = 0.4\,\sigma_Y$ and the axi-symmetric initial deflection: $\varepsilon_1 = 0$ and $\varepsilon_2 = \varepsilon_{max}$. Of course, the difference of types of residual stress distributions may affect insignificantly the ultimate strength so far as they are assumed herein.

From these results, it seems that, for intermediate values of the generalized radius-thickness ratio R in the elasto-plastic range, the ultimate strength is significantly more sensitive to the axi-symmetric mode ε_2 of initial deflections than to the asymmetric mode ε_1. Then, this sensitivity is visually confirmed by three-dimensional drawings of imperfection sensitivity surfaces. In the load-carrying capacity λ_m initial deflections (ε_1, ε_2) space, the ultimate strength can be easily represented in terms of the bifurcation sets of the truncated **parabolic umbilic** catastrophe in Eq. (3.2.12) from Eq. (3.2.10)(See, **Figs. 3.3.5**). Furthermore, **Fig. 3.3.6** shows the similar results with the parabolic residual stress $\sigma_r = 0.2\,\sigma_Y$ and the axi-symmetric initial deflections: $\varepsilon_1 = 0$, $\varepsilon_2 = \varepsilon_{max}$.

3.4 Conclusions

A simplified unified approach to the ultimate strength of compressed cylindrical shells is proposed in the light of the catastrophe theory. The main conclusions are:

(1) The residual stresses and the initial deflections may affect the evaluation of the elasto-plastic buckling stress and the form of the explicit imperfection sensitivity formula, respectively.

(2) The inelastic ultimate strength of the cylinders may be explicitly determined in the form of the bifurcation sets, i.e., the imperfection sensitivity curves for the initial deflections considered.

(3) The imperfection sensitivity of compressed cylindrical shell can be directly derived from the singularity condition on the equilibrium surfaces through the **elastic** pseudo-potential energy with considerations of **elasto-plasticity** of the material, which is defined near the elasto-plastic buckling point.

(4) The initial deflections are modified and replaced by the **equivalent imperfections** proposed herein.

(5) The present approach involves two types of analyses; the one-mode analysis (only asymmetric mode) and the two-mode analysis (asymmetric and axi-symmetric modes).

(6) The 2-mode analysis considers the interaction of both modes, and is more sufficiently practice than the 1-mode analysis.

(7) The elasto-plastic buckling may occur for the axi-symmetric buckling mode with the square asymmetric mode, and provides the near-coincident bifurcation for the trancated **parabolic umbilic** catastrophe. In the elastic range, the present formula identically gives the complete simultaneous bucklings, and the imperfection sensitivity for the axi-symmetric mode is just equal to the Koiter's formula.

(8) The reduction of the strength is more greatly affected by the axi-symmetric mode of initial deflections than the asymmetric initial mode, so far as the buckling modes are concerned herein.

(9) The form of distribution of residual stress assumed herein may insignificantly affect the present results.

(10) The general philosophy adopted herein may also be applicable to other types of engineering structures such as rigid frames, arches and trusses as well as columns, beams, plate panels and stiffened plates.

Bibliographies of Chapter 3 in PART III

1) Brush,D.O. and B.O.Almroth, Buckling of Bars, Plates and Shells. McGraw-Hill, 1975.
2) Flüge,W., Die Stabilitat der Kreiszylinderschade, Ing-Arch, Vol. 3, pp. 463-506, 1932.
3) Donnell,L.H., Stability of Thin-Walled Tubes under Torsion. NACA Report No. 479, 1933.
4) Donnell,L.H., A new theory for the buckling of thin cylindrical shells under axial compression and bending. Transactions of American Society of Mechanical Engineers, Vol. 56, pp. 795-806, 1934.
5) von Kármán,Th. and H.-S.Tsien, The buckling of thin cylindrical shells under axial compression. Journal of Aeronautical Sciences. Vol. 8, pp. 303-312, 1941.
6) Donnell,L.H. and C.C.Wan, Effects of imperfections on buckling of thin cylinders and columns under axial compression. Journal of Applied Mechanics, Vol. 17, pp. 73-83, 1950.
7) Koiter,W.T., Over de Stabiliteit van het Elastishe Evenwicht. Thesis, Delft, 1945 (English translation: On the Stability of Elastic Equilibrium. NASA Technical Transactions, F10, 833, National Aeronautics and Space Administration, 1967 and Technical Report AFFDL-TR-70-25, Air Force Flight Dynamics Laboratory, 1970).
8) Koiter,W.T., The Effect of axisymmetric imperfections on the buckling of cylindrical shells under axial compression. Proceedings of the Koniklijke Nederlandse Akademie van Watenshappen, Ser. B, Vol. 66, pp. 265-279, 1963.

9) Arbocz,J. and C.D.Babcock, The effect of general imperfections on the buckling of cylindrical shells. Journal of Applied Mechanics, Vol. 36, pp. 28-38, 1969.
10) Hutchinson,J.W., R.C.Tennyson and D.B.Muggeridge, Effect of a local axi-symmetric imperfection on the buckling behavior of a circular cylindrical shell under axial compression. AIAA Journal, Vol. 9, pp. 48-52, 1971.
11) Hansen,J.S., Influence of general imperfections in axially loaded cylindrical shells. International Journal of Solids and Structures, Vol. 11, pp. 1223-1233, 1975.
12) Croll,J.G.A. and R.C.Batista, Explicit lower bounds for the buckling axially loaded cylinders. International Journal of Mechanical Sciences, Vol. 23, pp. 331-343, 1981.
13) Batterman,S.C., Plastic buckling of axially compressed shells. AIAA Journal, Vol. 3, pp. 316-325, 1965.
14) Hutchinson,J.W., Plastic Buckling. Advances in Applied Mechanics, Vol. 14, Academic Press, pp. 67-144, 1974.
15) Croll,J.G.A., Elasto-plastic buckling of pressure and axial loaded cylinders. Proceedings of the Institution of Civil Engineers, Part 2, Vol. 73, pp. 633-652, 1982.
16) Niwa,Y., E.Watanabe and H.Isami, A new approach to predict the strength of steel columns. Proceedings of the Japan Society of Civil Engineers, No. 341, pp. 13-21, 1984.
17) Niwa,Y., E.Watanabe, H.Isami and Y. Fukumori, A new approach to predict the strength of compressed steel plates. Proceedings of the Japan Society of Civil Engineers, No. 341, pp. 23-31, 1984.
18) Niwa,Y., E.Watanabe and S.Suzuki, A new approach to the elasto-plastic lateral buckling strength of beams. Proceedings of the Japan Society of Civil Engineers, Structural Engineering/Earthquake Engineering, Vol. 1, No. 1, pp. 41s-49s, 1984.
19) Niwa,Y., E.Watanabe and H.Isami, A new approach to predict the strength of compressed steel stiffened plates. Proceedings of the Japan Society of Civil Engineers, Structural Engineering/Earthquake Engineering, Vol. 2, No. 2, pp. 281s-290s, 1985.
20) Niwa,Y., E.Watanabe and H.Isami, A new unified approach to predict the strength of steel structures. Proceedings of National Theoretical and Applied Mechanics, Vol. 34, 1985 (printing).
21) Taniguchi,N., An Evaluation of the Load-Carrying Capacity of Compressed Cylindrical Shells. Thesis presented to the Faculty of Engineering of Kyoto University in partial fulfillment of the requirements for the degree of Master of Engineering, 1985(in Japanese).
22) Bleich,F., Buckling of Metal Structures. McGraw-Hill, 1952.
23) Thom,R., Structural Stability and Morphogenesis. Benjamin, 1975.
24) ECCS, European Recommendations for Steel Construction: Buckling of Shells, 2nd Edition. European Convention for Constructional Steelwork, Publication No. 29, 1983.

APPENDIX for PART III

AUTOMATED TESTING OF THIN-WALLED STEEL STRUCTURES UNDER REPETITIVE LOADING BY MICROCOMPUTER SYSTEM

A.1 General Remarks

Structural engineers have been facing many intricate problems like geometrically and materially nonlinear structural behaviors. For instance, the strength, stability and the ductility of structures under repetitive loadings have great attentions, especially from the aseismic view point. The ultimate strength of slender members, in particular, depends on the geometrical and material parameters of the members, and may be thought to be predicted in a unified manner if the magnitudes of initial imperfections are known[1,2,3]. The measurement of the initial imperfections is thus very important, and several studies on their distributions have been reported on the prototype members during the temporary assembly of bridge superstructures at workshops and experimental structural models. Moreover, these imperfections may grow progressively through elasto-plastic large deflections, and gradual adverse deterioration may result in during the stochastic loading process in the lifetime of structures. This is partly a reason why the experimental investigations are called for attention on the strength of structures under repeated loadings.

This APPENDIX presents a servo-controlled testing system using a single or plural microcomputer(s) as its core, and a technique is reported on the precise detection of the load-carrying capacity and the deteriorating properties of thin-walled steel structures under repetitive loading causing large elasto-plastic deformations. The system will be named as **CATS: C**omputer **A**ided **T**esting **S**ystem[4,5].

The testing system provided herein can be illustrated in **Fig. A.1.1** and can be characterized by the following capabilities:

(a) easy and efficient measurement of initial and residual deflections on the surfaces of the test specimen using movable displacement transducers,

(b) quick real-time acquisition and processing of large quantities of test data for the swift decision making on the continuously varying state of the test specimens,

(c) digital feedback control of the servo-controlled testing machine,

(d) real-time display of the performance of the specimen,

(e) efficient storage of the acquired data,

(f) transmission of data to a large computer center for further large-scale computation via intelligent TSS terminal,

(g) cooperative task carried by multi-computer system, namely, plural number of microcomputers connected by the GP-IB(General Purpose Interface Bus), and

(h) applications of independent loadings in bi-axial conditions.

From this figure, the system is seen to consist of three groups of **SERVO TESTING MACHINE GROUP, DATA ACQUISITION GROUP** and **MICROCOMPUTER GROUP.** Several interfaces on microcomputers are controlled independently in the BASIC language. The software includes the method for detecting the ultimate strength of the specimen, generation of pulse signals to the function generator of the servo testing machine for its digital feedback control, and the data acquisition.

A.2 Hardware of Testing System

A.2.1 Servo testing machine group

This group is a servo-controlled electrohydraulic closed-loop system applicable to bi-axial test of repetitive bending and uniaxial compression (See, **Fig. A.2.1**). It mainly consists of the power pack, hydraulic actuator and servo controllers. The actuator is operated through the servo controller according to the prescribed voltage from the function generator: It accepts two inputs, one being the command signal from the function generator, and the other being a system analog feedback signal of either load or stroke; while it generates one principle output, the control signal to the servovalve.

The function generator on the servo testing machine is an 8-bit microcomputer independently programmable up to 16 steps. In each step, either of the sine, triangle, ramp, or hold wave form can be selected. On the other hand, the function generator can be controlled externally by the microcomputer named as the master controller through the digital input-output interface.

A.2.2 Data acquisition group

The response of the specimen subjected to the servo-controlled load or stroke displacement is detected by the devices of this group. These data are processed in real time so that they can be used as the digital feedback data, recorded on the floppy disks, and displayed by each microcomputer. The group mainly consists of the following: displacement transducers, digital strain amplifiers, dynamic strain amplifiers, normal switch box, hold-type switch box, pen strip chart recorder, and oscilloscope.

The readings of strains and displacements of the specimen under loading are sensored and amplified by some dynamic strain amplifiers and a digital strain amplifier. For a successful digital feedback control, the real time and continuous data acquisition is necessary, and thus the dynamic strain amplifiers are suited for this purpose. Whereas the digital strain amplifier is used to obtain the spatial distribution of the displacements and the stain readings of the test specimen. The amplifier is connected by two microcomputers through the GP-IB [4-7].

A.2.3 Microcomputer group

This group has two microcomputers as its core, and plays the key role as the master and the slave system controllers of the testing system. **Fig. A.2.2** shows the control relationship of two microcomputers and their main flow charts. Both microcomputers are independently executed by appropriate softwares as discussed in the next section.

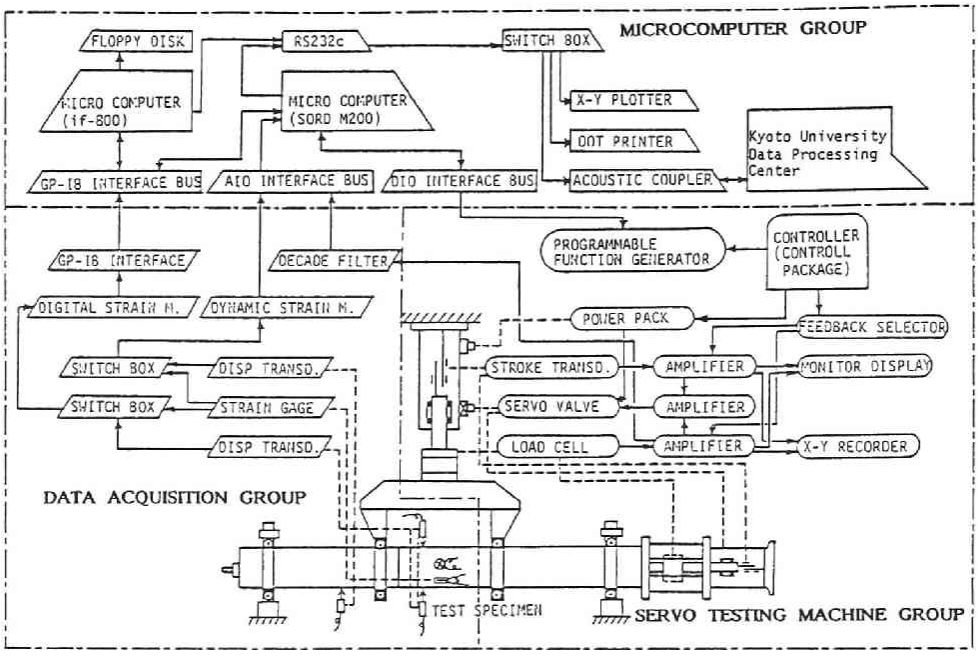

Fig. A.1.1 Automated Structural Testing System.

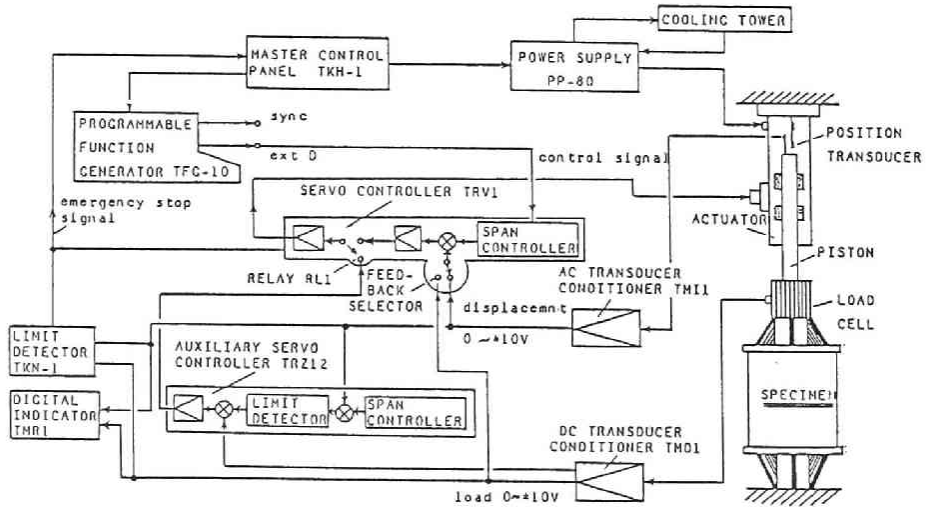

Fig. A.2.1 Servo-Controlled Hydraulic System.

One microcomputer is used as the master system controller so as to make a real-time, on-line control of servo-controlled testing system and is equipped with several interfaces: the Analog Input /Output (AIO) interface for the analog to digital transform, or vice versa; the Digital Input /Output (DIO) interface for the real-time control of the programmable function generator of the servo-controlled testing machine, and finally, the GP-IB for the digital data, its transmission and the control command to a slave microcomputer.

Another microcomputer is controlled as the slave system by the master controller through the GP-IB, and can be interrupted just before the execution of the subroutines: START, DISP, KLOAD and END, depending on each command signal as shown **Fig. A.2.2.** Then, the slave will execute the corresponding subroutine according to each command signal. At the same time, the master system controller independently controls the whole testing system. Also, the slave microcomputer stores a large amount of significant test data transmitted from the master controller through the GP-IB. Moreover, it also transmits a large amount of data to a large computer center via intelligent TSS terminal.

A.3 Software of Testing System

A.3.1 Testing procedures

Test specimens include stub columns with the cross sections of cruciforms, channels, cylindrical shells, and boxes with or without longitudinal stiffeners, which are subjected to uniform axial compression and tension. Furthermore, the box beam-columns are tested in repetitive bending under combined uniform axial compression as shown in **Fig. A.3.1.** Herein, details of the main softwares of these microcomputers are discussed on such box beam-columns for demonstrative purposes. **Fig. A.3.2** gives the setup of the software of the present testing system.

For a series of buckling tests of the box beam-columns under repetitive loadings, a single **loading cycle** corresponds to a sequence of a positive and a negative bending after measuring the initial deflections. The proposed testing procedures consists of (a) arrangement of the specimen, (b) adjustment and initialization of testing equipments, (c) application of uniaxial compression if necessary, (d) independent executions of both the master and the slave microcomputers in each BASIC language, (e) input several testing parameters to the master microcomputer, and (f) start of loading and a halt of loading after a half-loading cycle to get ready for (g) measuring the residual deflections.

A.3.2 Details of software

BASIC programs

Five BASIC programs: MAIN, START, DISP, PLOT and KLOAD are continuously executed on the master microcomputer, making use of the "CHAIN" command in Extended BASIC language, as its flow charts illustrated in **Fig. A.2.2.** Also, on the slave microcomputer, another testing program: BOX is independently executed and interrupted by the master system controller.

MAIN

This program is to form the trunk flow chart of the test and is chained

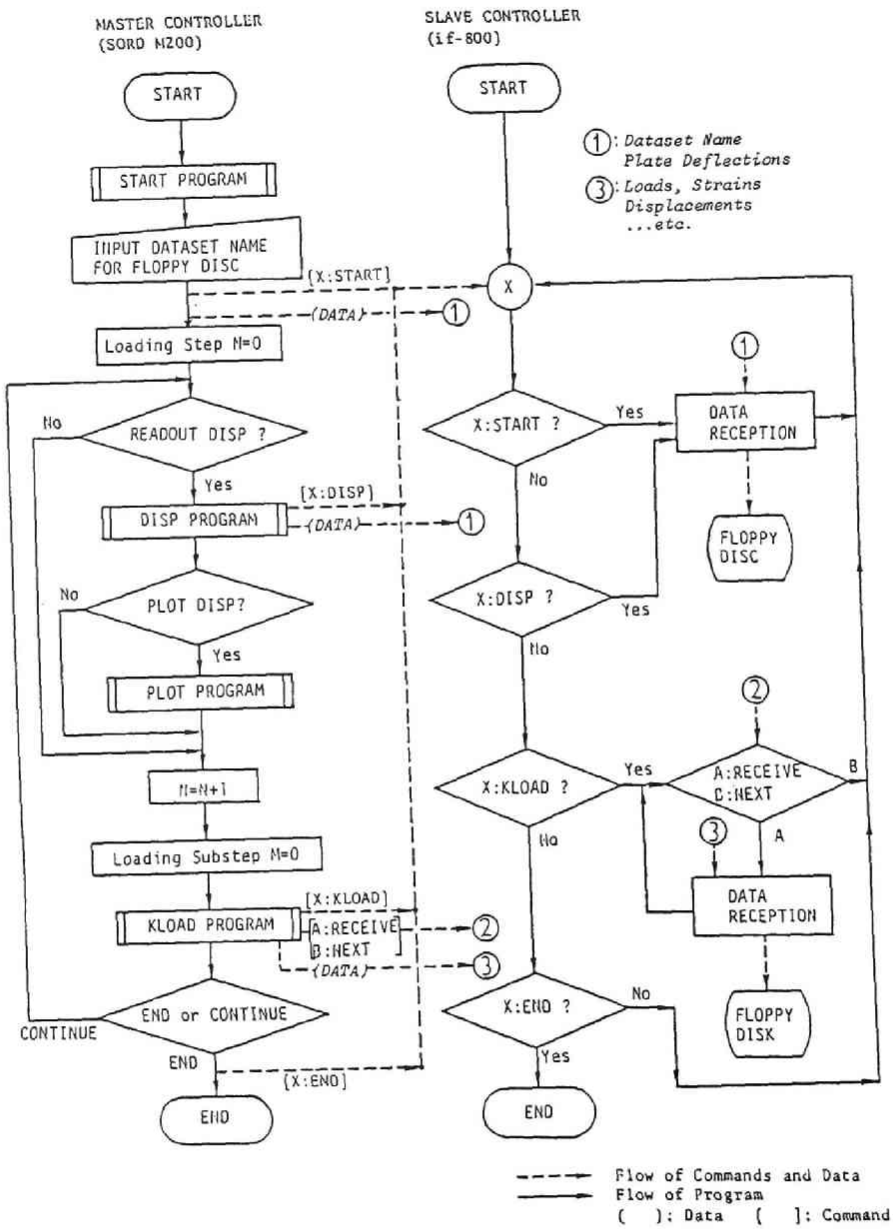

Fig. A.2.2 Relationship between Two Microcomputers.

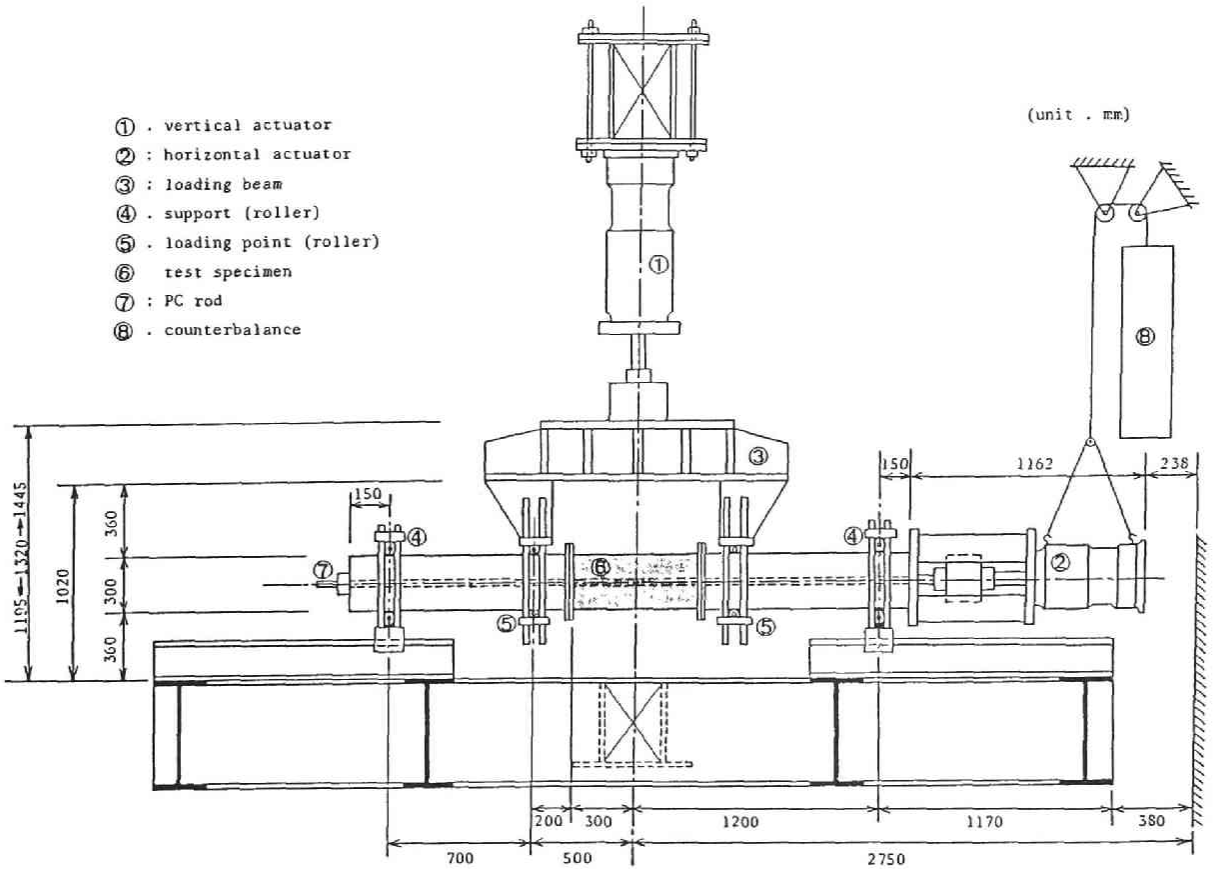

Fig. A.3.1 Test of Box Beam-Columns under Bi-Axial Loading.

with the others: START, DISP, PLOT and KLOAD. The right hand side of **Fig. A.2.2** or **Fig. A.3.3** shows the flow chart of the program.

START

This program is to input and initialize parameters after some confirmation to be ready for the test performance. The flow chart of the program is shown in **Fig. A.3.4.** In this figure, the "predicted maximum load" refers to the ideal load-carrying capacity of the specimen. The "control mode" refers to the type of control either by the load or the stroke displacement of the servo testing machine. Moreover, parameters for analog or digital data refer to those of AIO, or DIO, GP-IB interfaces, respectively.

The master system microcomputer interrupts the slave computer by the command "START" through the GP-IB. Then, these input data in the master microcomputer are transmitted to the slave computer through the GP-IB, and are stored in the floppy disks on the slave.

DISP

This program is to measure the displacements of the surfaces of the specimen, and the flow chart is illustrated in **Fig. A.3.5.** Several displacement transducers on the horizontally movable rig especially manufactured are connected with two microcomputers through the GP-IB of the digital strain amplifier and the hold-type switch box.

The master system microcomputer interrupts the slave computer by the command "DISP" through the GP-IB. Then, the measured digital data are transmitted from the master to the slave, and are stored in the floppy disks on the slave.

PLOT

This program is to draw two-dimensional distributions of the normalized displacements on the X-Y plotter. The flow chart is omitted.

KLOAD

This program is to select either loading or unloading, and to get both the analog and digital data through the AIO and GP-IB. The flow chart is illustrated in **Fig. A.3.6.**

In order to detect experimentally and automatically the ultimate strength of stub columns under compression and/or tension, two criteria of recognizing unloading is established: one being for sudden decrease of reaction load except for a causal erroneous reduction due to the action of the servo testing machine and the A/D converter on the AIO interface on the master system microcomputer in the lower range of the load; while another being for rapid and gradual change of the slope of the load-displacement curve considered[4]. If either of these criteria is satisfied during a test, then the servo testing machine is controlled and unloaded by the function generator through the DIO interface on the master system microcomputer.

On the other hand, in the case of the earthquake simulating tests of steel box beam-columns in repetitive bendings under uniform axial compression, the following unloading criterion is proposed[5]: The stroke displacement is controlled to

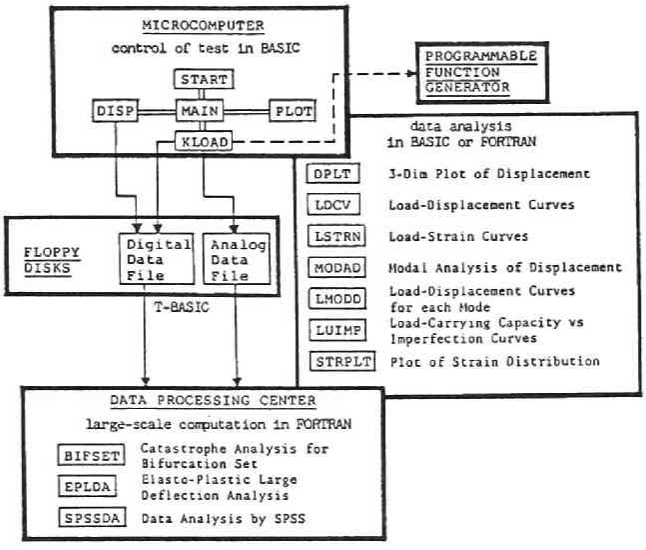

Fig. A.3.2 Software of the Testing System.

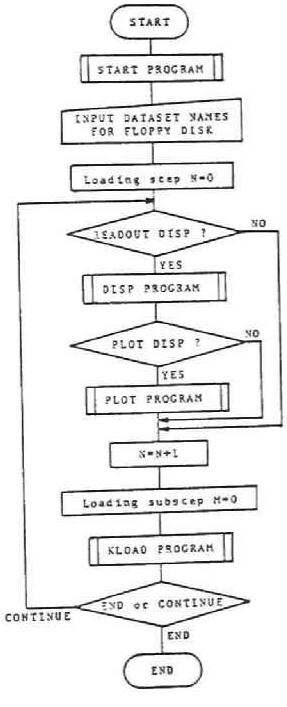

Fig. A.3.3 Flow Chart of MAIN.

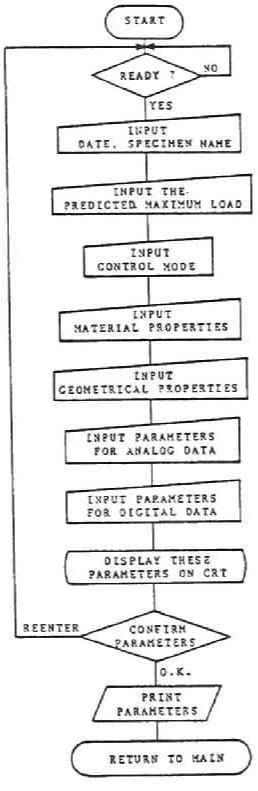

Fig. A.3.4 Flow Chart of START.

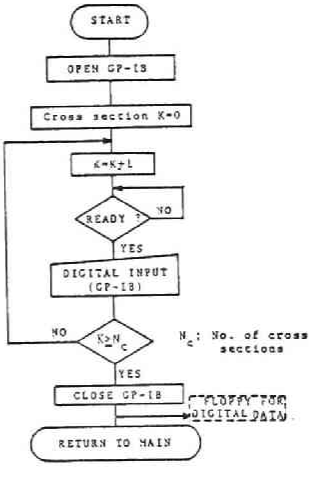

Fig. A.3.5 Flow Chart of DISP.

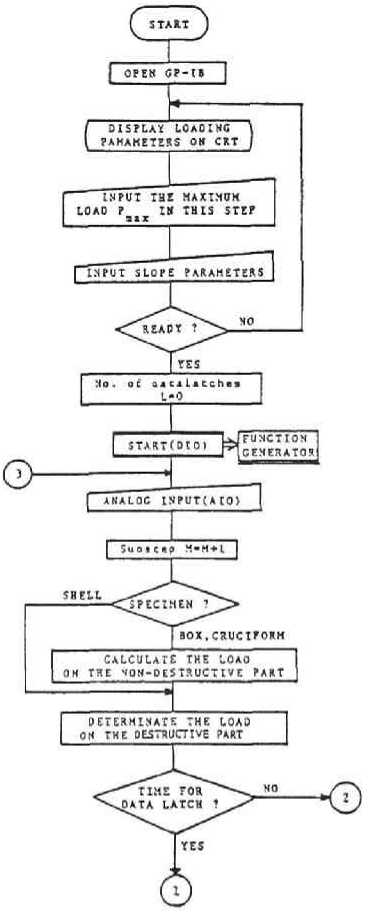

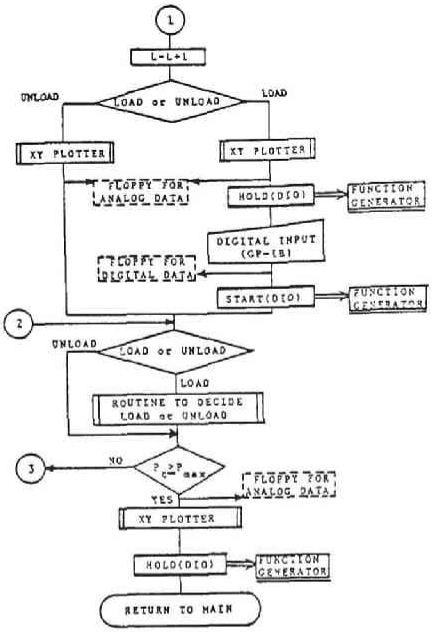

Fig. A.3.6 Flow Chart of KLOAD.

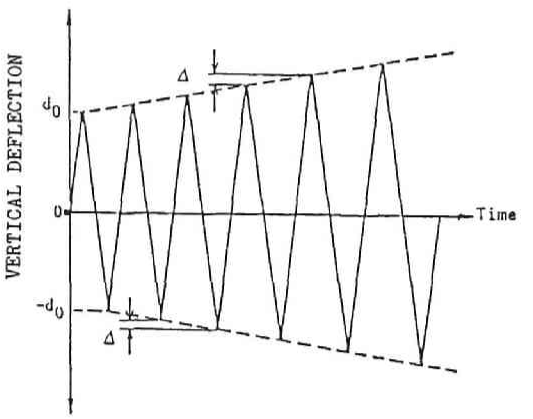

Fig. A.3.7 Sequential Ramp Wave for Vertical Deflection.

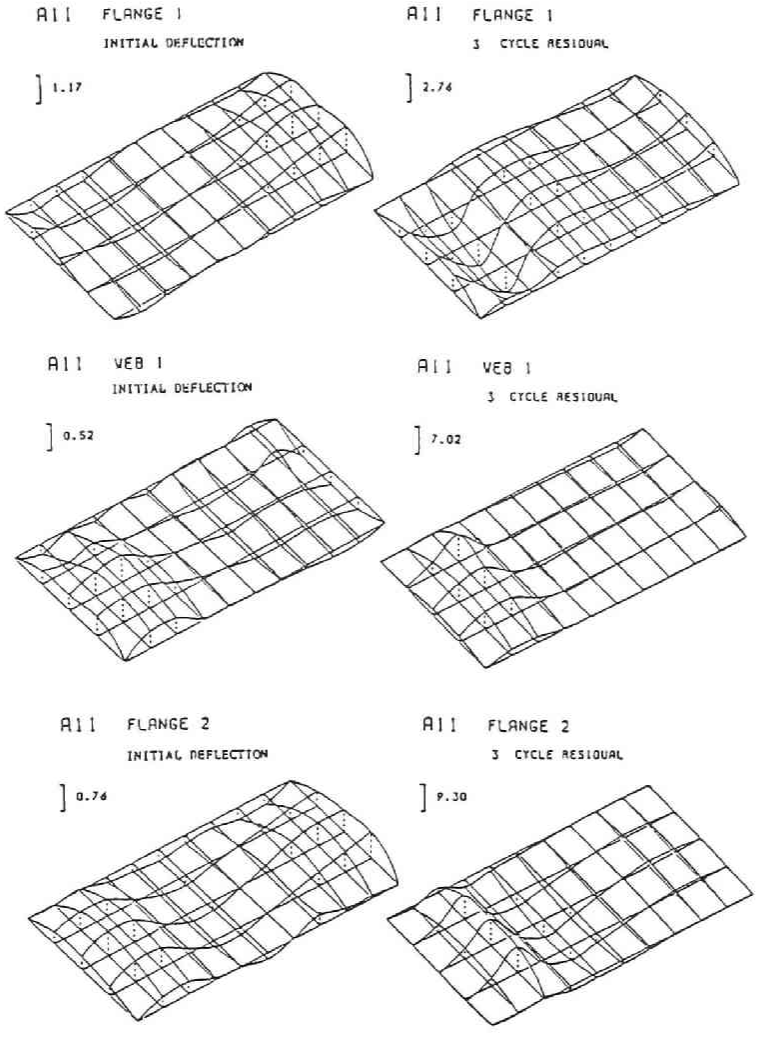

Fig. A.4.1 Initial and Residual Out-Of-Plane Deflections of Box Beam-Column Specimen.

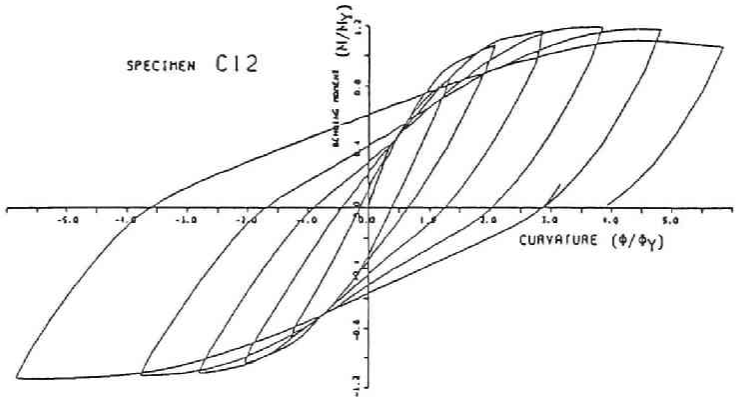

Fig. A.4.2 Relationship between Bending Moment and Curvature of Box Beam-Column Specimen. Based on Load-Cell and Curvature Gauge.

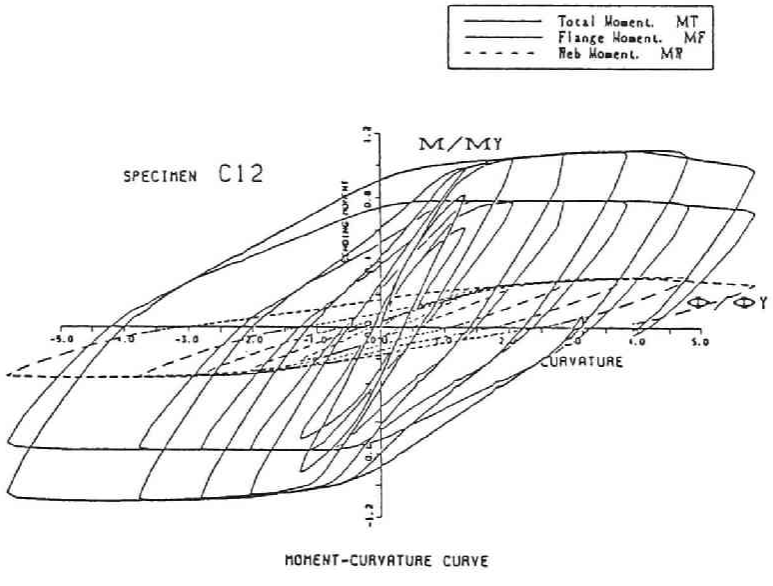

Fig. A.4.3 Relationship between Bending Moments and Curvature of Box Beam-Column Specimen. Based on Strain Gauges and Curvature Gauge. Load Distribution of Webs and Flanges.

conform the ramp wave form so that its peak value increases gradually in a linear form as shown in **Fig. A.3.7.** That is, the unloading criterion is represented as the limiting condition of the maximum deflection of the beam-column specimen:

$$d_n = (1 + (n \quad 1) \Delta) d_o$$

where d_n and d_o refer to the maximum vertical deflections in the n-th loading cycle and the prescribed first loading cycle, respectively. Also, Δ is specified from preliminary tests. The vertical deflection of the test specimen is continuously obtained as the analog data through the AIO interface on the master system microcomputer under loading (positive or negative bending). Then, the measured deflection is immediately compared with the specified deflection d_n in the above equation. If the unloading criterion for the maximum vertical deflection is satisfied, then the servo testing machine is controlled by the function generator through the DIO Interface on the master system microcomputer. Herein, another actuator is maintained to yield the constant horizontal thrust load during a test for uniaxial compression of the beam-column.

A.4 Experimental Displays

Fig. A.4.1 shows an example of the displays of the initial and residual out-of-plane deflections of the beam-column specimens.

Fig. A.4.2 shows another example of the moment curvature relationship of the beam-column specimens obtained by the reading of the load cell of the servo machine and the curvature gauge. Whereas **Fig. A.4.3** illustrates the similar relationship of strain gauges and the curvatures gauge. The load distribution by the structural components, namely, the bending moments carried by the webs and the flanges are also indicated herein.

A.5 Conclusions

In this APPENDIX, a new automated structural testing system is presented. This system is especially named as the **CATS**, Computer Aided Testing System. The main conclusions are:

(1) The system is found to work precisely and quickly. The plural microcomputers connected by the GP-IB as the controllers of the testing system is also found to be very efficient.

(2) The testing system is mainly composed of three groups: Servo testing machine group, Data acquisition group, and Microcomputer group.

(3) Several series of buckling tests have been conducted on the specimens: steel stub columns and box beam-columns under repetitive loading.

(4) The testing system has the following advantages: (a) easy and efficient measurement of initial and residual deflections of the surfaces of the specimen, (b) quick real-time acquisition and computation of large quantity of data for the swift decision making on the continuously varying state of the specimen, (c) quick digital feedback control of the servo testing machine, (d) real-time display of the performance of the specimen, (e)

storage of a large quantity of acquired data, (f) cooperative task carried by especially two microcomputers connected by GP-IB, and (g) swift transmission of data to large computer center via the TSS terminal.

Bibliographies of APPENDIX in PART III

1) IDMC, Statistical study on the initial deformations and the ultimate strength of steel bridge members, JSSC, Vol. 16, No. 179, 1980, pp. 10-43(in Japanese).
2) Niwa,Y., E.Watanabe and Y.Iwashimizu, On the initial imperfections and their relations to the strength of web-plates of actual steel bridges, Memoirs of the Faculty of Engineering, Kyoto University, Vol. 43, 1981, pp. 240-264.
3) Komatsu,S., Y.Niwa and E.Watanabe, Statistical study on imperfections of steel webs, Journal of Structural Division, Proc. ASCE, 1983, pp. 419-438.
4) Niwa,Y., E.Watanabe and H.Isami, Automated structural testing using microcomputer system, Proceedings of the Japan Society of Civil Engineers, No. 332, 1983, pp. 145-158.
5) Niwa,Y., E.Watanabe and H.Isami, Automated testing of thin-walled steel structures under repetitive loading by microcomputer system. Proceedings of the 2nd International Conference on Civil and Structural Engineering Computing, Vol. 2, 1985, pp. 337-343.
6) Ramirez,E.V. and M.Weiss, Microprocessing Fundamentals Hardware and Software, McGraw-Hill, 1980.
7) Hiramatsu,K. and T.Saito, Interfaces of microcomputer, Ohmusha, 1979(in Japanese).

CONCLUDING REMARKS

This dissertation is concerned with applications of the catastrophe theory to evaluation procedures of the ultimate strength of typical structural members in both elastic and elasto-plastic ranges. Firstly, a numerical method of elastic catastrophe analysis is proposed for discrete structural systems, and its flow chart is illustrated in **Fig. 1.2.1** of the PART II. Secondly, a new method of approach to predict the elasto-plastic strength of steel members is unified in details, and its flow chart is illustrated in **Fig. 1.3.1** of the PART III. The present formulations do not involve the so-called nonlinear process to trace the relevant equilibrium paths up to the ultimate strength of the members in the elastic or elasto-plastic range.

The main conclusions in the PART I are summarized as follows:

The chapter 1 reviews on the general theory of elastic stability in a topological sense using the catastrophe theory. The potential function of structural system can be defined by a function of the generalized internal state variables and several external control parameters. Then, an explicit form of the potential function of the imperfect system can be determined by the Taylor's expansion at the critical point of the potential function of the associated perfect system. Herein, the generalized state variables correspond to the essential instability modes, while the control parameters correspond to a single loading parameter and the associated initial modes. Moreover, an effect of the initial displacements on the load-carrying capacity of the system is obtained from the bifurcation set in the catastrophe theory.

The chapter 2 presents an introduction to the catastrophe theory in the light of the singularity theory of mappings in pure mathematics. Then, broad, but concise, historical reviews on the catastrophe theory and its applications in engineering sciences are provided. There exists a family of potential functions characterized by the control parameters as they vary smoothly. This family is thought as the common potential function in the engineering sciences. Also, the stable state of the system corresponds to that at which the potential function has its local minimum for prescribed control parameters under the Perfect-delay convention. Thus, the catastrophe may take place at a peculiar point where the number of such minima changes suddenly. The Thom's Theorem asserts that a family of potential functions can be described locally in either typical form of the seven elementary catastrophes or universal unfoldings under the state variables ≤ 2 and the control parameters ≤ 4. The bifurcation set in the control-parameter space through the catastrophe map of elementary catastrophe unfolding plays a significant role in order to evaluate the imperfection sensitivity in structural mechanics.

The main conclusions in the PART II are:

The chapter 1 proposes a numerical formulation of catastrophe analysis for static instabilities of multi-degree-of-freedom structural systems in civil engineering field. The present procedure makes use of discretization methods such as a finite element method(FEM) and a simplified element method(SEM: See, APPENDIX A), and also of several modal transformations in the light of the Thom and Thompson's theories. Thus, the instability phenomena for the original potential

function with the multiple state variables can be numerically realized as those for either of the Thom's seven elementary catastrophes with one or two state variables through some diffeomorphisms in the APPENDIX B. The present formula will be applicable to the common instability problems with no, linear or nonlinear prebuckling equilibrium paths for engineering structures.

The chapter 2 presents a direct computational approach to determine the imperfection sensitivity of structures in terms of the bifurcation set through the catastrophe theory. The singularity condition on the equilibrium surface is definitely consistent with the zero-determinant condition of the associated map. The bifurcation set for a typical **fold** catastrophe can be explicitly realized by the 1/2-power rule. Also, the bifurcation set for a typical **dual cusp** catastrophe can be realized by the 2/3-power rule. Furthermore, the bifurcation sets for typical **hyperbolic umbilic** catastrophes can be consequently composed of three explicit imperfection sensitivity surfaces and their combinations. Then, each bifurcation set may be visually drawn in the three-dimensional load-imperfections space, and may confirm Thompson's results.

The chapter 3 provides a comparative study on the numerical results among three catastrophe analyses for the two-degree-of-freedom, continuous and discrete inextensible column models neglecting the axial deformations. The results of the discrete analysis are shown to converge to those of the continuous analysis, as the number of discrete finite elements increases. For a legitimate evaluation of the **cusp** and **dual cusp** catastrophe, the 4th order terms of the buckling mode in the total potential function must be considered rigorously in expressions for both the strain energy and the external work of the potential function. Thus, the catastrophes of **fold, cusp, dual cusp** and **umbilics** can be shown to be realized numerically for each column model. Herein, the value of each stability coefficient calculated herein may converge to that by the continuous analyses; also the results by the FEM may tend to overestimate slightly in comparison with the SEM, as the number of discrete finite elements increases.

The chapter 4 presents several applications of the discrete catastrophe analysis in order to predict the nonlinear behavior of structural models such as columns and compressed plates with or without stiffeners. In this chapter, the catastrophe analysis accompanies with the static condensation procedure under the certain control types of loads and displacements in the initial postbuckling range.

The first application is made to extensible column models considering the axial deformations. So far as the first-order approximations of the axial strain and the curvature are considered, the 4th order terms of the buckling mode in the potential function always disappear, and the potential function leads to only an eigenvalue problem for the ideal buckling load in an analytical sense. Then, the column model has no postbuckling strength. The present numerical results analyzed by the SEM confirm the first-order approximate extensible column. However, the results by the FEM may tend to slightly overestimate the nonlinear characteristics. This quantitative difference depends on the kind of the shape function adopted in each discrete method. Herein, an extensibility of the neutral axis of column will not affect the cubic terms of the potential function, and the terms equal to those in the case of the inextensible column as the number of the discrete elements increases.

Secondly, the nonlinear solutions of elastic large deflection for compressed rectangular plates are predicted by the proposed numerical formulation without recourse to solving the nonlinear simultaneous equilibrium equations. In the case of

square unstiffened plates, the numerical results are found to be in excellent agreement with those by Timoshenko, Coan, Yamaki, Williams and Rhodes under various supporting conditions and the two control types. Herein, from the results, the difference between two control types of load and displacement may become little significant quantitatively and qualitatively within the accessible range of elastic large deflection.

Moreover, the present analysis is applied to the compressed rectangular stiffened plates with the symmetric and eccentric stiffeners for the global and local bucklings. The compressed stiffened plate with the symmetric stiffener has the stable symmetric bifurcation point, **cusp**, for both the global and the local buckling modes at smaller and larger flexural rigidities, respectively. Further applications to the compressed stiffened plates with the eccentric stiffener are made herein. For the distinct global buckling with the asymmetric bifurcation point, the load-carrying capacity can be determined from the **fold** in terms of the downward mode of the global initial deflection. Whereas, the distinct local buckling has the stable symmetric point of bifurcation, **cusp**, and the load-carrying capacity can never be predicted in the stability and the catastrophe theories of elastic structures. At their coincident bifurcation, the imperfection sensitivity surfaces are expressed in the form of the **hyperbolic umbilic** catastrophe with the homeoclinal bifurcation. The load-carrying capacity is commonly more sensitive to the global initial mode than to the local initial mode for their magnitudes being the same.

The PART III is summarized as follows:

The chapter 1 unifies a new simplified approach for evaluation of the strength of slender steel structural members such as columns, plates and shells. The residual stresses and the initial displacements may affect the evaluation of the elasto-plastic buckling strength and the form of the explicit imperfection sensitivity formula, respectively. Therefore, the inelastic strength prediction of the members may be explicitly evaluated in terms of the bifurcation sets or the imperfection sensitivity curves. Herein, the bifurcation set can be defined explicitly near the **equivalent bifurcation point** being the intersection point of the elasto-plastic postbuckling path with the plastic failure mechanism curve for typical members with neutral and stable postbuckling equilibria. While, in the case of members with unstable postbuckling equilibria like cylindrical shells, their normal elasto-plastic bifurcation point is taken to be the equivalent bifurcation point. Then, the bifurcation set can be directly determined from evaluating stability characteristics at the point. However, in the proposed approach, the actual initial geometrical imperfections are modified in the form of the proposed **equivalent imperfections.** The equivalent imperfection can be determined in a unified form on the basis of the previous strength curves and practical design curves.

In this chapter, several numerical illustrations for axially compressed columns are calculated using appropriate form of the equivalent initial deflections. The results are compared with some design curves and analytical results. The demonstrations are found to be in good correlation with those by such various investigations and experimental results, and the form of distribution of residual stress assumed herein may insignificantly affect the present results.

The chapter 2 formulates the simple unified approach of the elasto-plastic ultimate strength for the compressed steel plates with and without stiffeners. The inelastic strength prediction of the plate members may be explicitly determined

from the bifurcation sets for both global and local bucklings. Herein, the bifurcation sets can be defined explicitly near the equivalent bifurcation point being the intersection point of the elasto-plastic parabolic postbuckling path with the plastic mechanism curve. Also, the initial imperfections are modified and replaced by the equivalent imperfections proposed herein. The present ultimate strength curves are numerically shown to be in good correlation with some design specification curves and several test data.

Furthermore, using the proposed strength formula expressed as the imperfection sensitivity, a Monte Carlo simulation is performed on appropriate statistical distributions of the residual stresses and the initial deflections for compressed plates and stiffened plates. Then, the most frequent combinations of such imperfections can be explicitly determined from both their joint probability density function and the 5%-fractile ultimate strengths.

The final chapter 3 formulates the simplified unified approach of the elasto-plastic ultimate strength for the compressed cylindrical shells. The inelastic ultimate strength of the cylinders may be explicitly determined in the form of the bifurcation sets. Herein, the imperfection sensitivity of compressed cylindrical shell can be directly derived from the singularity condition on the equilibrium surfaces through the **elastic** pseudo-potential energy with considerations of **elasto-plasticity** of the material, which is defined near the elasto-plastic buckling point. Also, the initial deflections are modified and replaced by the equivalent imperfections proposed herein. The present approach involves two types of analyses; the one-mode analysis (only asymmetric mode) and the two-mode analysis (asymmetric and axi-symmetric modes). The two-mode analysis treats with the interaction of both modes, and is more sufficiently practice than the one-mode analysis. Then, the imperfection sensitivity can be predicted by the incomplete **parabolic umbilic** catastrophe with the paraclinal bifurcation, and the potential is trancated up to the 3rd-order terms. The elasto-plastic buckling provides the near-coincident bifurcation; whereas, in the elastic range, the present result identically gives the complete simultaneous bucklings. Particularly, the elastic imperfection sensitivity for the axi-symmetric mode is just equal to the Koiter's formula. Also, the formula is in good correlation with the ECCS strength curve for the compressed cylinder. The reduction of the strength is more greatly affected by the axi-symmetric initial mode than the asymmetric initial mode in the two-mode analysis.

In this PART III, all the calculations can be made using mainly a microcomputer with small memory storage. The general philosophy adopted herein may also be applicable to other types of engineering structures such as rigid frames, arches and trusses as well as columns, beams, plate panels, stiffened plates and cylindrical shells.